INVESTIGATION OF FACTORS AFFECTING SURROGATE LIMB MEASUREMENTS IN THE TESTING OF LANDMINE PROTECTED VEHICLES

By
Tamlin Whyte

Thesis presented for the degree of Master of Science
in Mechanical Engineering

In the special field of Impact Biomechanics

University of Cape Town

March 2007

ABSTRACT

Abstract:	Landmine protected vehicles (LPVs) are designed to minimise the risk of injury to occupants. In order to quantify this risk, human surrogate measurement devices (HSMDs) are placed in the vehicle to record data which is then related to risk of injury using injury criteria that have been defined in test standards. Experience in testing LPVs and studies conducted have indicated that the lower leg is very vulnerable to injury and much speculation exists over the tibia injury criterion and the lower limb surrogates with which this criterion is measured. A lower limb impactor (LLI) system was thus designed to test lower limb surrogates and to explore factors that may affect the measurements obtained using the surrogates. The factors that were investigated in this study were the position of the lower limb, the wearing of a boot and the hip and knee joint stiffness. Simulations detailed in [6] were used as the basis for the experiments conducted to examine the effect that lower limb position has on the lower tibia axial force. For all but one case the experimental and simulated results were similar, with the conventional seating position resulting in the highest axial tibia force which was decreased by approximately half when the seating position was altered. However, only injury due to pure axial loading of the lower tibia is considered and the risk of injury due to other loading regimes and injury mechanisms may in fact show an increase at different limb positions. It is recommended that post mortem human surrogate (PMHS) tests be conducted at the various limb positions in order to determine the effects of injury mechanisms other than pure axial loading of the lower limb. Wearing a standard issue (South African) army boot was found to decrease the lower tibia axial force by more than 10%. The effect of hip and knee joint stiffness produced inconclusive results and further testing is required to ascertain the ability of this factor to influence the lower tibia axial force.
Keywords:	Landmine protected vehicle, human surrogate measurement devices, lower limb impactor, lower limb position, boot, joint stiffness.

ACKNOWLEDGEMENTS

This study was part of a larger project which was conducted as a deliverable by the Council for Scientific and Industrial Research (CSIR), Landwards Sciences (LS) for Armscor. As such it has involved many people performing various tasks in order that the project deliverable could be submitted within the designated time period. In particular, Leon Broodryk and Deon Malherbe are acknowledged for the manufacture of the Lower Leg Impactor (LLI) and played a crucial role in the practical elements of the design of the LLI. Rayeesa Ahmed was solely responsible for the lumped parameter modelling conducted throughout this study and assisted in the characterisation of the spring stiffness. Jimmy Hannan and Piet Ramaloko provided test and measurement support and assisted in the instrumentation of both the original Lower Leg Testing System (LLTS) and LLI and the lower limb surrogates. Vacation work students Valrich Grundling and William Mtshweni, assisted with the testing. David Reinecke managed the larger project deliverable from LS and provided much guidance and support and ensured that the relevant resources were available.

As this thesis was conducted through the University of Cape Town (UCT), the support of the Blast, Impact and Survivability Research Unit (BISRU) added further depth to this project. Victor Balden conducted the finite element simulations of both the original LLTS and LLI and assisted Rayeesa and the author of this dissertation in interpreting the simulation results and formulating ideas for improving the original system. Professor Gerald Nurick supervised this study. His involvement with LS and Armscor meant that he understood the larger project of which this study was a part and thus he could provide insight at all stages of the project and guidance to keep this study focused.

Frans Beetge from Armscor must be thanked for his role in managing the larger project. His support and inputs to this study were invaluable as his wealth of experience gives him much insight into the field of landmine protected vehicles (LPVs).

I am grateful for the guidance and financial support from the CSIR, LS and Armscor, without which this study could not have taken place.

Photograph of the LLI team (from left to right): Deon Malherbe, Piet Ramaloko, Jimmy Hannan, ATD 2, Valrich Grundling, Tamlin Whyte, Victor Balden, William Mtshweni, Rayeesa Ahmed and Leon Broodryk.

EXECUTIVE SUMMARY

Title:	INVESTIGATION OF FACTORS AFFECTING SURROGATE LIMB MEASUREMENTS IN THE TESTING OF LANDMINE PROTECTED VEHICLES
Background:	Landmine protected vehicles (LPVs) are designed to minimise the risk of injury to the occupants during times of conflict as well as to protect members of humanitarian organisations to allow them to bring aid to post-conflict countries. The protection capabilities of LPVs are tested using human surrogate measurement devices (HSMD). The results recorded by the HSMDs are then related to injury criteria (or allowable injury levels) that have been specified in test standards. Studies conducted in the field and through simulations indicate that the lower leg is very vulnerable to injury and much speculation exists over the tibia injury criterion and the lower limb surrogates with which this criterion is measured. The LLTS was thus commissioned by Armscor (as part of a larger project focussing on LPVs) in the hope that the apparatus would supply a force of similar magnitude and duration to a surrogate limb as that limb would be presented within a vehicle exposed to an anti-vehicle (AV) mine explosive event. The original LLTS was transferred to the CSIR Landwards Sciences for characterisation and modification after which it was redesigned, recharacterised and renamed the Lower Leg Impactor (LLI). The LLI could be used to test various factors which may effect measurements obtained by lower limb human surrogates.
Objectives:	The first objective of this thesis was to modify the original LLTS so that it would supply a force to a surrogate limb as it could experience within an LPV during an anti-vehicle (AV) mine explosive event. The second objective was then to use the modified system, the LLI, to assess the effect of various human surrogate limb parameters (such as lower leg position, the wearing of a boot and joint stiffness) on measurements obtained.

Methodology:	In order to determine the required performance of the original LLTS, a literature review was conducted through which the specific aim of the system was clarified in terms of the forces that a surrogate limb could be exposed to within an LPV. The original LLTS was inherited from an external company, thus the system required characterisation in order to determine what modifications needed to be made. This was done via a series of experiments to evaluate the range of forces that could be generated by the original LLTS. In addition, simulations were conducted by Victor Balden and Rayeesa Ahmed in order to better understand the operation of the original system, to identify possible shortcomings and to investigate proposed modifications. Based on the experimental results and the simulations, modifications were made to the original LLTS and it was renamed the LLI. The LLI was then characterised to determine whether it was an improvement over the original system and whether it could meet its specifications. The effect of various factors on the measurements obtained by surrogate limbs, namely the positioning of the lower limb, the wearing of a boot and the stiffness of the knee and hip joints, was then investigated.
Conclusions:	The LLI meets the desired specifications for a system to provide a force to a surrogate limb as it could experience from within an LPV during an explosive event. The effect of lower limb position on the peak lower tibia axial force recorded by a surrogate limb is significant. The conventional lower limb position (seated with hip, knee and ankle joints at right angles) produced the most severe axial loading. The effect of wearing a standard issue (South African) army boot significantly decreases the peak lower tibia axial force. The effect of joint stiffness on the peak lower tibia axial force is inconclusive.

Recommendations:	It is recommended that post mortem human surrogate (PMHS) tests be conducted at the various limb positions in order to determine the effects of injury mechanisms other than pure axial loading of the lower limb. The effect of different types of boots on the peak lower tibia force should be investigated as the effect of wearing a standard issue (South African) army boot has been shown to significantly decrease the peak force recorded by the lower tibia. The effect of joint stiffness of the surrogate leg hip and knee joints when the leg is subjected to both low and high loads should be further investigated.

ABBREVIATIONS LIST

AIS	Abbreviated Injury Scale
Armscor	Armaments Corporation of South Africa Limited
ATD	Anthropomorphic Test Device
AV	Anti-vehicle
BISRU	Blast Impact and Survivability Research Unit
CSIR	Council for Scientific and Industrial Research
DAQ	Data Acquisition unit
FEM	Finite Element Model
HIC	Head Injury Criterion
HSMD	Human Surrogate Measurement Device
ISS	Injury Severity Score
LLI	Lower Leg Impactor
LLTS	Lower Leg Testing System
LMT	Land Mobility Technologies
LPV	Landmine Protected Vehicle
LS	Landwards Science competency area of the CSIR
NATO	North Atlantic Treaty Organisation
NHTSA	National Highway Traffic Safety Administration
PMHS	Post Mortem Human Surrogate
RTI	Revised Tibia Index
SABS	South African Bureau of Standards
SI	Severity Index
TI	Tibia Index
TNT	Trinitrotoluene
TROSS™	Test Rig for Occupant Safety Systems™
UCT	University of Cape Town
WSTC	Wayne State Tolerance Curve

CONTENTS

LIST OF FIGURES

Chapter 2:

LIST OF TABLES

Chapter 2:

Chapter 3:

1 INTRODUCTION

1.1 Background

Anti-vehicle (AV) mines present not only a threat to vehicles during times of conflict, but their humanitarian impact extends into the future. AV mines prevent humanitarian organisations from gaining access to populations in need of aid and the clearing of these mines is time-consuming and costly [1]. Landmine protected vehicles (LPVs) must be designed to minimise the risk of injury to the occupants during times of conflict as well as to protect members of humanitarian organisations to allow them to bring aid to post-conflict countries.

Standards have been developed to test the protection capability of LPVs (e.g. RSA-MIL-STD-37 [2], AEP-55 version 2 [3]). These standards specify injury criteria which give an indication of what injuries a person might sustain if they were exposed to certain measured forces or accelerations. Human surrogate measurement devices (HSMD) (e.g. Hybrid III [4], Surrogate Leg [5]) are used to record data in vehicles being subjected to testing with AV mine surrogates. The data being recorded depends a great deal on the measurement device being used and thus the HSMD must be carefully designed and calibrated to record results that reflect as closely as possible what a person would experience in the vehicle in the field.

Studies conducted in the field and through simulation indicate that the lower leg is very vulnerable to injury in an AV mine strike as this is the part of the body closest to the vehicle floor [6]. In addition, this is the criterion through which many LPVs fail during testing. Much speculation exists over the tibia injury criterion and the lower limb surrogates with which this criterion is measured.

The Lower Leg Testing System (LLTS) was thus commissioned by Armscor in the hope that the apparatus would be able to supply a force of similar magnitude and duration to a surrogate limb as that limb would be exposed to within a vehicle subjected to an AV mine detonation. The original LLTS was transferred to the CSIR, LS for characterisation and modification. After modification the system was renamed the Lower Leg Impactor (LLI).

The LLI lends itself to the testing and validation of lower limb surrogates as the limbs can be positioned as they would in an LPV. It is necessary to explore the factors that affect the surrogate limb measurements in order to better understand injury mechanisms and criteria and to allow one to better relate these readings to injuries which would be sustained by vehicle occupants. The effect of lower leg position on lower extremity injury levels is one of these factors. This knowledge will enable LPVs to be designed that will offer greater protection to the vehicle occupants.

1.2 Objectives

The main objectives of this thesis were as follows:

- To modify and characterise the LLTS to enable testing of human surrogate limbs through the application of forces as the limb would expect to experience within a landmine protected vehicle during an explosive event.
- To then use the modified system, the LLI, to assess the effect of various human surrogate limb parameters (such as lower leg position, the wearing of a boot and joint stiffness) on measurements obtained. These measurements can then be used to comment on the influence that these parameters may have on vehicle occupant injury levels.

1.3 Plan of development

A literature survey was conducted that focussed on reviewing the body of knowledge surrounding the following topics:

- Injury mechanisms and injury criteria of the lower limb;
- Lower limb surrogate measurement devices used in LPV validation tests;
- Factors that affect measurements obtained using lower limb surrogates;
- Typical injuries that occur within LPVs; and
- Apparatus used in the testing and validation of lower limb surrogates.

The literature was then used to clearly define the aim and requirements of the LLI.

The aim of the LLI is to apply forces to surrogate limbs as they may experience within an LPV during an explosive event. In order to determine whether the original LLTS was capable of meeting this aim (and to compare the characterisation results with those obtained by the manufacturer) it was first characterised through a series of experiments. Lumped parameter and finite element models were built by Rayeesa Ahmed (CSIR LS) and Victor Balden (BISRU) to aid in understanding the operation of the current system and to investigate the effects of possible modifications to the system. Changes were then made to the original LLTS and another series of experiments were conducted using the LLI to ascertain whether the LLI complied with the desired requirements.

A further objective of this dissertation involved using the LLI to asses the role that the various lower limb HSMA parameters play in measured injury levels. The parameters that were explored were lower limb position, wearing a boot and hip and knee joint stiffness.

Finally, conclusions were drawn and recommendations were made for future research.

2 LITERATURE STUDY

The first section of the literature study focussed on reviewing the body of knowledge surrounding injury mechanisms, injury scales and injury criteria of lower limb. Lower limb surrogate measurement devices used in LPV validation tests, factors that affect these measurements and typical injuries that occur within LPVs were then explored. In order to investigate the parameters that affect lower limb surrogate measurements, systems to test and validate the surrogates are required. Typical lower limb surrogate testing and validation apparatus used prior to LPV validation tests were thus reviewed. One of these systems was the original LLTS. Thus the literature provided by the manufacturer describing the original LLTS concept, design and initial characterisation was carefully considered. Typical vehicle test results with LPVs were also reviewed and the assembled body of literature was used to more clearly define the aim and requirements of the LLI.

2.1 Lower limb mechanisms of injury, injury scales and injury criteria

Mechanisms of injury describe the manner in which injuries can occur and injury criteria[1] specify the limits at which these injuries occur. Injury scales offer a means by which injuries can be described and graded in terms of severity.

2.1.1 Mechanisms of injury

Bone responds to repetitive loading over time by reabsorbing bone where the loading conditions are mild and depositing bone where the loading conditions are severe. However, if the magnitude and frequency of the loading exceeds the ability of the bone to adapt, injury occurs [8].

As the lower limb is the focus of this study, mechanisms of injury of the tibia, ankle and foot were explored.

Tibia fractures can be caused through direct or indirect impact to the leg and are the most common fractures in long bones [7]. Injury mechanisms of the ankle and foot are closely related to the possible range of motion of the ankle and hind foot (See Figure 1).

[1] Injury criteria are proposed and validated on the basis of experimental studies and, depending on the type of experiment, the terms injury criterion, damage criterion and protection criterion are used. When living tissue is used in the experiments, the term injury criterion is used. When PMHS are used, then the criterion is referred to as a damage criterion. The use of ATDs requires the use of the term protection criterion. However, the terms injury, damage and protection criteria are often related to one another and not clearly differentiated and thus the term injury criteria is widely used, and is used in this study, as any index meant to quantify impact severity [7].

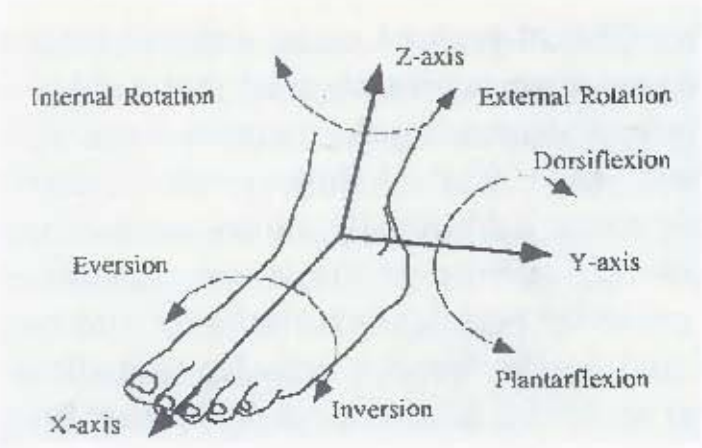

Figure 1: Anatomical motions of the hind foot joints [7].

In frontal collisions, 58% of ankle injuries are due to axial load, 15% to inversion and 11% to eversion Axial loading can result in talus (See Figure 3 and Figure 4) fractures and pylon[2] fractures by driving the talus into the tibia. Dorsiflexion (See Figure 1) and entrapment of the knee can increase axial forces [7]. This can be related back to the occupant of an LPV, if an occupant is sitting with the front of the foot raised and a heavy object on the lab, the axial ankle force will be higher which could result in a pylon fracture

[2] Intra-articular fractures of the distal tibia involving the calcaneus, talus and distal tibia (see Figure 3 and Figure 4).

Inversion and eversion (See Figure 1) account for most malleolar (See Figure 2) injuries, especially ankle fractures. The rate of rotation, orientation of the ankle and occupant specific factors such as age or pre-existing damage also affects the probability of malleolar injury [7].

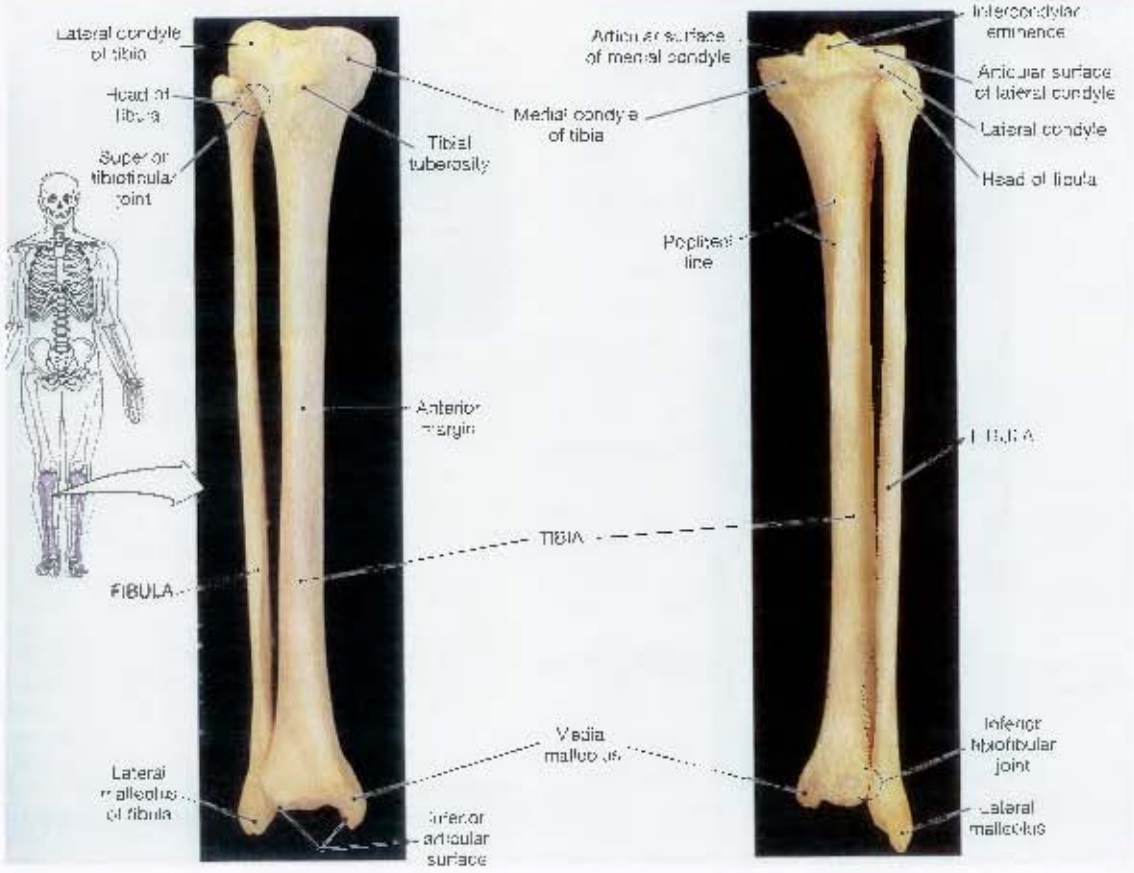

Figure 2: Anterior (left) and posterior (right) views of the right tibia and fibula [9].

Foot or metatarsal (See Figure 3 and Figure 4) fractures sustained in automotive accidents result mainly from contact to the foot pedals. If the heel also strikes the floorboard then the local loading may cause a calcaneus (See Figure 3 and Figure 4) fracture [7].

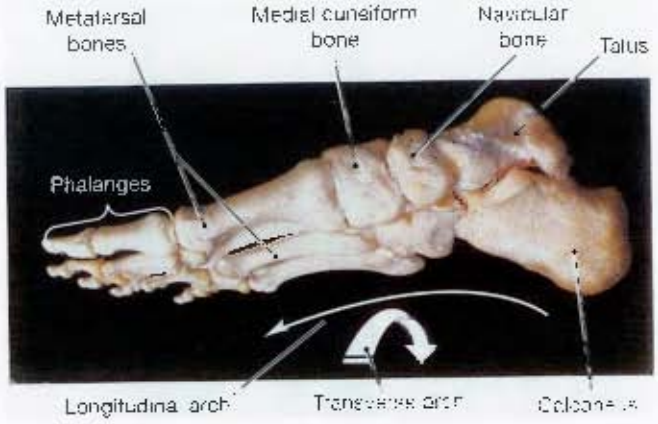

Figure 3: Medial view of the right foot [9].

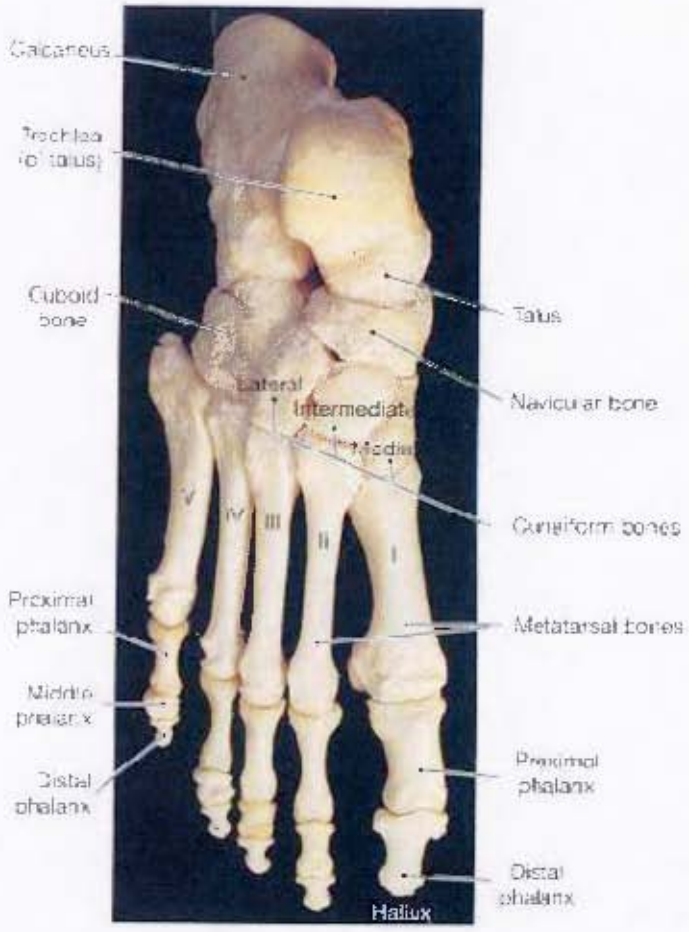

Figure 4: Superior view of the right foot [9].

2.1.2 Injury scales

Injury scales are used to describe the type and severity of an injury and are based on medical diagnosis [7]. Examples of anatomic injury scales are the Abbreviated Injury Scale (AIS), the Injury Severity Score (ISS), the Probability of Death (POD) and the Occupant Injury Classification (OIC) [10]. In trauma research, the most commonly used scale is the Abbreviated Injury Scale (AIS).

The AIS dates back to 1971 to fill a need for a standardised system for classifying the type and severity of injuries resulting from vehicular crashes [11]. The AIS has been revised over the years to describe more injuries and the latest version is AIS 2005. In [11] the AIS is defined as "an anatomically-based, consensus-derived, global severity scoring system that classifies each injury by body region according to its relative importance on a 6-point ordinal scale." In the AIS code the injury is given a number which describes the specific injury and a severity rating from 1 to 6, where 1 is considered a minor injury and 6 is an untreatable injury

In the current military standards [2] an injury measurement must be less than an injury risk of 10% of an AIS 2+ injury[3]. An AIS 2 injury is a moderate severity injury with a 0.1 to 0.4% fatality range. In terms of the AIS code for the lower extremities this could be a tibia, fibula, calcaneus or metatarsal fracture (AIS 2) or a traumatic amputation below the knee (AIS 3) [11].

2.1.3 Injury criteria

Injury criteria attempt to relate parameters (such as forces or accelerations) measured by human surrogates (anthropomorphic test devices (ATDs) or cadavers) to injuries that a person would sustain if subjected to those measured parameters. Many different injury criteria exist and debate continues as to how accurate these criteria are as a prediction of actual injuries that would be sustained.

One of the most well known[4] injury criterion is the head injury criterion (HIC). This may be due to the fact that head injuries sustained in automotive accidents is a leading cause of death and disability [7]. The HIC was developed over 30 years ago and has a historical basis in the work of Gadd [12] who used the Wayne State Tolerance Curve (WSTC) to develop the severity index (SI). The version of the HIC that is used today was proposed by the US National Highway Traffic Safety Administration (NHTSA). Hertz [13] developed a curve that related the HIC to a probability of skull fracture [7]. Although the HIC is still the most commonly used criterion for head injury in automotive research, it is not currently included in the standard for the testing of LPVs, AEP-55 Volume 2 [3]. One of the reasons for this is that the HIC is only valid for a frontal impact of the skull and in LPVs the skull is more likely to impact the roof of the vehicle which would result in an impact to the top of the skull.

[3] An AIS 2+ injury could be an AIS 2, AIS 3, AIS 4, AIS 5 or AIS 6 injury. Thus, less than 10% risk of AIS 2+ injury means the risk of injuries greater than and including AIS 2 injuries is less than 10%.

[4] The HIC is mentioned as an introduction to injury criteria in books such as [14] which deal with the broader field of impact mechanics.

In the testing of LPVs, the lower limb criteria are often discussed as the lower leg is very vulnerable to injury in an AV mine strike as this is the part of the body closest to the vehicle floor [6]. In addition, the lower limb criterion is often the criterion through which many LPVs fail during testing. Much speculation exists over the tibia injury criterion and the lower limb surrogates with which this criterion is measured. This section will thus focus on the lower limb injury criteria, the development thereof using PMHS tests and a detailed description of the currently available criteria.

2.1.3.1 The development of lower limb injury criteria using post mortem human surrogates

In order to determine injury criteria, a variety of tests have been conducted with PMHS specimens. There is not complete agreement in the literature on injury mechanisms and criteria for the foot and ankle complex as significantly different test protocols have been used [15]. These differences arise from differences in the individual factors of cadaver specimens (e.g. age, gender); the level at which the limb is amputated (e.g. above, at or below the knee); the manner in which the limb is interfaced with the system (e.g. strapped to the test fixture, attached to an ATD) and the specifications of the impactor (e.g. rate of loading and force of impact).

The most commonly used criteria in predicting lower limb injuries are outlined in 2.1.3.2. The experimental setups that were used in PMHS tests are described below to highlight the different methods that are used which may result in discrepancies in injury criteria definitions.

Bergeman and Prasad [16] conducted tests to investigate ankle injuries in automobile accidents that often involve dorsiflexion of the ankle caused by impact loading to the bottom of the foot. Nine pairs of cadaver limbs (from both male and female subjects ranging in age from 38 to 71 years) that were amputated below the knee were impacted on the bottom of the foot with a pneumatically propelled linear impactor with velocities between 3 and 8m/s. The peak axial loads ranged between 1.1kN and 5.0kN. The study focussed on the effect of dorsiflexion on likelihood of ankle injury and found a strong correlation between them. Injuries that occurred were malleolus (See Figure 2) fractures and ligament avulsions and ruptures. No correlation between injury levels and peak loads, moments or loading rates was observed.

Schueler et al. [17] did not amputate the lower limbs and used 12 fresh PMHS ranging in age between 24 and 67 years. The plantar foot surface was impacted using a pneumatic impactor with an impact mass of 38kg and impact velocities of between 6.7 to 12.5m/s. Fractures of the calcaneus were the main injuries that were observed. A sole force of 15kN was found to indicate a significant risk of lower limb injury.

Yoganandan et al. [18] used 26 lower limbs amputated at the knee and applied dynamic loading to the plantar surface of the foot. Calcaneus and distal tibia fractures were observed at forces ranging from 4.3 to 11.4kN. The resulting injury criteria are described in 2.1.3.2.

Funk et al. [19] looked at the effect of Achilles tension on the axial tolerance of the foot/ankle complex. 43 PMHS lower limb specimens were amputated above the knee and impacted with a pneumatic impactor which provided a footplate velocity of about 5m/s. Calcaneal, talar and tibial pilon fractures were observed and it was found that fracture initiated at the distal tibia more frequently with the addition of Achilles tension.

2.1.3.2 Injury criteria applicable to the lower limb

The most common injury criteria applicable to the lower limb are axial criteria ([18],[20]) and the tibia index (TI) and revised tibia index (RTI) that take into account bending moments ([21], [22]).

Axial criteria:

The Hirsh criterion[5] [20] is aimed at provided an injury criterion for unrestrained standing personnel to shipboard shock motions. A tolerance curve of stiff-legged standing men to shock motion of short duration is provided (See Figure 5).

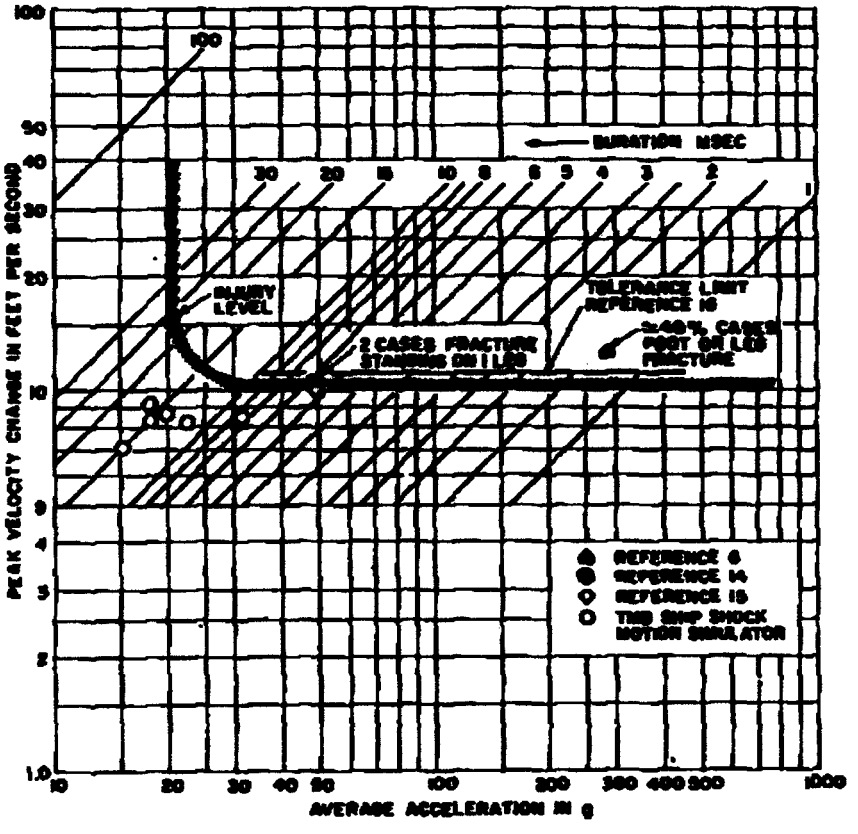

Figure 5: Tolerance of stiff-legged standing men to shock motion of short duration (from [20]).

[5] Although Hirsh [20] also provides injury criteria for the seated man, this criterion is for the lower spine and not for the lower limb. Thus, although the standing man criterion is not ideal as the human surrogates used during vehicle validation tests are usually seated, it does provide one with some idea of the tolerance of the lower limb to shock motion. In addition, the standing man data was used by the manufacturer to specify the desired peak tibia forces and peak durations that the LLTS was to simulate. Thus this paper is mentioned here so as to better understand the design requirements employed by the manufacturer of the original LLTS.

Hirsh states that the maximum tolerable loading of a single-degree-of-freedom mechanical system will be related to a peak acceleration when the duration of the loading pulse is long compared to the natural period of the system, and that the maximum tolerance is related to a peak velocity change when the duration of the loading pulse is short compared to the natural period of the system[6]. Hirsh indicates that the subject would sustain compressive injuries in the limbs near the point of load application when exposed to a peak velocity change of 3 to 4m/s for a pulse duration less than 10ms.

The Yoganandan et al. [18] criterion is the criterion currently referenced in RSA-MIL-STD-37 [2] and AEP-55 volume 2 [3]. Yoganandan et al. [18] supplies an equation for calculating the risk of calcaneus-talus-tibia fracture under axial loading. The fracture forces ranged from 4.3kN to 11.4kN.

The closed form equation for the risk based solely on dynamic axial load curve is:

P= 1 – exp [-exp{(w-2.036057)/0.3323456}]
where P indicates the probability of injury (fracture)
and w=ln(x) where x is the force measured by the tibia load cell in N.

However, this equation does not take into account age which was found to be one of the most significant discriminating variables (along with dynamic axial force which is reflected by x in the above equation) that define the injury risk function. Thus, a function based on cadaver data (based on both male and female subjects) is presented in [18] that does take age into account. The probability distribution curve is shown in Figure 6. The formula for the x-axis of the curve is as follows:

x-axis value = 0.0348*<age> + 0.415*<axial force>

The x-axis value that corresponds to a 10% probability of an abbreviated injury scale (AIS 2+[7]) injury can be read off the probability distribution curve (See Figure 6). The age of the subject can then be inserted into the equation and the corresponding axial force can be calculated. Thus, for a 45 year old subject, an axial force of 5.4kN is the limit. Based on an age of 45 years and an axial force of 5.4kN, the x-axis value is 3.8. A table comparing age and axial force limits for a 10% probability of injury was thus created to illustrate the implications of the graph shown in Figure 6 which is the effect of age on the axial force limits (See Table 1).

[6] The natural frequency of a standing man is 10 Hz (10cps), thus the natural period is 0.1s.
[7] An AIS 2 injury represents a moderate injury (0.1 to 0.4% fatality range). AIS 2+ injuries relating to the lower limb include tibia, fibula, calcaneus and metatarsal fractures and traumatic amputations below the knee [11].

Table 1: The axial force limits for a 10% probability of injury versus age as determined from the curve presented in Figure 6.

Age (years)	Axial force (kN)
20	7.5
25	7.1
30	6.6
35	6.2
40	5.8
45	5.4
50	5.0
55	4.5
60	4.1
65	3.7
70	3.3

The peak force duration is not included in the criterion[8]. This is problematic as it will influence the injury level [7].

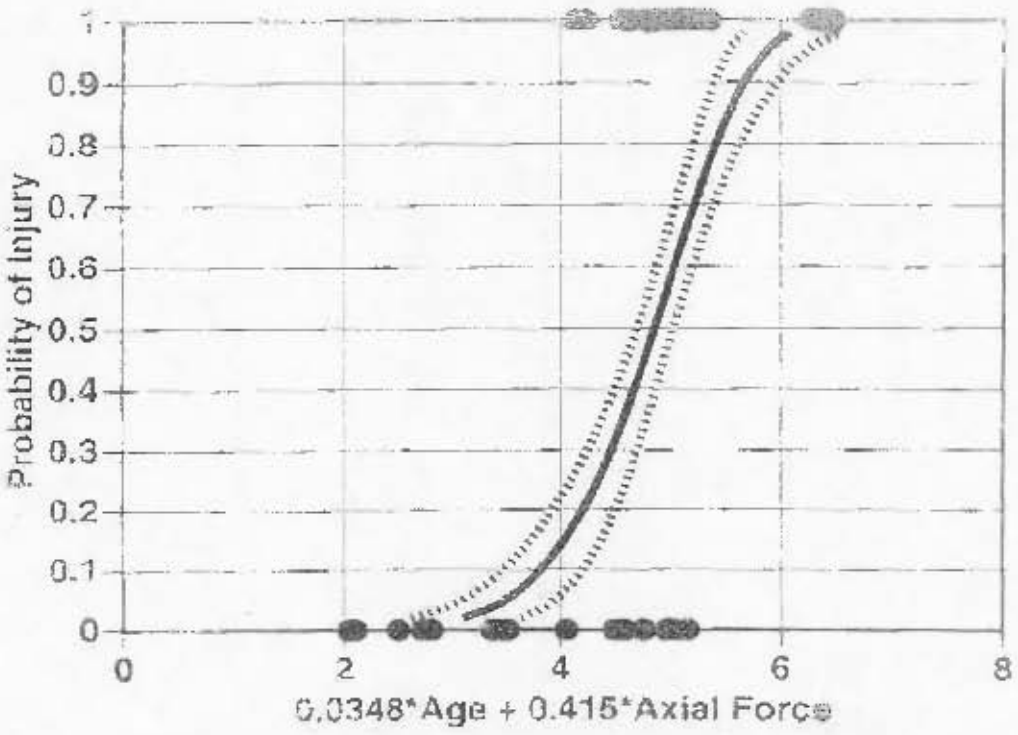

Figure 6: Probability distribution for foot-ankle injury as a function of age and dynamic axial force derived from cadaver tests (from [18]).

[8] A criteria referred to as the LLth Criteria that is mentioned in [23] does take into account the duration of the peak force (or exposure time), however, this criteria is not yet included in the current international standard developed by NATO [3]. Thus this criterion is not included in this study.

The peak lower tibia axial force can also be used to determine the probability of calcaneal, talar, ankle and midfoot fractures [22]. A 10% probability of AIS 2+ injury of the calcaneus, talus, ankle or midfoot corresponds to a lower tibia axial force that can be calculated from the following equation.

P= 1 /[1 + e^(4.572 - 0.670*F)]

where P indicates the probability of injury (fracture or AIS 2+) and F is the force measured by the tibia load cell in N.

The calculated force corresponding to a 10% probability of AIS 2+ injury is 3.54kN.

The relationship is shown graphically in Figure 7

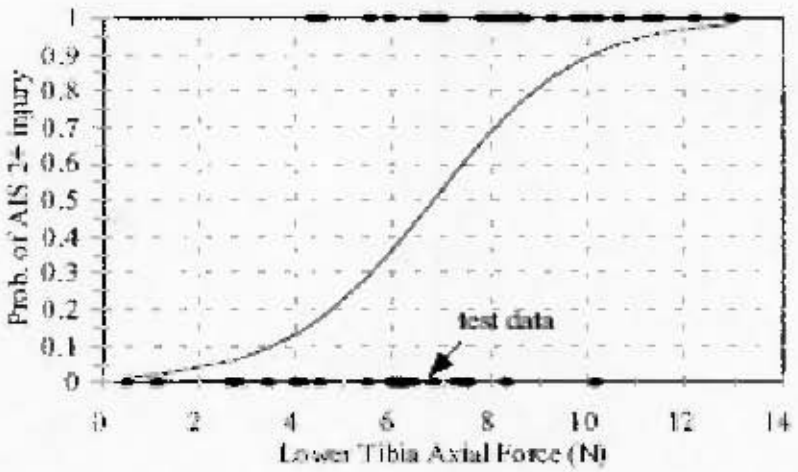

Figure 7: Probability of AIS 2+ calcaneus, talus, ankle and midfoot fractures as a function of axial lower tibia force (from [22]).

The tibia index (TI) takes into account bending moments as well as the axial force in the tibia. It is aimed at preventing tibia shaft fractures and can be calculated as follows:

TI = M/Mcrit + F/Fcrit < 1.3 and F<8kN

where M is bending moment,
F is compressive force and
Mcrit=225Nm and **Fcrit=35.9kN** are the critical intercept values for 50th percentile male (from [24]).

There is much debate surrounding the TI and its ability to be a predictor of fracture in axial impacts [25] [26]. A revised trauma index (RTI) was developed as testing by Schreiber [1997] with cadaveric leg specimens showed that the critical force limit indicated by Mertz was too high and the critical moment was too low. Thus the revised values were specified as **Fcrit=12kN** and **Mcrit=240Nm** [22]. Figure 8 shows how the probability of AIS 2+ leg shaft fracture can be found from the RTI.

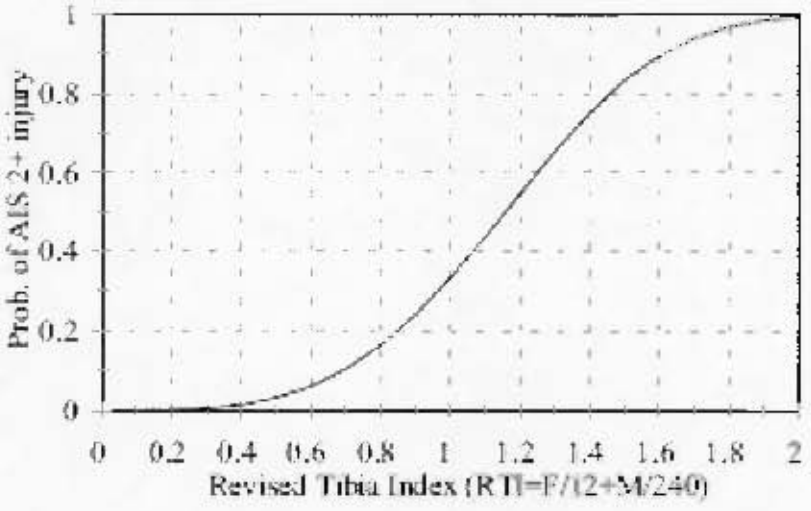

Figure 8: Probability of AIS 2+ leg shaft fracture versus RTI (from [22]).

Table 2 shows typical injury limits for the tibia and fibula

Table 2: Mechanical strength (average values) of the bones of the lower limbs as reported by Levine [27] (from [7]).

	Tibia		Fibula	
	Male	**Female**	**Male**	**Female**
Torque[Nm]	89	56	9	10
Bending[kN]	3.36	2.24	0.44	0.3
Average maximum moment [Nm]	207	124	27	17
Long axis compression[kN]	10.36	7.49	0.6	0.48

It must be noted that these criteria are derived from cadaver data and thus a Hybrid III ATD may need some correction as it would not measure the same force as a cadaver would. As stated in [25], "it appears that the axial force measured on the Hybrid III tibia is 2 to 3 times greater than the value observed on a cadaveric specimen. Limiting the axial force on the ATD tibia to 8kN should thus ensure significantly smaller axial forces in the human tibia."

2.2 Mechanical lower limb human surrogate measurement devices

Anthropomorphic test devices (ATDs) are mechanical models of the human body that are meant to represent the human body, but are robust enough to withstand a high number of tests and loading that would cause damage to the human body [7]. ATDs must be repeatable and reproducible to allow test results to be compared. As the measurements obtained from the ATD are used to determine injury levels (based on injury criteria), they must be regularly calibrated. Over 20 different dummy types are available (See Table 3 from [7]), but the current standard used in the testing of LPVs is the Hybrid III 50th percentile dummy.

Table 3: List of available dummies and their field of application (from [7]).

application	anthropomorphic test devices
frontal impact	Hybrid III family, THOR
lateral impact	EuroSID, EuroSID2, SID, SID-HIII, SID IIs, BioSID, WorldSID
rear-end impact	BioRID, RID2
pedestrian	POLAR
children	P0, P3/4, P3, P6, P10, Q-dummies, CRABI
belt	TNO-10
impactor	free motion head impactor, head/hip impactor for pedestrian impact

The mechanical human surrogate measurement devices that are currently available at the CSIR, LS are the male Hybrid III 50th percentile dummy [4] (See Figure 9) and the surrogate leg [5] (See Figure 10). A number of the surrogate legs are available at the CSIR, LS as they are used, together with the Hybrid III ATD, in the certification testing of LPVs. However, they have been found to measure peak tibia forces that are up to 2kN different from one another when drop tested from the same height. The legs have thus been assigned unique serial numbers and are not interchangeable with one another during tests.

Figure 9: The male Hybrid III 50th percentile ATD.

Figure 10: The surrogate leg.

Very little documentation [27] exists on the surrogate leg and commenting on its biofidelity or how closely its behaviour mimics that of a real human. The Hybrid III however has been the focus of many investigations into its biofidelity [25] [29].

The measurements obtained from human surrogates need to be related to injuries that a human subject would sustain via injury criteria. As mentioned in the previous section, as stated in [25] it appears that the axial force measured on the Hybrid III tibia is 2 to 3 times greater than the values observed on a cadaver specimen. Limiting the axial force on the ATD tibia to 8kN should thus ensure significantly smaller axial forces in the human tibia.

2.3 Factors affecting mechanical lower limb human surrogate measurements

The focus of this section of the literature review is on factors that are explored in this study, which are lower limb position, wearing of a boot and hip and knee joint stiffness.

2.3.1 Lower limb position

Lower limb position is defined by the angle of the hip, knee and ankle joints. Bergeman and Prasad [16] conducted tests to investigate ankle injuries in automobile accidents that often involve dorsiflexion of the ankle caused by impact loading to the bottom of the foot. The study found that the best correlation for an injury prediction was with a maximum angle of dorsiflexion. The foot was initially positioned at 90 degrees to the limb. The test setup is shown in Figure 11.

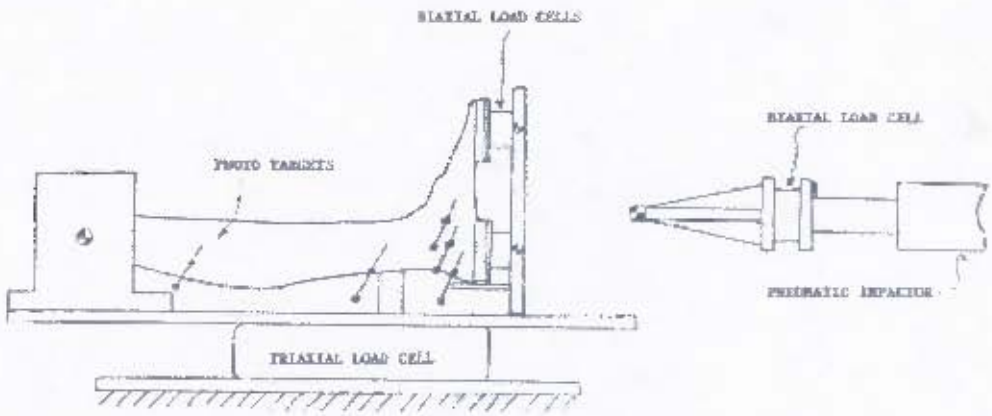

Figure 11: Impact testing arrangement (from [16]).

If the resulting angle of dorsiflexion after impact was less than 45 degrees, no injuries occurred. The peak axial loading ranged between 1.1kN and 5kN and no correlation between injury levels and peak loads (5kN is below the 10% risk of AIS 2+ injury to the lower tibia, thus this is expected), moments or loading rates was observed. This study was conducted with the limb parallel to the impactor and thus only the angle of the ankle joint was taken into account.

Klopp et al. [15] investigated the effect of the initial position of the foot on injury outcomes and found that a dorsiflexed foot was more resistant to injury than a neutral or plantarflexed foot. The test setup is shown in Figure 12. This seems to contradict the results from [16]. However, in [15] it was shown that if the initial position of the foot was in dorsiflexion it was more resistant to injury, whereas in [16] it was shown that if the impact caused the foot to dorsiflex more than 45 degrees from a neutral position, injury was likely.

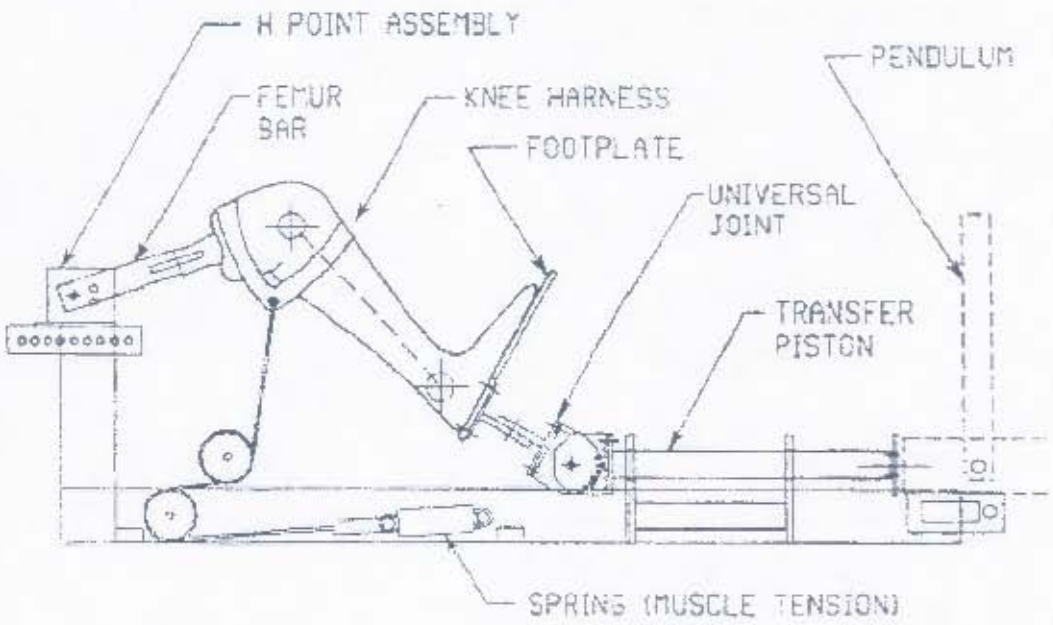

Figure 12: Schematic of test apparatus from [15].

A study was conducted by van der Horst et al. [6] which included not only the position of the ankle joints, but the positioning of the entire lower limb. The paper consisted of simulations that were conducted for four different lower limb positions. As the experimental design of this dissertation was based on that described in [6], this paper will be discussed in detail.

The aim of the study was to validate the Madymo Hybrid III Denton leg model using the TROSS™ experimental data (for details on TROSS™ see section 2.5.1 of this dissertation).

Three different loading conditions of increasing severity of explosive loads (denoted by db1, db2 and db3 respectively) were used to gather experimental data using the TROSS™, with and without shoes (denoted by db and dbns respectively). Only the conventional lower limb position was used with the hip, knee and ankle joints all at 90 degrees as shown in Figure 13.

Figure 13: TROSS™ test setup (from [6]).

Simulations were then conducted using Madymo As in the experimental data. three loading conditions of increasing severity of explosive loads (db1,db2. db3) were used, with and without shoes (db, dbns). Four different lower leg positions were simulated (See Figure 14). all with the same vertical displacement of the footplate. It must be noted that only Position A was validated with experimental data and the results of the effect of boots were not presented in this paper.

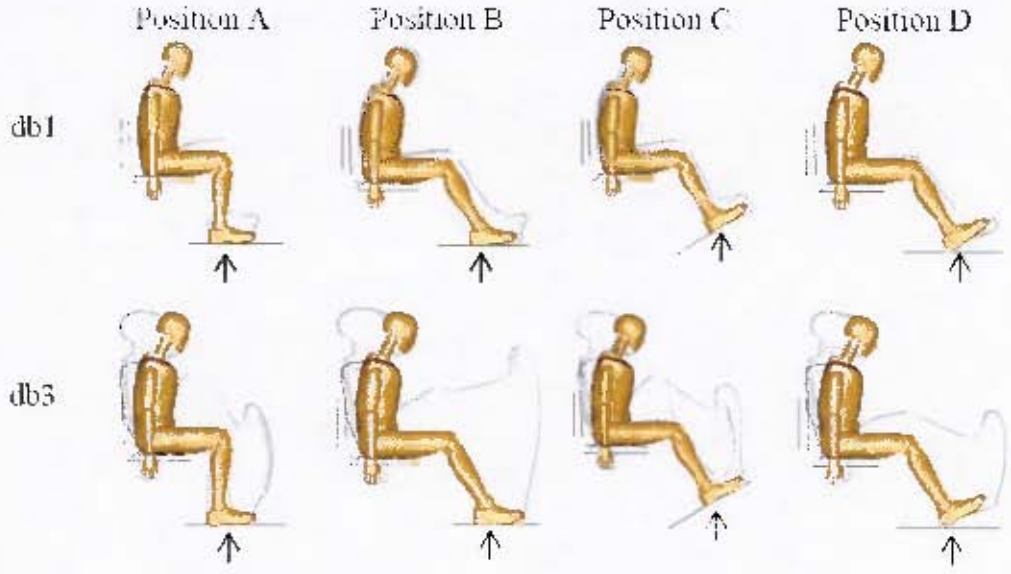

Figure 14: Tracing view using Altair Hyperworks: crash dummy motion during pure vertical footplate displacement for four initial positions at two different loading conditions (from [6]).

Experimental and simulation results were presented on the three loading conditions of increasing severity of explosive loads (db1, db2. db3) but only for Position A (See Figure 14) as this position was used to validate the model

The results of the validation of the model for Position A, at loads db1, db2 and db3 from left to right, are presented in Figure 15. Approximate experimental peak forces are marked in red and approximate simulated peak forces are marked in green. The db1, db2 and db3 loads correspond to approximate lower tibia axial forces of about 3.5kN, 7kN and 10kN respectively. The corresponding motion diagrams are shown below the force diagrams

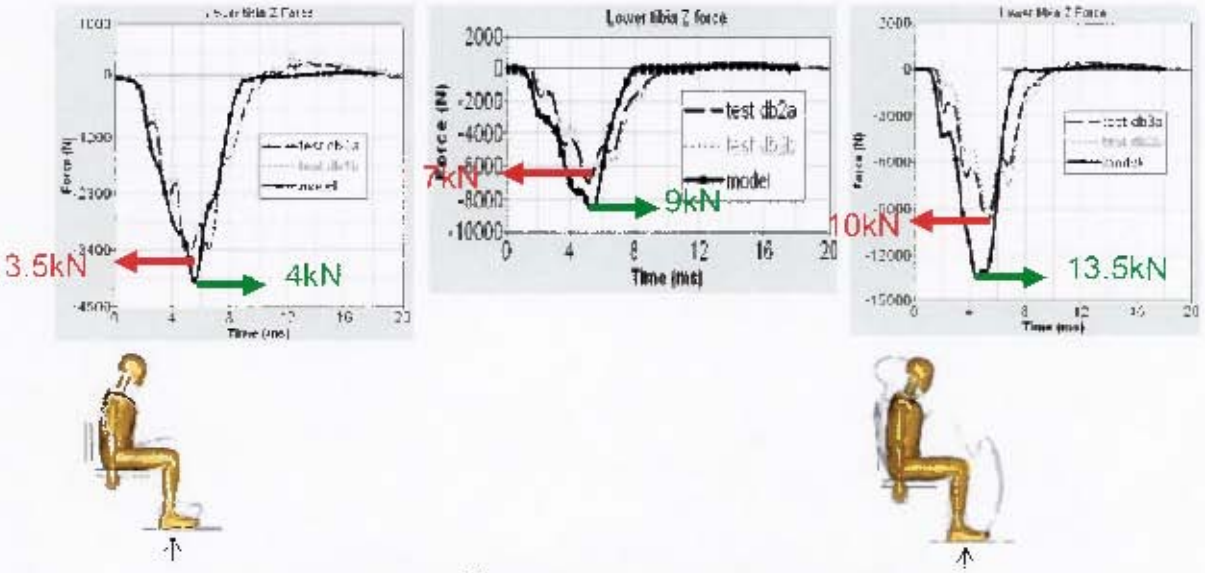

Figure 15: TROSS™ and simulated results for three loading conditions with the limb in Position A (Pictures extracted from [6]).

The simulated db3 results for axial force through the lower tibia for Positions A, B, C and D (shown from left to right) are presented in Figure 16.

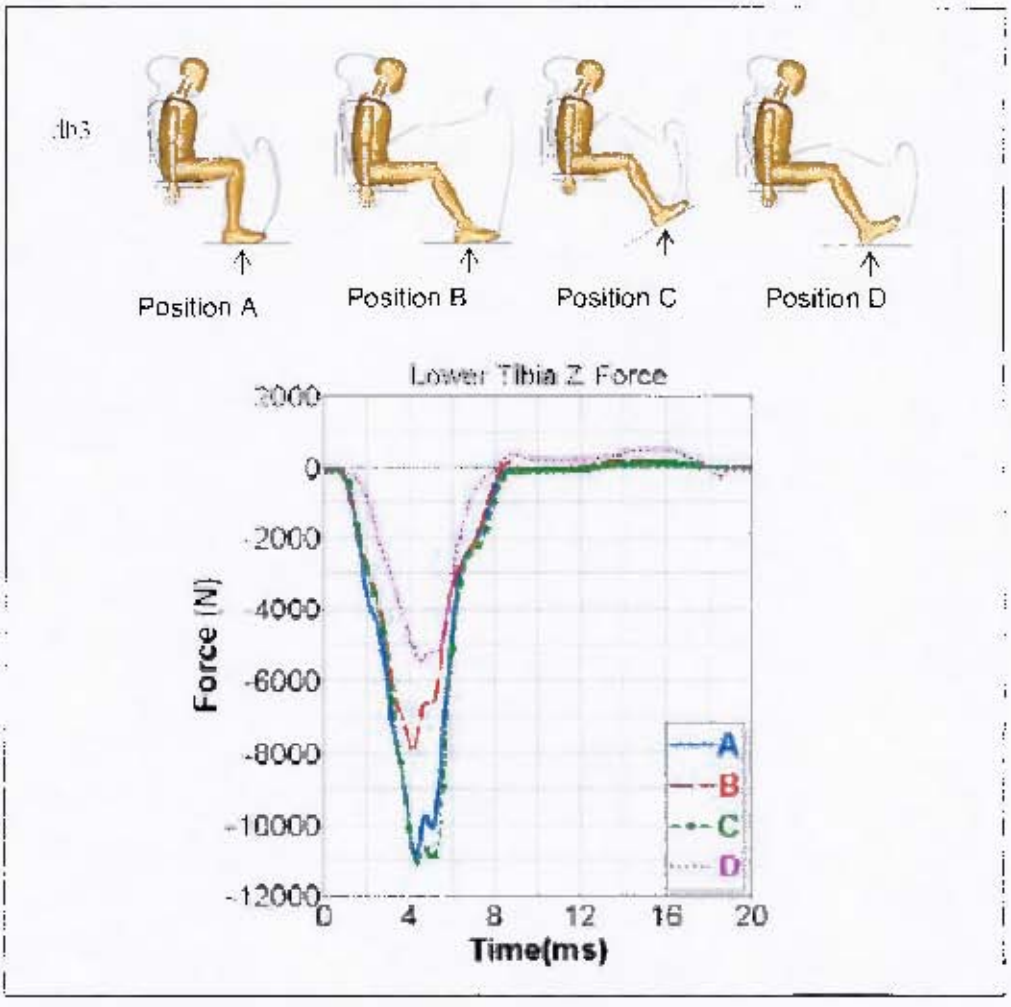

Figure 16: Loading condition db3 results (from [6]).

It must be noted that a higher peak axial force does not necessarily mean a higher injury risk as the injury mechanisms may be different when the foot is in different positions (i.e. The force may not be purely axial).

In terms of injury criteria, the Yoganandan et al. [18] axial tibia load injury model is accepted by the NATO working group. This is a maximum peak force of 5 4kN, at an age of 45 years and corresponds to a 10% risk of AIS 2+ injuries on lower leg. However, this may not be valid for positions other than Position A where the loading is not purely axial and loading mechanisms may vary due to the initial leg position.

The paper concluded that Madymo showed very good correlation to the experimental data and that the approach was suitable for future use in injury assessment The parameter study showed that the occupant positioning had a considerable influence on the lower leg loading during a mine strike

2.3.2 Wearing a boot

The effect of wearing a boot on the axial tibia force recorded by the Hybrid III ATD has been found to be significant in a number of studies.

Manseau and Keown [30] presented results that show the axial tibia force decreases from 17.4kN, when a boot is not used, to 13.3kN when a boot used. This is about a 24% decrease in force. The same trend was reported by Geurts et al. [31] where a 40% reduction in axial tibia force was found in experimental results and a 15% reduction in simulated results with the use of a boot. Similarly, Bir et al. [32] presented results of tests conducted with the TROSS™ (See Table 4). The conditions 1, 2 and 3 are similar to the loading conditions *db1*, *db2* and *db3* in [6], where the loading increases from 1 to 3. It was found that wearing a boot decreased the overall loading by about 30 to 40%.

Table 4: Results from testing conducted using TROSS™ system and Hybrid III surrogate (from [32]).

Hybrid III	Plate displacement (mm)	Peak plate velocity (m/s)	Tibia Force - Z (N)
Condition 1 no boot	12.3	2.0	5970
Condition 1 boot	12.6	2.0	3709
Condition 2 no boot	21.8	3.4	10740
Condition 2 boot	20.5	3.4	7000
Condition 3 boot	27.1	4.5	9984

2.3.3 Joint stiffness

The concept of joint stiffness can prove problematic to define as the physical definition of the term appears to differ from the understanding of the term in the medical field. This issue was explored in [33]. In the medical or biomechanics field joint stiffness describes the ability of muscles and joints to resist motion, whereas in physics the term is used to characterise properties of deformable bodies under an influence of external forces. Without the external forces the bodies should maintain a constant shape. However, muscles and joints cannot be considered bodies in this context, but rather they act as links between bodies or conglomerates of bodies [33]. The solution that was presented in [33] was that studies that make use of the term should clearly specify what the term describes.

When the joint stiffness is set for a mechanical lower limb, the term refers to a torque setting that is applied to the joints. This setting is specified for the Hybrid III ATD and the surrogate leg, but the manner in which it is set is fairly subjective. Various studies that have been conducted may aid in setting the stiffness of the surrogate limbs so they are more representative of the human lower limb. The results of studies of joint stiffness are presented here.

Joint stiffness is responsible for maintaining joint stability. The knee joint is stiffer than the ankle joint and the stiffness ratio between the two joints affects the internal leg stability [34] [35]. Muscle activity and the load against which the muscles are acting affects joint stiffness [36] [37] [38], but tendons, ligaments, skin and muscles affect the joint stiffness even when they are merely passive [39] [40] [41] [42].

In [20] it was stated that fracture initiated at the distal tibia more frequently with the addition of Achilles tension and Hardin et al. [43] supported this theory that muscle activation level could exacerbate axial loading injuries. Joint stiffness is also related to the position of a particular joint [44] [45] [46]. Another factor that can influence lower extremity joint stiffness is carrying a load such as a backpack. Holt et al. [47] conducted a study that showed that if the backpack load increased, the lower limb joint stiffness increased. In addition, as the walking speed increased so did the joint stiffness [47]. Yet another factor that affects joint stiffness is age [48], elderly men show lower joint stiffness than younger men [49].

2.4 Typical lower limb injuries within an armoured vehicle

Few publications are available detailing AV landmine incidents and even fewer describe the injuries in detail.

Stiff [50] presents a large number of AV landmine incidents that occurred during the Rhodesian War (December 1972 to January 1980), but only the number of people killed or injured are reported on. The specific injuries are not described, as is the case with most documentation concerning AV landmine incidents.

However, two papers describing injuries sustained by occupants of vehicles involved in an AV mine explosion were found.

Medin et al. [51]

This paper details an AV landmine (6.5kg TNT) incident involving a Swedish armoured personnel carrier in Bosnia in January 1996. Of the nine occupants, two needed below knee amputations, three suffered from heel bone fractures, one sustained a ligament injury of the knee and three others sustained no physical injuries. It must be noted that the occupants were standing and not sitting at the time of the incident.

Radonic et al. [52]

Radonic et al. [2004] analyses antitank mine casualties in South Croatia which occurred from 1991 to 1995. Of 464 occupants, 9% (42) were injured and 3% (12) were fatal. They conclude that although injuries from antitank mines are frequently fatal, a large percentage of occupants survived their injuries or were unharmed. Of the 42 patients that were injured, 2 sustained traumatic amputations of the lower leg with fractured calcaneus in the opposite leg, 6 calcaneus fractures of which 2 had fractured tibia and 3 patients had only tibia fracture. Thus, only 11 of the 464 occupants sustained lower limb injuries. Of the 12 patients who died 3 of them sustained lower limb injuries in addition to other injuries.

2.5 Lower limb testing and validation apparatus

In order to test, verify and calibrate lower limb HSMDs used in the validation of LPVs, lower limb testing and validation apparatus are required. Although sled testers are often used in frontal and side impact crash tests [7] [53], surrogate limbs within LPVs are exposed to vertical impacts. Thus a validation apparatus that can supply vertical loads is preferred. A drop test rig is one such apparatus and makes use of the constant acceleration provided by gravity. The peak velocity attained is independent of the mass of the object being dropped and can be calculated by

$$v = \sqrt{g.h.2}$$

which is calculated by equating gravitational potential energy (Eg = mgh [54]) with kinetic energy (Ek = ½ mv^2) [54]), where m is the mass which cancels out, g is the acceleration due to gravity and h is the height from which the object is dropped.

A problem with the drop test rig when used to calibrate HSMDs is that it is difficult to accurately define the position of the limb on impact. This is due to the movement of the limb both when it is lifted and when it is dropped.

Alternative calibration and validation systems are the German TROSS™ and the LLTS. The rest of this chapter will describe the TROSS™, on which the concept of the LLTS was based, and the original LLTS documentation. This documentation was provided by the manufacturer of the original LLTS and covers the concept, design and initial characterisation that was performed by the manufacturer.

2.5.1 Test Rig for Occupant Safety Systems (TROSS)™

The Test Rig for Occupant Safety Systems (TROSS™) was developed to load a human surrogate with a force (approximately 3 to 10kN) comparable to a real mine (2 to 10kg TNT) detonation under a light military vehicle. It was developed by IABG (Lichtenau, Germany) in cooperation with WTD 91 (Meppen, Germany) [6].

This test fixture consists of a membrane bottom plate with a footplate mounted on top of it. The seat is attached to a structure surrounding the plate which is uncoupled from the floor so that seat motion does not affect lower limb loading. The footplate is loaded by small explosive charges under the bottom plate [32]. Figure 17 shows the TROSS™ from the outside and Figure 18 shows the inside of the TROSS™ with a Hybrid III ATD and instrumentation.

Figure 17: The outside of the TROSS™ (from [32]).

Figure 18: The inside of the TROSS™ with a Hybrid III ATD and instrumentation (from [6]).

Figure 19 provides an indication of typical lower tibia peak forces and peak force durations that can be applied using the TROSS™ (*db1* represents the lowest loading condition and *db3* represents the highest loading condition as presented in [6]). Peak forces of up to approximately 10kN can be generated with typical durations of around 9ms.

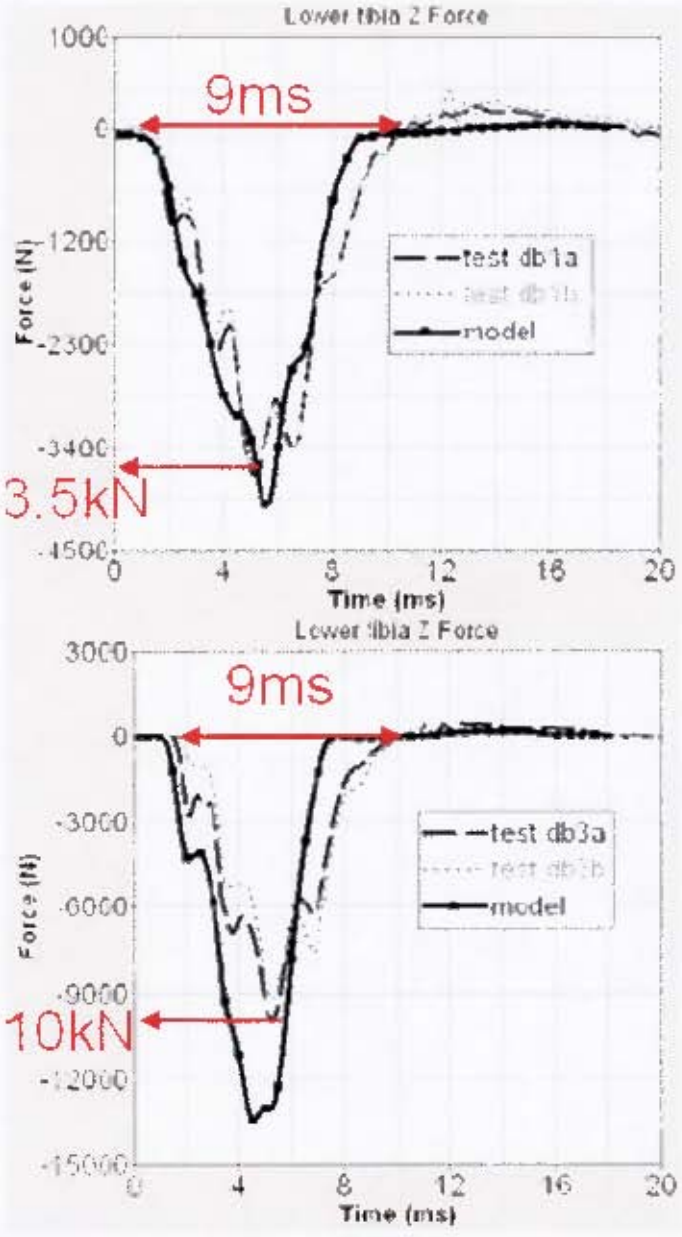

Figure 19: Typical lower tibia peak force and duration results obtained using the TROSS™ (figures extracted from [6]).

2.5.2 Original lower limb testing system (LLTS)

The aim of the LLTS is to load a HSMD with a realistic and repeatable peak force and time duration to allow for different configurations and HSMDs to be compared. This portion of the literature study was performed by reviewing the documentation on the LLTS that was provided by the manufacturer [55] [56] [57]. The essential aspects necessary to understand the current and intended functioning of the LLTS are outlined in this section.

As described in [55], the basic requirement was for a system that could:

- Load a HSMD with a realistic peak force and time duration to allow for different configurations and HSMDs to be compared
- Apply a signal to the Hybrid III ATD and other human surrogates to allow for their validation.
- Supply a repeatable signal to the foot of the instrument and to identify trends or effects by changing variables

In terms of performance, it is specified in [55] that the LLTS will subject a lower limb surrogate to loads that it could expect to experience in the field and allow provision for the load to be increased until the damage threshold of the Hybrid III is reached. It is explicitly stated in [55] that the loading will be defined as the response of the applicator and not the measuring instrument.[9]

2.5.2.1 Background

In [55] the desired input signal range is defined in terms of the measuring instrument as follows:

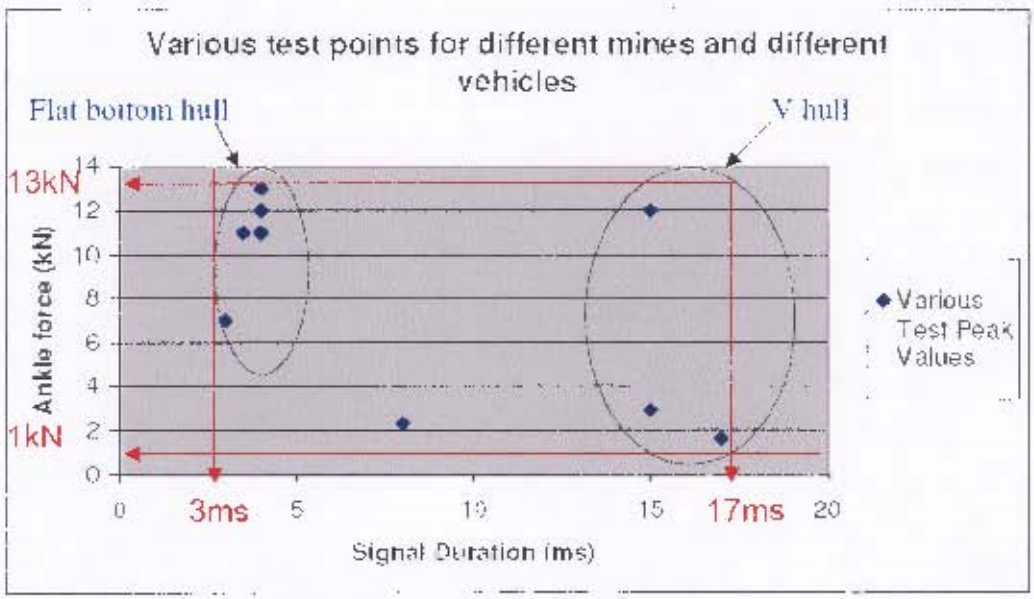

Figure 20: Range of data collected for different mines and different vehicles by the manufacturer (adapted from [55]).

From Figure 20 it can be seen that the measured ankle force ranges from about 1 to 13kN and the signal duration is about 3 to 17ms.
A peak velocity change of 4.5m/s is the required velocity to be achieved [55], based on this value being selected as 1.5 times the Hirsh injury line [20]

[9] This is significant as the response of the applicator is inextricably linked to the properties of the measuring instrument and thus a method of isolating the input force to the measuring instrument should be investigated.

2.5.2.2 Simulation results

A four-degrees-of-freedom Matlab™ model was built to simulate results (See Figure 21) and the following observations were made [55]:

- The force response at the ankle or load cell appears to be driven mostly by the stiffness of the lower leg.

- The item that influences the design the second most is the foot stiffness. This comprises of the stiffness anywhere from the ankle down to and including the sole of the boot

- High force long duration signals are problematic to achieve. It is thus suggested in [55] to use a stiffer boot to obtain high force long duration events. However, this is problematic as the surrogate limb is the measurement apparatus under investigation and it would not be appropriate to modify the apparatus under investigation in order to manipulate the force input to it.

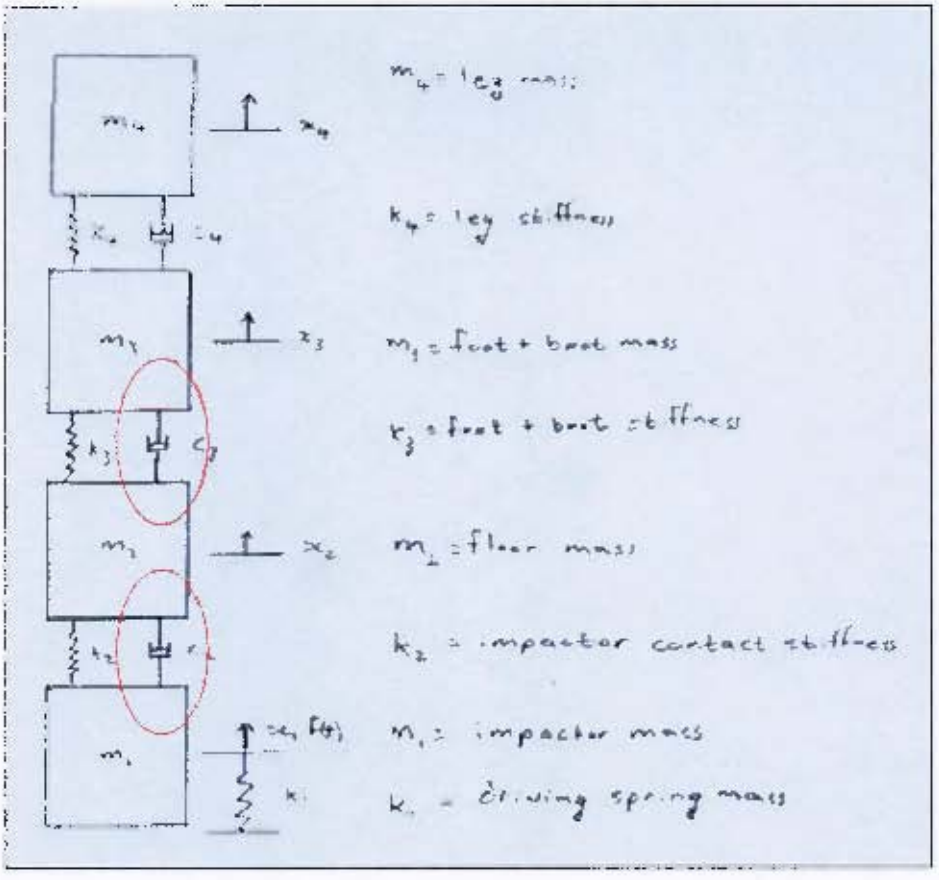

Figure 21: 4 degree of freedom system as illustrated in [55].

The following conclusion was drawn from the simulation results [55]:

- The LLTS will not be able to meet the high force, long duration signals that were included into the original specification.

2.5.2.3 Method of operation of the LLTS

The following instructions are provided for operating the LLTS (See Figure 22):

- Adjust seat height horizontally and vertically to achieve the desired seating position.
- Connect spinnaker quick release.
- Set offset distance[17] (to control the **duration** of the peak velocity of top plate or peak force of the leg)
- Close the front lower access panel.
- Use the jack with the load cell display to apply required preload to the spring (to control the **peak velocity** of the top plate/ **peak force** of the leg).
- Pull quick release rope and trigger DAQ.

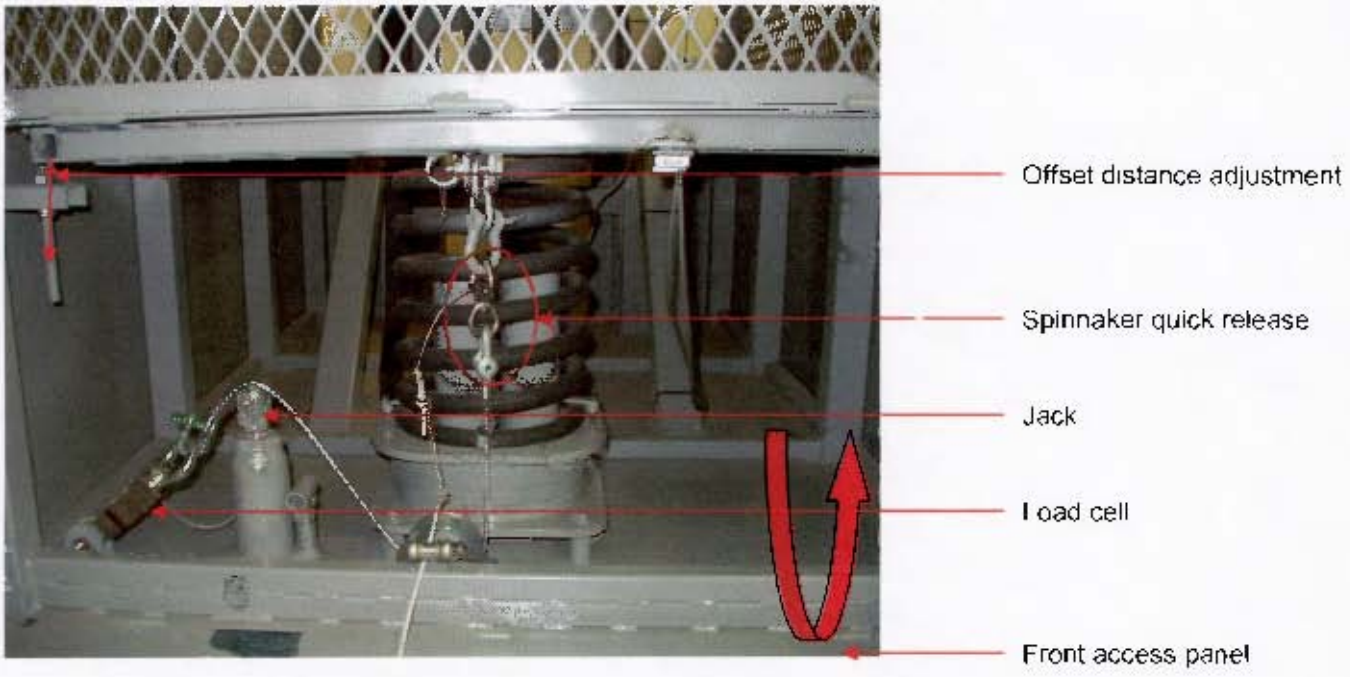

Figure 22: The elements involved in the operation of the LLTS.

[17] Distance by which the top plate is lowered from its resting position.

2.5.2.4 Summary of results and data analysis

One test at each test domain location was conducted by the manufacturer. The test domain is defined in Table 5 and covers 3 different offset/travel distances at 5 different spring preloads. A further 3 tests were conducted to examine the repeatability of the system (See Table 6).

Table 5: The test domain covered by the manufacturer to characterise the LLTS (from [57]).

Influence Factor		Travel distance	Travel distance	Travel distance
	Value	10 mm	30 mm	50 mm
Preload	400 kg	Test 1	Test 6	Test 11
Preload	500 kg	Test 2	Test 7	Test 12
Preload	600 kg	Test 3	Test 8	Test 13
Preload	700 kg	Test 4	Test 9	Test 14
Preload	800 kg	Test 5	Test 10	Test 15

Table 6: Tests conducted to assess the repeatability of the LLTS (from [57]).

Test	Travel distance	Preload
Test 16	30 mm	600 kg
Test 17	30 mm	600 kg
Test 18	30 mm	600 kg

A 1000g accelerometer was fitted to the top plate near the leg. This data was passed through a filter box and filtered at 300Hz. The results were then integrated to obtain velocity results. The leg has a lower tibia load cell with which force results were obtained. The durations of the peak velocities and forces were taken from the zero intersection points of the peak velocity or force axes on either side of the peak (See Figure 23).

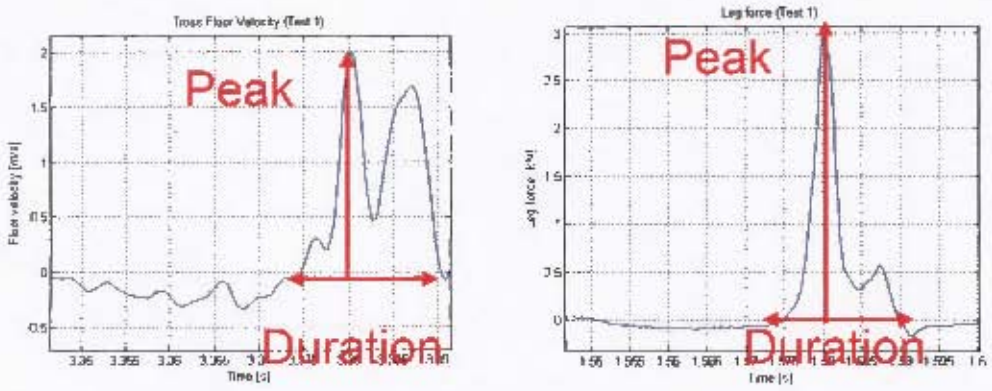

Figure 23: Graphs showing how the peak velocity (right) and peak force (left) and the respective durations are obtained (adapted from [57]).

The trends in the peak velocity and peak velocity duration of the top plate and the trends in the peak force and peak force duration of the surrogate leg are shown in Figure 24 to Figure 27.

The following trends were observed[1]:

- The **peak top plate velocity** and the **peak leg force** increase as the spring preload is increased, as intuitively expected (See Figure 24 and Figure 26).
- The **peak top plate velocity** shows no obvious trend with regards to altering the offset (travel) distance (See Figure 24).
- However, the **peak leg force** decreases as the offset distance increases (See Figure 26). This trend is curious as one would expect the top plate velocity to reflect a similar trend to that observed in the surrogate leg (which rests on the top plate)
- The **peak top plate velocity duration** decreases as spring preload increases and increases very definitely as the offset distance increases (See Figure 25)
- The **peak leg force duration**, however, shows no obvious trends (See Figure 27). Again this trend is curious as it does not correspond to the trend observed in the top plate velocity duration.

Note: Top plate peak velocity was not recorded in Test 7 as the accelerometer came loose during testing

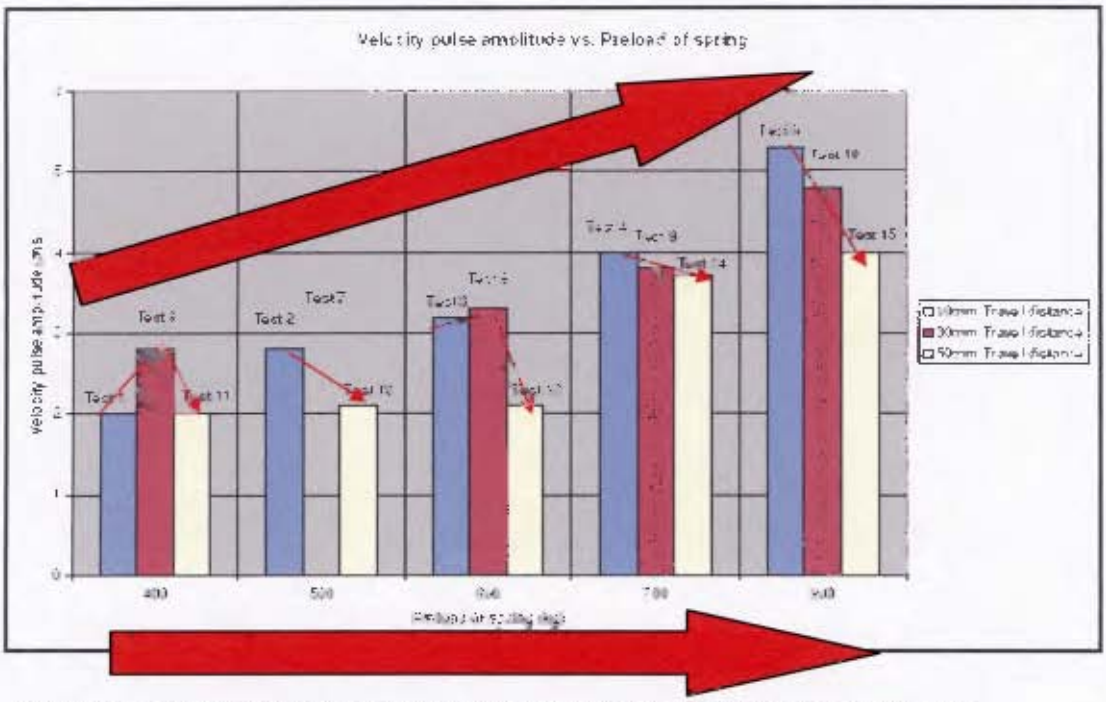

Figure 24: Top plate peak velocity showing trends in increasing preload of the spring and adjusting the offset (travel) distance (adapted from [57]).

Figure 25: Top plate peak velocity duration showing trends in increasing preload of the spring and adjusting the offset (travel) distance (adapted from [57]).

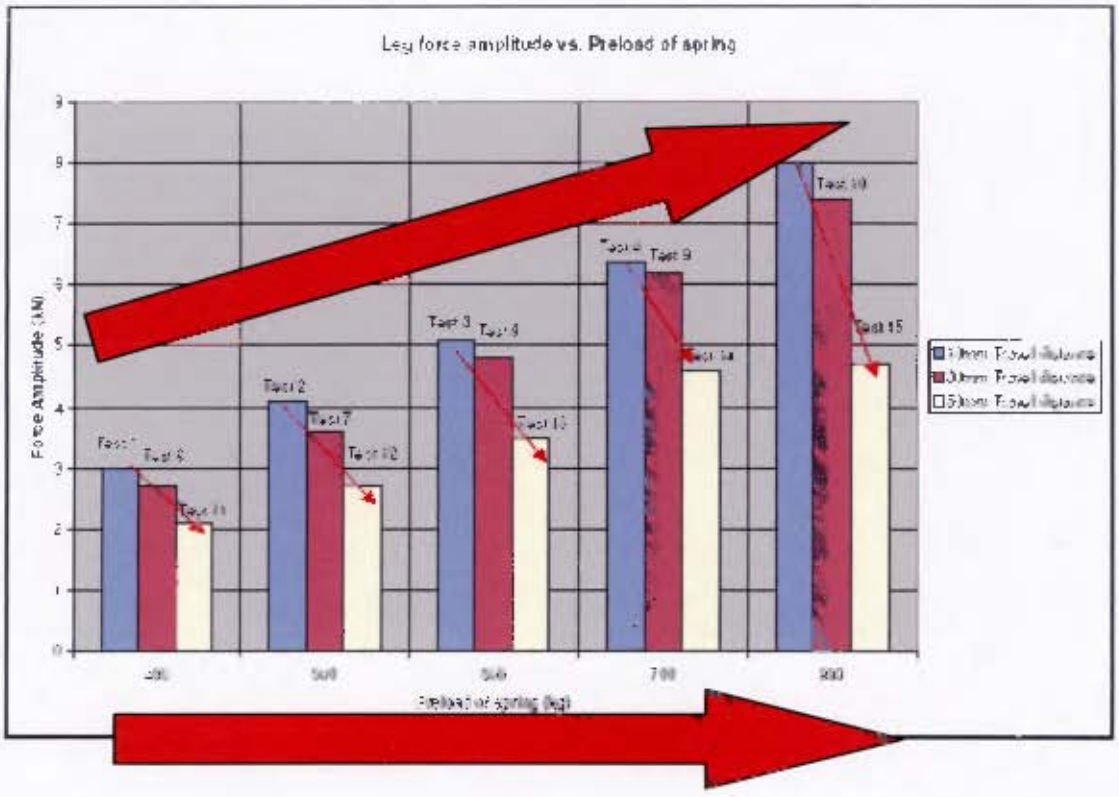

Figure 26: Surrogate leg peak force showing trends in increasing preload of the spring and adjusting the offset (travel) distance (adapted from [57]).

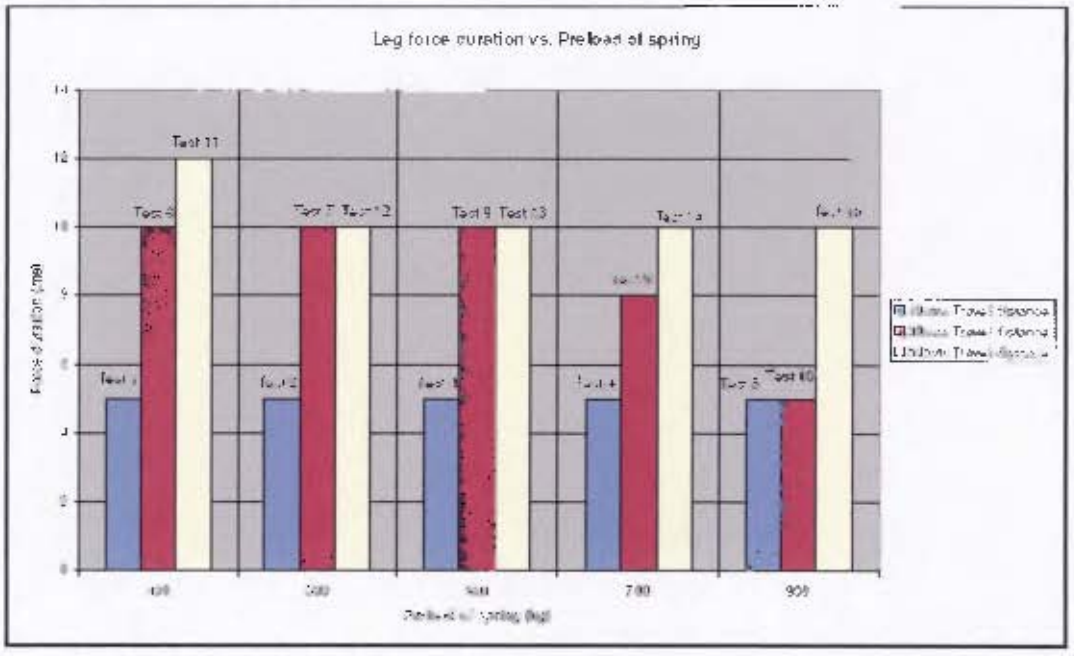

Figure 27: Surrogate leg peak velocity duration showing trends in increasing preload of the spring and adjusting the offset (travel) distance (from [57]).

In terms of repeatability, the results of Tests 16 to 18 which reflect a spring preload of 600kg at an offset distance of 30mm are shown in Figure 28 and Figure 29.

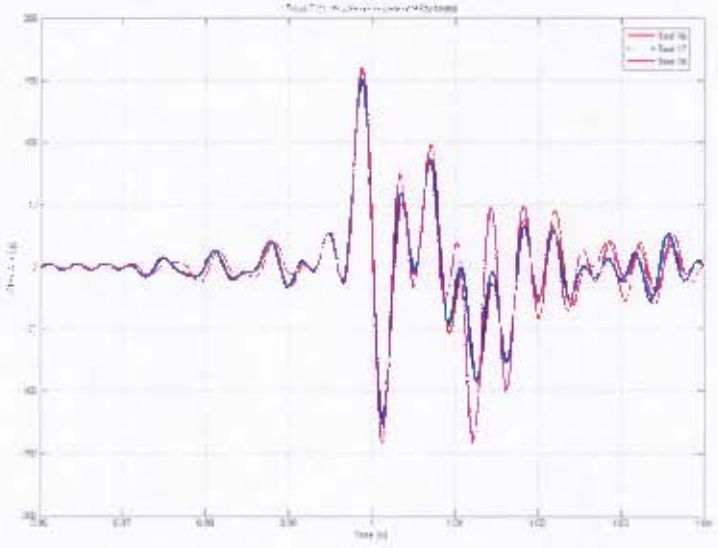

Figure 28: Top plate acceleration [g] plotted against time [s] (from [57]).

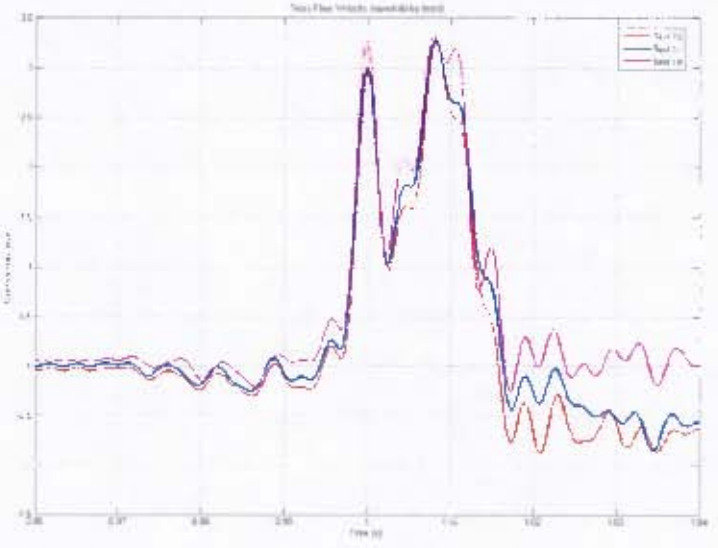

Figure 29: Top plate velocity [m/s] plotted against time [s] (from [57]).

It is interesting to note the variation in top plate velocity duration. In Figure 29 the velocity duration ranges from approximately 0.02 to 0.028 seconds. In Test 8 shown in Figure 25 the velocity duration is 0.015 seconds at the same offset and spring load. In addition to this, in Figure 25 the velocity duration is 0.025 seconds at the 50mm offset at the same preload (which falls into the range displayed in Figure 29 for the 30mm offset). This shows that the velocity duration (as measured between the zero time axis intersection points on either side of the peak velocity) may not be a reliable parameter with which the system can be characterised.

2.6 Typical vehicle validation tests with anti-vehicle landmines

Two distinct accelerations occur in the vehicle structure and occupant bodies during a blast event. Firstly, very high acceleration levels with only small displacements, and secondly a more global response resulting from a lower level of acceleration with larger displacements (e.g. In car crash incidents). The effect of the very high accelerations on the human body causes injuries due to the passage of the shock front through the body, at a rate greater than that at which the body can absorb the energy [58].

When high accelerations are applied to the vehicle floor they may result in lower limb injuries. Thus, to simulate the acceleration with which the vehicle floor impacts the foot (as is the aim of the LLTS), the values of typical vehicle floor accelerations will be investigated. Typical surrogate leg measurements recorded during LPV tests will provide an indication of the forces that should be applied by the LLTS and thus the results of some of these tests will be presented in this section.

2.6.1 Typical floor accelerations

Very little literature seems to be available regarding the acceleration of the floor of a vehicle during an AV landmine blast. Wang et al. [59] stated that in a medium-sized armoured vehicle localised floor average acceleration and peak velocity change may typically exceed 100g and 12m/s respectively during an AV landmine blast. Two other papers were found that describe the measurement of the acceleration of steel plates subjected to explosive blast loading. These papers are outlined below.

Boyd [58]

The aim of this study was a first step in quantifying the acceleration loads on the lower limbs and/or torso of personnel on a deck subjected to blast loading from below. It is hoped that eventually the severity of injury will be possible to predict from the acceleration of an explosively loaded deck plate.

Piezoelectric 50000g accelerometers were mounted on a 1m square, 5mm thick mild steel plate free to move under load (The plates were bolted to a heavy steel frame with 24 high tensile bolts, tensioned to 11.06Nm). The accelerometers were mounted diagonally opposite each other at 100mm and 200mm (A1 and A2 respectively) from the centre of the plate. A 250g Pentolite sphere was centrally detonated at a standoff distance from the plate of 250mm to 500mm. Table 7 shows the typical accelerations recorded.

The peak accelerations measured vary from around 13000g to 41000g with durations of around 0.0002s.

These accelerations are significantly greater than the maximum accelerations of around 300g with durations of around 0.005s recorded using the LLTS. It should thus be kept in mind that the modified LLTS should produce higher floor accelerations than the original system.

Table 7: Measured accelerations of a steel plate presented in (from [58]).

Standoff distance from plate (mm)	A1 peak acceleration (g)	A2 peak acceleration (g)
500	14657	14748
500	13185	14239
400	17529	15052
250	40969	30049

Kaufman et al. [61]

This paper investigated the shock reduction power of different materials in plate targets. As the human body sustains injury when momentum changes rapidly, protection measures must aim to reduce the momentum transfer into the occupant compartment.

60000g piezoresistive accelerometers were mounted on the centre of the test plate. 700mm square steel plates of 8mm thickness were fixed between two rectangular steel frames with a circular opening of 500mm. The frame is fixed to a construction and loaded with 4 concrete cuboids of 500kg each. A 1kg plastit load (explosive gelatine) placed 500mm under the plate results in an acceleration of around 800000m/s^2 (81633g) and a velocity of around 100m/s. The peak acceleration duration is around 0.0002s.

Again, these accelerations are significantly greater than the maximum accelerations of around 300g with durations of around 0.005s recorded using the LLTS. The modified LLTS should aim to produce greater floor accelerations than the original system.

2.6.2 Typical surrogate limb measurements

The Hybrid III ATD and surrogate leg are instrumented with load cells in the lower tibia. A number of vehicle certification tests have been conducted by the CSIR, LS using these surrogates. In order to investigate the typical forces recorded by surrogate limbs in a vehicle subjected to an AV mine explosion, the data that was collected was processed to obtain both peak force and peak force duration results[13] (See document on the disk accompanying this thesis titled *Matlab™ Script Files* for the Matlab™ code). These results were then plotted to obtain a range of typical values that we would expect to find in the field and would thus want to simulate using the LLTS. One can see in Figure 30 that peak force varies from 158.4N to 43372.4N and the peak force duration varies from 0.002 seconds to 0.0704 seconds.

[13] Vehicle tests may include wheel shots, where the test charge is positioned beneath a wheel of a vehicle, or hull shots, where the test charge is positioned under the hull at a positioned which is thought to produce the most severe loading on the ATD occupant.

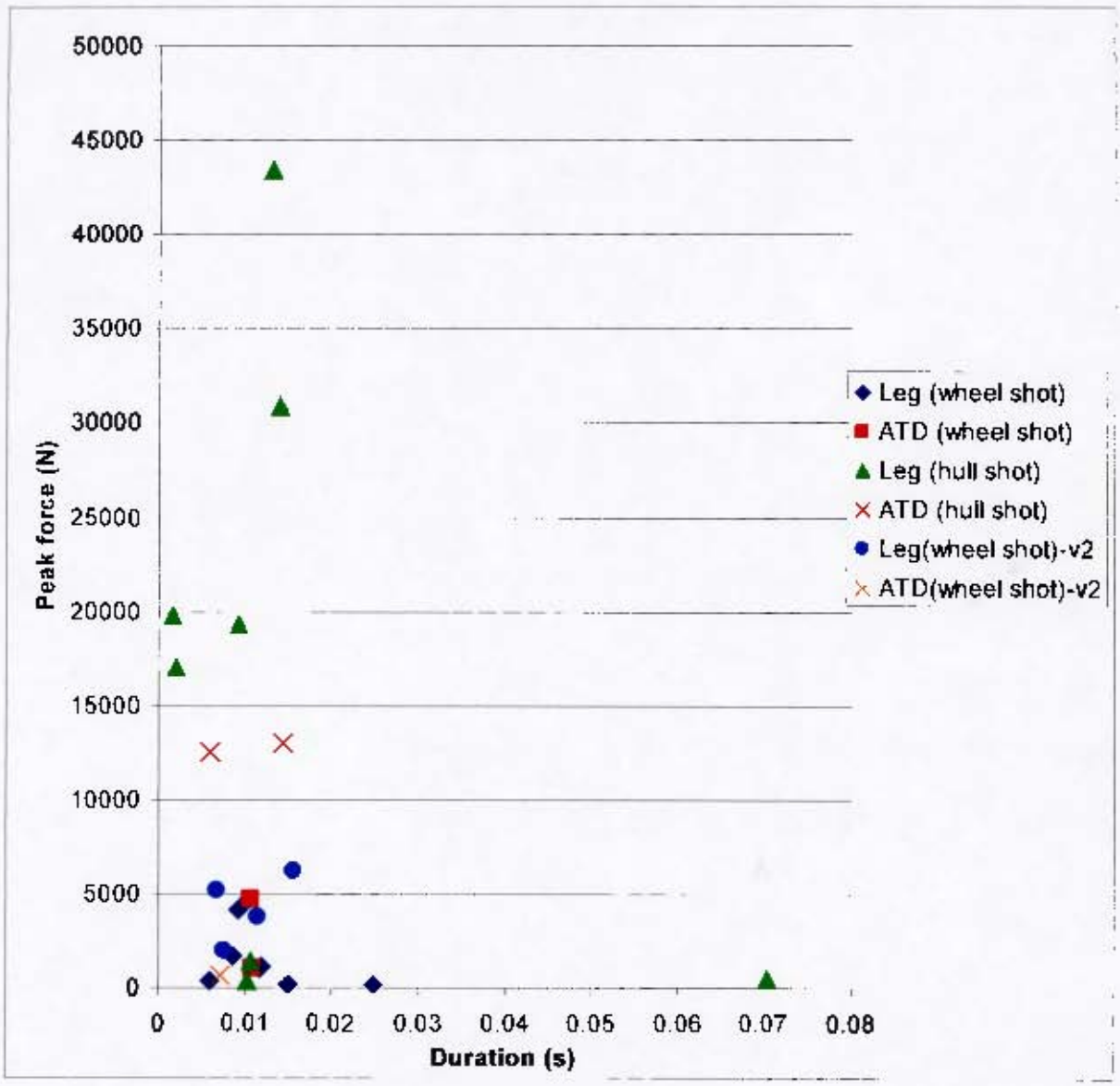

Figure 30: Typical peak force and peak force duration results as seen by the lower tibia load cell of the ATDs and surrogate legs during vehicle tests.

2.7 Clarification of the aim of the LLTS

The aim of the LLTS is to subject a lower limb surrogate to loads that it could expect to experience in the field. Based on vehicle tests conducted by the CSIR (1 in Figure 31) and the manufacturer (2 in Figure 31), a surrogate limb can typically experience forces ranging from about 0.15kN to at least 15kN in the field. The peak force durations range from about 2 to 20ms. The data presented using the TROSS™ reaches a peak force of 10kN with a duration of 9ms which falls into this range.

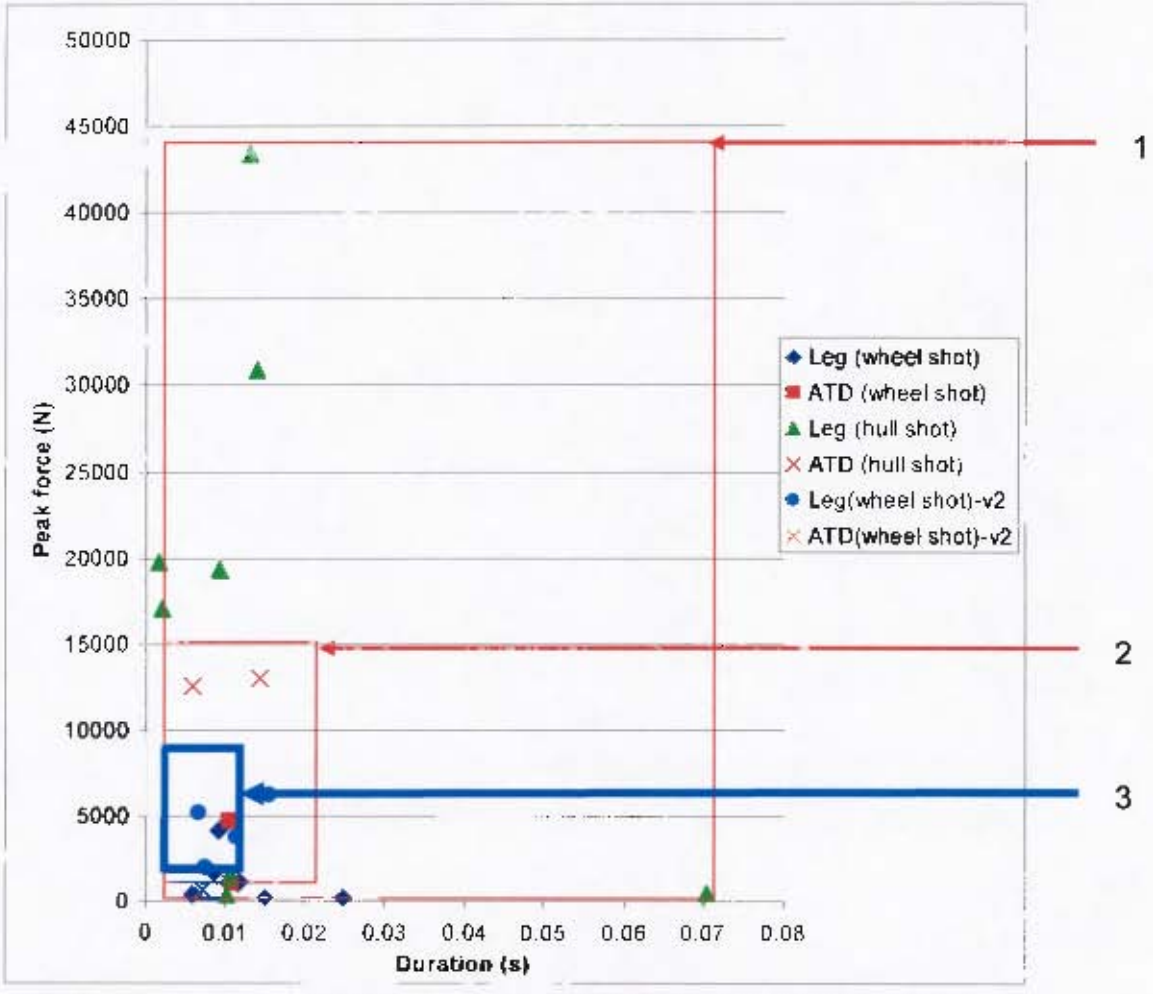

Figure 31: Peak lower tibia forces and durations typically experienced by a surrogate limb or ATD in an AV landmine incident the field (1 and 2) and applied by the LLTS (3).

The aim of the LLTS is thus to supply the surrogate limb with a peak force of at least 10kN, but preferably higher (15kN), and a peak force duration of between 2 and 20ms.

3 MODIFICATION AND CHARACTERISATION OF THE LLTS

The original LLTS was inherited from an external company, thus the system required characterisation in order to determine what modifications needed to be made. This was done via a series of experiments to evaluate the range of forces that could be generated by the original LLTS. In addition, simulations were conducted by Victor Balden and Rayeesa Ahmed in order to better understand the operation of the original system, to identify possible shortcomings and to investigate proposed modifications. Based on the experimental results and the simulations, modifications were made to the original LLTS and it was renamed the LLI. The LLI was then characterised to determine whether it was an improvement over the original system and whether it could meet its specifications.

3.1 Characterisation of the original LLTS

Before the characterisation testing was conducted, the spring constant needed to be validated[12], repairs needed to be made to the LLTS and the instrumentation and data acquisition systems needed to be set up. Thereafter the testing was conducted and the results were recorded and analysed.

3.1.1 Spring constant validation

As the spring is central to the performance of the LLTS, it was decided to verify the spring constant that was supplied by the manufacturer. In order to perform this task a downward force was applied to the bottom (strike) plate from its resting position to compress the spring. The displacement of the plate was measured at discrete levels and the corresponding loads were read off the load cell display. The setup that was used for the validation of the spring constant is shown in Figure 32.

Figure 32: Set up used for validation of LLTS spring constant.

The procedure was repeated three times so that an average spring constant value could be obtained. The results of the tests are shown in Table 8.

[12] Rayeesa Ahmed assisted the author of this dissertation in validation of the spring constant using the original LLTS.

Table 8: Recorded displacement and force values.

Test 1		Test 2		Test 3	
Displacement (m)	Force (N)	Displacement (m)	Force (N)	Displacement (m)	Force (N)
0	39.24	0	98.1	0	88.29
0.017	804.42	0.012	863.28	0.013	922.14
0.028	1628.46	0.030	1922.76	0.030	1991.43
0.049	2707.56	0.047	2913.57	0.049	2962.62
0.072	3757.23	0.066	3874.95	0.066	3904.38
0.088	4738.23	0.086	4914.81	0.088	4924.62
0.106	5591.70	0.106	5895.61	0.106	6052.77
0.125	6680.61	0.128	7023.96	0.126	7161.30
0.143	7769.52	0.135	7848.00	0.139	8191.35

Due to the initial compression of the spring being unknown, a direct comparison of force and displacement values could not be included when determining the spring constant (k). For this reason the first values recorded (at zero displacement) were omitted in the calculations as the change in applied spring force ($\Delta F = F_2 - F_1$) is related to the displacement (or change in distance: $\Delta x = x_2 - x_1$) by k. The equation used in the calculations was therefore:

$$\Delta F = k\Delta x \text{ or } (F_2 - F_1) = k(x_2 - x_1).$$

The last values in the table were also omitted as it was observed that at loads above 7.5kN, the bottom plate starts to visibly bend and distort and the jack begins to press up against it. The displacement values were measured at the front of the bottom plate (See Figure 32). However, the strike plate does not move only in a vertical direction, but rotates about a point through an angle. The amount that the plate displaced is therefore more than the amount that the spring compresses.

The arm length (l) = 1580mm and the distance from the pivot point to where spring acts (d) = 1356mm. The bottom plate rotates through an angle θ from its initial position.
Thus, s_1 is the measured displacement value and
s_2 is the amount that the spring is compressed.

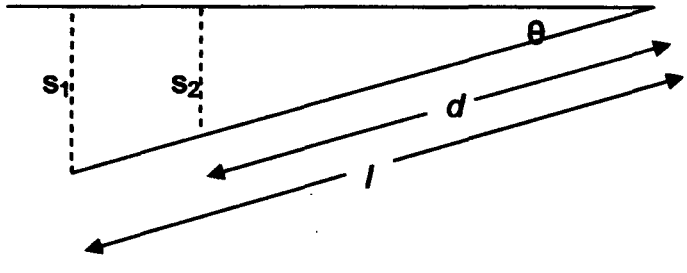

θ was calculated using the following equation:

$$\frac{s_1}{l} = \sin\theta$$

s_2 was then calculated by substituting θ into:

$$\frac{s_2}{d} = \sin\theta$$

The adjusted displacement values were calculated using the above equations and are shown in Table 9.

Table 9: Adjusted displacement values.

Test 1		Test 2		Test 3	
s_1 (m)	s_2 (m)	s_1 (m)	s_2 (m)	s_1 (m)	s_2 (m)
0.017	0.015	0.012	0.010	0.013	0.011
0.028	0.024	0.030	0.026	0.030	0.026
0.049	0.042	0.047	0.040	0.049	0.042
0.072	0.062	0.066	0.057	0.066	0.057
0.088	0.076	0.086	0.074	0.088	0.076
0.106	0.091	0.106	0.091	0.106	0.091
0.125	0.107	0.128	0.110	0.126	0.108

Two methods were used to calculate the spring constant which give slightly different results.

Method 1:

In the first method, F_1 and x_1 were the preceding sets of values in each instance (I.e. The F_1 and x_1 measurements were not fixed at the first F and x measurements). The displacement and force values that were calculated are shown in Table 10.

Table 10: Calculated Displacement and Force Values (varying F_1 and x_1).

Test 1		Test 2		Test 3	
Δx (m)	ΔF (N)	Δx (m)	ΔF (N)	Δx (m)	ΔF (N)
0.009	824	0.016	1059	0.015	1069
0.018	1079	0.014	991	0.016	971
0.020	1050	0.017	961	0.015	942
0.014	981	0.017	1040	0.019	1020
0.015	853	0.017	981	0.015	1128
0.016	1089	0.019	1128	0.017	1109

A spring constant value was then calculated for each set of points (See Table 11).

Table 11: Calculated spring constant values.

Test 1	Test 2	Test 3
Spring constant (k) (N/mm)	Spring constant (k) (N/mm)	Spring constant (k) (N/mm)
91.6	66.2	71.3
59.9	70.8	60.7
52.5	56.5	62.8
70.1	61.2	53.7
56.9	57.7	75.2
68.1	59.4	65.2

The average k values for each test:

Test 1: k = 66.5 N/mm
Test 2: k = 62.0 N/mm
Test 3: k = 64.8 N/mm

Therefore **k = 64.4 N/mm** (method 1).

Method 2:

The second method of calculating the new values was based on fixing F_1 and x_1 (as the first sets of values after zero displacement) for all the calculations.

The results obtained using method 2 (fixed F_1 and x_1) with the adjusted displacements (to take into account the angular rotation of the bottom plate) are shown in Table 12 and Figure 33.

Table 12: Calculated displacement and force values (fixed F_1 and x_1).

Test 1		Test 2		Test 3	
Δx (m)	ΔF (N)	Δx (m)	ΔF (N)	Δx (m)	ΔF (N)
0.009	824	0.015	1059	0.015	1069
0.027	1903	0.030	2050	0.031	2040
0.047	2953	0.046	3012	0.045	2982
0.061	3934	0.064	4052	0.064	4002
0.076	4787	0.081	5033	0.080	5131
0.093	5876	0.100	6161	0.097	6239

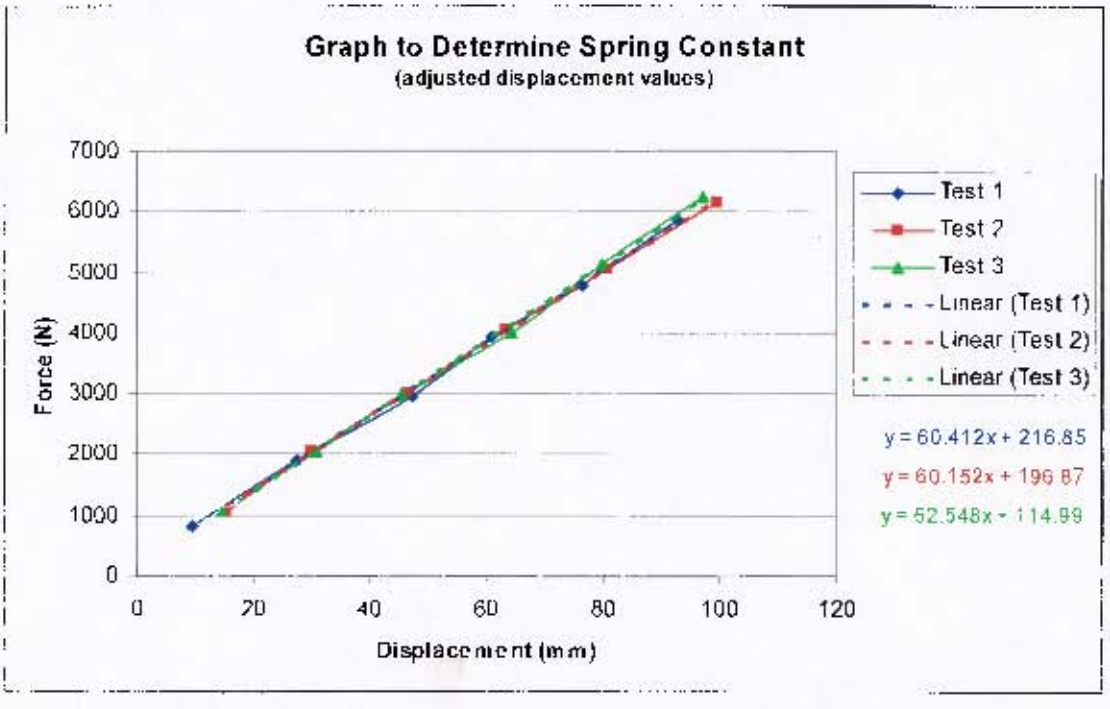

Figure 33: Graph to determine spring constant with adjusted displacement values.

The average k values for each test:

Test 1: k = 60.4 N/mm
Test 2: k = 60.2 N/mm
Test 3: k = 62.5 N/mm

Therefore k = **61.0 N/mm** (method 2).

According to the spring manufacturer, the spring constant is specified as 49.36N/mm or 49.36kN/m. The test certificate can be found in Appendix A1. There is a substantial deviation between the above results and the value specified for the spring stiffness by the manufacturer. This difference could be due to a number of reasons.

The force values were recorded by means of a load cell attached to a cable which was in turn attached to the bottom plate. The bottom plate was pulled down, compressing the spring, and the tension in the cable was the input for the force values captured (due to the positioning of the load cell in the system). Of the total input force value recorded, it is uncertain whether all the force or whether only a percentage of the force was acting to compress the spring. Force may also be dissipated in the bending of the bottom plate whilst the spring is being compressed, as is shown in the finite element model (See Appendix B).

Due to the movement of the strike plate being angular, it is also uncertain exactly how the spring reacts when the strike plate is pulled down. It is unlikely that the spring will compress completely vertically, and whether the spring shifts or slides along the strike plate to initiate compression at a different position is unknown.

Finally, the measurement of the displacement values were recorded manually and therefore human error contributes to the deviation. As the strike plate was moved down and the spring compressed, the edge of the strike plate from where the measurements were taken, moved away from the edge of the frame where the tape measure setup and aligned. These values were therefore captured across a space and subject to inaccuracy. In addition, other factors such as the straightness of the tape measure could also affect the measurements.

For these reasons, until another set of spring characterisation tests can be conducted with the above inconsistencies eliminated, the spring stiffness of 50 N/mm as specified will be used in the simulations.

Basic spring calculations:

The spring constant and other spring specifications can be used to calculate the maximum force that a spring of a certain length should be able to achieve.

The following specifications were provided by the spring manufacturer:

- Spring stiffness 49.36N/mm (49.36kN/m).
- Free length 402mm.
- Bar diameter 25mm.
- Number of coils 8.25.

Using these measurements one can determine the maximum spring preload:

- Maximum compression = 402mm (8.25 x 25mm) = 195.75mm.
- Maximum spring preload = 195.75 x 49.36 = 9662.22 N.

Thus, a longer spring may be needed to facilitate a higher preload which could supply a 10 to 15kN force to the surrogate limb.

3.1.2 Initial observations and repairs

A limited number of characterisation tests were performed by the manufacturer of the original LLTS. However, in order to determine what modifications needed to be made to the system, further characterisation tests were necessary. Before this testing could be conducted various repairs were required and are summarised in this section (See section 2.5.2.3 of this dissertation for a description of the LLTS components).

In order for characterisation tests to continue various repairs were required:

- As the cable began to fray it needed to be replaced. On purchasing a new cable it was discovered that the 5mm cable that was being used was only certified (SABS) to carry loads of up to 200kg. This is a problem as the cable needs to be loaded to a minimum of 800kg which would require a 10mm cable. As the LLTS system was designed to operate with the 5mm cable it was decided to continue to use this type of cable, but to replace it regularly as signs of ware became visible.

Figure 34: Photograph of frayed cable in position over the jack.

Figure 35: Photograph of frayed cable when removed from the jack.

- Removing the old cable and replacing it with a new cable proved problematic as the entire spring needed to be lifted Thus the cables were crimped at either end and D shackles used to enable the cable to be replaced more easily.

Figure 36: Photograph showing the labour intensive procedure necessary to replace the cable.

Figure 37: Photograph of the D-shackle mechanism implemented to make replacing the cable less labour intensive.

- The spring was not adequately secured. The latches slipped and bent and the bolts worked loose

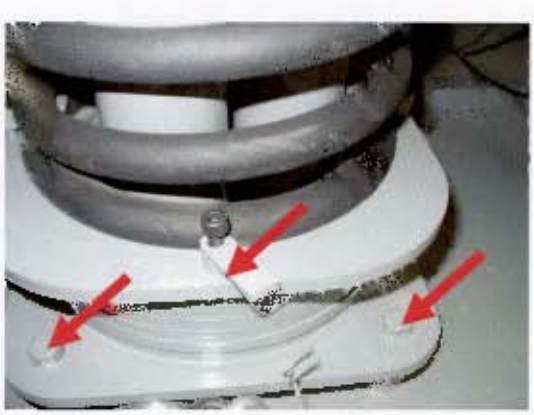

Figure 38: Photograph showing a slipped latch and bolts that are loose.

- The bolts used to set the offset distance were rusty and difficult to move and thus required lubrication.

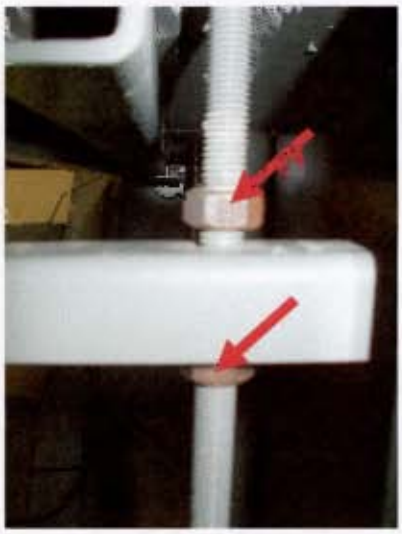

Figure 39: Photograph showing the rusty bolts that are used to set the offset distance.

- The quick release rope was often caught in the pulley mechanism. If the front panel was transparent this could be prevented.

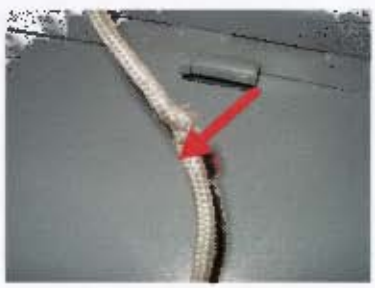

Figure 40: Photograph showing the damaged quick release rope.

- Towards the end of the characterisation tests it was discovered that the spacers were beginning to slip out of alignment and that the spring was shifting the base.

Figure 41: Photograph showing the spacers that are out of alignment.

- The seat height adjustment system was problematic as the seat system was heavy and not accurately aligned. It required much physical strength and took a fair amount of time to adjust the seat. In addition to this, the discrete levels meant that fine adjustments to the seat height were not possible.

Figure 42: Photograph showing the misalignment in the seat height adjustment system.

3.1.3 Instrumentation for initial characterisation

A surrogate leg [5] number 5 with a lower tibia load cell and a 500g accelerometer (serial number 0639-005) was used as the measurement device in the characterisation testing. 500g accelerometers were attached to the top and bottom plates of the LLTS (with serial numbers 0639-008 and 0639-013 respectively).

Figure 43: Surrogate leg number 5 with load cell and accelerometer.

Figure 44: 500g accelerometer as was fitted in the foot and on the top and bottom plates of the LLTS.

Figure 45: LLTS fitted with accelerometers.

The calibration certificates for the instrumentation can be found in Appendix A2.

3.1.4 Description of tests conducted

The characterisation testing was initially aimed at repeating the characterisation results provided by the manufacturer in [57]. However, the following factors necessitated different characterisation test procedures:

- In communications with the manufacturer it was stated that the joint torque of the surrogate leg was assumed to be 25Nm, but this was not confirmed. As our initial testing showed a difference in forces recorded at various joint torque setting, it was decided to test at joint torque settings of both 25Nm and 6Nm values.

- The manufacturer did not state the serial numbers of the specific surrogate legs (See section 2.2 of this dissertation for a description of the surrogate legs) were used in the characterisation, but in communications it was conveyed that three different legs were used. It was decided to use only one leg (leg number 5) in the characterisation of the LLTS as this would reduce the number of variables present in the process.

- The manufacturer specified spring preloads of 800kg in [58], however, it was noted that the bottom plate is pulled skew and down to the right at preloads above 750kg (due to the jack pushing up on the left hand side of the plate) which may influence the results as the bottom plate would impact the top plate at more of an angle. Thus, in the characterisation testing the spring preload was limited to 750kg.

- In an attempt to highlight the trends the test domain was later extended to include a set of samples at 200kg of spring preload and another set of samples at an offset distance of 70mm. The test domain is presented in Table 13.

- The manufacturer conducted only one test at each test domain location, except at one location where the repeatability was assessed using three samples. Although it was decided that repeatability should be assessed at as many test domain locations as possible, certain limitations in this regard were noted. It was decided to first populate as much of the test domain as possible and then determine the repeatability of the samples by conducting further tests at each test domain location. Due to the fact that problems were encountered towards the end of the LLTS which require repair and modification before safe testing could continue, not all of the test domain locations contain more than one sample.

- The test method as described by the manufacturer in the test instruction [56] was used. The seat height needed to be adjusted as the foot of the leg did not touch the top plate at certain offsets. A problem was encountered with adjusting the seat height for each top plate offset value as the seat can only be adjusted in increments or decrements of 25mm. Thus, one seat height was used for the 10mm and 30mm offsets and the seat was lowered by about 5cm for both the 50mm and 70mm offsets.

The number of samples at each test domain location is described in Table 13.

Table 13: Number of samples per test domain location.

Offset distance	Number of samples per test domain location at various spring preloads [kg] and leg joint torque settings [Nm]							
[mm]	200kg		400kg		600kg		750kg	
	6Nm	25Nm	6Nm	25Nm	6Nm	25Nm	6Nm	25Nm
10	2	2	3	3	1	1	1	1
30	2	2	1	4	1	4	1	1
50	2	1	2	1	4	3	2	1
70	1	1	2	1	2	1	2	1

The total number of samples throughout the test domain is 57.

3.1.5 Data acquisition, processing and analysis

Data acquisition:

The first four channels of the middle row of a custom designed data acquisition unit (DAQ) (serial number 03062006) were used to record the leg load cell force, bottom plate acceleration, top plate acceleration and leg acceleration respectively. The gain of the channels is 188.75 and the excitation voltage is 4.998 volts. Each of the channels was sampled at 10kHz for 2 seconds (of which 0.25 seconds is pre-trigger data). The DAQ was manually triggered when the spring was released.

Data processing and analysis:

The raw data was down loaded from the DAQ[13]. Before this data could be analysed calibration factors needed to be taken into account.

The calibration factors (k) are as follows:

- Surrogate leg 5: k = 52.6664.
- Bottom plate accelerometer: k = 62.3296.
- Top plate accelerometer: k = 62.3296.
- Surrogate leg accelerometer: k = 61.6048.

The calibration documents can be found in Appendix A2.

A program was written in Matlab™ to process the data called *data_reader.m*. All of the Matlab™ script files written for this dissertation can be found on the disk accompanying this dissertation in a document titled *Matlab™ Script Files*. In addition to applying calibration factors this code was used to group relevant test domain samples and save them in data files that are then easier to access and process.

[13] A 12 bit analogue to digital converter (ADC) spans -10V to +10V which gives 20V span in the DAQ. Thus, the number of discrete levels is 2^12 which gives a resolution of 20/(2^12) V. To make the raw data meaningful one must multiply it by k*(20/(2^12)).

The sets of test samples that were incorporated into the data (*.mat*) files can be found on the disk accompanying this dissertation in a document titled *Detailed Results*. The convention used in the results is as follows:

- Blue – top plate.
- Red – bottom plate.
- Green – foot.

The accelerometer results were further processed using the Matlab™ files *accprocbasic.m* and *accprocfiltering.m*. The surrogate leg load cell results were processed using *loadcellproc.m*.

A typical example of one of the sets of test samples in shown in Figure 46. The heading in bold gives the name of the data set denoted by a certain offset distance and spring preload. The original files included in this set are specified and graphs of the accelerations and velocities are displayed. The peak velocities and durations are listed.

data10200

DROP_290806_1028.dlp
DROP_290806_1031 dlp

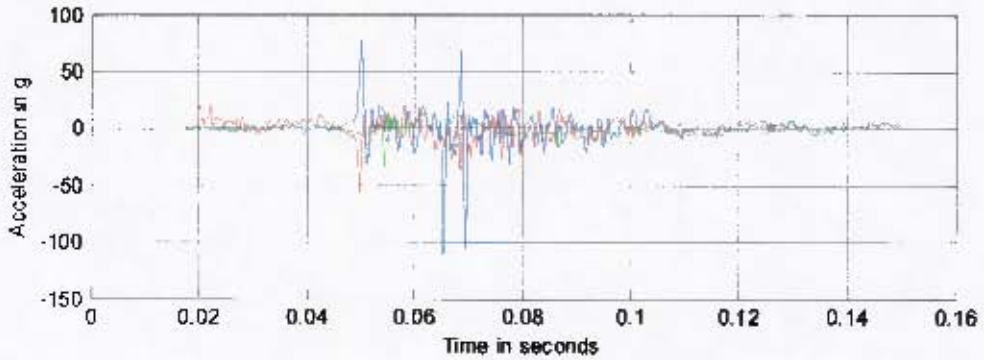

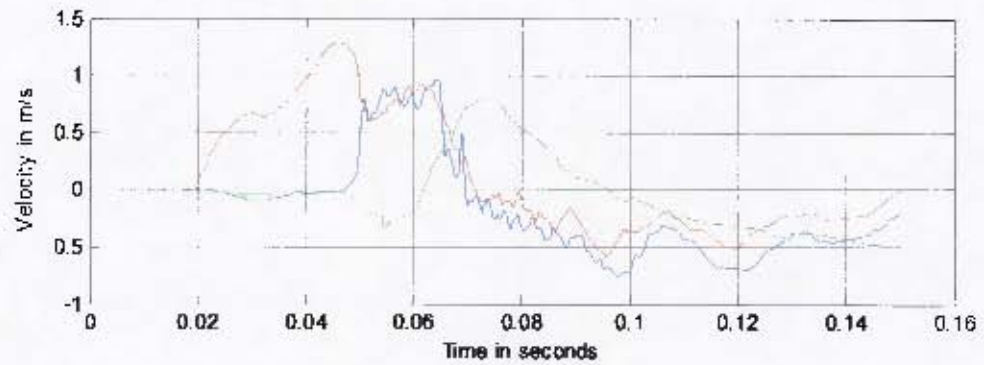

Peak top plate velocity:
0.9713
Duration :
0.0223
Peak bottom plate velocity:
1.2949
Duration :
0.0522
Peak leg velocity:
0.7994
Duration :
0.0343

Figure 46: Example of test domain sample from the accompanying *Detailed Results* document.

Integrating accelerometer signals to obtain velocity signals:

The accelerations were integrated using the above mentioned codes to provide velocity signals. There is much debate[14] as to whether this can be done or not, but as this was the method used by the manufacturer in the initial characterisation it was decided to use the same method in this characterisation. However, caution must be taken with regards to the validity of velocities obtained using this method.

The effect of offsets in initial acceleration data was magnified when integrating the acceleration data as can be seen in Figure 47.

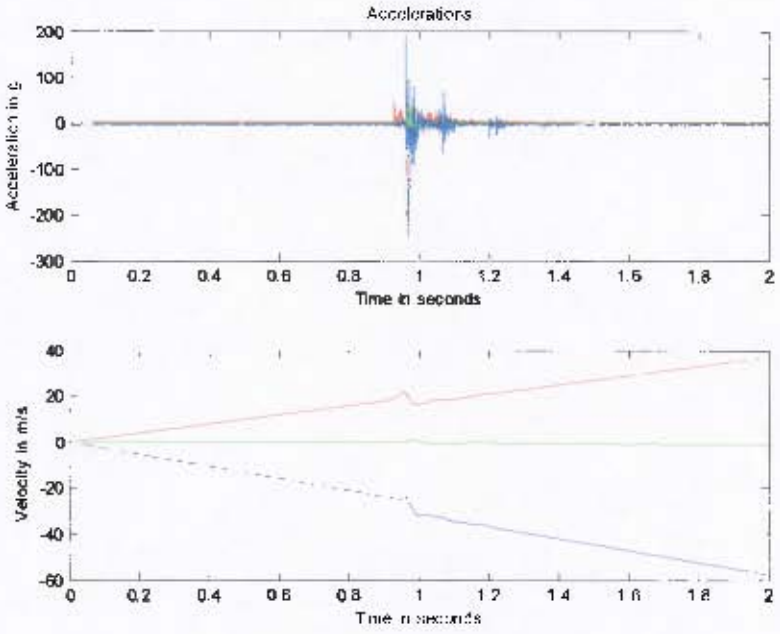

Figure 47: The effect of offsets in acceleration signals when integrating to obtain velocity signals.

This effect was reduced by subtracting the average of the first 100 acceleration samples from the entire acceleration signal. The result is shown in Figure 48.

[14] An accelerometer comes with a calibration certificate that describes a linear calibration factor. However the voltage output by the accelerometer is not only a function of the acceleration, but the velocity and displacement coefficients also play a role. If the accelerometer can be calibrated to more than a linear calibration factor (eg. Using a vibration table), then perhaps the acceleration readings can be more accurately obtained by numerical integration.

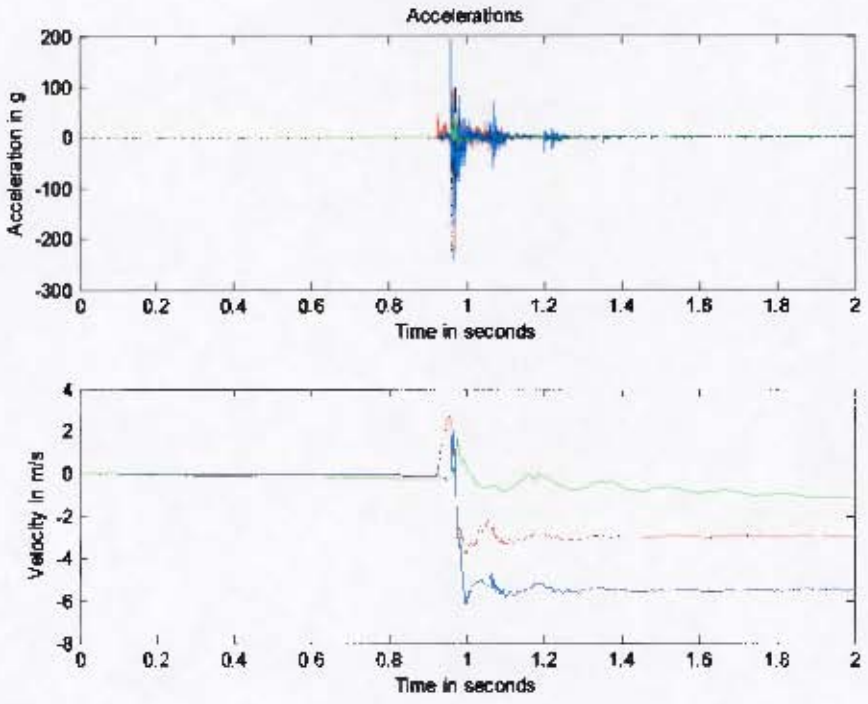

Figure 48: The velocity signals produced by removing the initial offset in the acceleration data.

Figure 49 shows a zoomed in view of Figure 48 .

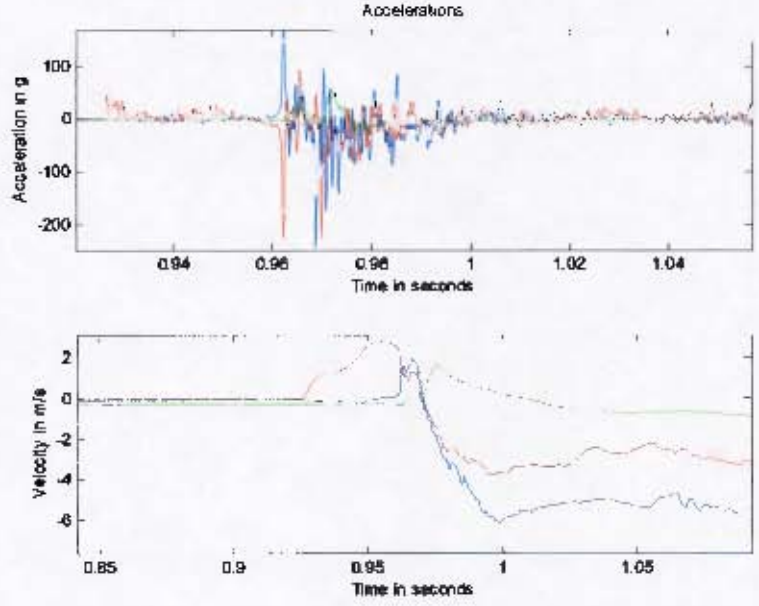

Figure 49: A magnified view of the accelerations and velocities with the initial offset removed.

Filtering of results:

Acceleration results are presented unfiltered (in post processing), but as the manufacturer mechanically filtered the data at 300Hz, to allow comparison of test results, a few of the results were filtered at this value. Unfiltered results are presented in Figure 50 and the same results filtered at 300Hz are presented in Figure 51. The peak top plate acceleration (indicated in blue in the figures) dropped from about 200g to about 80g when the data was filtered, but interestingly, the peak velocity only dropped from 2.08m/s to 2.03m/s. The filtered results in Figure 51 are comparable to those obtained by the manufacturer at the same offset and spring preload. The acceleration and velocity results obtained by the manufacturer are presented in Figure 52 and Figure 53 respectively and show a peak acceleration of around 105g and peak velocity of 2m/s. The acceleration and velocity results are summarised in Table 14.

Table 14: Summary of filtered and unfiltered top plate acceleration and velocity results.

	Raw data	Data filtered at 300Hz	Manufacturer data filtered at 300Hz
Peak acceleration[g]	200	90	110
Peak velocity[m/s]	2.08	2.03	2.00
Peak velocity duration[s]	0.0185	0.0184	0.0125

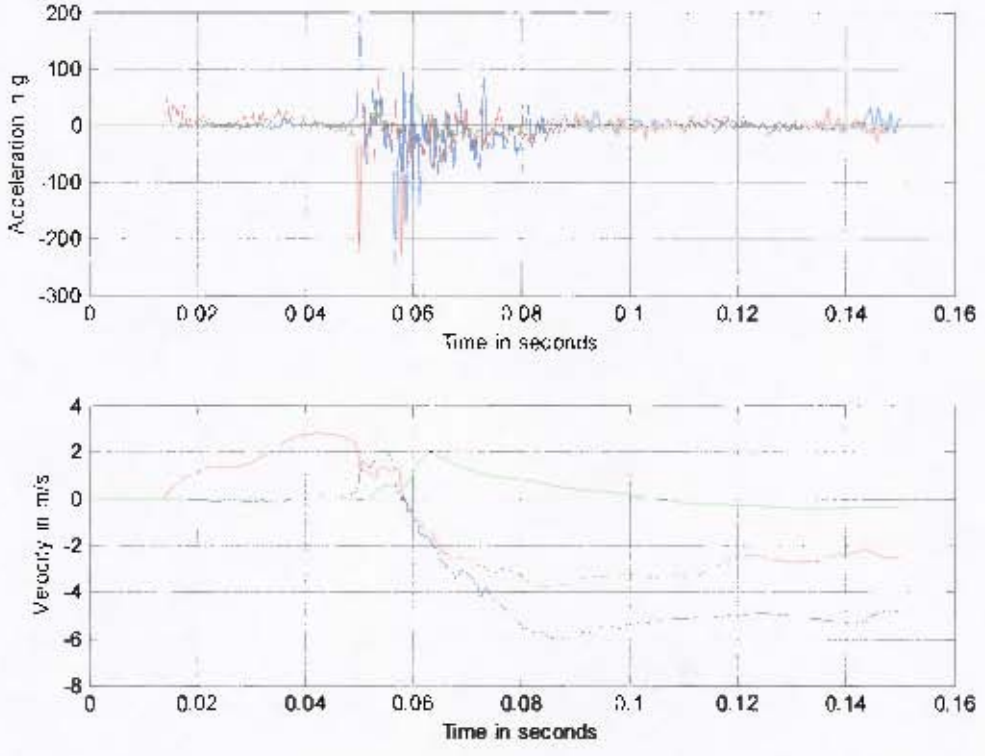

Figure 50: Unfiltered acceleration and velocity data for 10mm offset, 400kg spring preload and 25Nm surrogate leg joint torque setting.

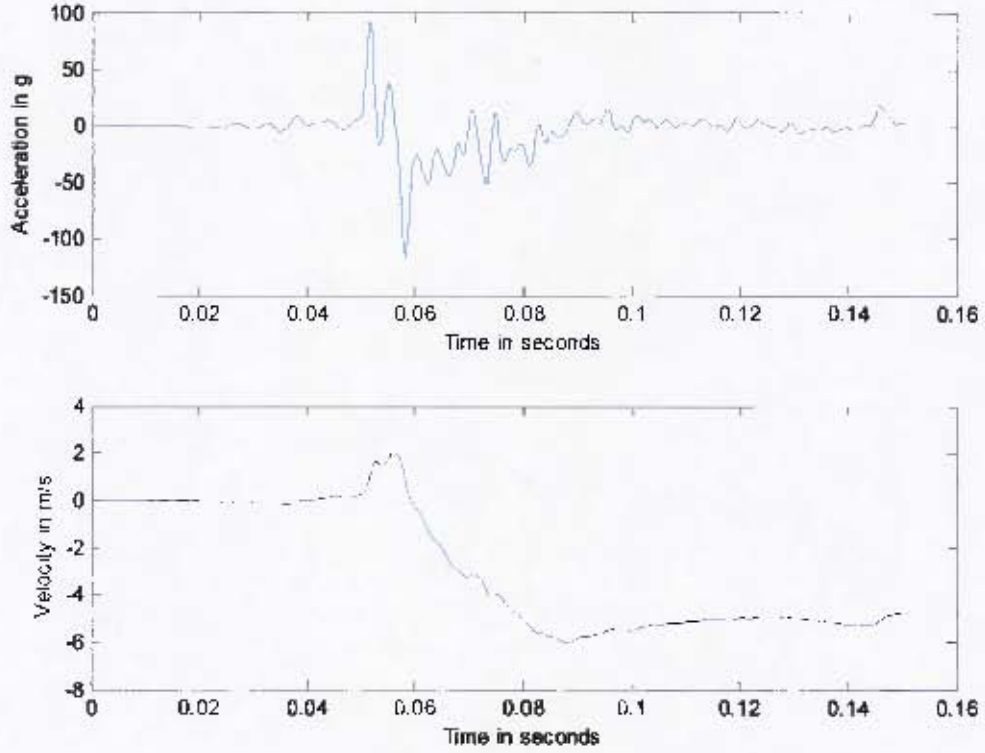

Figure 51: Acceleration and velocity data filtered at 300Hz for 10mm offset 400kg spring preload and 25Nm surrogate leg joint torque setting

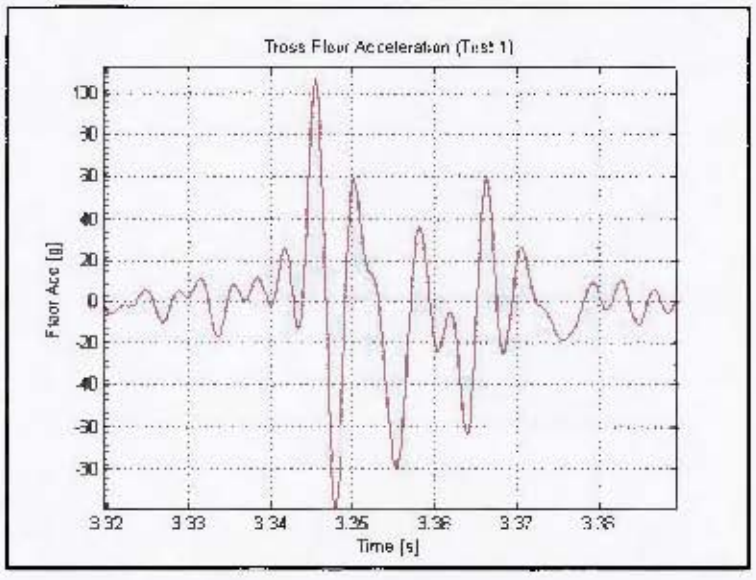

Figure 52: Acceleration data filtered at 300Hz for 10mm offset, 400kg spring preload presented by the manufacturer (from [57]).

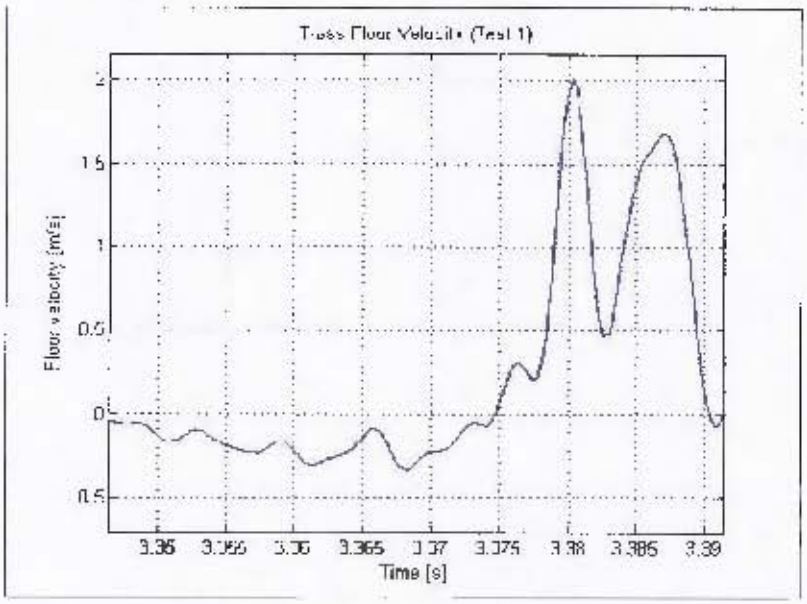

Figure 53: Velocity data for 10mm offset, 400kg spring preload presented by the manufacturer (from [57]).

The surrogate leg peak force was obtained using data that was not filtered in post processing, but in order to get a peak force duration the data was filtered at 300Hz to smooth out the signal.

Determining duration of peak velocity and peak leg force:

The durations of the peak velocity and peak leg force were measured between the zero time axis intersection points on either side of the peaks as illustrated in Figure 54.

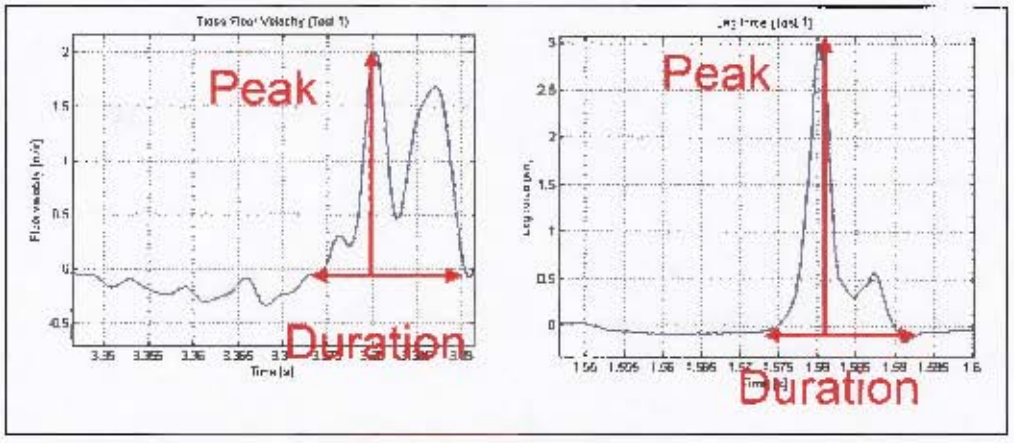

Figure 54: Illustration of how the peak velocity duration and peak leg force duration are determined.

However, this method can be problematic if the dip is just greater than zero and thus does not actually cross the zero axis where one would expect the peak duration to end. Figure 55 and Figure 56 illustrate this problem.

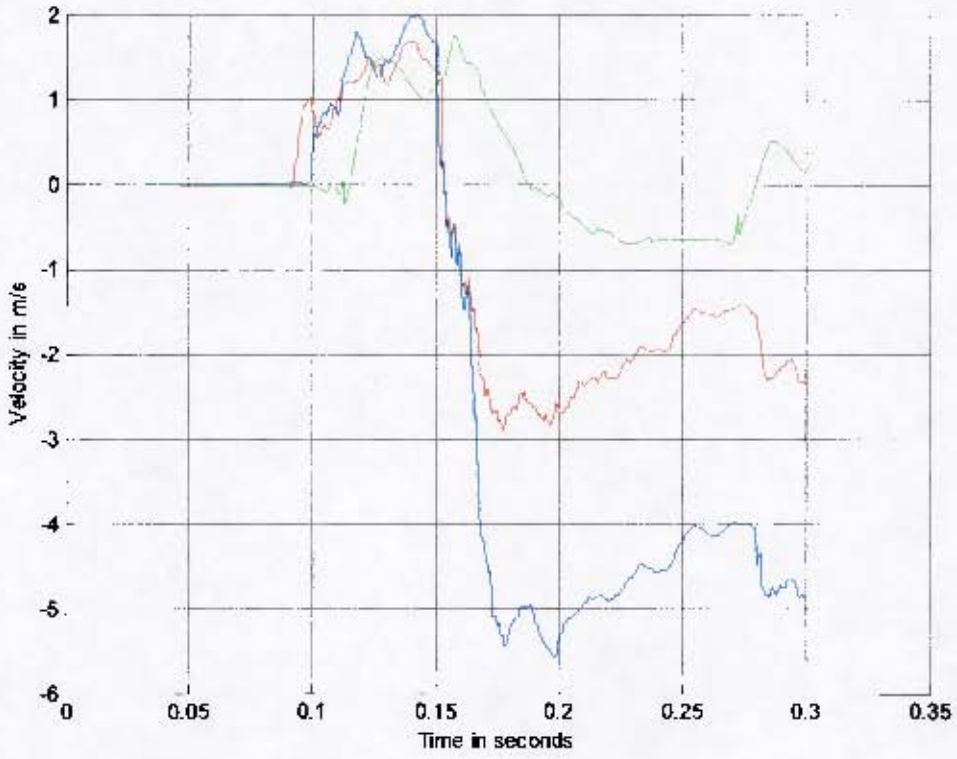

Figure 55: Illustration of determination of peak velocity duration (400kg spring preload at 70mm offset – blue is the top plate, red is the bottom plate and green is the surrogate leg).

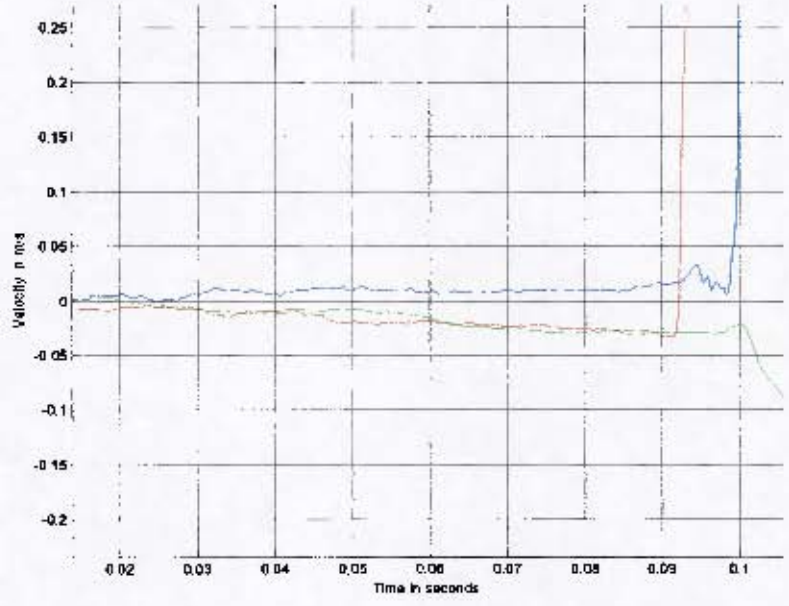

Figure 56: Zoomed in version of Figure 55.

If the duration was determined using the zero crossing of the velocity axis, then the durations would be as follows:

Peak top plate velocity duration (blue in Figure 55 and Figure 56):	**0.1248s.**
Peak bottom plate velocity duration (red in Figure 55 and Figure 56):	0.0580s.
Peak leg velocity duration (green in Figure 55 and Figure 56):	0.0350s.

If the duration was set using a 0.01m/s threshold rather that a zero threshold, the durations would be as follows:

Peak top plate velocity duration:	**0.0516s.**
Peak bottom plate velocity duration:	0.0579s.
Peak leg velocity duration:	0.0349s.

The method of using the zero crossing must be applied with caution as the results may be misleading. A threshold method of determining the duration should be investigated for future studies. For this study the zero crossing method was implemented as this was the method used by the manufacturer which allowed for comparison of characterisation results.

3.1.6 Summary of test results

In order to match the data provided by the manufacturer, the top plate peak velocity and duration and the surrogate leg peak force and duration were more closely examined. All of the top plate velocity and surrogate leg peak force results will be presented and plotted and trends will be identified. The repeatability will be examined as will the effect of changing the seat height.

It must be noted that the results for 200kg spring preload at 50mm and 70mm offset distances are not presented as the spring is not displaced enough by the 200kg preload to result in these displacements.

The full processed results from which the peaks and durations were obtained for each joint torque and spring preload are presented in the accompanying document *Detailed Results*. It is of importance to report these results in full as if discrepancies in the results are observed, it would be possible to discover why they may have arisen by studying the original plots (e.g. If a duration seems strange one can study the corresponding plot and might find that if a threshold was set instead of using a zero crossing to determine the duration, it might produce a more expected result).

Top plate velocity results:

Table 15: Summary of top plate velocity results.

Joint stiffness (Nm)	Preload on spring (kg)	Offset distance (mm)			
		10	30	50	70
		Peak velocity of top plate (m/s)			
25	200	0.94	1.00		
	400	1.88	1.74	1.51	1.99
	600	2.26	2.36	2.26	2.11
	750	2.75	2.85	2.94	2.64
6	200	0.94	1.16		
	400	1.74	1.77	1.67	2.04
	600	2.28	2.52	2.40	2.09
	750	2.64	3.03	3.12	2.56
		Peak velocity duration of top plate (s)			
25	200	0.0239	0.0684		
	400	0.0172	0.0243	0.0407	0.0516
	600	0.0148	0.0152	0.0125	0.0334
	750	0.0146	0.0113	0.0069	0.0086
6	200	0.0320	0.0624		
	400	0.0197	0.0288	0.0399	0.0542
	600	0.0176	0.0141	0.0145	0.0348
	750	0.0156	0.0121	0.0086	0.0084

The results in Table 15 are plotted in Figure 57 and Figure 58.

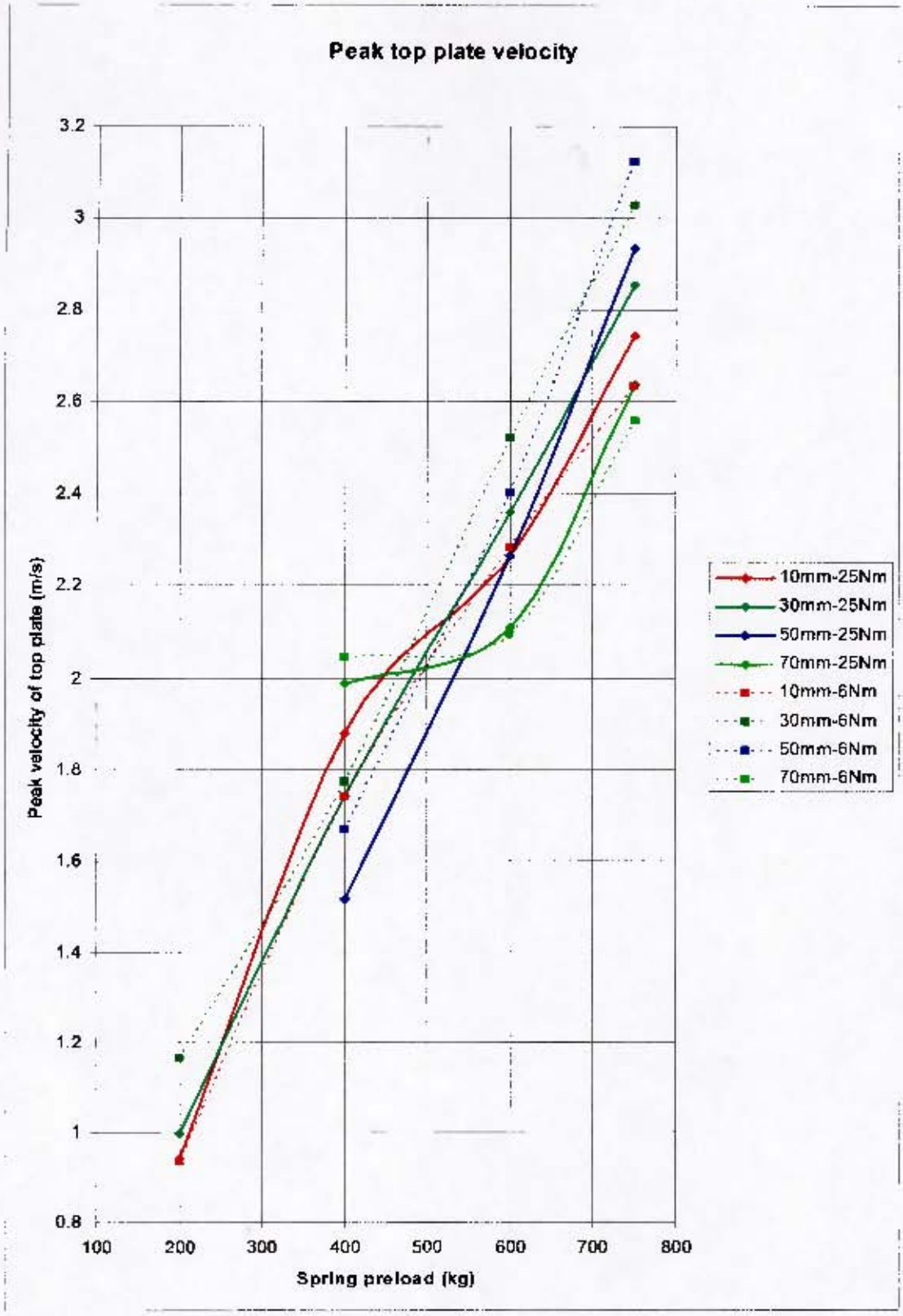

Figure 57: Peak top plate velocity at various spring preloads and offset distances at joint torques of 25Nm and 6Nm.

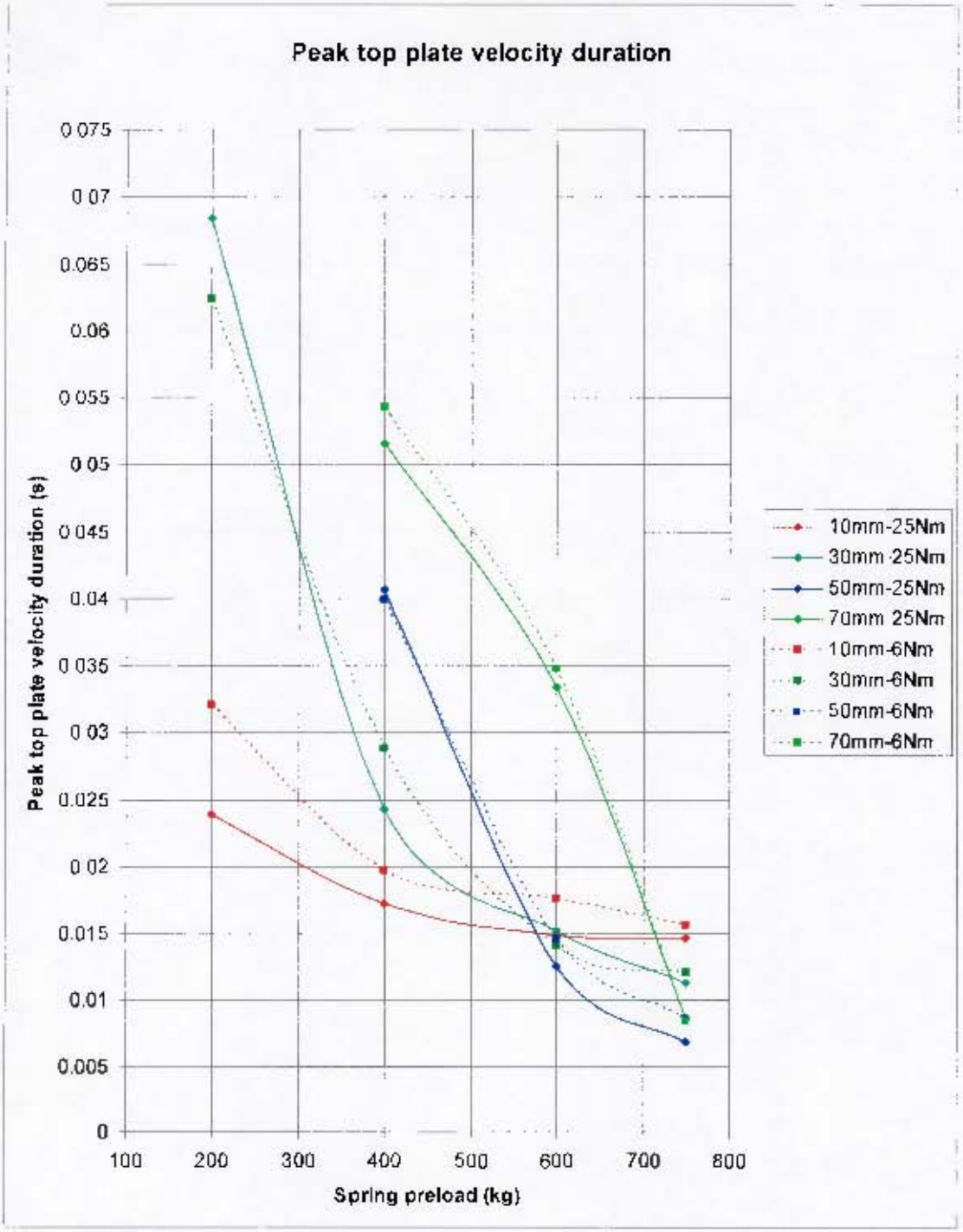

Figure 58: Peak top plate velocity duration at various spring preloads and offset distances at joint torques of 25Nm and 6Nm

If the results are separated into 25Nm and 6Nm joint torques and plotted as the manufacturer presented the results, trends can be compared. The trends are presented in Figure 59 and Figure 60.

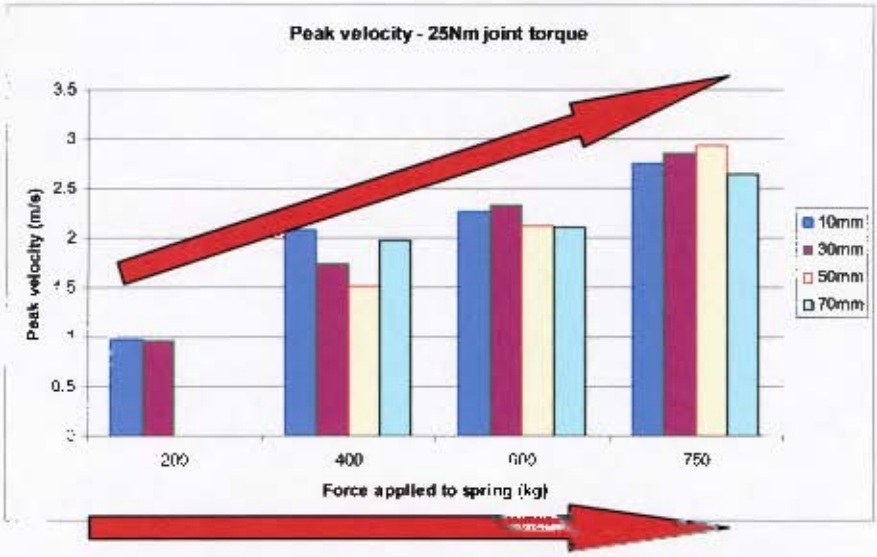

Figure 59: Peak velocity at various spring preloads and offset distances with 25Nm joint torque setting.

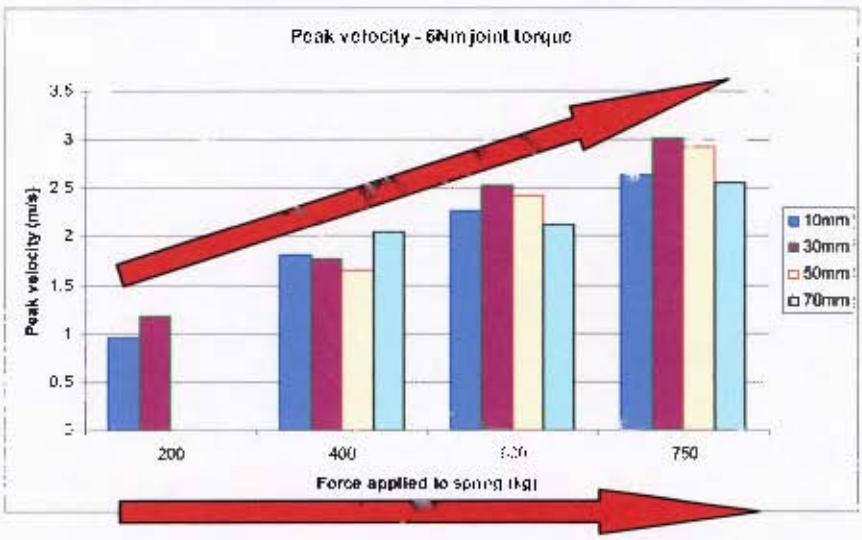

Figure 60: Peak velocity at various spring preloads and offset distances with 6Nm joint torque setting.

For both joint torques one can see the general trend that as spring preload increases, peak velocity increases. However no obvious trend with offset distances was observed. This is to be expected as varying the offset distances, according to the manufacturer, should vary the duration of the peak velocity.

In order to identify trends in the peak velocity duration, the graphs in Figure 61 and Figure 62 were plotted.

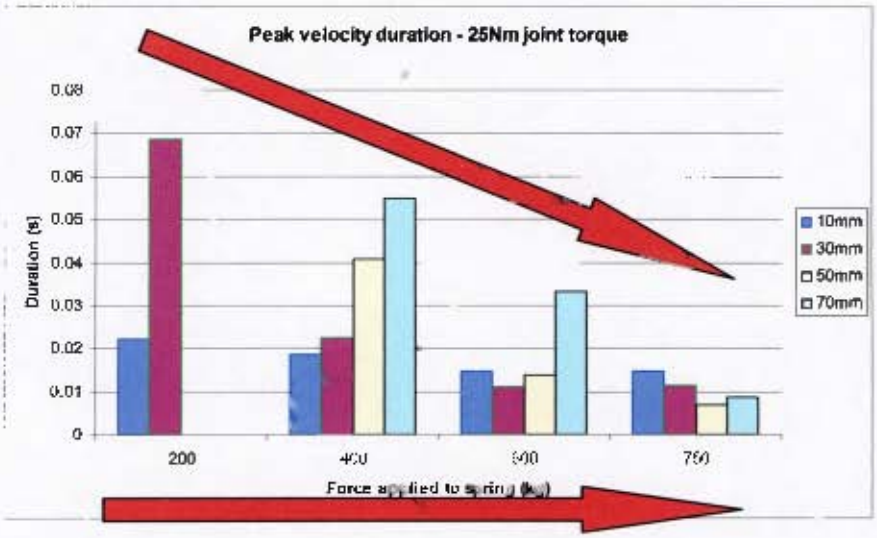

Figure 61: Peak velocity duration at various spring preloads and offset distances with 25Nm joint torque setting.

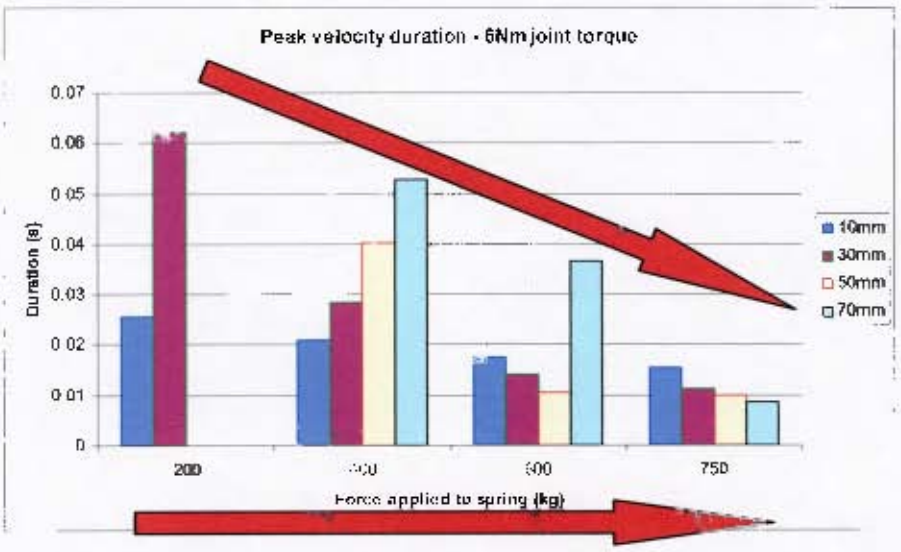

Figure 62: Peak velocity duration at various spring preloads and offset distances with 6Nm joint torque setting.

For both joint torques one can see the general trend that as spring preload increases, peak velocity duration decreases. However, no obvious trend with offset distances was observed. According to the manufacturer, increasing the offset distance should increase the duration of the peak velocity, however, this trend was not apparent throughout the data range.

Surrogate leg load cell results:

Table 16: **Summary of surrogate leg load cell results.**

Joint stiffness (Nm)	Preload on spring (kg)	Offset distance (mm)			
		10	30	50	70
		Peak leg force (kN)			
25	200	1.33	0.87		
	400	2.28	2.45	1.81	1.83
	600	3.59	3.65	2.85	2.83
	750	3.86	4.37	3.38	3.37
6	200	1.04	0.81		
	400	2.27	1.75	1.50	1.02
	600	4.53	2.55	3.07	2.82
	750	6.59	4.87	3.85	4.10
		Peak leg force duration (s)			
25	200	0.0324	0.0687		
	400	0.0201	0.0406	0.0519	0.0568
	600	0.0142	0.0183	0.0304	0.0418
	750	0.0102	0.0156	0.0513	0.0418
6	200	0.0174	0.0574		
	400	0.0205	0.0200	0.0274	0.0408
	600	0.0172	0.0222	0.0233	0.0223
	750	0.0086	0.0211	0.0250	0.0182

The results in Table 16 are plotted in Figure 63 and Figure 64.

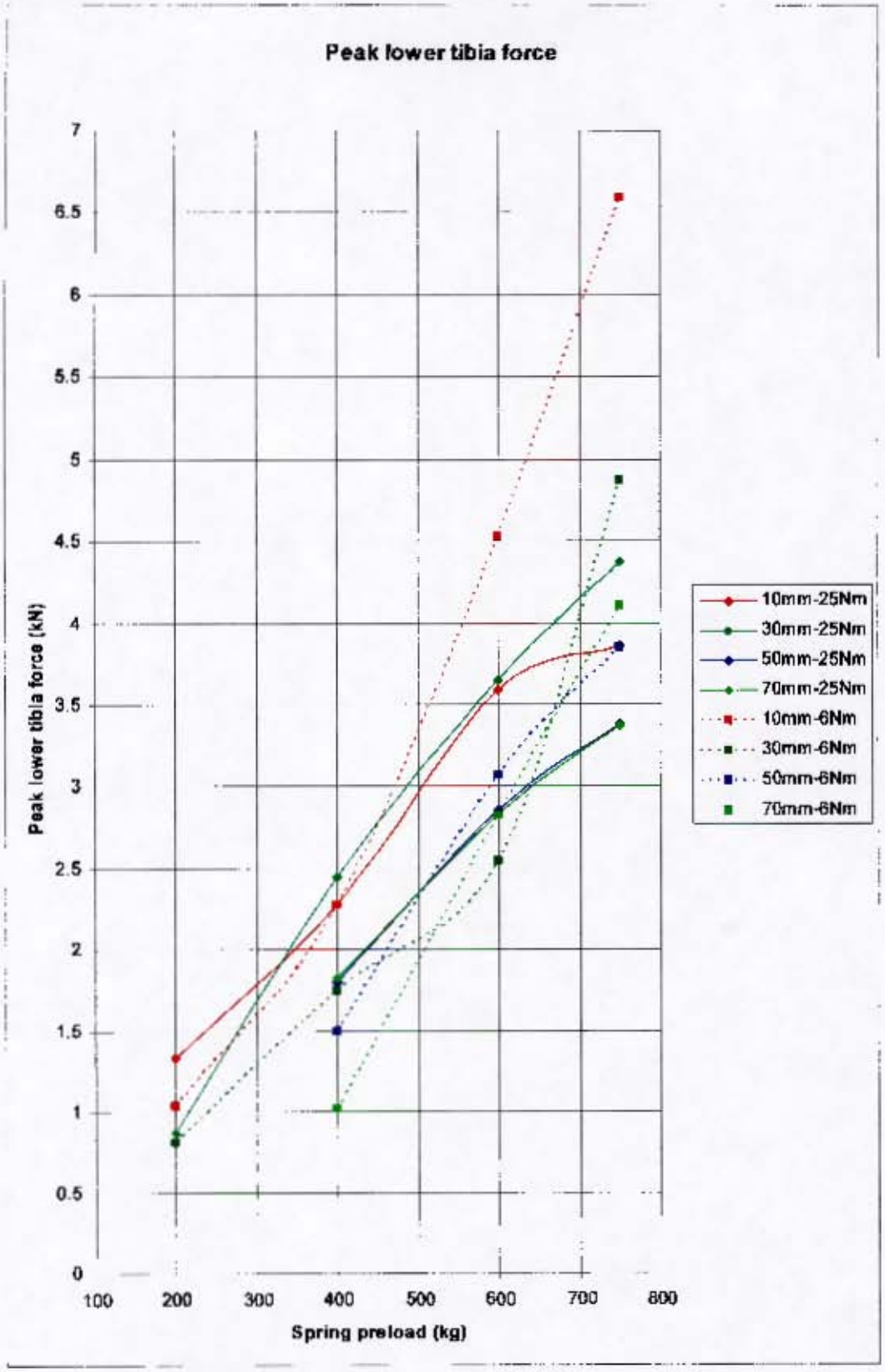

Figure 63: Peak leg force at various spring preloads and offset distances at joint torques of 25Nm and 6Nm.

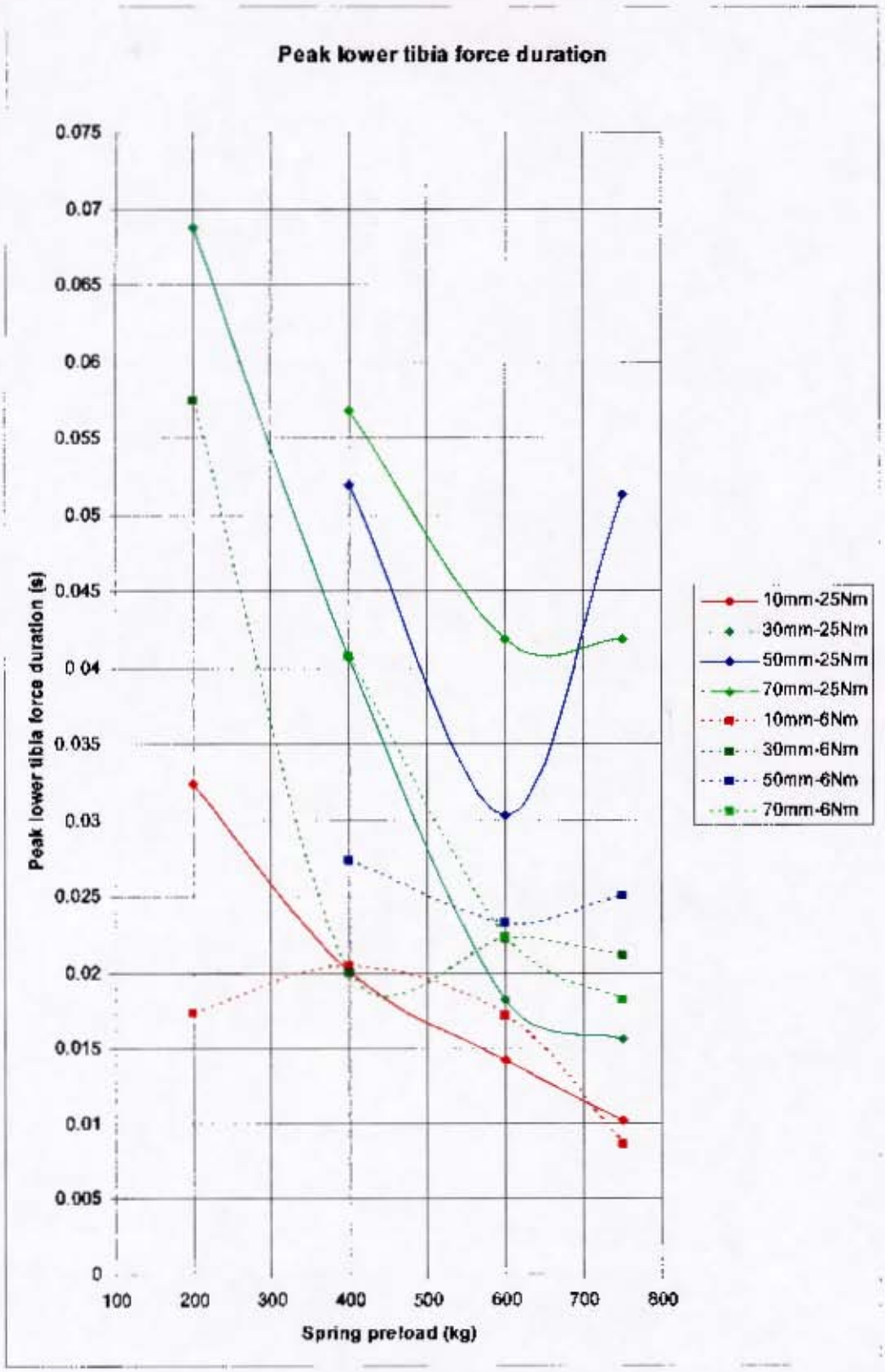

Figure 64: Peak leg force duration at various spring preloads and offset distances at joint torques of 25Nm and 6Nm

Analysing these results more closely, the following trends can be observed.

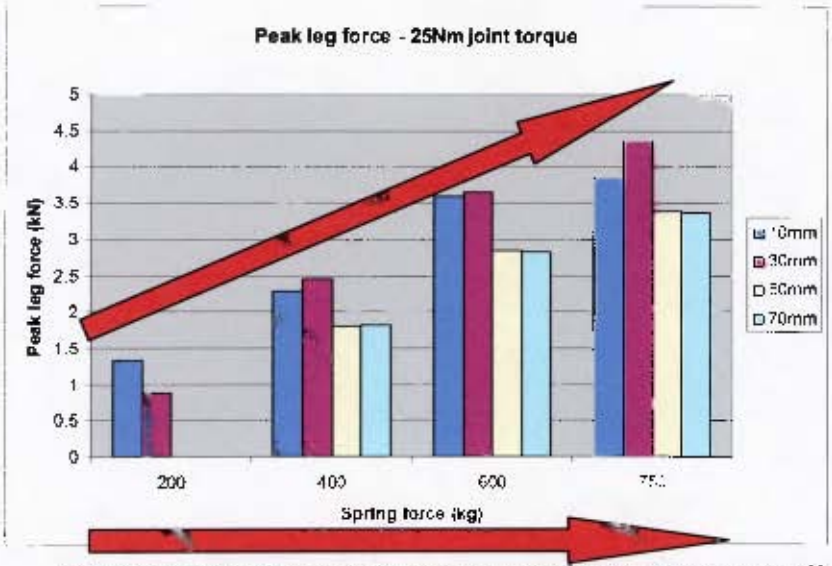

Figure 65: Peak leg force at various spring preloads and offset distances with 25Nm joint torque setting.

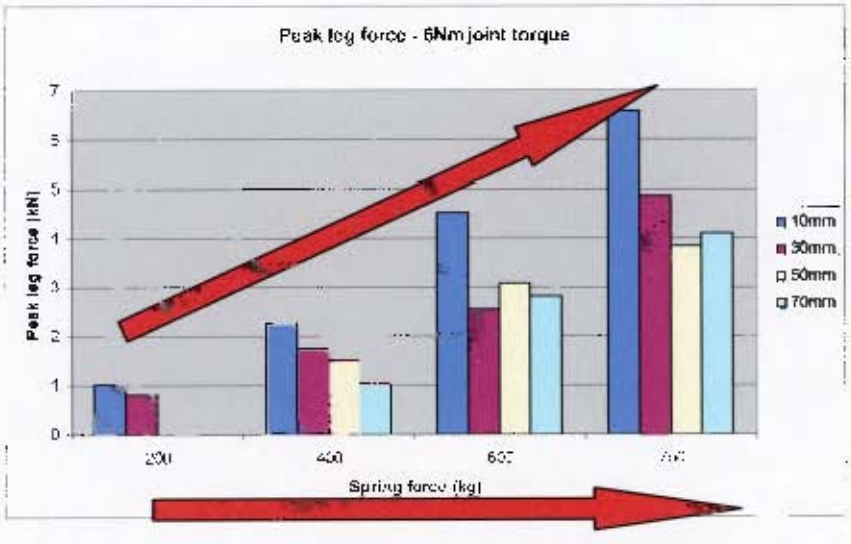

Figure 66: Peak leg force at various spring preloads and offset distances with 6Nm joint torque setting.

As with the peak top plate velocity, the general trend is that as spring preload increases, the peak leg force increases for both 25Nm and 6Nm joint torque settings and no obvious trends with offset distances were observed.

Trends in the peak leg force duration are explored in Figure 67 and Figure 68.

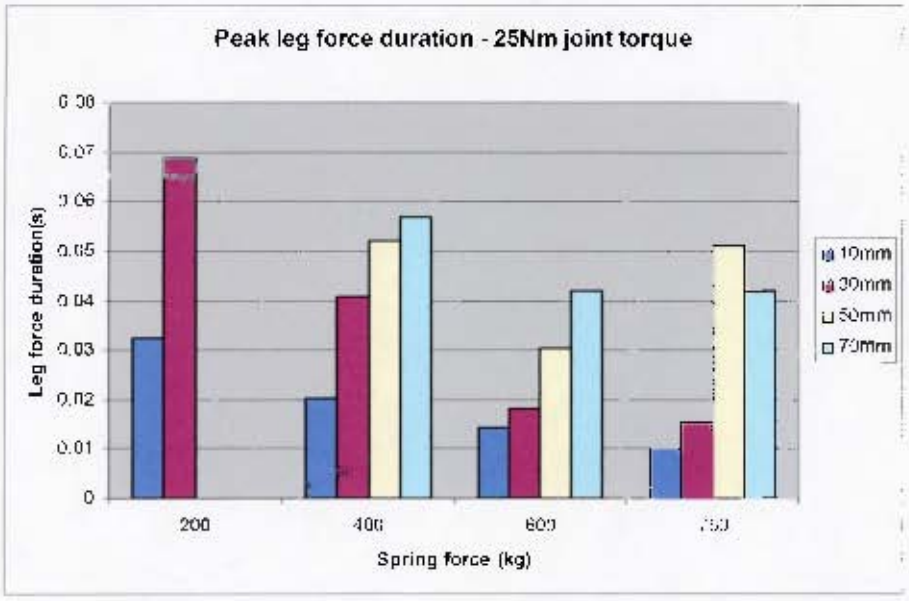

Figure 67: Peak leg force duration at various spring preloads and offset distances with 25Nm joint torque setting.

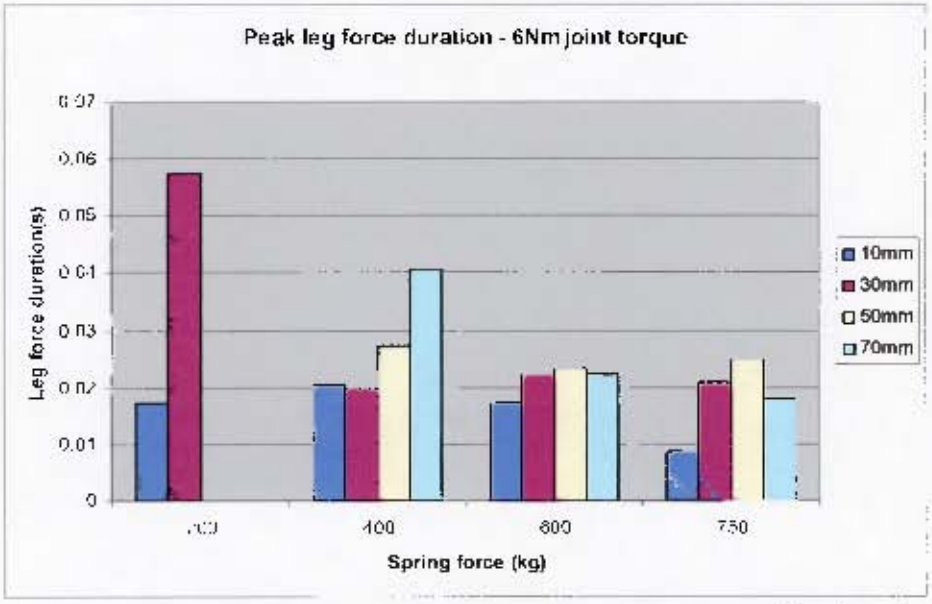

Figure 68: Peak leg force duration at various spring preloads and offset distances with 6Nm joint torque setting.

No obvious trends could be identified in the peak leg force duration with increasing spring preload or varying the offset distance.

Repeatability investigation:

The repeatability of the signal supplied by the LLTS is of great importance as this is one of the primary aims of the system. Due to the fact that problems were encountered towards the end of the LLTS characterisation process which require repair and modification before safe testing can continue, not all of the test domain locations contain more than one sample. However, as a preliminary investigation into the repeatability of the data, the samples taken at the 30mm, 600kg spring preload were examined at a joint torque of 25Nm. The repeatability of the LLTS was then compared to the repeatability of the drop test rig.

The graphs in Figure 69 and Figure 70 contain 3 repeats of the experiment done at 30mm offset with 600kg spring preload and joint torque of 25Nm.

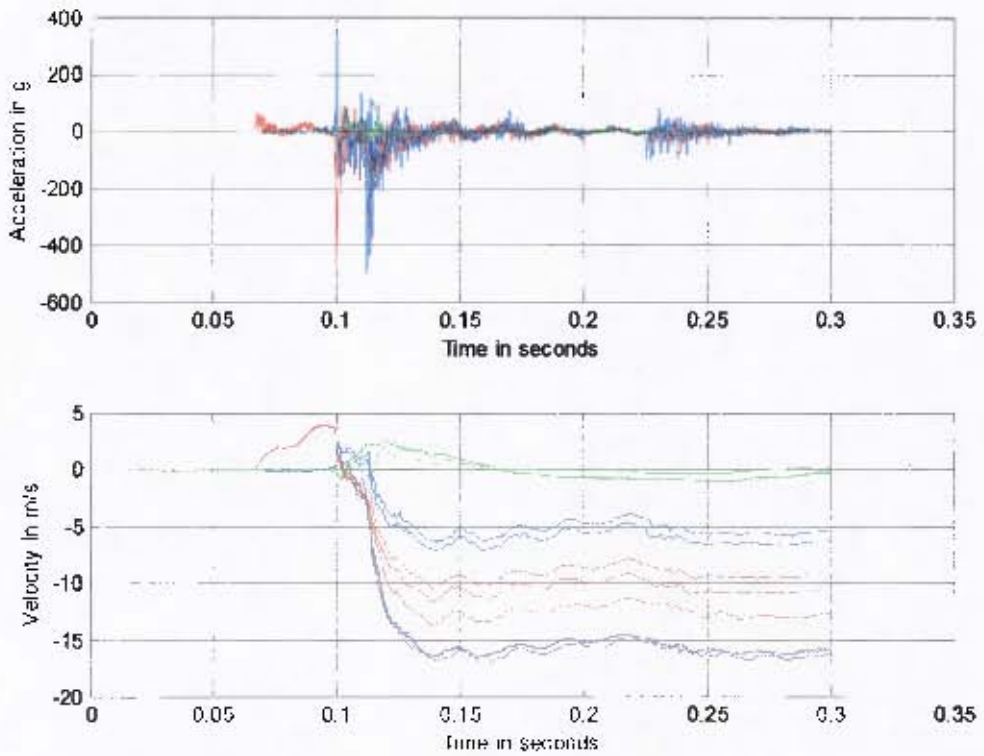

Figure 69: 3 repeats with 30mm offset and 600kg spring preload plotted on top of one another (blue – top plate, red- bottom plate, green – surrogate leg).

Figure 70 shows a zoomed in view of Figure 69.

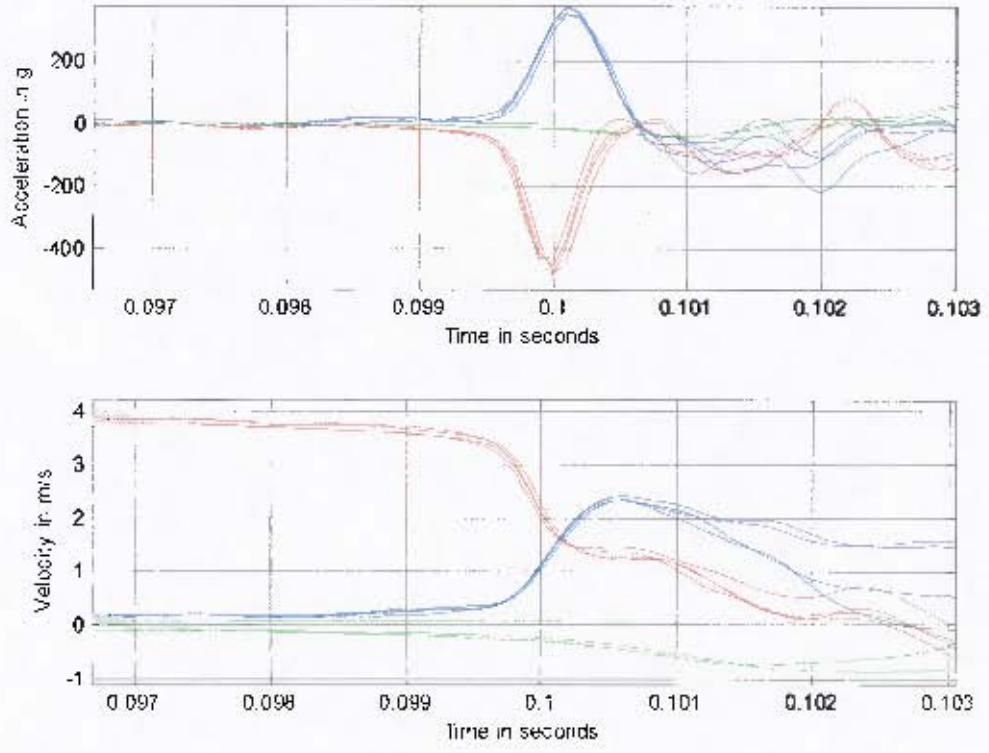

Figure 70: Zoomed in view of 3 repeats with 30mm offset and 600kg spring preload plotted on top of one another (blue – top plate, red- bottom plate, green – surrogate leg).

The repeatability of the peak velocity (indicated in blue in Figure 70) is assessed in Table 17. The peak velocity results are within 1% of one another and the velocity durations are within 35% of one another.

Table 17: Repeatability assessment of top plate peak velocity and peak velocity duration.

	Peak velocity (m/s)	Peak velocity duration (s)
Sample 1	2.36	0.0191
Sample 2	2.34	0.0106
Sample 3	2.33	0.0110
Average	2.34	0.0136
Standard deviation	0.02	0.0048

The repeatability of the leg force recorded during the same test is assessed in Figure 71 and Figure 72. The average and standard deviation are calculated in Table 18.

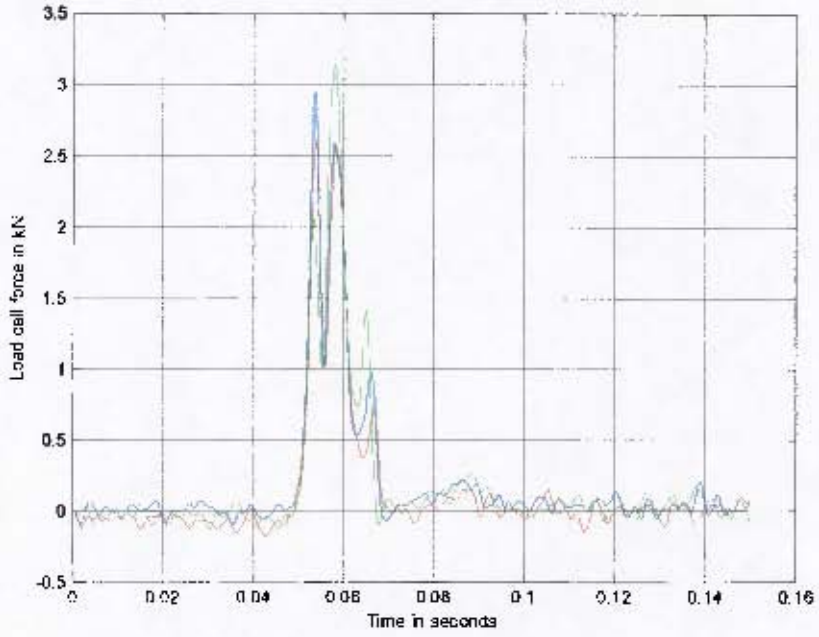

Figure 71: 3 repeats with 30mm offset and 600kg spring preload plotted on top of one another.

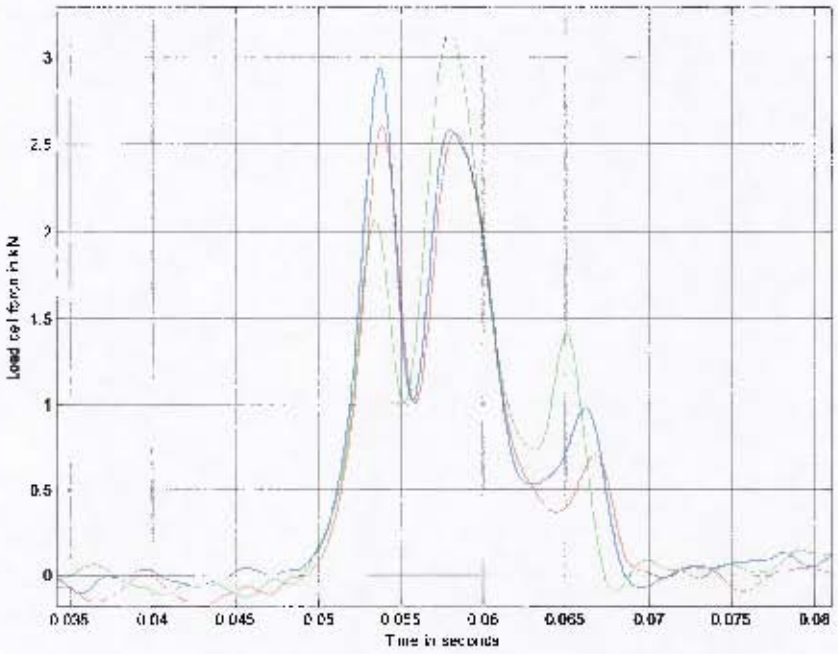

Figure 72: Zooming into the peaks in Figure 71.

Table 18: Repeatability assessment of peak leg force and peak leg force duration.

	Peak leg force (kN)	Peak leg force duration (s)
Sample 1	2.93	0.0212
Sample 2	3.53	0.0240
Sample 3	3.27	0.0183
Average	3.25	0.0212
Standard deviation	0.30	0.0029

From Table 18 it can be deduced that the peak leg forces are within 10% of one another and the peak leg force durations are within 14% of one another.

This repeatability of the LLTS was compared to the repeatability of a drop test rig for similar peak leg force values. The drop tests were performed using the same surrogate leg at 25Nm joint torque setting and dropped from 500mm. The drop test results are presented in Figure 73 and Figure 74.

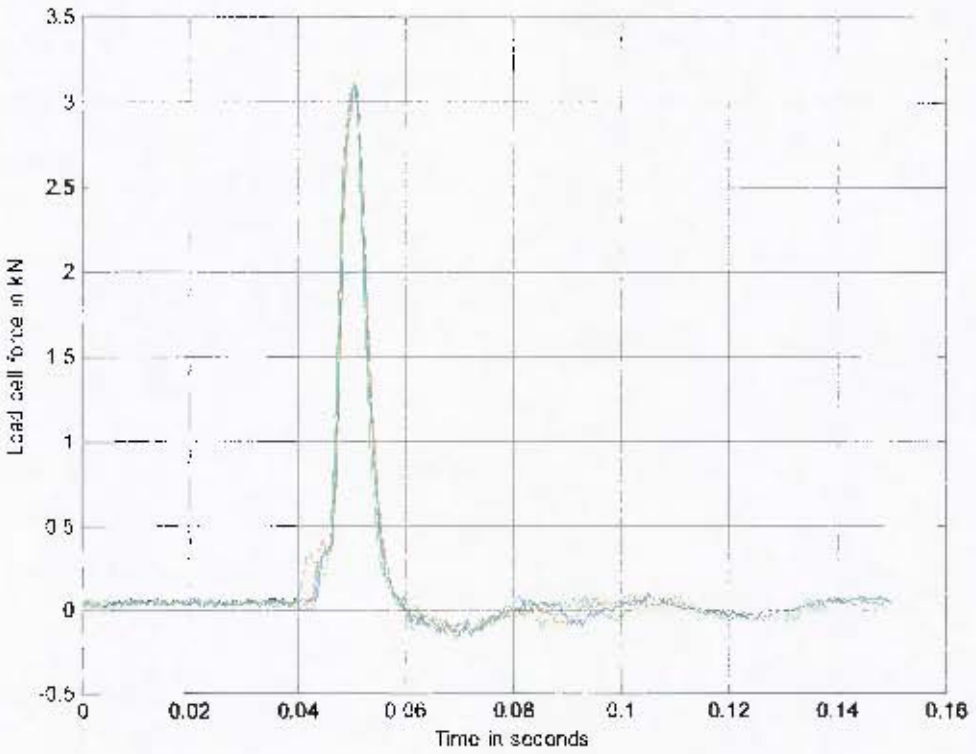

Figure 73: Drop test results analysed for repeatability (5 drops plotted on top of one another).

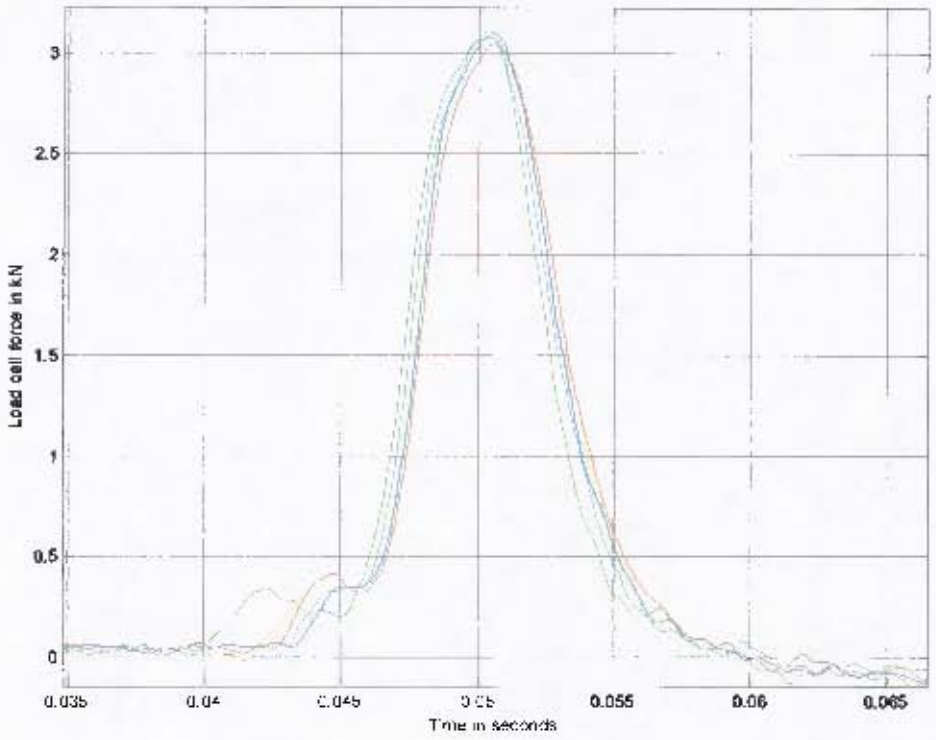

Figure 74: Zoomed in Figure 73.

Table 19: Repeatability assessment of peak leg force and peak leg force duration obtained with a drop test rig.

	Peak leg force (kN)	Peak leg force duration (s)
Sample 1	3.07	0.0168
Sample 2	3.14	0.0156
Sample 3	3.14	0.0183
Sample 4	3.10	0.0151
Sample 5	3.17	0.0166
Average	3.12	0.0165
Standard deviation	0.04	0.0012

From Table 19 it can be deduced that the peak leg forces are within 2% of one another and the durations are within 8% of one another.

Effect of varying the seat height:

The seat height can currently only be adjusted in discrete levels. The effect of this was examined by conducting tests at two slightly different heights. The lower seat height is approximately 25mm (one discrete level on the LLTS) lower than the original seat height. The top plate velocity and leg force results are shown in Figure 75 to Figure 78.

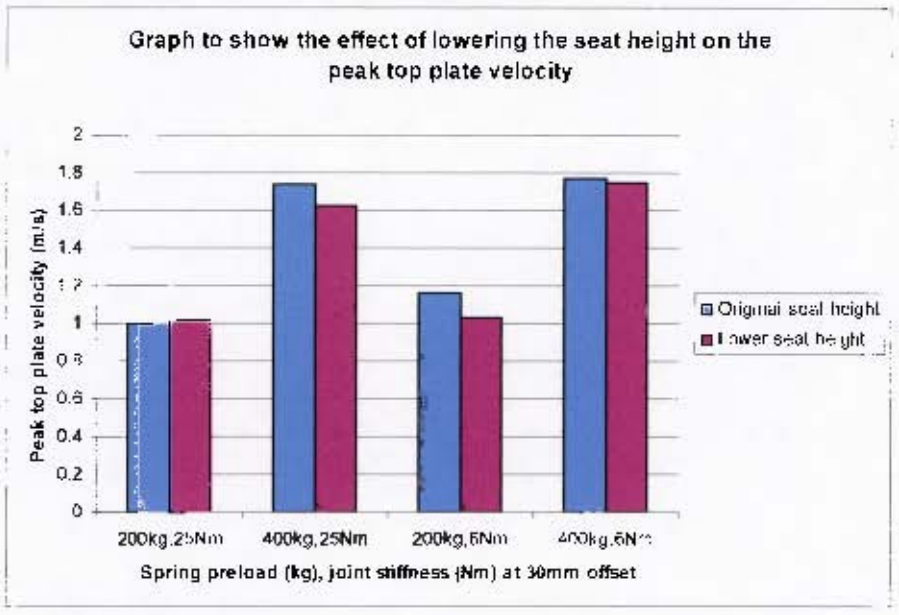

Figure 75: Effect of seat height on peak top plate velocity.

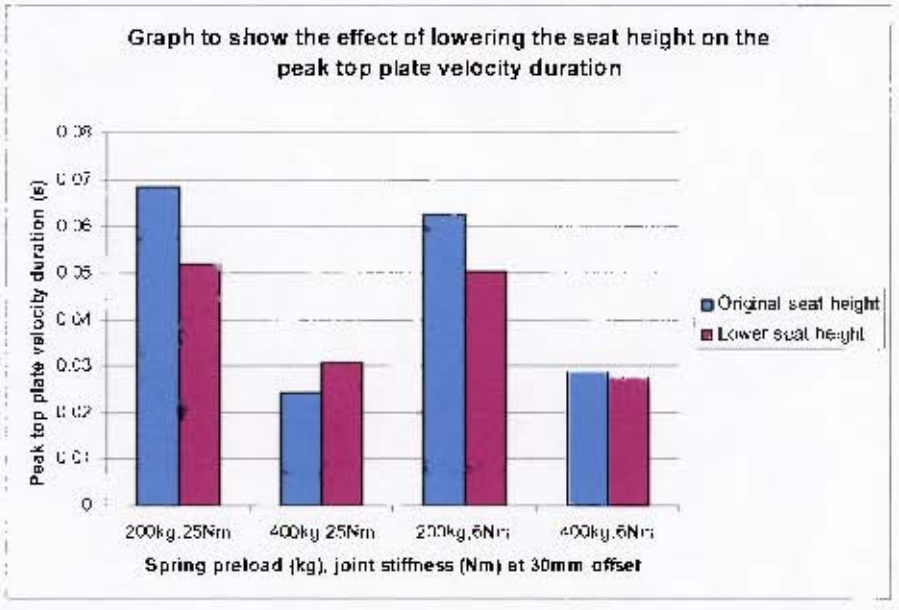

Figure 76: Effect of seat height on peak top plate velocity duration.

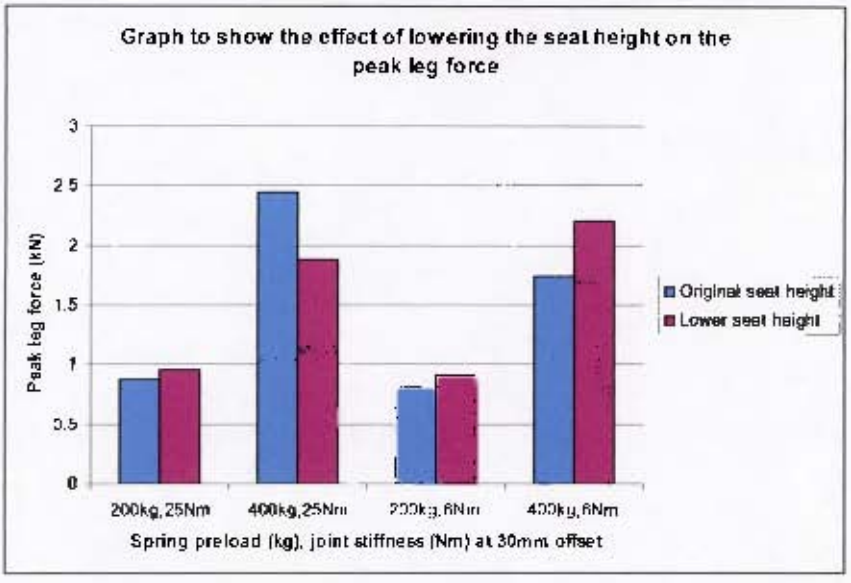

Figure 77: Effect of seat height on peak leg force.

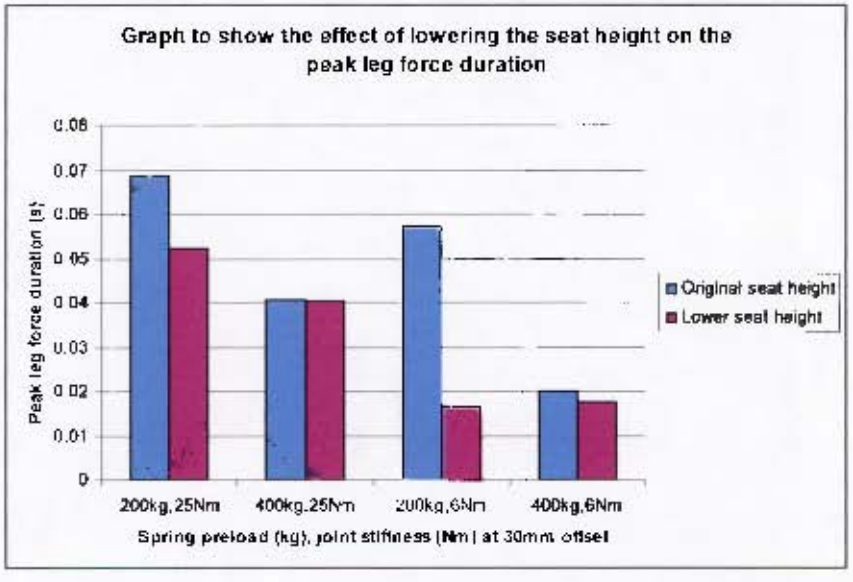

Figure 78: Effect of seat height on peak leg force duration.

Although it is clear that adjusting the seat height does have an effect on the results, distinct trends cannot be identified. It should be kept in mind that the 10mm and 30mm offsets were conducted at one seat height, whilst the 50mm and 70mm offsets were conducted at a lower seat height [15]

[15] A lower seat height was necessary at the 50mm and 70mm offsets as the shoe could not rest flat on the top plate at the higher seat height.

3.1.7 LLTS simulation

In order to understand the fundamental functioning of the LLTS a lumped parameter model was created in MSC Adams by Rayeesa Ahmed. In addition to this model a finite element model was built by Victor Balden to assess the structural strengths and weaknesses of the LLTS.

3.1.7.1 Lumped parameter model

Due to safety reasons, a front cover is in a position that restricts viewing of what is actually happening to the various components during testing. In addition, tests take place over very short time intervals, again making it difficult to see what is happening. It was therefore decided to simulate the LLTS in order to gain a better understanding of how the system works in practice.

Another reason for having a simulation of the LLTS is that it is easier and more cost (and time) effective to first simulate any possible changes or modifications to see what their effects are before actually implementing them. Similarly, there are no restrictions in a simulated version of the system as to how many load cells and accelerometers can be implemented to capture data, making it possible to monitor what is happening at more places throughout the system than is practically feasible.

The performance of the LLTS was simulated using the software package MSC.Adams by Rayeesa Ahmed. Adams is a motion simulation package used to analyse the behavior of complex mechanical assemblies.

Libraries of options are available to model geometries, constraints, joints and forces to simulate how components act with and in relation to each other. Once the model is set up and checked, Adams runs simultaneous equations for kinematic, static, quasi-static and dynamic simulations. Results can be viewed as graphs, data plots, reports and animations.

The main advantage to using Adams is the very quick run time of simulations as compared to other packages. This is due to the Adams solver using a lumped parameter approach. Adams was chosen to evaluate the dynamic performance of the LLTS.

Figure 79 shows the model of the LLTS in Adams. The entire LLTS was not modeled, but rather the moving parts of the system. The top plate and bottom (strike) plate were drawn using the geometry provided in the LLTS data pack and constrained to move about the same fixed pivot point. A spring of the same length and stiffness as specified was inserted between the strike plate and a block representing the spacers. A fixed frame, floor and stopper were also modeled as they constrain the space in which the top plate is allowed to move. The leg was replaced with a dummy mass.

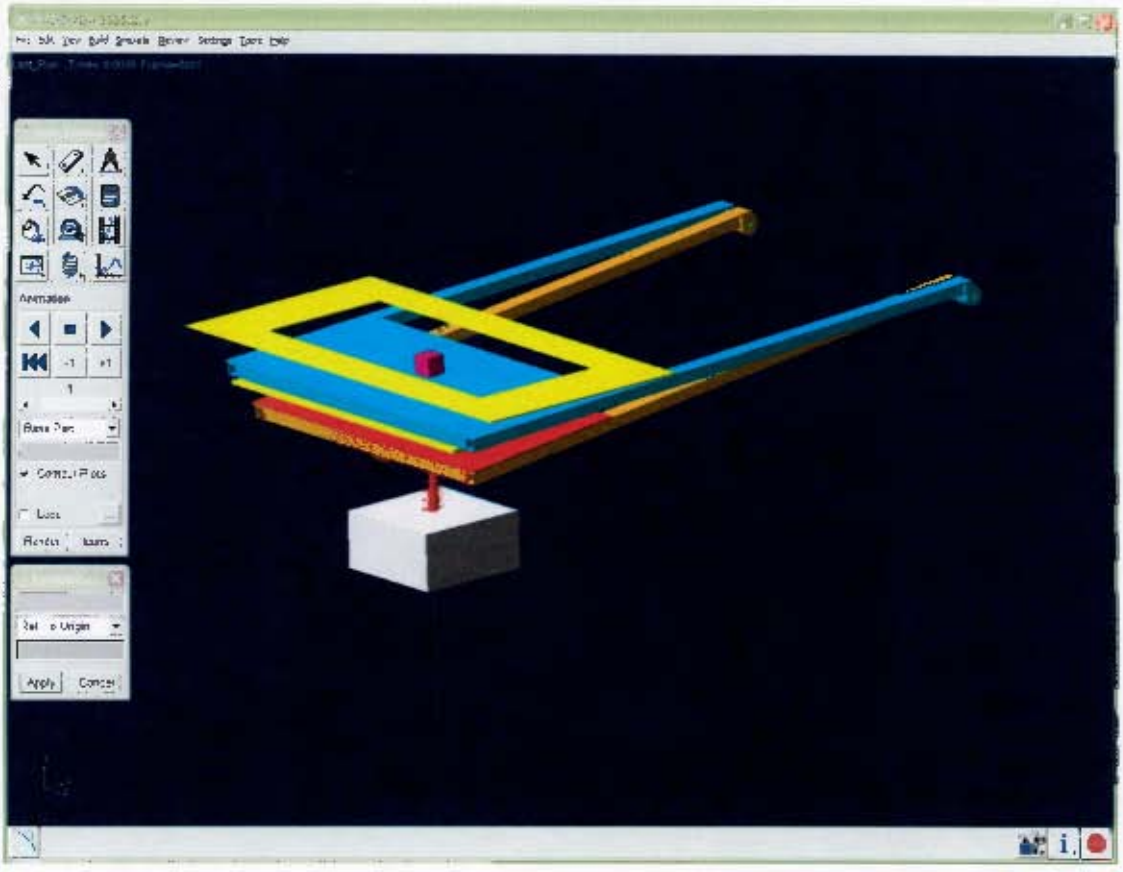

Figure 79: Model of the LLTS in MSC.Adams (by R Ahmed).

For each simulation run, the bottom plate was moved down and the spring compressed to the desired preload. The stopper was also adjusted and the top plate (and dummy mass) moved down to model the desired offset distance. Measures were placed at the same positions as the physical system and graphs for the accelerations and velocities were obtained for the top plate, strike plate and dummy mass. The peak force on the dummy mass was also measured.

The results of the simulation are presented in Table 20 to Table 23.

Table 20: Summary of top plate simulation results (by R Ahmed).

Preload on spring (kg)	Offset distance (mm)			
	10	30	50	70
	Peak velocity of top plate (m/s)			
200	0.59	0.63		
400	1.15	1.36	1.60	1.45
600	1.74	2.18	2.52	2.37
750	2.20	2.67	3.11	3.15
	Peak velocity duration of top plate (s)			
200	0.0202	0.0637		
400	0.0096	0.0231	0.0335	0.0490
600	0.0063	0.0138	0.0199	0.0298
750	0.0050	0.0113	0.0160	0.0219

Table 21: Summary of bottom plate simulation results (by R Ahmed).

Preload on spring (kg)	Offset distance (mm)			
	10	30	50	70
	Peak velocity of bottom plate (m/s)			
200	1.14	1.10		
400	2.45	2.45	2.43	2.12
600	3.77	3.76	3.76	3.75
750	4.75	4.74	4.74	4.74
	Time to Impact (s)			
200	0.0417	0.0239		
400	0.0436	0.0349	0.0268	0.0184
600	0.0442	0.0384	0.0329	0.0277
750	0.0440	0.0397	0.0353	0.0311

Table 22: Summary of dummy mass simulation results (by R Ahmed).

Preload on spring (kg)	Offset distance (mm)			
	10	30	50	70
	Peak velocity of dummy mass (m/s)			
200	0.56	0.58		
400	1.08	1.29	1.53	1.33
600	1.65	2.11	2.46	2.30
750	2.10	2.61	3.04	3.11

Table 23: Summary of dummy mass peak force simulation results (by R Ahmed).

Preload on spring (kg)	Offset distance (mm)			
	10	30	50	70
	Peak Force on Dummy Mass (kN)			
200	1.27	1.24		
400	2.89	3.74	4.72	3.23
600	5.08	7.01	9.56	7.35
750	7.36	8.86	12.7	12.6

The results are plotted in Figure 80 and Figure 81.

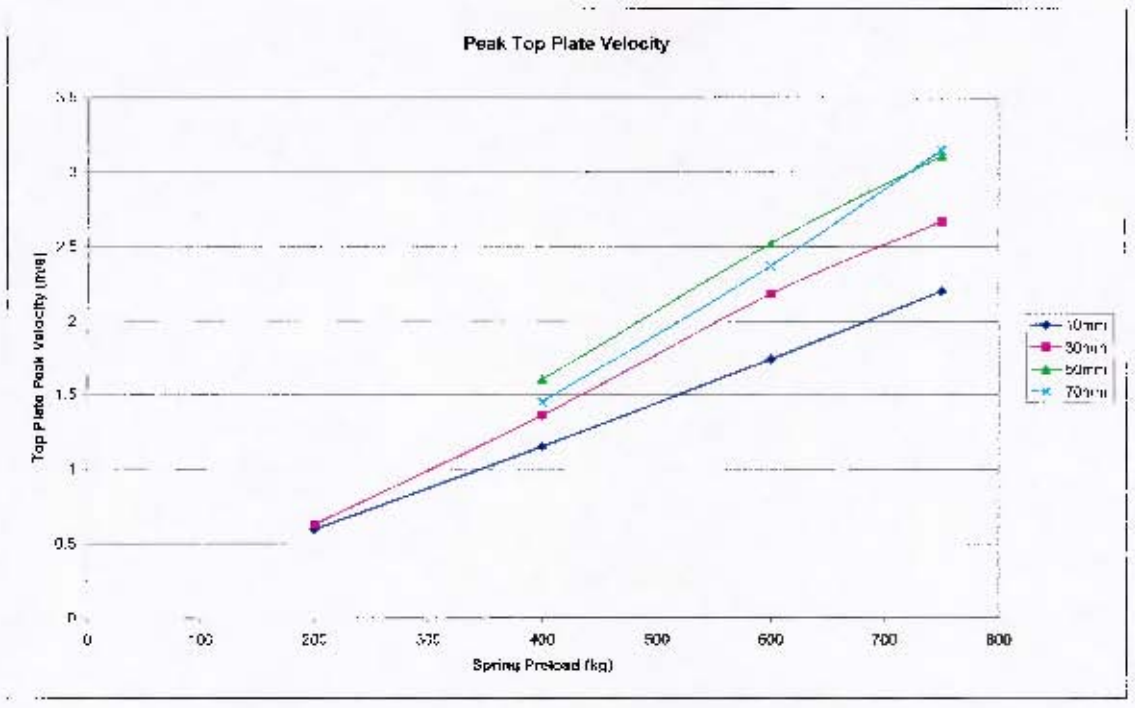

Figure 80: Graph of peak top plate velocity (by R Ahmed).

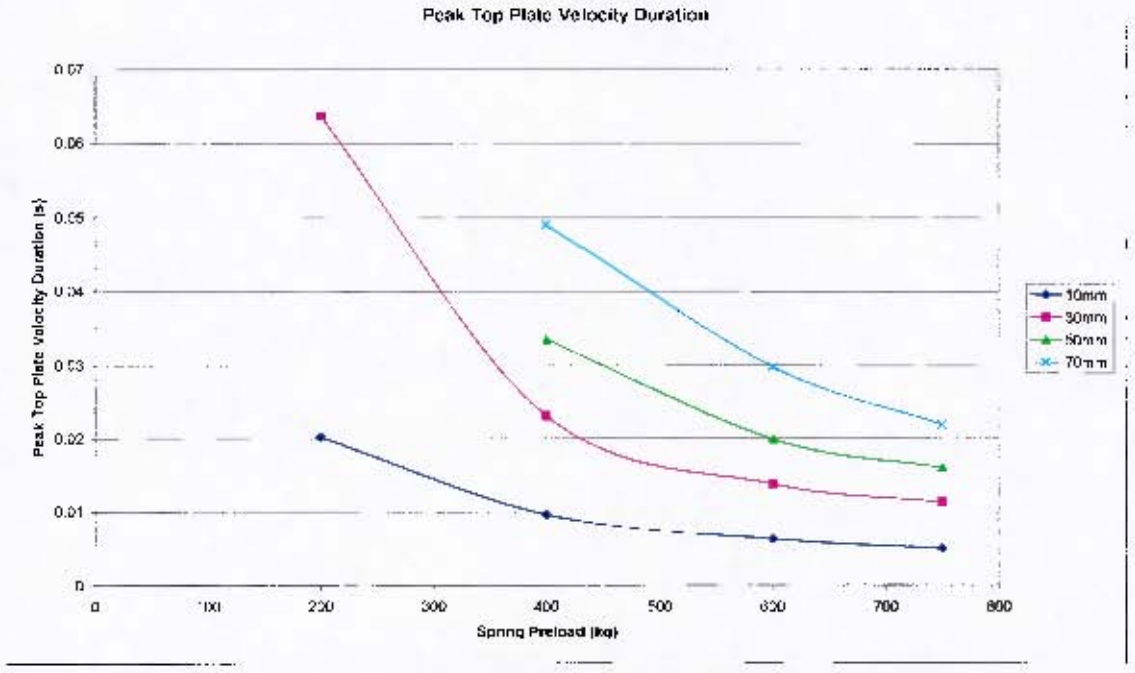

Figure 81: Graph of peak top plate velocity duration (by R Ahmed).

It must be noted that as the dummy mass was unconstrained realistic dummy mass peak velocity durations could not be obtained from the model. In reality the surrogate leg is constrained and future models of the LLTS will contain a surrogate leg model and not only a dummy mass.

3.1.7.2 Finite element model

The finite element model was executed by Victor Balden of BISRU, UCT in ABAQUS. The FEM model highlighted structural weaknesses in the LLTS. The plates were found to have much unwanted movement (bending and rotating) as was the seat (which visibly moved up and down in practice as well as in the simulation). The full report on these simulations can be found in Appendix B1.

3.1.8 Conclusions on the original LLTS

The conclusions on the original LLTS were drawn by comparing the characterisation results to the two main aims which were defined for the system:

- **Aim 1: Apply a force of varying peak amplitude and peak amplitude duration to a surrogate limb as the limb might see in the field.**

  In terms of varying the peak amplitude of the force, it has been identified that increasing the preload on the spring increases the peak force.

  No obvious trends were observed in varying the offset distance which is meant to control the duration of the peak force. However, increasing the peak force does appear to decrease the peak force duration irrespective of the offset distance setting.

  The current LLTS is not able to reproduce the larger peak forces of short duration that a limb may be subjected to in the field (see Figure 82).

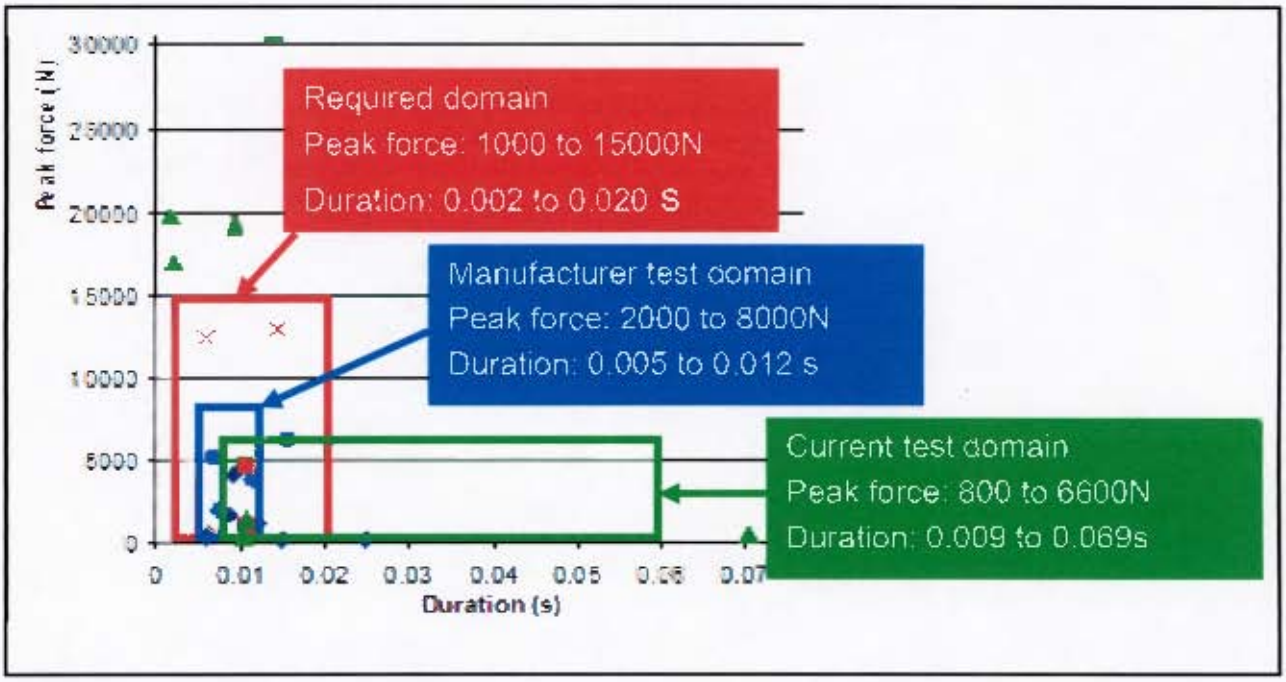

Figure 82: Illustration of typical forces that a limb may be subjected to in the field and domains currently covered by the LLTS.

- **Aim 2: The force must be repeatable to allow various parameters to be explored.**

  As it was not possible to obtain multiple samples at each point in the test domain, the repeatability cannot be commented on with confidence. Preliminary results indicate good repeatability in peak top plate velocity results (within 1% of one another), but poor repeatability in the durations (within 35% of one another). However, peak leg forces seem less repeatable (within 10% of one another with durations within 14%) which is even less repeatable than similar tests conducted on the same leg using a drop test rig (peak forces within 2% of one another with durations within 8%).

In summary, the current LLTS can apply loads that just exceed the injury criterion for the lower limb. Repairs and modifications are recommended to extend the force range and to improve the safety and "user friendliness" of the LLTS. The repeatability of the LLTS must be assessed using complete test domain with multiple samples at each test domain location.

3.1.9 Investigation of proposed modifications

In order to investigate a range of possible modifications, simulations were performed by Rayeesa Ahmed and Victor Balden.

3.1.9.1 Aim of modifications

Based on both characterisation tests and simulation results various short comings were observed. The primary aim of the modifications is to increase peak force applied to the surrogate limb.
In addition to this the structure requires modification in order to reduce the effect of vibrations and other unwanted movements that were identified in the FEM model. It is hoped that by implementing various changes the system will become more robust and produce more repeatable results.
The user would also benefit from modifications resulting in the LLTS being less labour intensive to operate.
Various modifications are investigated (using simulations where applicable) in order to determine which are the most promising ideas for improving the LLTS.

3.1.9.2 Descriptions of proposed modifications and simulations

Firm up seat suspension:
Problem: FEM eigenmode analysis confirmed excessive seat movement which was visually observed during impact.
Solution: Threaded bars with wing nuts can be used between the seat and the floor and at the back of the seat structure. Tracks can be used on the floor of the LLTS to maintain horizontal seat movement when the bars have been introduced.

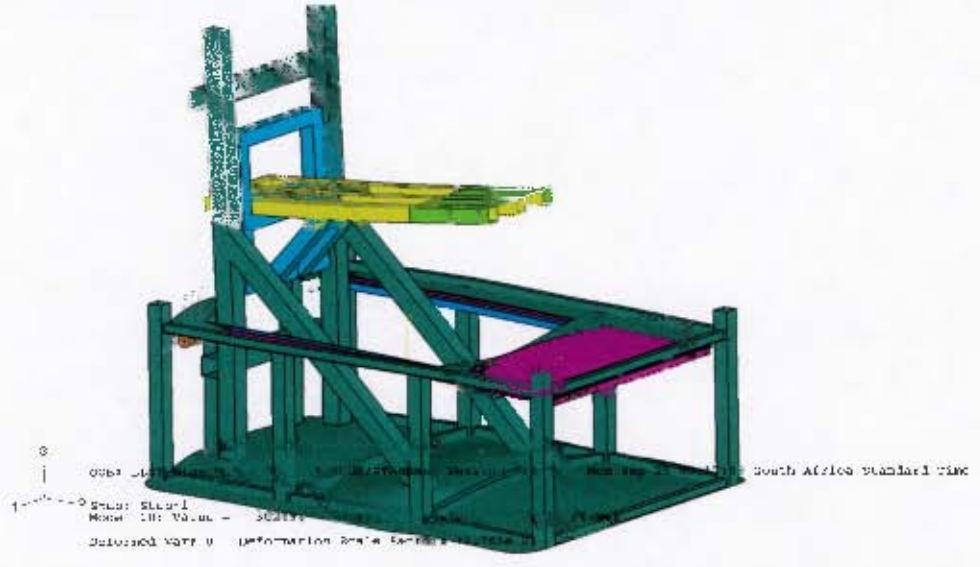

Figure 83: Diagram of simulation to illustrate seat movement (by V Balden).

Simulation description:

This modification was not simulated using the Adams model as it did not include the whole LLTS system and as the Adams model is a rigid body model it cannot simulate bending and flexing of the plates.

Remove the top plate:

Problems:

- The peak force applied by the LLTS is too low.
- The top plate adds weight and flexes unnecessarily which may introduce unexpected behavior into the system.

Solution:

- Remove the top plate. This will reduce the mass which will in turn increase the peak velocity which the system is able to achieve.

Simulation description:

Figure 84 shows the model of this modification in Adams. The top plate and stopper plate were removed. The bottom plate was left to move about the fixed pivot point. The contact forces were updated to reflect that contact would now occur from the bottom plate directly onto the dummy mass and frame floor.

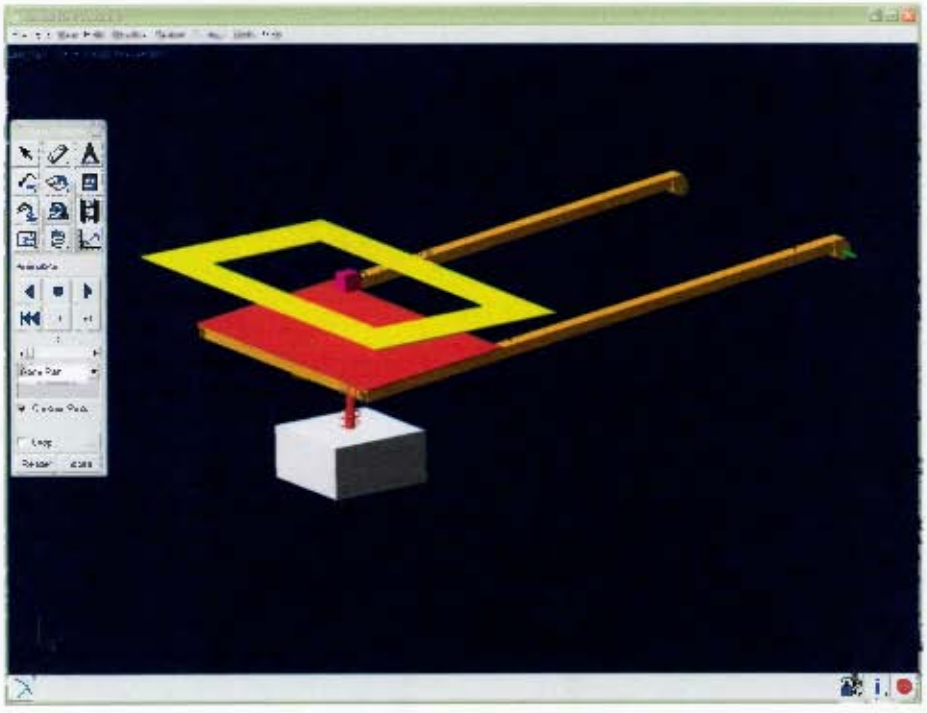

Figure 84: Adams model showing removal of top plate

(by R Ahmed).

For each simulation run, the bottom plate was rotated down and the spring compressed to the desired preload. The dummy mass was suspended at a position ±10mm below the frame floor to ensure that the strike plate impacts the dummy mass first. The dummy mass in the model drops from its initial position slightly (prior to impact) due to the effect of gravity; however this will not affect the results significantly. Graphs for the accelerations and velocities were obtained for the bottom plate and dummy mass. The peak force on the dummy mass was also measured.

Replace plates with impactor and steel guiding tubes:

Problems.

- The peak force applied by the LLTS is too low.
- The plates add weight and flex unnecessarily which may introduce unexpected behavior into the system.
- The spring is not utilised efficiently as it is not compressed straight, but rather at an angle by the pivoting plates. The spring will also be released at an angle.

Solution:

- Remove the plates. This will reduce the mass which will in turn increase the peak velocity which the system is able to achieve.
- Use an impactor mounted on the spring and guide the spring straight (should it extend skew) with hard chrome plated steel guiding tubes.

Simulation description:

Figure 85 shows the model of this modification in Adams. The top and bottom plates were removed as well as the stopper plate. Four guiding tubes were modeled equidistantly around the spring, of lengths just short of reaching the frame floor. A new cylindrical strike plate was modeled to just fit within the boundary of the four tubes, to which the spring is attached. A constraint was added to restrict the impactor (strike plate) to only be able to move vertically with respect to the tubes

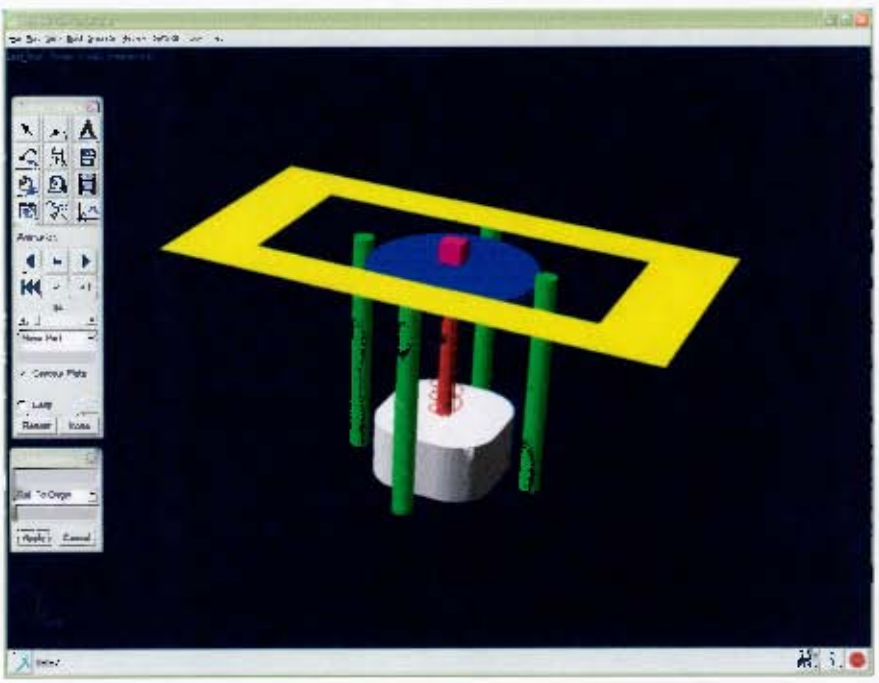

Figure 85: Adams model showing impactor and guiding tubes

(by R Ahmed).

For each simulation that was run, the impactor was moved down and the spring compressed to the desired preload. The dummy mass was suspended at a position +10mm below the frame floor to ensure that the impactor impacts with the dummy mass first. The dummy mass in the model drops from its initial position slightly (prior to impact) due to the effect of gravity; however this will not affect the results significantly. Graphs for the accelerations and velocities were obtained for the impactor and dummy mass. The peak force on the dummy mass was also measured

A set of simulations were done at various plate thicknesses to see what the effect the weight of the impactor would have.

Replace plates with impactor and guiding steel sleeve:

Problems: Same as above.

Solution:

- Remove the plates. This will reduce the mass which will in turn increase the peak velocity which the system is able to achieve.
- Use an impactor mounted on the spring and guide the spring straight (should it extend skew) with a hard chrome plated steel guiding sleeve.

Disadvantage:

- Much friction may be introduced by the impactor and sleeve contact.

Simulation description:

Figure 86 shows the model of this modification in Adams. It is very similar to the previous concept with the tubes merely being replaced by the sleeve. The constraint to restrict the impactor to only be able to move vertically with respect to the tubes was updated to the sleeve. The main difference between the two concepts is the amount of friction that the impactor will experience during testing, with the tubes having the smaller contact area. However, during these initial simulations, friction effects were omitted and the results of the two simulations are expected to be the same.

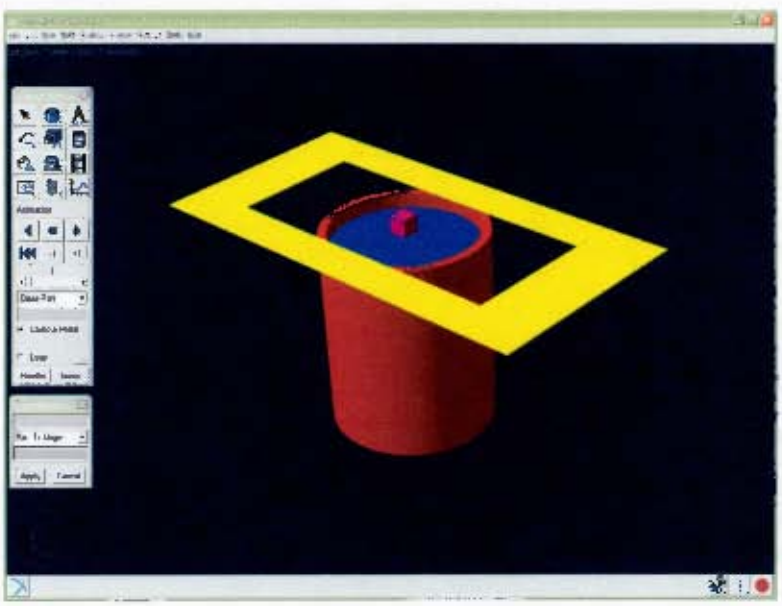

Figure 86: Adams model showing impactor and guiding sleeve (by R Ahmed).

For each simulation run, the impactor was moved down and the spring compressed to the desired preload. The dummy mass was suspended at a position ±10mm below the frame floor to ensure that the impactor impacts with the dummy mass first. The dummy mass in the model drops from its initial position slightly (prior to impact) due to the effect of gravity; however this will not affect the results significantly. Graphs for the accelerations and velocities were obtained for the impactor and dummy mass. The peak force on the dummy mass was also measured.

A set of simulations were done at various plate thicknesses to see what the effect the weight of the impactor would have.

Replace plates with impactor guided with sliding tubes:
Problems: Same as above.
Solution:

- Remove the plates. This will reduce the mass which will in turn increase the peak velocity which the system is able to achieve.
- Use an impactor mounted on the spring and guide the spring straight (should it extend skew) using sets of tubes which slide inside each other.

Disadvantage:

- Much friction may be introduced as the tubes make contact with one another.

Simulation description:
Figure 87 shows the model of this modification in Adams. Once again, it is very similar to the tubes concept. The tubes were shortened and hollowed out. The impactor was increased in diameter so that instead of fitting within the boundaries of the tubes, was now large enough to cover them. Attached to the impactor, four additional cylinders were modeled that fit into the hollow tubes to provide guiding for the impactor during testing. The constraint to restrict the impactor to only be able to move vertically with respect to the tubes was updated.

In addition to the amount of friction (and contact area) changing, this concept differs only in that the impactor is made stiffer and heavier by attaching the upper cylinders directly onto it. However, the performance of the impactor remains the same and since during these initial simulations friction effects were omitted, the results of the different simulations are expected to be the same.

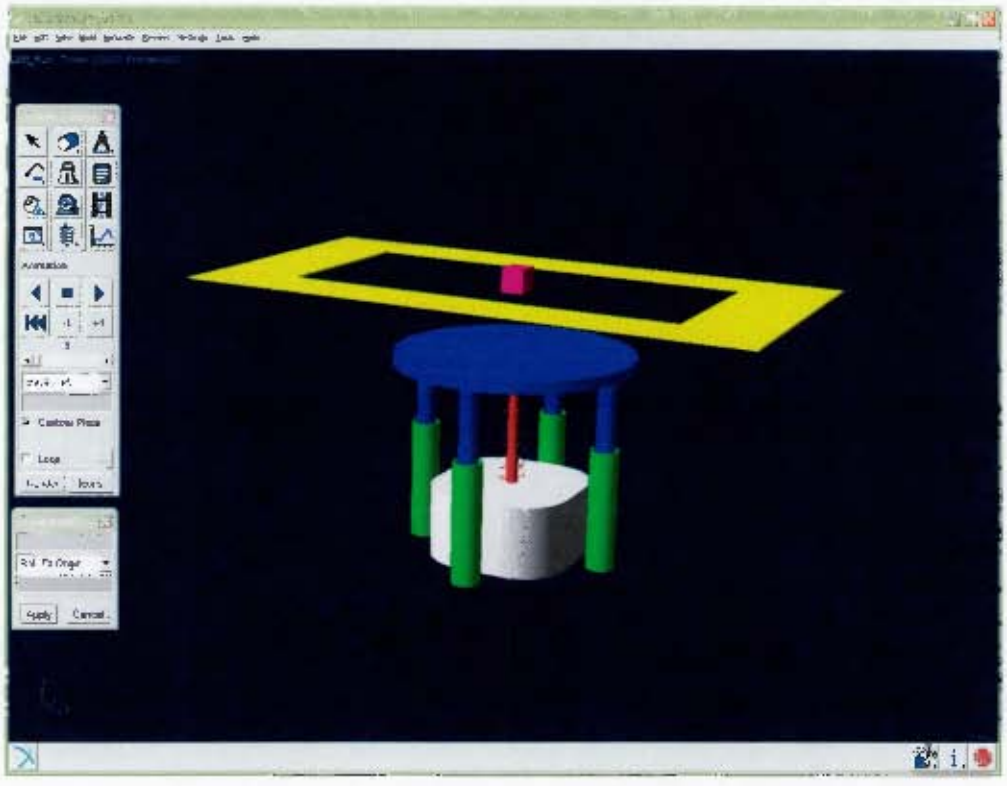

Figure 87: Adams model showing impactor with sliding tubes

(by R Ahmed).

For each simulation run, the impactor was moved down and the spring compressed to the desired preload. The dummy mass was suspended at a position ±10mm below the frame floor to ensure that the impactor impacts with the dummy mass first. The dummy mass in the model drops from its initial position slightly (prior to impact) due to the effect of gravity, however this will not affect the results significantly. Graphs for the accelerations and velocities were obtained for the impactor and dummy mass. The peak force on the dummy mass was also measured.

An alternative set of simulations were run after replacing the vertical motion constraint with a contact force between corresponding sliding tubes.

Replace spring with springs of varying stiffness:

Problem: Peak force is too low and durations cannot be manipulated.

Solution:

- Manufacture a number of springs of varying stiffness that can be swapped into the LLTS to achieve different peak forces and durations.

Disadvantages:

- It is labour intensive to remove and replace springs.
- The system would have to be characterised for each spring
- The springs are fairly costly.

Simulation description:

A series of simulations were run on the LLTS model using different spring stiffness values. Using the maximum displacement practically achievable on the LLTS, the maximum preload for the various springs were calculated. This preload was used in the simulations and the resulting peak forces on the dummy mass and top plate velocities were compared.

Replace spring with a longer spring with the same stiffness:

Problem: Peak force is too low and durations cannot be manipulated.

Solution:

- Manufacture a longer spring with the same stiffness as the current spring. This will allow one to achieve greater preloads which should result in higher peak forces and shorter durations which is where the current LLTS falls short of its aim

Simulation description:

With the current LLTS system, increasing the spring length will not have an effect on the results because the maximum possible displacement of the spring is limited i.e. the strike plate can only be pulled down a limited distance without interfering with the bottle jack used to pull the strike plate down.

There is however space available for a longer spring if the spacers beneath the spring are removed. The space available is 150mm so the maximum total spring free length that will be able to fit there will be 550mm. Bearing in mind that the length of the spring should not exceed the mean diameter of the spring by more than four times, a length of 550mm compared to the outer diameter of 250mm should not result in any buckling of the spring

A longer spring will theoretically be able to achieve higher preloads due to greater displacements being possible. However, the displacements will also depend on the geometry of the spring. Assuming that the wire diameter and the outer diameter remain the same, and assuming that the ratio of number of coils to spring free length stays the same, a simulation to determine the effect of using a longer spring can be done.

For this simulation, the concept outlined in the sliding tubes modification was used to demonstrate the effect of the spring length. A spring length of 500mm was used, with a maximum displacement corresponding to ±1200kg preload.

Other modifications that could be made in the future:

- Addition of a membrane plate
  - Provisions could be made to the LLI to accommodate an "oven grid" type mechanism for swapping in plates of differing stiffness.
  - *Advantages*:
    - Will be able to position the foot accurately
    - Will possibly be able to manipulate the duration of the signal.
  - *Disadvantages*:
    - Will add damping and a distributed mass that will decrease the velocity whilst distributing the impulse over a larger area.

- Addition of a leaf spring on which to position foot
  - *Advantage*: lower leg positioning without adding too much damping or mass.
  - *Disadvantage*: may not be able to handle the high loading.

- Suspended plate for lower leg positioning
  - A thin, light plate could be suspended by bungees or a mesh net.
  - *Advantages*
    - Will be able to position the foot accurately and at an angle
    - Will be able to set the height at which the spring impacts the foot.
    - Could use plates of different stiffness to manipulate the duration of the signal.
  - *Disadvantages*:
    - Will add damping and a distributed mass that will decrease the velocity whilst distributing the impulse over a larger area.

- Use of hydraulic system to compress spring
  - *Advantage*: Neater, less cumbersome, more robust system that is less labour intensive to use.
  - *Disadvantage*: More expensive.

- Use a hydraulic / air coupler modified for quick release in place of the spinnaker quick release.

- Add extra strengthening to base of LLTS to stabilise the system.

- Add damping where the impactor makes contact with the frame after it has made contact with the foot. This will offer some protection to the frame.

- A transparent front protection cover should replace the current steel front panel to allow visual confirmation of system functioning as well as the use of photography. This will enable one to better interpret the measurements

3.1.9.3 Results of simulated modifications

As expected, the guiding tubes and guiding sleeve results were the same. The sliding tubes results correspond to the 50kg simulation using the guiding tubes or sleeve as the mass of the impactor was predefined for the sliding tubes simulation.

Table 24: Simulation results of modifications to the LLTS (by R Ahmed).

Practical Results (10mm offset results were used for comparison)				
Preload (kg)	200	400	600	750
Top Plate Peak Velocity (m/s)	0.935	1.740	2.281	2.635
Top Plate Velocity Duration (s)	0.0320	0.0197	0.0176	0.0156
Peak Force on Leg (kN)	1.039	2.273	4.526	6.591
Simulation Results – LLTS (10mm offset results used)				
Preload (kg)	200	400	600	750
Top Plate Peak Velocity (m/s)	0.594	1.15	1.74	2.20
Top Plate Velocity Duration (s)	0.0202	0.0096	0.0063	0.0050
Bottom Plate Peak Velocity (m/s)	1.14	2.45	3.77	4.75
Dummy Mass Peak Velocity (m/s)	0.555	1.08	1.65	2.10
Peak Force on Dummy Mass (kN)	1.27	2.89	5.08	7.36
Simulation Results - No Top Plate				
Preload (kg)	200	400	600	750
Bottom Plate Peak Velocity (m/s)	1.14	2.18	3.77	4.76
Dummy Mass Peak Velocity (m/s)	1.17	2.07	3.49	4.18
Peak Force on Dummy Mass (kN)	8.15	15.9	37.7	41.3
Simulation Results – Guiding Tubes & Guiding Sleeve (10kg)				
Preload (kg)	200	400	600	750
Impactor Peak Velocity (m/s)	1.41	2.90	4.38	5.50
Dummy Mass Peak Velocity (m/s)	0.993	1.73	2.42	3.09
Peak Force on Dummy Mass (kN)	20.9	34.1	46.8	58.2
Simulation Results – Guiding Tubes & Guiding Sleeve (25kg)				
Preload (kg)	200	400	600	750
Impactor Peak Velocity (m/s)	1.01	2.15	3.29	4.15
Dummy Mass Peak Velocity (m/s)	0.91	1.85	2.75	3.39
Peak Force on Dummy Mass (kN)	16.9	35.0	48.2	59.4
Simulation Results – Guiding Tubes, Guiding Sleeve & Sliding Tubes (50kg)				
Preload (kg)	200	400	600	750
Impactor Peak Velocity (m/s)	0.672	1.57	2.47	3.14
Dummy Mass Peak Velocity (m/s)	0.649	1.49	2.34	3.04
Peak Force on Dummy Mass (kN)	15.8	22.5	42.5	52.9
Simulation Results – Sliding Tubes (no vertical constraint)				
Preload (kg)	200	400	600	750
Impactor Peak Velocity (m/s)	0.654	1.54	2.42	3.08
Dummy Mass Peak Velocity (m/s)	0.701	1.81	2.62	3.37
Peak Force on Dummy Mass (kN)	15.1	27.2	29.7	36.9

Because there is no top plate in the modified simulations, the graphs in Figure 88 and Figure 89 compare the peak velocities of the bottom plate or impactor and dummy mass respectively.

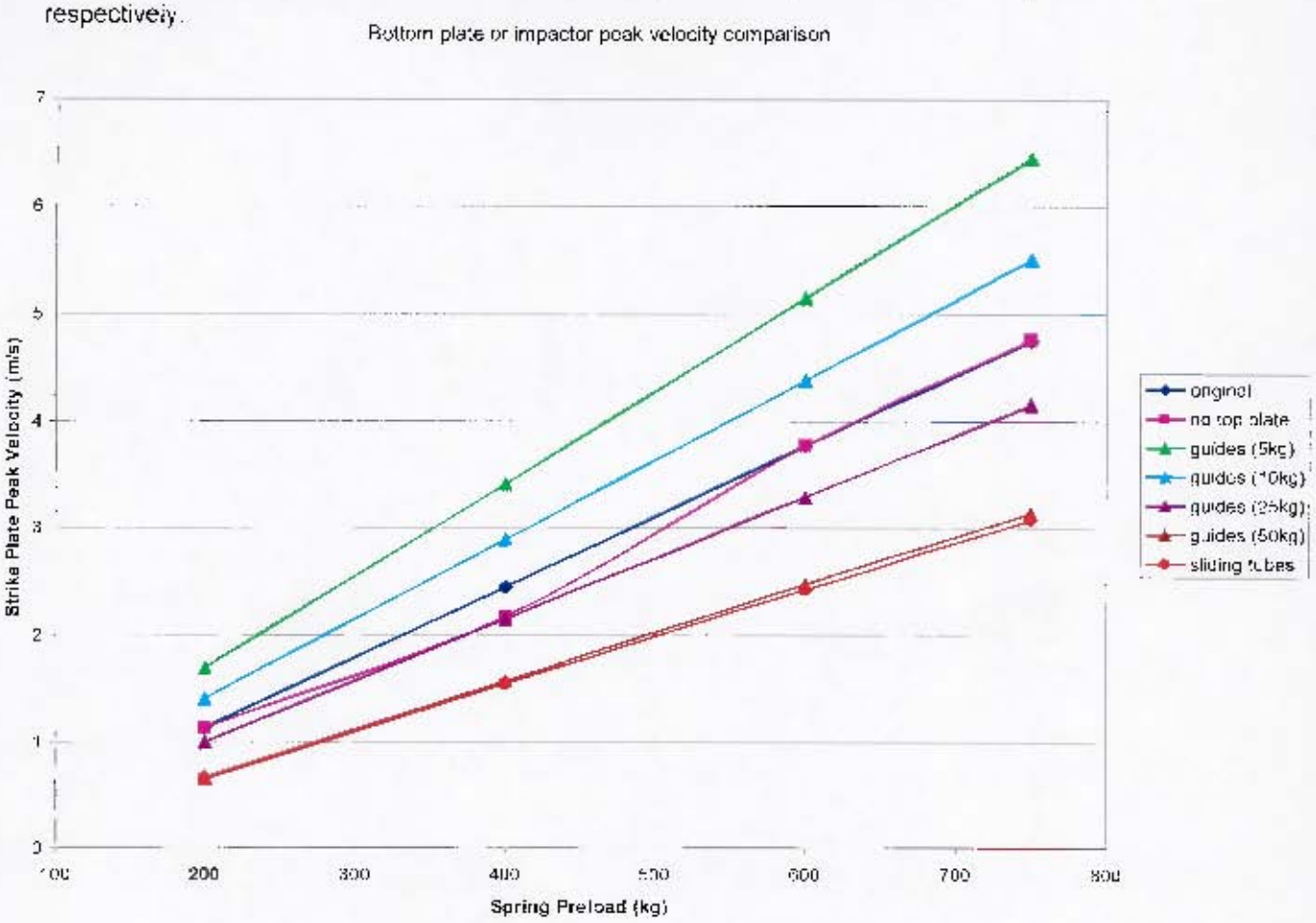

Figure 88: Graph showing bottom plate or impactor peak velocities for simulated modifications (by R Ahmed).

Figure 88 confirms the fact that decreasing the mass of the impactor or bottom plate (against which the spring must work) increases the peak velocity of the impactor or bottom plate [16]

[16] It may at first appear incorrect in Figure 88 that the peak velocity with no top plate is the same as the original which does have a top plate. However, it is intuitively realised that the peak velocity with no top plate would be the peak velocity of the bottom plate which is what is plotted for the original case.

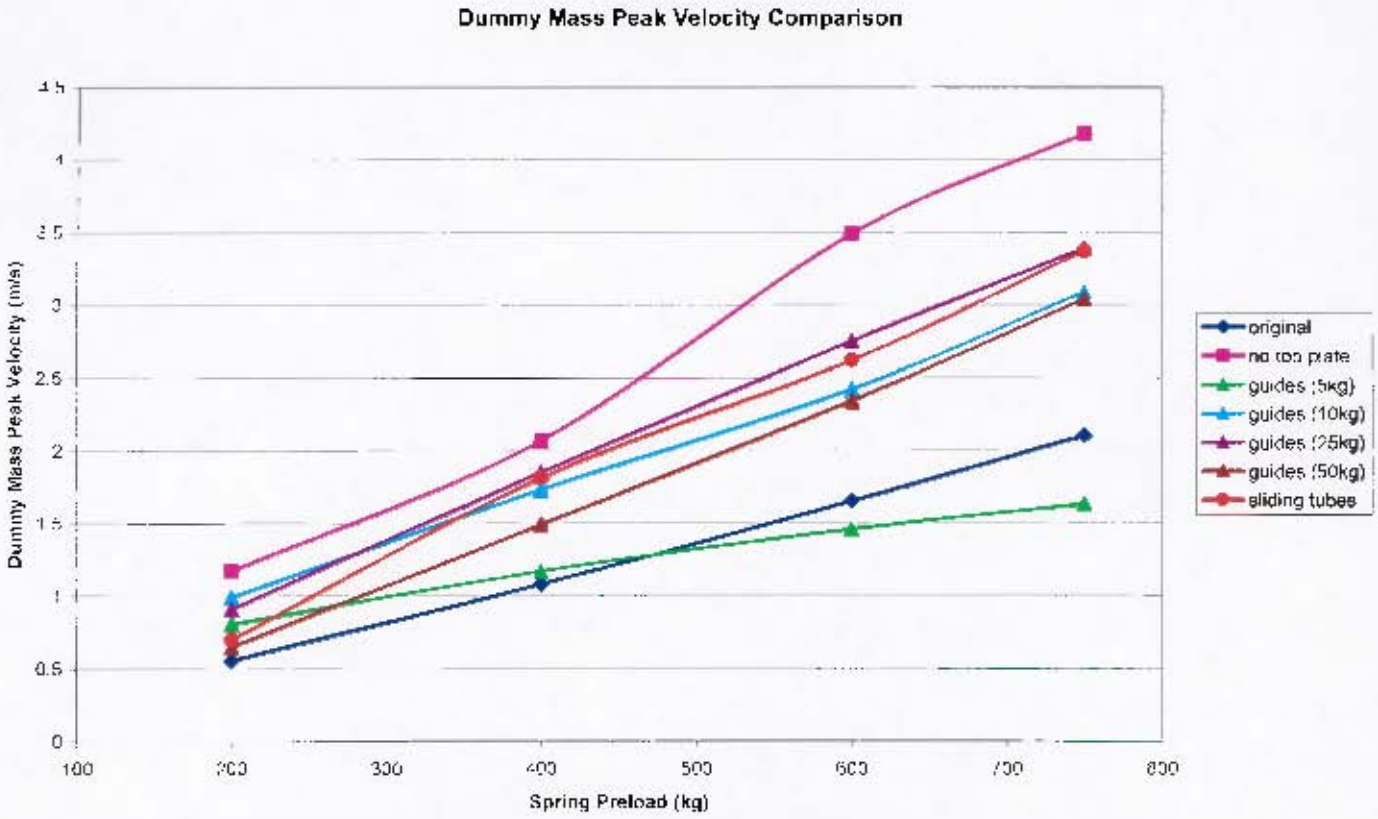

Figure 89: Graph showing dummy mass peak velocities for simulated modifications (by R Ahmed).

At first glance, Figure 89 may appear suspicious as the dummy mass peak velocity does not behave in the same manner as the impactor peak velocity in that it does not increase as impactor mass decreases. However, this can be explained by considering the momentum of the system. A larger mass can transfer more momentum as it is proportional to the mass multiplied by the velocity. This concept was clearly explained in a chapter of [14] which describes the elementary aspects of inelastic impact. If a stationary mass M_1 is struck by a mass M_2 travelling with an initial velocity V_2, conservation of linear momentum demands that:

$$M_2 V_2 = (M_1 + M_2) V_2$$

where V_2 is the common velocity of both masses immediately after an inelastic impact [14]. If $M_2 >> M_1$ then approximately no kinetic energy is lost during the event. The initial kinetic energy (E_k) of mass M_2 is $E_k = M_2 (V_2)^2$. Thus, if the kinetic energy before the impact is equal to the kinetic energy after the impact, the amount of kinetic energy (E_k) to be transferred to mass M_1 is directly proportional to both M_2 and V_2. Thus one can increase the kinetic energy transferred to M_1 by increasing the moving mass M_2 and/or the initial velocity of the moving mass V_2

Figure 89 clearly shows that the maximum dummy mass peak velocity achievable increases for all the modification proposals (except the 5kg guiding tubes).

The results of varying the spring stiffness are presented in Figure 90. It can be seen that the peak force and top plate peak velocity increase as spring stiffness increases.

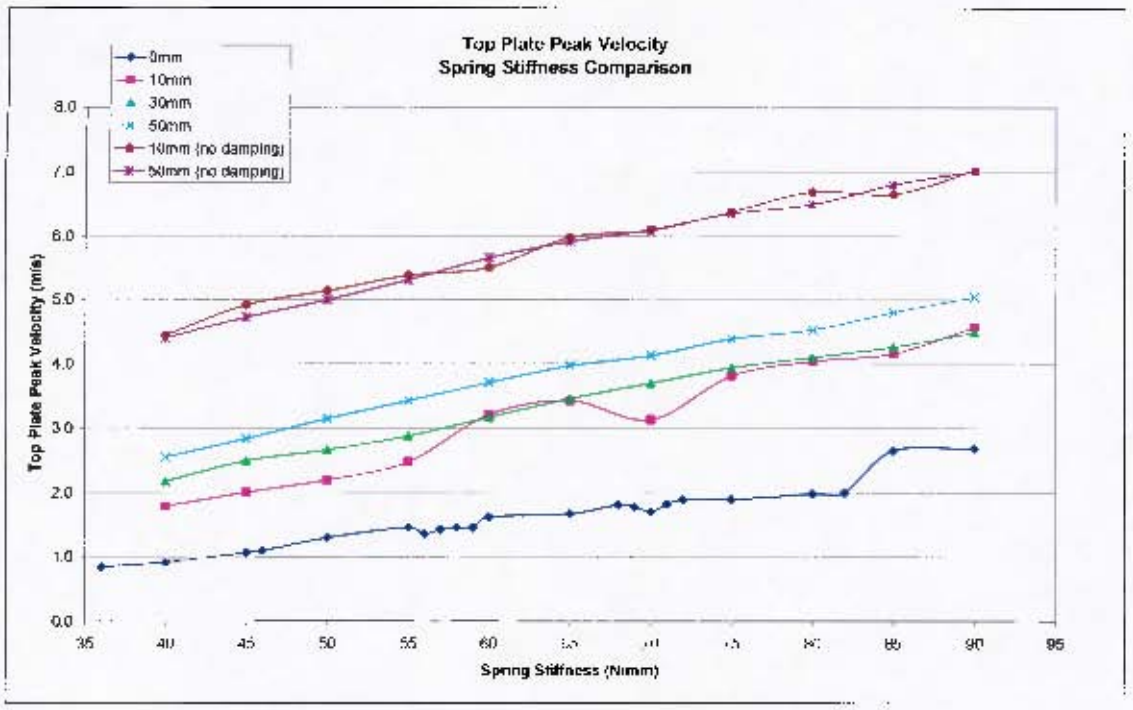

Figure 90: Top plate peak velocity with varying spring stiffness (by R Ahmed).

However, as mentioned before, using multiple springs with differing spring stiffness may not be practical. Thus, a longer spring with the same spring stiffness as the current spring was considered and the simulation results are presented in Table 25 and Figure 91.

Table 25: Simulation results using a longer spring (by R Ahmed).

Simulation Results – Longer Spring Length (Sliding Tubes)			
Preload (kg)	Strike Plate Peak Velocity (m/s)	Dummy Mass Peak Velocity (m/s)	Peak Force on Dummy Mass (kN)
200	0.679	0.658	16.68
400	1.58	1.49	22.54
600	2.48	2.37	42.81
750	3.16	3.12	54.59
900	3.83	3.61	60.83
1050	4.51	4.34	71.26
1200	5.18	5.08	82.43

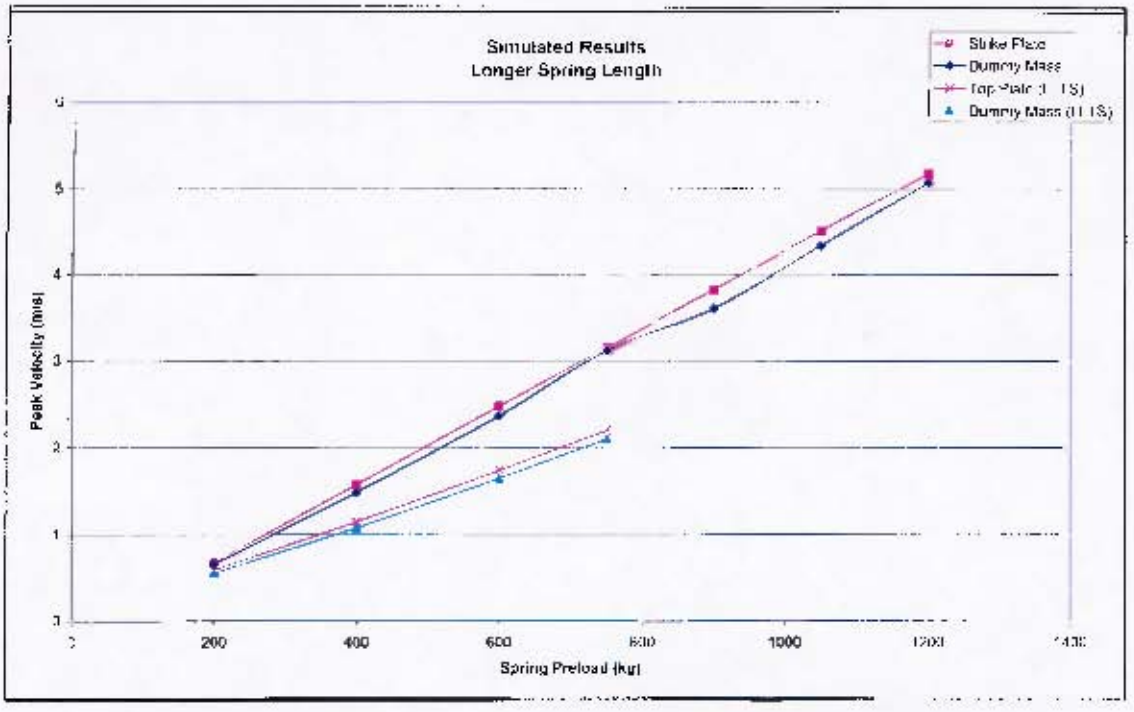

Figure 91: Graph of peak velocities achieved using a longer spring (by R Ahmed).

The two upper lines in the graph in Figure 91 represent the impactor (strike plate) and dummy mass peak velocity results from the simulation using the longer spring, while the lower lines in the graph are the top plate and dummy mass peak velocity results from the original simulation of the LLTS.

Comparing the two sets of graphs, we can see that an increase in the length of the spring can result in an increase in the peak velocities.

3.2 Description of modifications made to LLTS

The LLTS was modified and renamed the LLI (See Figure 92). The basic operation principles of the LLI are as follows

- Position the foot on the impactor plate. The required position can be obtained by lifting or lowering the drop test rig seat and then using the seat height adjustment system to secure the position. The angle of the limb can be set by loosening the bolts on the adjustable base plate, moving the spring system backwards or forwards and then tightening the bolts on the base plate to secure the system to the ground. Further angle adjustment to the foot can be achieved using the piping attached to the seat of the drop test rig to suspend the foot using flat tie-downs.

- Hook the hydraulic slave cylinder to the impactor plate and pump the hydraulic master cylinder to compress the spring until the desired preload is achieved (This can be read off the force gauge attached to the hydraulic master cylinder).

- Insert the foot pedal piping into the foot pedal adaptor. Release the compressed spring by standing on the foot pedal piping.

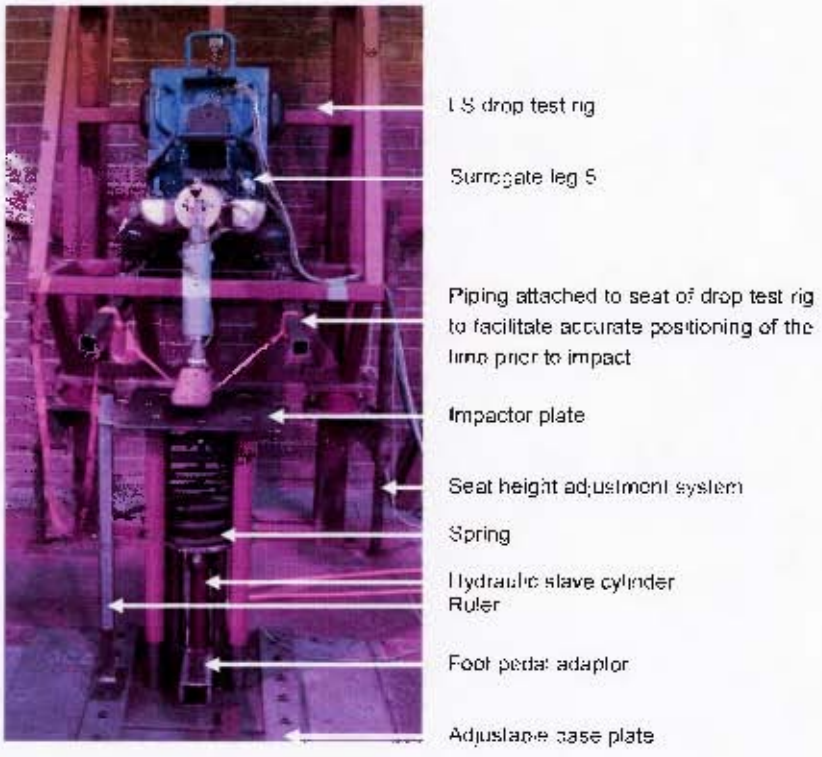

Figure 92: Labelled diagram of the LLI.

The details of the modifications are described as follows:

- The top and bottom plates of the original LLTS were removed and replaced with an impactor system. The modified system reduced the weight upon which the spring must act. This in turn increased the peak velocity of the impactor plate and thus increased the peak force that was applied to the surrogate leg. The spring can thus be compressed vertically and not at an angle. An alternative compression mechanism and release mechanism was implemented with the use of a hydraulic system (See Figure 93).

Figure 93: Hydraulic master cylinder (pump system) with force display pressure gauge.

Figure 94 shows the bearings that were used at the top and bottom ends of the hydraulic slave cylinder to make the release mechanism more efficient. Figure 95 shows the release mechanism during the manufacture and development process of the LLI.

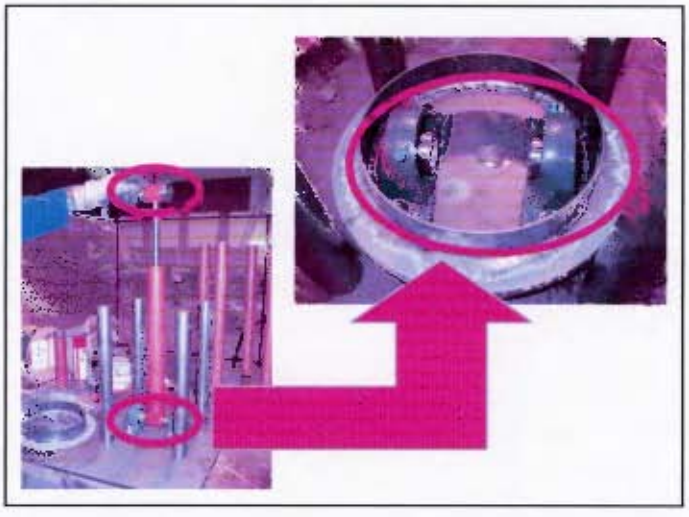

Figure 94: Diagram showing the bearings that were used at the top and bottom of the hydraulic slave cylinder.

Figure 95: Diagram showing the release mechanism during the manufacture of the LLI.

- The sliding tubes concept as described and simulated in section 3.1.9 was implemented to guide the spring when it is released. Figure 96 shows how the sliding tubes concept was implemented during the manufacture of the LLI.

Figure 96: The sliding tubes concept being implemented during the manufacture of the LLI.

- It was initially recommended after the characterisation of the original LLTS that in order to further increase the peak forces applied to the surrogate limb a longer spring should be purchased. However, it was decided to first observe the peak forces that could be achieved with the current spring in the LLI before another spring was purchased. As the spring is no longer compressed and released at an angle and the wasteful movements in the plates will no longer be an issue, and as the mass against which the spring must act is greatly reduced and thus the velocity of the impactor plate increased, it was felt that the original spring should perform better in the LLI than in the original LLTS.

- The LS drop test rig was used to position the limb on the impactor plate (See Figure 92 and Figure 97). All modifications to the drop test rig to enable it to be used with the drop test rig were designed to be removable. Thus the drop test rig can be converted back for drop testing and the modifications can be used with another drop test rig or seat system should the LLI be relocated at any stage. One of the recommendations for the modification of the original LLTS was to add extra strengthening to the base of the LLTS to stabilise the system. With the system being securely mounted to the cement floor this was no longer necessary. The frame of the original LLTS was abandoned as it introduced unnecessary vibrations to the system and was unnecessary in the modified system where the seat and impactor system are separate entities.

Figure 97: Threaded bar and wing-nut mechanism that forms the seat height adjustment system.

3.3 Characterisation of LLI

The LLI was characterised to determine whether its functionality was an improvement on the original system. This was assessed in terms of the aim of the system which was to provide a repeatable signal that was representative of that which a limb could experience within a vehicle subjected to a landmine blast. In order to characterise the system, firstly the spring constant was validated and then various surrogate limbs were used to record measurements which could then be compared to those obtained using the original LLTS, the TROSS™, the drop test rig and actual vehicle test results.

3.3.1 Spring constant validation

The spring was again characterised within the LLI system as discrepancies arose regarding the spring constant obtained using the original LLTS and the constant specified by the spring manufacturer (See section 3.1.1 for further details). A ruler was erected beside the spring with a marker attached to the impactor plate to minimise the human error introduced when reading the displacement values (See Figure 98).

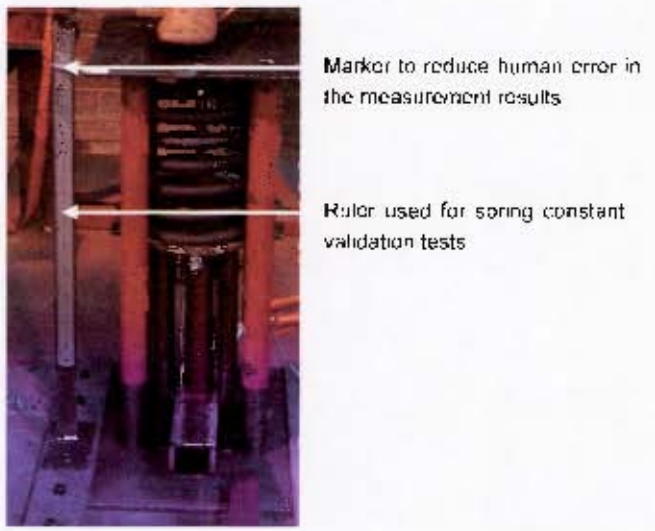

Figure 98: LLI setup for spring constant validation.

The test was repeated three times so that an average value could be obtained. The results are listed in Table 26 to Table 28.

Table 26: Sample 1 of spring preload force and spring displacement readings to validate the spring constant.

Sample 1		
Force (N)	Displacement reading (mm)	Change in displacement (m)
0	7	
1000	17	0.010
2000	32	0.025
3000	50	0.043
4000	66	0.059
5000	84	0.077
6000	103	0.096
7000	119	0.112
8000	135	0.128
9000	151	0.144
10000	164	0.157

Table 27: Sample 2 of spring preload force and spring displacement readings to validate the spring constant.

Sample 2		
Force (N)	Displacement reading (mm)	Change in displacement (m)
0	7	
1000	16	0.009
2000	31	0.024
3000	49	0.042
4000	67	0.060
5000	85	0.078
6000	103	0.096
7000	119	0.112
8000	136	0.129
9000	151	0.144
10000	165	0.158

Table 28: Sample 3 of spring preload force and spring displacement readings to validate the spring constant.

Sample 3		
Force (N)	Displacement reading (mm)	Change in displacement (m)
0	7	
1000	15	0.008
2000	32	0.026
3000	49	0.042
4000	67	0.061
5000	86	0.079
6000	102	0.096
7000	118	0.111
8000	135	0.129
9000	150	0.144
10000	165	0.159

The spring constants derived from each of the different samples showed excellent repeatability and were within 0.5% of one another (See Figure 99). This indicates great confidence in the spring constant obtained from the plots. An additional trend line was fitted to a graph containing every test point as a separate entity in each of the three samples (See Figure 100). This produced a very similar value for the spring constant and was within 0.002% of the average spring constant obtained from plotting the test points from each sample separately. The details are described below.

The average spring constant obtained from Figure 99 was:

- 59.373kN/m.

The spring constant obtained from Figure 100 was:

- 59.371 kN/m.

Thus, a spring constant of 59.37kN/m was determined in both in Figure 99 and Figure 100.

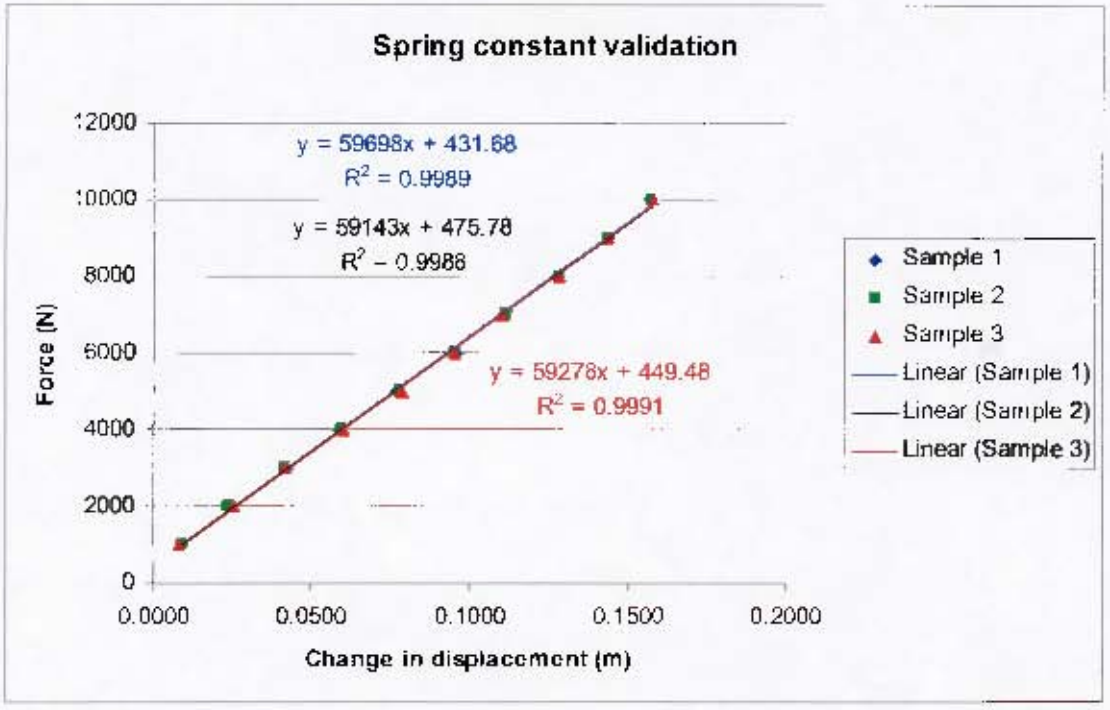

Figure 99: Graph showing the spring constants derived from each of the 3 sample sets.

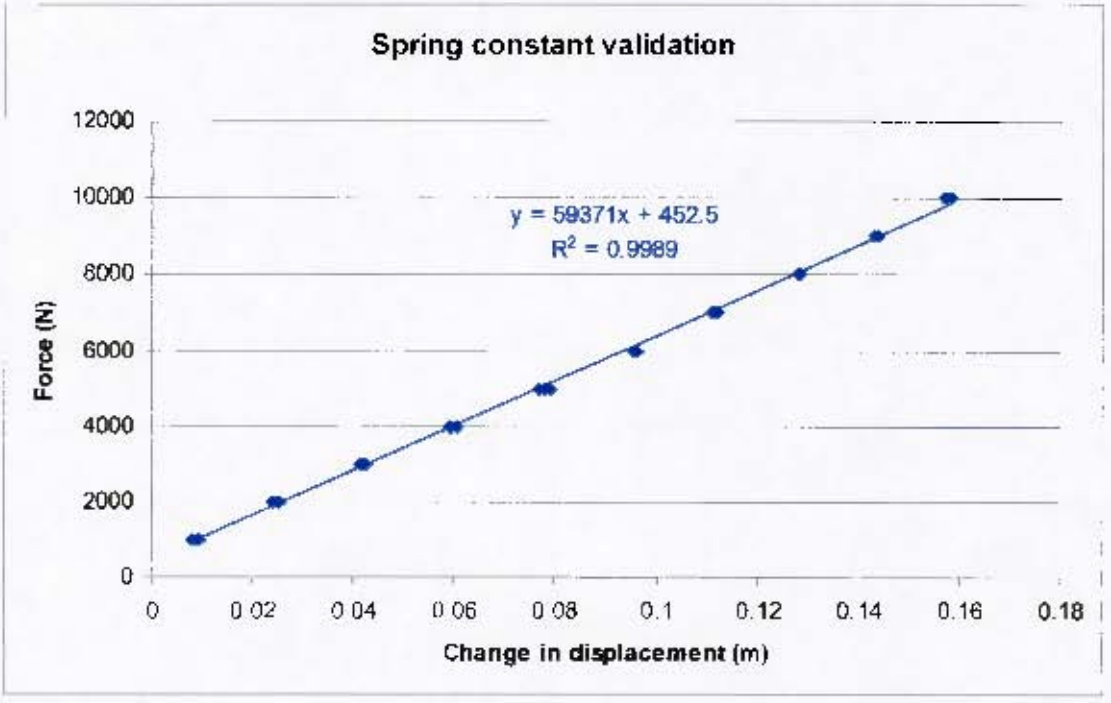

Figure 100: Graph showing the spring constant derived by plotting all 3 sample sets in the same series.

Check using basic spring calculations:

The spring constant and other spring specifications were used, as before, to calculate the maximum force that a spring of a certain length should be able to achieve.

The following specifications were provided by the spring manufacturer:

- Spring stiffness 49.36N/mm (49.36kN/m)
- Free length 402mm
- Bar diameter 25mm.
- Number of coils 8.25

Using these measurements the maximum spring preload was determined:

- Maximum compression = 402mm – (8.25 x 25mm) = 195.75mm.
- Maximum spring preload = 195.75 x 49.36 = 9662.22 N.

However, using the spring stiffness that was derived from the LLI, the maximum spring preload can be calculated as follows:

- Maximum spring preload = 195.75 x 59.37 = 11621.68 N.

This seemed like a reasonable value as the spring was not fully compressed by 10kN preload during the spring constant validation tests. The fact that the spring could be compressed to 10kN in practice, but calculating the maximum spring preload using the data provided by the manufacturer gives only 9.7kN, indicates that the spring constant provided may be incorrect

3.3.2 Description of tests conducted

Initially it was decided that a loose mass should be used in place of the surrogate leg to characterise the LLI. This would eliminate variables and degrees of freedom that would be introduced by the leg, however due to safety considerations it was decided that a loose mass could not be safely used with the current setup. It was thus decided that a surrogate leg should be used as before. This also allowed the LLI test results to be compared to the characterisation tests performed using the original LLTS. In addition to this two adaptor modules were manufactured for use with the surrogate leg to reduce the inherent degrees of freedom and possible variability in the response of the limb. Firstly, a discarded Hybrid III ATD foot (as was used on the surrogate leg) was modified to allow the moving ankle joint to be replaced with a solid structure. Secondly, the foot was replaced with a stiff steel foot of similar mass to eliminate the damping that would be introduced by the prosthetic rubber coating of the Hybrid III ATD foot.

Thus, the LLI was characterised using a surrogate leg setup in four different configurations:

- Setup 1: Surrogate leg 5 as is with shoe (as was used during the characterisation of the original LLTS). The foot with the boot weights 2.3kg.

- Setup 2. Surrogate leg 5 with shoe removed (to eliminate any variables that the shoe may introduce). The foot without the boot weights 1.3kg. Figure 101 shows this setup.

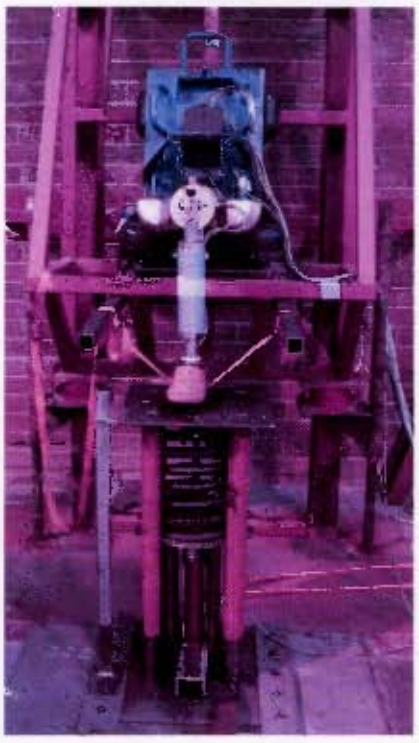

Figure 101: The LLI with the surrogate leg for setup 2.

- Setup 3: Surrogate leg 5 with adapted foot (See Figure 102) attached directly to the lower limb (to remove the degrees of freedom introduced by the ankle). The foot without the moving ankle joint weighs 1.3kg.

Figure 102: Adapted foot with no ankle joint for setup 3.

- Setup 4: Surrogate leg 5 with the steel foot (to remove the damping introduced by the prosthetic rubber coating the Hybrid III foot). The steel foot weights 1.2kg. The steel foot is shown in Figure 103.

Figure 103: Adapted steel foot for setup 4.

Using these four different setups, the effect that the surrogate limb properties have on the characteristics of the force transferred from the LLI was assessed.

The following test procedure was followed to characterise the LLI:

- The spring was characterised in the LLI (where it was compressed vertically) to confirm the spring stiffness indicated by the manufacturer. This was done by taking a range of displacement and force measurements whilst compressing the spring. Approximately 10 measurements were taken at 1kN intervals up to a spring preload of 10kN. This process was repeated 3 times and an average obtained for the actual spring stiffness.

- A series of tests were conducted without the surrogate leg in the system in order to evaluate the input plate velocity to the system both with and without a surrogate limb. 5 samples were taken at spring preloads of 4kN, 6kN, 8kN and 10kN. The test domain for Setup 1 is shown in Table 29.

Table 29: Test Domain for Setup 1 without a surrogate leg

Spring preload (kN)	Number of samples
4	5 samples
6	5 samples
8	5 samples
10	5 samples

- In order to characterise the LLI with a surrogate leg a single offset was chosen 30mm below the impactor plate rest position. This translates to the spring being compressed until the impactor plate was pulled down by 30mm. The foot was then positioned on the LLI impactor plate whilst it was slightly preloaded This ensures that the impact occurred between the foot and the impactor plate before the spring extended beyond its rest position.

- The spring was preloaded to 4kN[17], 6kN, 8kN and 10kN. 5 samples were taken with the surrogate leg joint torques set to 6Nm and another 5 samples with the joint torques set to 25Nm at each of the specified preloads The test domain for Setup 1 is shown in Table 31.

Table 30: Test Domain for Setup 1

Spring preload (kN)	6Nm joint torque	25Nm joint torque
4	5 samples	5 samples
6	5 samples	5 samples
8	5 samples	5 samples
10	5 samples	5 samples

- For setup 2, 5 samples were taken at 4kN and 6kN for both 6Nm and 25Nm joint torques. 1 sample was taken at 8kN for 6Nm joint torque. but as the axial lower tibia force exceeded 20kN testing was discontinued at this point to prevent damage to the surrogate leg and to ensure that the implementation of the calibration factor for the lower tibia load cell remains valid[18]. The test domain for Setup 2 is shown in Table 31.

Table 31: Test Domain for Setup 2

Spring preload (kN)	6Nm joint torque	25Nm joint torque
4	5 samples	5 samples
6	5 samples	5 samples
8	1 sample	0 samples

[17] Initialy tests were to be conducted at 2kN. but the spring could not compress to the 30mm offset with the 2kN spring preload.

[18] The surrogate leg load cells have a full scale capacity of 20kN and thus the calibration factor cannot meaningfully be applied beyond this value.

- For setup 3 5 samples were taken at 4kN, 6kN and 8kN for the 25Nm joint torque setting. Testing could not continue to 10kN as the axial lower tibia force at 10kN would exceed 20kN. The modified ankle joint was found to be damaged (See Figure 104 and Figure 105) after the 8kN set of tests and thus testing could not be conducted for the 6Nm joint torque. The test domain for Setup 3 is shown in Table 32.

Table 32: Test Domain for Setup 3

Spring preload (kN)	25Nm joint torque
4	5 samples
6	5 samples
8	5 samples

Figure 104: Photograph of damaged weld on modified ankle joint.

Figure 105: Photograph of bent bolt from modified ankle joint.

- For setup 4 the spring could only be loaded to 4kN before the limit of the tibia load cell was exceeded. At the 6Nm joint torque setting, 1 sample was taken at 6kN spring preload, but the limit of the tibia load cell was exceeded. Another sample was taken at 5kN spring preload, but this too exceeded the limit of the tibia load cell. The test domain for Setup 4 is shown in Table 34.

Table 33: Test Domain for Setup 4

Spring preload (kN)	6Nm joint torque	25Nm joint torque
4	5 samples	5 samples
5	1 sample	0 samples
6	1 sample	0 samples

- In addition to the effect that the various surrogate leg setups have on the functioning of the LLI, it was decided to investigate the effect of increasing the mass of the impactor plate and to compare results with yet another human surrogate limb, the Hybrid III ATD surrogate limb. The Hybrid III ATD was used in addition to the surrogate leg to allow the LLI results to be compared to results obtained using the TROSS™. A steel plate weighing 7.8kg was manufactured and was mounted on the LLI impactor plate (See Figure 106).

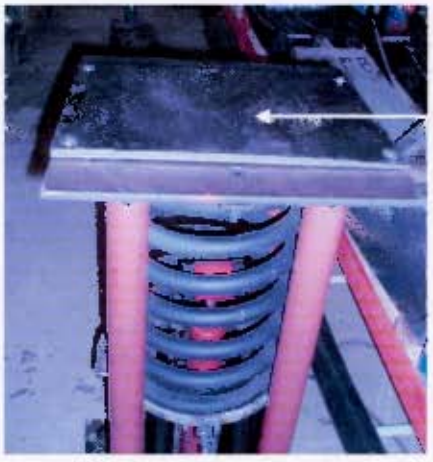

Steel plate bolted onto the LLI impactor plate

Figure 106: Steel plate mounted on the LLI impactor plate.

3.3.3 Instrumentation for characterisation

The following transducers were used in order to characterise the LLI (See Figure 107 for the location of the transducers).

- Two 500g accelerometers were fitted to the impactor plate (Setups 3 and 4 were only be fitted with one accelerometer as the results showed that the impactor plate moved up straight and not at fluctuating angles to the horizontal).
- One 500g accelerometer was fitted to the surrogate leg foot or adapted foot.
- Surrogate leg 5 was fitted with a load cell in the lower tibia.
- Hybrid III ATD with an ankle load cell, lower tibia load cell and foot accelerometer.

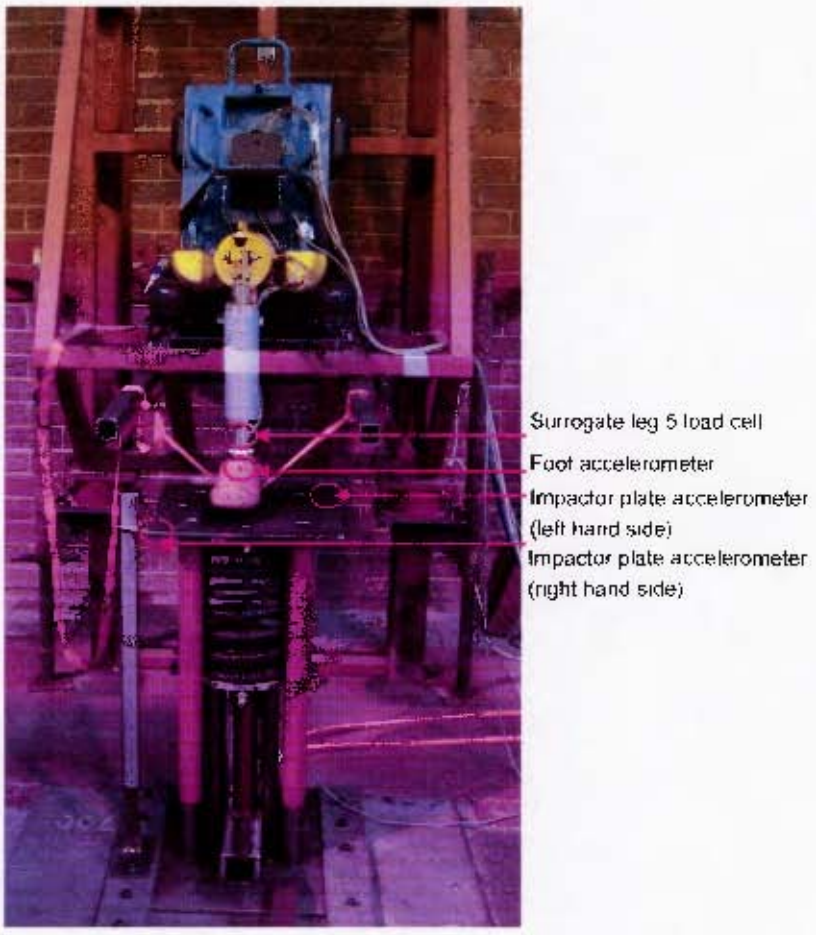

Figure 107: Diagram showing the location of transducers on the LLI and surrogate leg 5.

The hydraulic master cylinder was fitted with a calibrated force gauge (See Figure 108) and both the hydraulic master and slave cylinders were inspected, repaired and given a safety rating (See Appendix A3 for calibration information).

Figure 108: Photograph of the hydraulic master cylinder (pump) and the calibrated force gauge.

Table 34 shows the relevant serial numbers of the instrumentation and the sensitivities of the transducers. All calibration certificates and documentation can be found in Appendix A2.

Table 34: Description of the instrumentation used in the characterisation of the LLI and the sensitivities of the transducers.

Instrumentation description:	Serial number:	Sensitivity:
Surrogate leg 5	5	N/A
Surrogate leg 5 load cell	5	0.00010mV/N
Surrogate leg 5 500g foot accelerometer	0639-005	0.086mV/g
Impactor plate 500g accelerometer (left hand side)	0639-013	0.085mV/g
Impactor plate 500g accelerometer (right hand side)[19]	0639-008	0.085mV/g
Hybrid III ATD 2	294	N/A
Hybrid III ATD foot accelerometer	6491-003	0.107mV/g
Hybrid III ATD lower tibia load cell	3287-792	Fz=0.00048mV/N Mx=0.03685mV/Nm My=0.03715mV/Nm
Hybrid III ATD ankle load cell	4218J-80	Fx=0.00126mV/N Fy=0.00127mV/N Fz=0.00048mV/N Mx=0.01931mV/Nm My=0.01914mV/Nm
ATD DAQ data acquisition system	01062006	N/A
LEG DAQ data acquisition system	05062006	N/A
Hydraulic pump and cylinder	(ENERPAC P84 hand pump, medium pressure double acting cylinder)	N/A (calibrated with hydraulic cylinder force gauge)
Hydraulic cylinder force gauge	147851	N/A

[19] The right hand side impactor plate accelerometer was removed from the plate and used as a foot accelerometer with the adapted foot modules as surrogate leg 5 foot accelerometer stopped working.

3.3.4 Data acquisition, processing and analysis

Data acquisition:

Data was acquired using two Compact RIO DAQ systems. The signals were sampled for 2 seconds at 10kHz, 0.25 seconds of which was pre-trigger data.

Data processing:

The signals were processed in Matlab™ where the offset was subtracted from each of the channels and the calibration factors (calculated from the sensitivities of the transducers and the channel gains and excitation voltages) were applied. Filtering was also conducted in accordance with AEP-55 Volume 2 [3]. The script files that were used to process the data were named as follows:

- *data reader_llts_version1.m* – Used to process the LLI results obtained without a surrogate on the system and the results obtained using setup 1.
- *data_reader_llts_version2.m* – Used to process the LLI results obtained with a surrogate leg using setup 2, 3, 4 and the results obtained using an additional mass plate on the LLTS impactor plate[23].
- *data reader_llts_ATD_version1.m* – Used to process the LLI results obtained with the Hybrid III ATD.

Data analysis:

The manner in which the data was analysed played a large role in the results that were obtained. There is often no standard rule as to how to analyse the data and thus certain decisions were made regarding the analysis of the results. However, as the results could be analysed differently depending on the focus of the research, each of the test graphs were presented in the *Detailed Results* document that can be found on the disk accompanying this dissertation. This will allow the results to be analysed in an alternative manner should the need arise in the future. A typical example of the graphs that were provided in this document was outlined below.

[23] Version 1 and 2 of this code is different as the LLI impactor plate (right hand side) accelerometer was used as the foot accelerometer in tests conducted after setup 1.

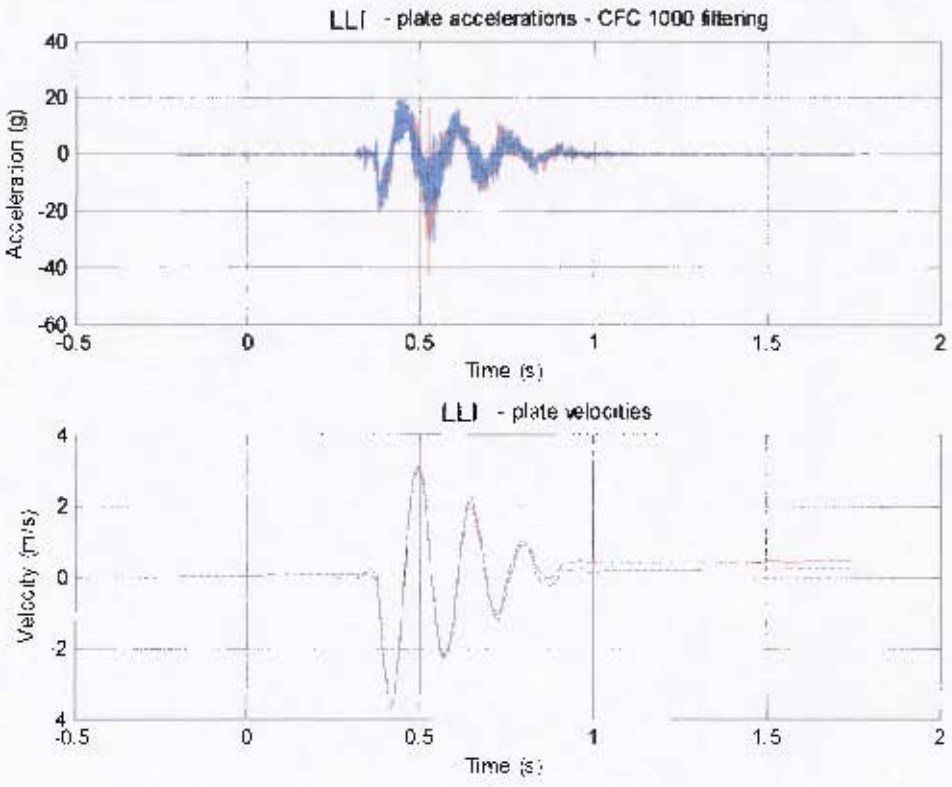

Figure 109: A typical example of the impactor plate accelerations (red - right hand side, blue - left hand side) and velocities that are presented in the *Detailed Results* document.

Whilst most of the graphs in the *Detailed Results* document display similar shapes and trends, unusual results were occasionally recorded by the right hand side impactor plate accelerometer (See Figure 110). A study of the notes made during the testing revealed that the unusual results corresponded with a bending of the ruler marker that occurred on multiple occasions. As the ruler marker was mounted above the right hand side impactor plate accelerometer (making use of the same holes that were drilled into the steel impactor plate), it would seem plausible that if this marker caught on the ruler during the test that it should influence the recorded acceleration.

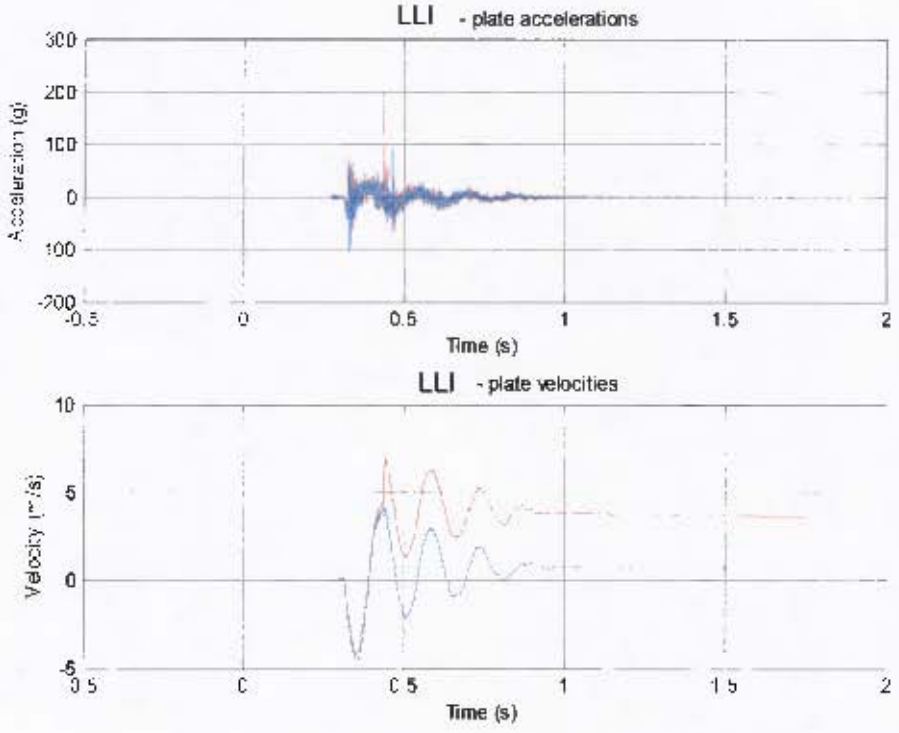

Figure 110: Unusual impactor plate acceleration and velocity (red - right hand side, blue - left hand side) for the 8kN spring preload case.

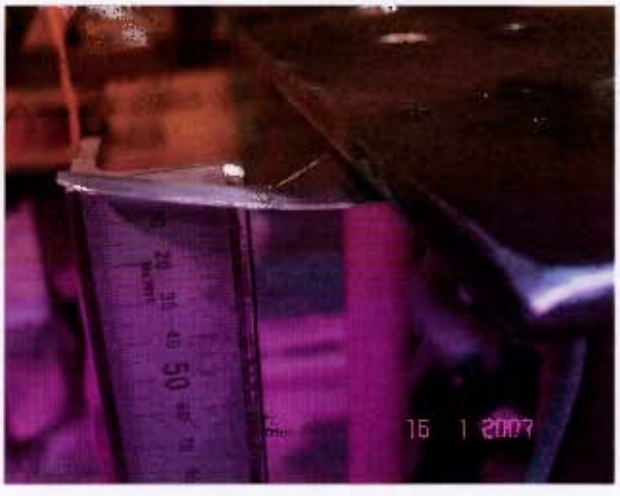

Figure 111: Photograph of bent ruler marker.

The data that needed to be extracted form the results in order to characterise the LLI was the peak leg force and peak impactor plate velocity and the durations of these peaks. The peak leg force and peak impactor plate velocity were obtained directly from the filtered results. However, the determination of the durations of these peaks proved less obvious. To illustrate this point an impactor plate velocity (red) and a leg force (blue) were plotted in Figure 112 (Note: The figure is not to scale as it is merely to illustrate a point). If the duration of the peak velocity was obtained for the y-axis zero crossing, the duration would be approximately 0.6s (See the green line in Figure 112). However, this did not seem to accurately reflect the duration of the peak.

Thus, a threshold method could be applied where the y-axis -0.05m/s crossing could be used (See the navy line in Figure 112). This would appear to be a satisfactory method, but the shape of the peak may change and the same problems would be experienced using this threshold as if the zero crossing was used.

One of these problems is illustrated in Figure 112 as a slight variation in the velocity peak could cause the duration to change from 0.05s to 0.1s which is double the actual duration. Thus it was decided that a threshold value of 10% of the peak value would be the most objective way of determining the duration of the peak (See the orange line in Figure 112). The duration of the peak leg force was similarly obtained using a threshold of 10% of the peak force.

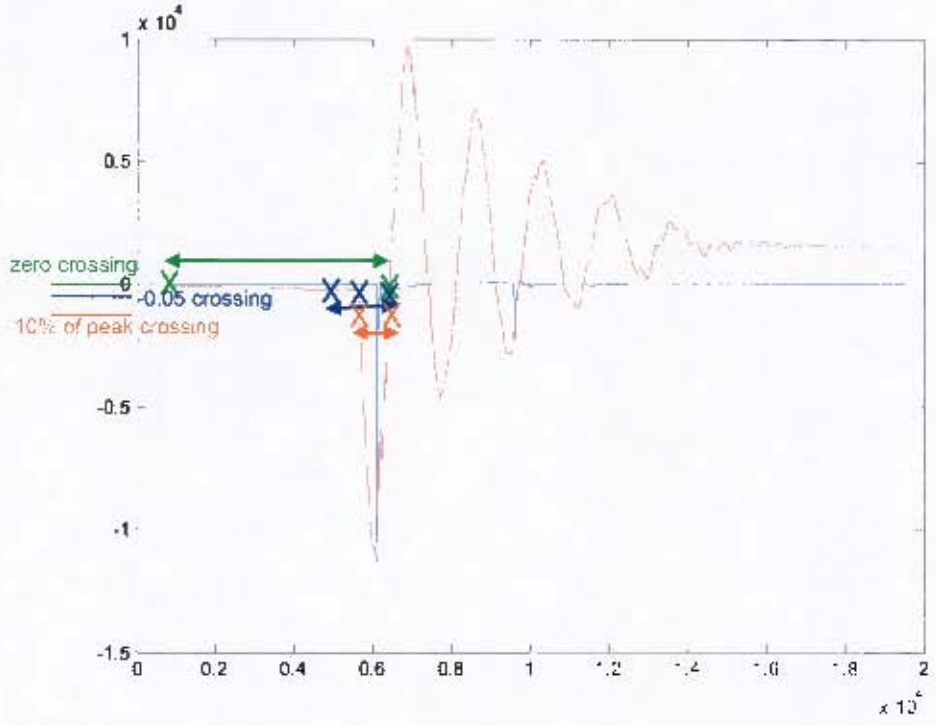

Figure 112: Illustration of the determination of the duration of the peak velocity.

Another point to note regarding the analysis of the data was the time at which the peak velocity and peak leg force occur. Without exception the peak velocity of the impactor plate was achieved before impact with the surrogate leg. This phenomenon is relevant as the impactor plate and surrogate leg results were not all analysed on the same axes, however, it plays a large role in the interpretation of the relationship between the peak leg force and peak velocity that is discussed in section 3.5.1. Figure 113 shows the peak leg force and the peak impactor plate velocity plotted at the same time. The y-axis is not to scale, but it is clear that the peak velocity occurs before the peak leg force and that the leg influences the velocity of the impactor plate after the impact has occurred. It is also clear that the leg responds more quickly than the impactor plate which would make sense since the impactor plate is heavier and thus carries with it more momentum than the surrogate leg.

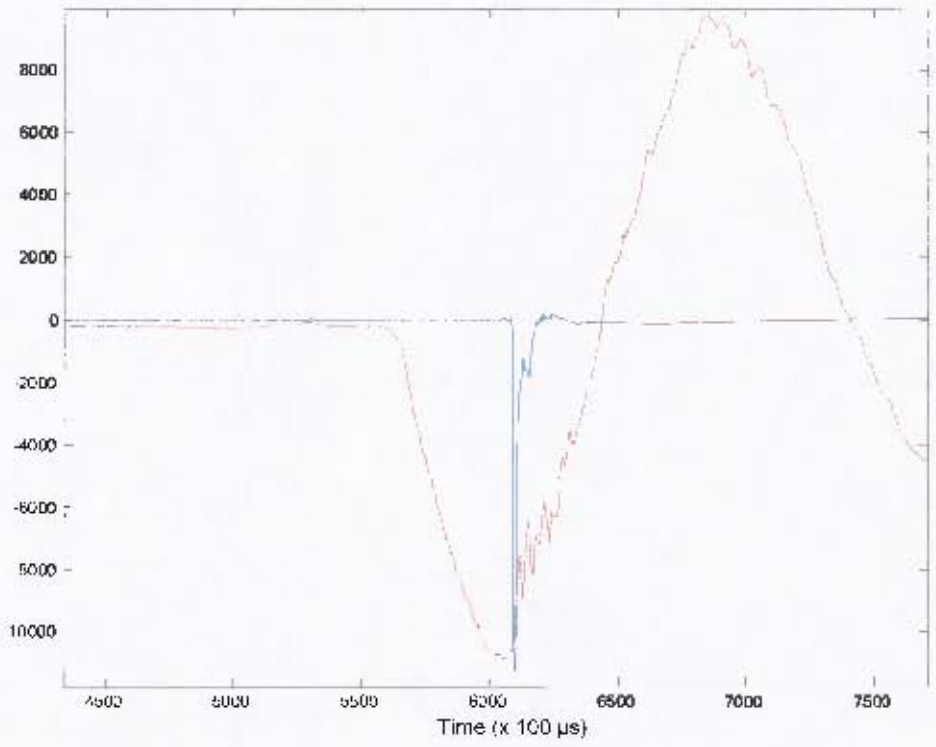

Figure 113: Graph showing the impactor plate velocity and the surrogate leg force.

3.3.5 Summary of results of LLI characterisation

The LLI was characterised using the same surrogate leg as was used to characterise the original LLTS to allow the functionality of each of the systems to be meaningfully compared. In addition, a series of tests were conducted without the surrogate leg in the system in order to evaluate the input plate velocity to the system both with and without a surrogate limb. This would allow one to ascertain the effect that the surrogate leg has on the system during operation. The peak plate velocity and peak leg force were measured at various spring preloads and the repeatability was assessed in each setup.

3.3.5.1 Characterisation without a surrogate leg

The spring was compressed to various spring preloads before being released. Samples were taken at each spring preload of 4kN, 6kN, 8kN and 10kN. The results are shown in Table 35.

Table 35: Results of characterisation of LLI without a surrogate leg.

Spring preload (kN)	Peak plate velocity 1 (m/s)	Peak plate velocity 2 (m/s)	Average peak plate velocity (m/s)	Peak plate velocity duration 1 (s)	Peak plate velocity duration 2 (s)	Average peak plate velocity duration (s)
4	2.13	1.88	2.00	0.0820	0.0768	0.0794
4	1.82	1.67	1.74	0.0773	0.0731	0.0752
6	3.72	3.60	3.66	0.0735	0.0719	0.0727
6	3.43	3.52	3.48	0.0715	0.0709	0.0712
6	3.71	3.64	3.68	0.0744	0.0720	0.0732
8	4.25	4.68	4.46	0.0703	0.0709	0.0706
10	5.62	5.89	5.75	0.0702	0.0678	0.0690
10	5.30	5.61	5.46	0.0700	0.0691	0.0696
10	5.93	6.13	6.03	0.0701	0.0718	0.0710

The first factor that is of interest in the LLI characterisation is whether there is lateral movement of the plate once the compressed spring has been released. Lateral movement may cause the outer metal cylinders mounted to the impactor plate to make contact with the inner metal cylinders mounted to the base of the system, thus reducing the peak velocity of the plate. However, by analysing the results in Table 35, it was found that the peak plate velocities were, on average, within 5.8% of one another whilst the peak plate velocity duration were within 0.02% of one another. Thus, the lateral movement of the plate is deemed to be minimal in terms of the performance of the system. Figure 114 shows a typical example of the accelerations and velocities obtained from accelerometers mounted on each side of the plate.

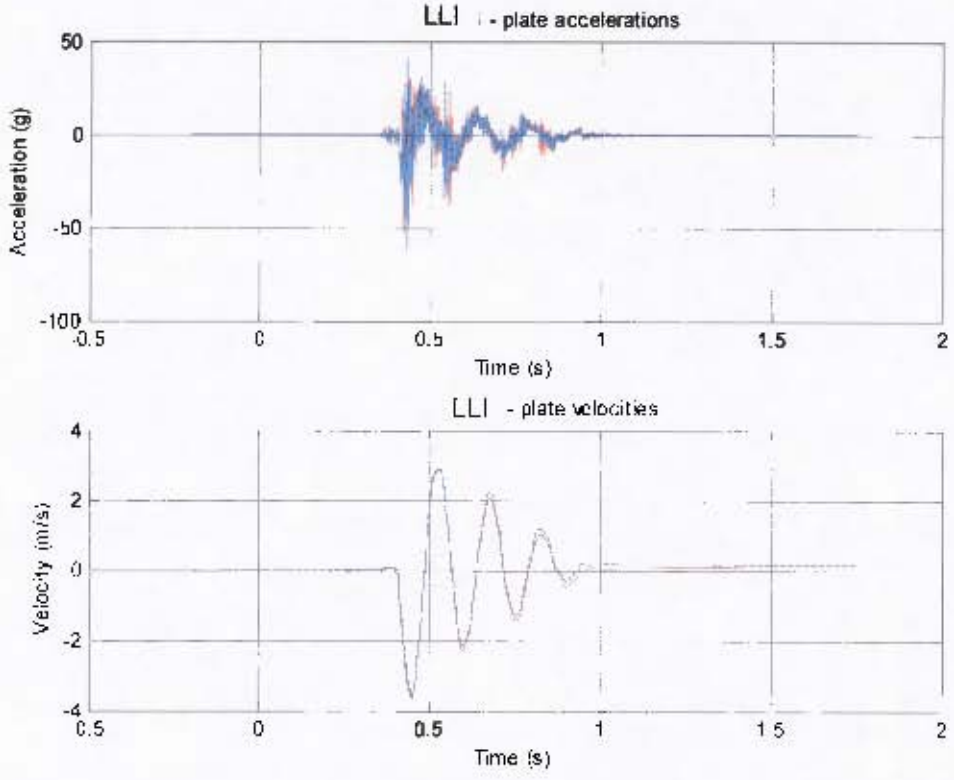

Figure 114: Graph of plate acceleration and plate velocities obtained from accelerometers mounted on each side of the impactor plate when released from a spring preload of 6kN.

The average of the two measurements obtained from each side of the plate was used in comparing the peak velocity and peak velocity duration after each test. Figure 115 shows a plot of the peak plate velocity versus the spring preload. A strong linear relationship can be observed as expected. The trend line fits the data points with an R^2 value[21] of 0.97 which is close to 1 and thus shows that the trend line is a very good fit.

[21] A trend line value is most reliable when its R^2 value is at or near 1. R^2 is known as the coefficient of determination and it is a measure of the proportion of the variation in the y-axis variable that is explained by the variation in the x-axis variable [60].

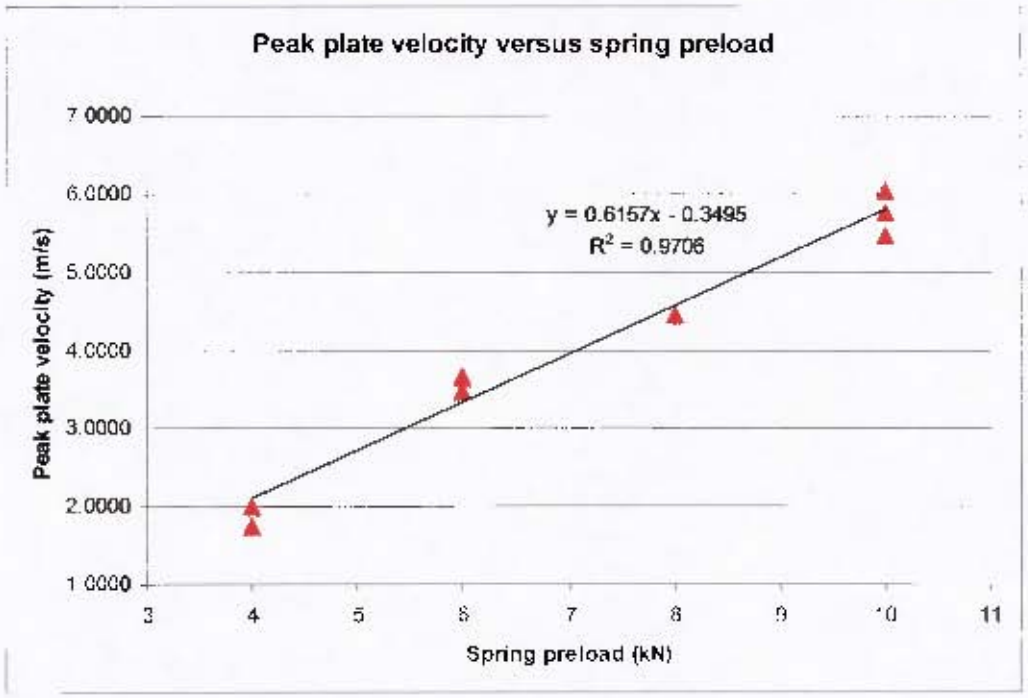

Figure 115: Graph showing the peak plate velocity versus the spring preload during the characterisation of the LLI without a surrogate leg.

Figure 116 shows a plot of the duration of the peak velocity versus the spring preload. The peak velocity duration appears to decrease as the spring preload increases as expected

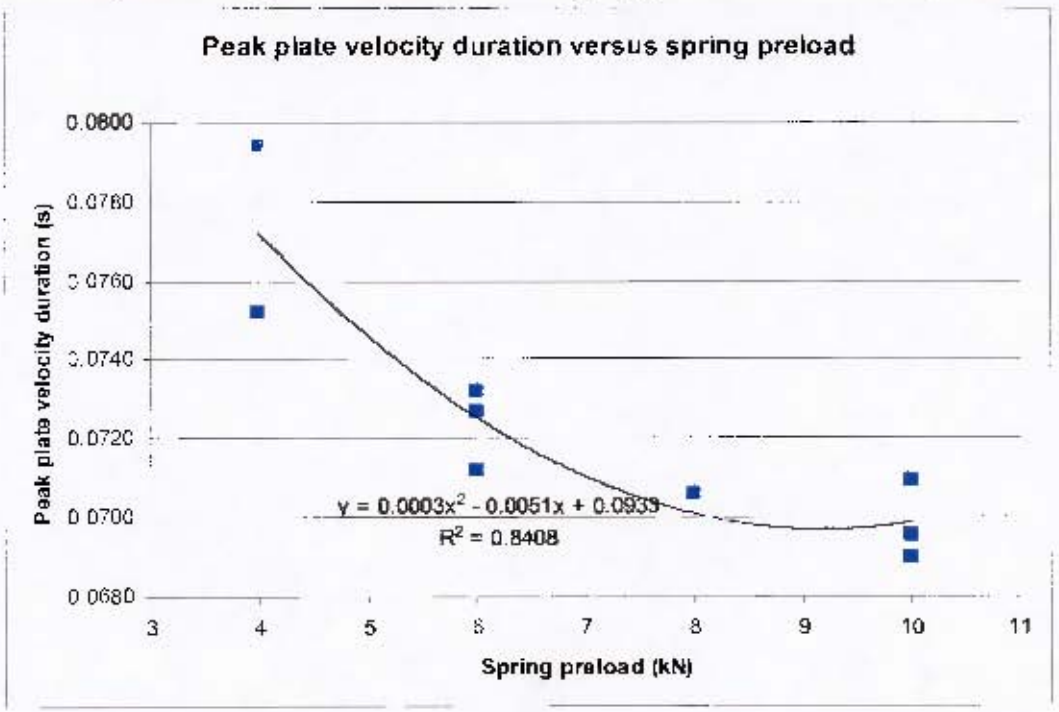

Figure 116: Graph showing the peak plate velocity duration versus the spring preload during the characterisation of the LLI without a surrogate leg.

3.3.5.2 Characterisation with a surrogate leg

A number of tests were conducted as various spring preloads in order to explore the effect that a surrogate leg has on the performance of the LLI and to allow for comparisons to be made with the original LLTS.

The results are listed in Table 36 and Table 37. The joint torque of the surrogate leg was set to 25Nm in each of the tests.

Table 36: Peak plate velocity results for characterisation of the LLI with a surrogate leg.

Spring preload (kN)	Peak plate velocity 1 (m/s)	Peak plate velocity 2 (m/s)	Average peak plate velocity	Peak plate velocity duration 1 (s)	Peak plate velocity duration 2 (s)	Average peak plate velocity duration (s)
4	1.79	1.79	1.79	0.0763	0.0773	0.0768
4	2.00	1.80	1.90	0.0790	0.0777	0.0784
4	1.98	1.74	1.86	0.0794	0.0743	0.0769
4	1.71	1.63	1.67	0.0752	0.0766	0.0759
4	1.90	1.69	1.79	0.0791	0.0759	0.0775
6	3.18	2.89	3.04	0.0716	0.0656	0.0686
6	3.15	3.11	3.13	0.0694	0.0657	0.0676
6	3.25	3.06	3.16	0.0757	0.0691	0.0724
6	3.16	3.08	3.12	0.0743	0.0704	0.0724
6	3.12	3.15	3.14	0.0692	0.0654	0.0673
8	4.23	4.34	4.28	0.0682	0.0669	0.0676
8	3.94	4.21	4.07	0.0681	0.0663	0.0672
8	4.01	4.25	4.13	0.0648	0.0664	0.0656
8	4.19	4.12	4.16	0.0676	0.0657	0.0667
8	4.04	4.12	4.08	0.0646	0.0645	0.0646
10	5.86	5.89	5.87	0.0673	0.0627	0.0650
10	5.84	5.68	5.76	0.0666	0.0623	0.0645
10	5.73	5.73	5.73	0.0642	0.0628	0.0635
10	5.66	5.66	5.66	0.0644	0.0641	0.0643
10	5.51	5.49	5.50	0.0668	0.0648	0.0658

Table 37: Peak leg force results for characterisation of the LLI.

Spring preload (kN)	Peak leg force (kN)	Peak leg force duration (s)
4	3.23	0.0092
4	3.22	0.0089
4	3.07	0.0090
4	3.17	0.0090
4	2.78	0.0099
6	7.78	0.0072
6	8.79	0.0057
6	8.77	0.0058
6	9.03	0.0056
6	8.68	0.0056
8	14.56	0.0045
8	14.45	0.0047
8	14.58	0.0046
8	14.34	0.0047
8	14.67	0.0046
10	20.01	0.0041
10	20.98	0.0040
10	21.18	0.0039
10	20.59	0.0040
10	20.39	0.0041

A very strong linear relationship between the peak plate velocity, that was measured with the surrogate leg on the LLI, versus spring preload can be seen in Figure 117

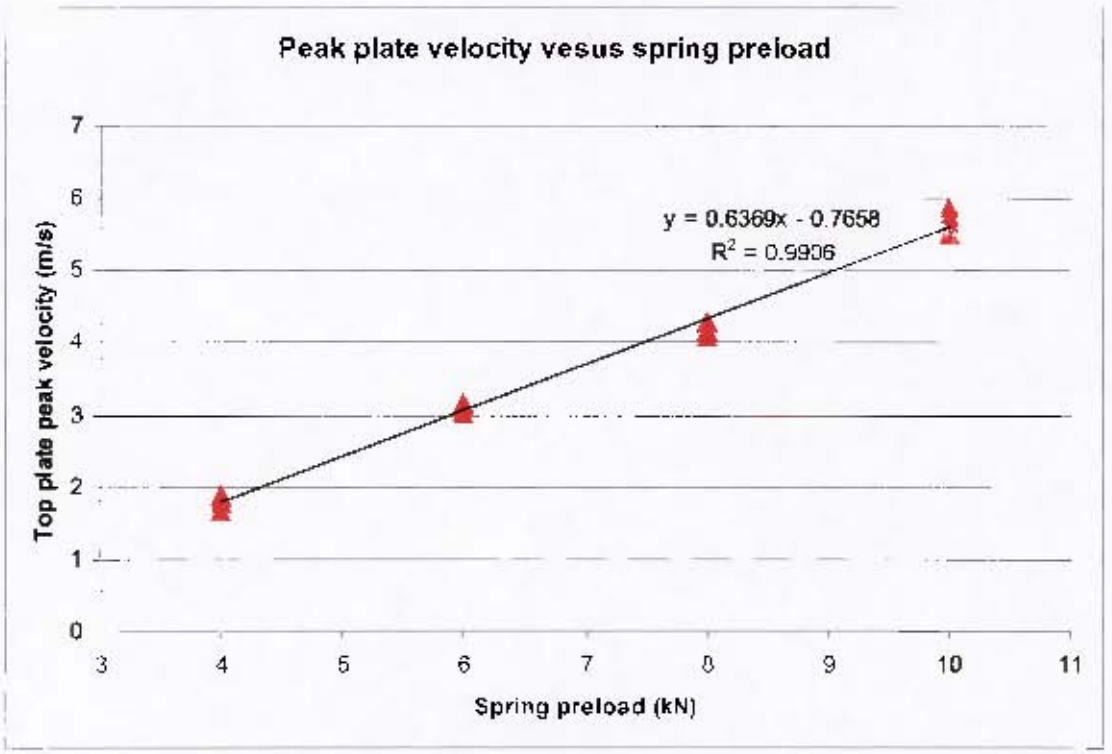

Figure 117: Plot of peak plate velocity results for characterisation of the LLI with a surrogate leg.

The peak plate velocity duration is also very dependant on the spring preload as can be seen in Figure 118.

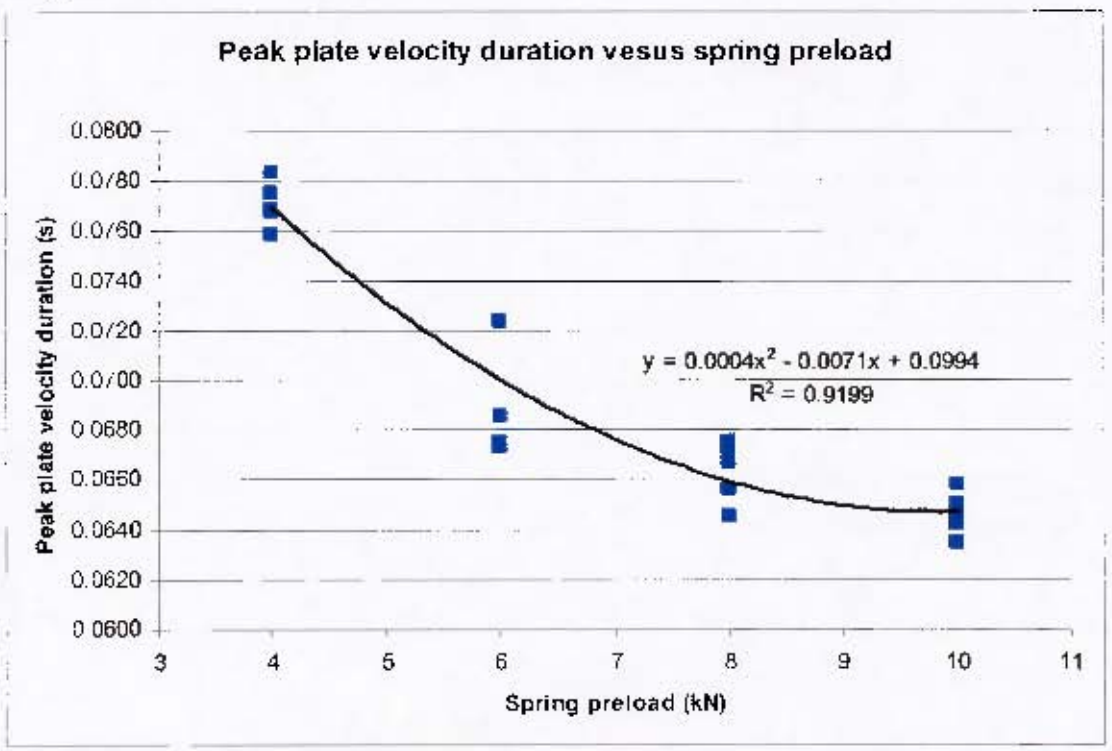

Figure 118: Plot of peak velocity duration results for characterisation of the LLI with a surrogate leg.

A very strong relationship can be seen between the peak surrogate leg force versus the spring preload (See Figure 119). The repeatability is also very good as the peak leg force values at each spring preload are (on average) within 3.7% of one another. The duration of the peak leg force versus the spring preload is plotted in Figure 120. As was observed in Figure 118 a nonlinear relationship exists between these variables.

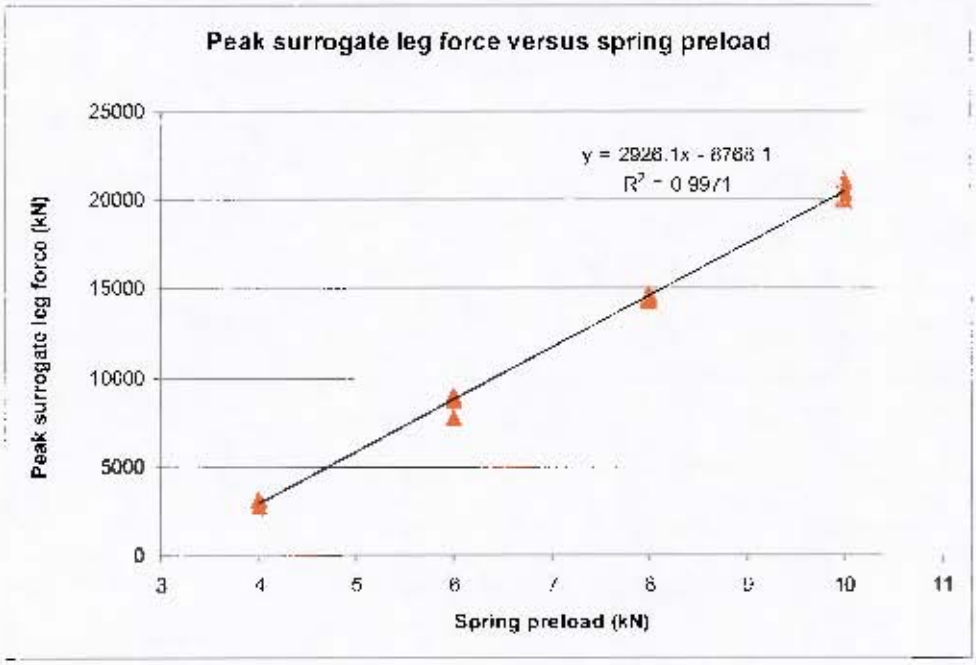

Figure 119: Plot of peak leg force results for characterisation of the LLI with a surrogate leg.

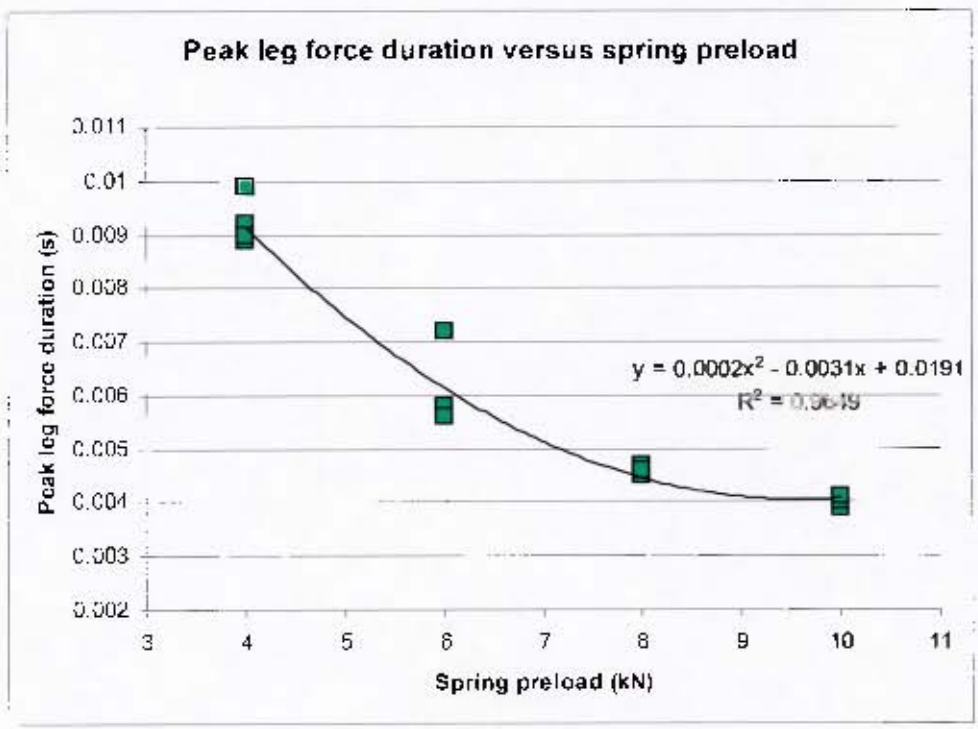

Figure 120: Plot of peak leg force duration results for characterisation of the LLI with a surrogate leg.

3.3.6 Simulation of LLI

A simulation was conducted in MSC ADAMS by Rayeesa Ahmed to allow the impactor plate velocity of the model to be compared with that of the actual LLI.

Figure 121 shows a typical simulation of the impactor plate velocity at 6kN spring preload. The actual result is shown in Figure 122[22].

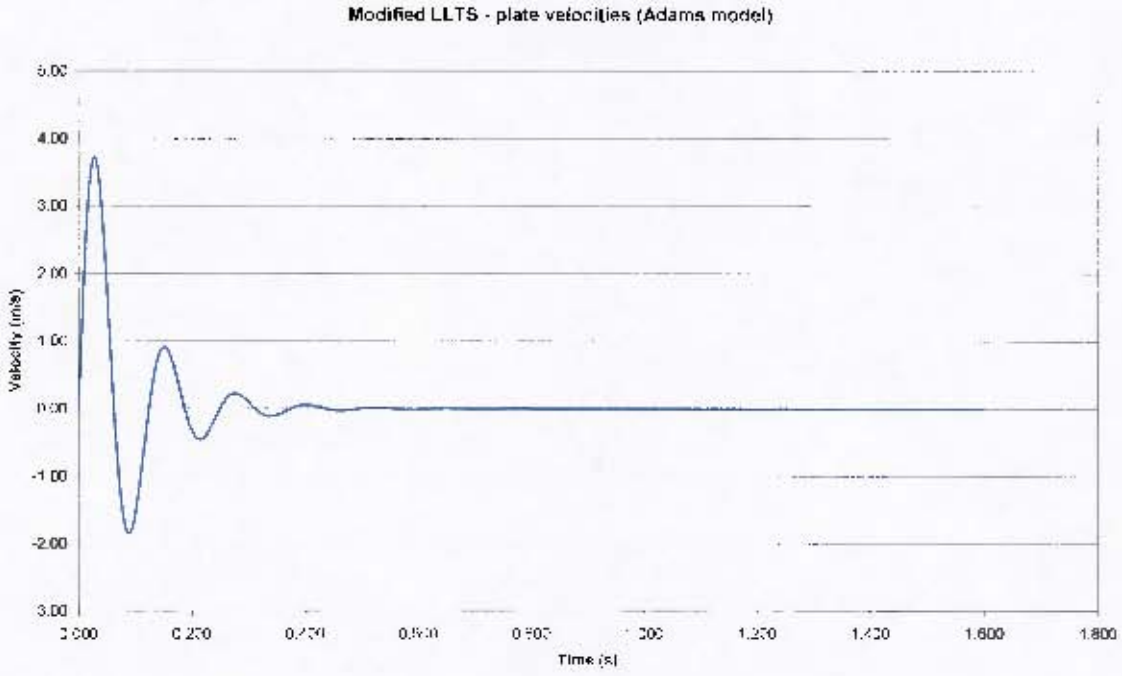

Figure 121: Graph of the simulated peak impactor plate velocity at 6kN spring preload (by R Ahmed).

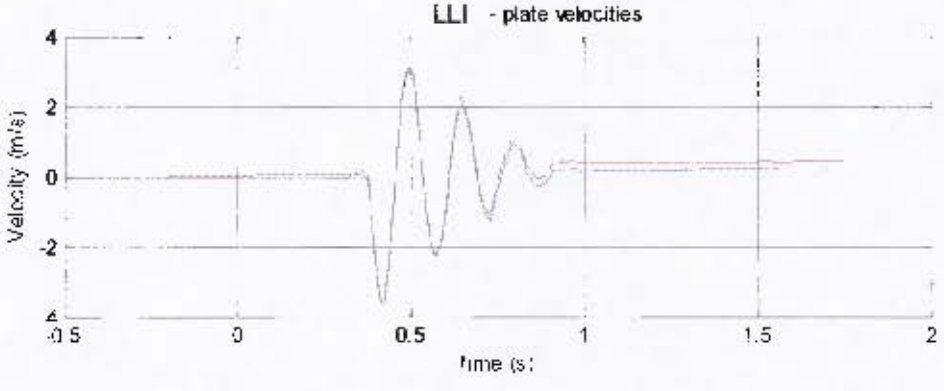

Figure 122: Graph of the actual peak impactor plate velocity at 6kN spring preload.

[22] The orientation of the simulated and actual velocity is opposite due to assumptions that were made. In the actual results a negative velocity indicates an upward velocity whilst in the simulation the opposite assumption has been made.

Simulations were conducted for the LLI with the added mass plate and without so that the results could be compared. Table 38 and Table 39 list the results which are plotted in Figure 123 and Figure 124. The results are as expected and show that as the mass of the impactor plate increases the peak plate velocity decreases.

Table 38: Simulated plate velocity results without an added mass plate.

Spring preload (kN)	Peak plate velocity (m/s)	Peak plate velocity duration (s)
4	2.44	0.057
6	3.72	0.057
8	5.01	0.057
10	6.30	0.057

Table 39: Simulated plate velocity results with an added mass plate

Spring preload (kN)	Peak plate velocity (m/s)	Peak plate velocity duration (s)
4	2.13	0.066
6	3.28	0.066
8	4.43	0.066
10	5.59	0.066

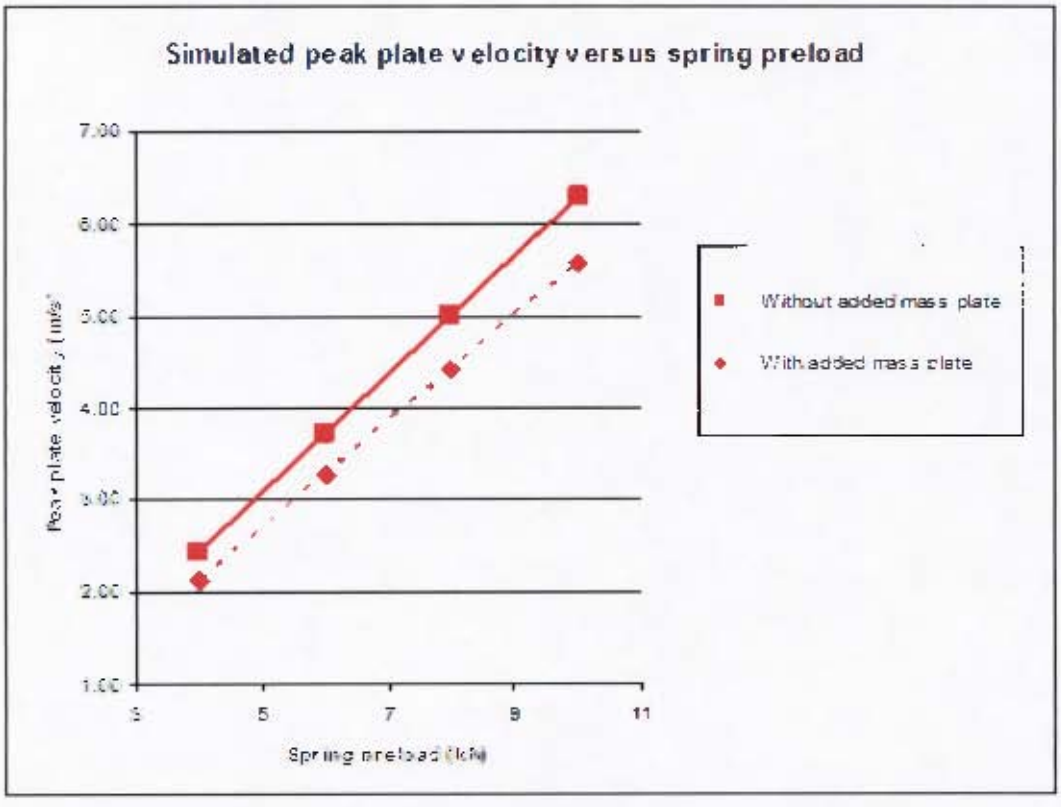

Figure 123: Graph showing simulated peak plate velocity results with and without an added mass plate.

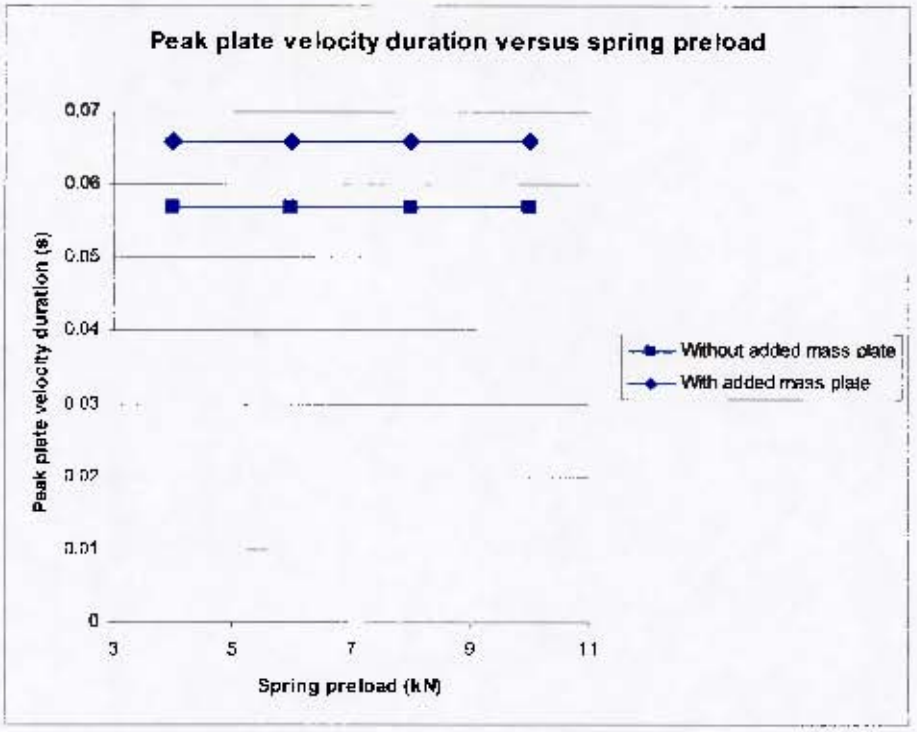

Figure 124: Graph showing simulated peak plate velocity duration results with and without an added mass plate.

3.4 Factors affecting characterisation and performance of LLI

In order to better understand the functioning of the LLI, other factors such as the effect of adding extra mass on the impactor plate and the use of different surrogate limbs to measure the force supplied by the impactor were investigated.

3.4.1 Effect of adding a mass plate

As can be seen in Figure 125 a mass plate of 7.8kg was added to the impactor plate to increase the mass which is accelerated by the preloaded spring. The impactor plate with the tubes but without the added mass, weights 22.2kg. Thus the increase in mass is 35% of the original mass.

Figure 125: Photograph showing the additional mass plate mounted on the LLI.

Figure 126 shows that the peak plate velocity decreases, on average, from about 5.7m/s to about 4.6m/s as a result of the added mass. This represents a 19% drop in the velocity with the increase in mass by 35%. The duration of the peak plate velocity shows no obvious trend as can be seen in Figure 127.

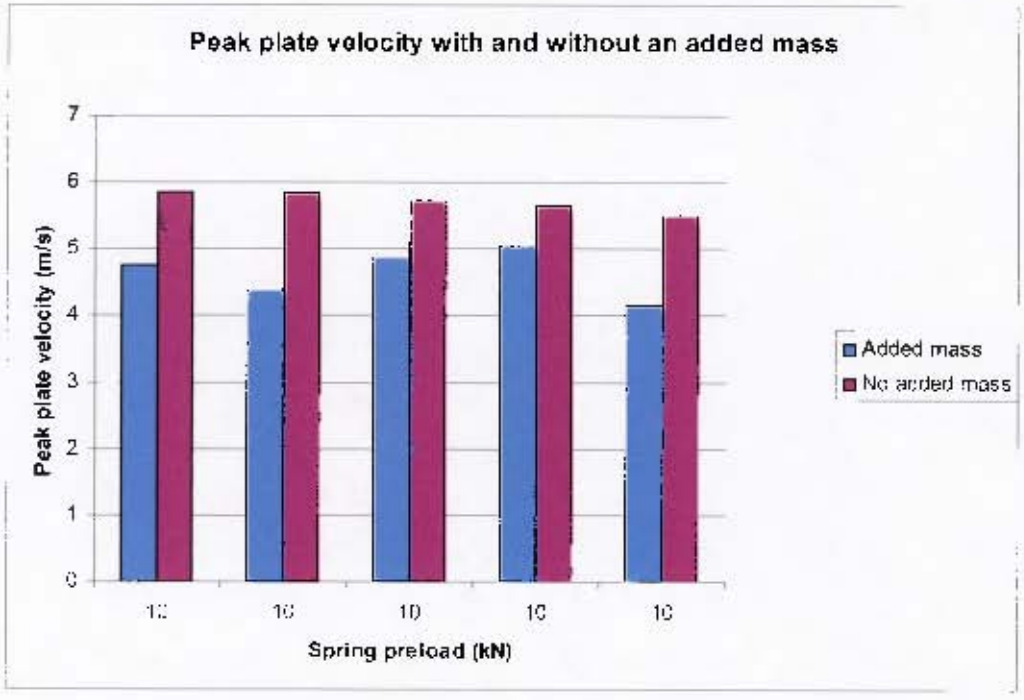

Figure 126: Graph showing 5 samples of peak plate velocity with and without an added mass at a spring preload of 10kN.

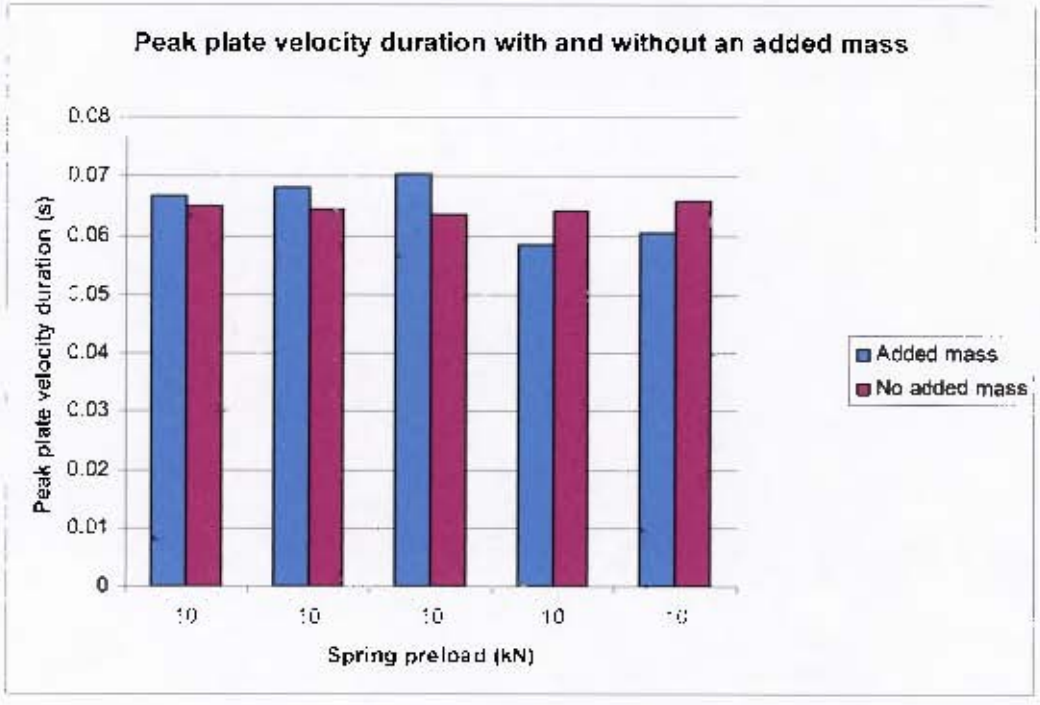

Figure 127: Graph showing 5 samples of the duration of the peak plate velocity with and without an added mass at a spring preload of 10kN.

The trend in peak leg force corresponds to the peak plate velocity as it decreases from an average value of 20.6kN to an average value of 18.5kN with the addition of the mass to the top plate (See Figure 128). No obvious trend is observed in the duration of the peak leg force (See Figure 129).

The repeatability of the peak plate velocity and duration decreases with the added mass from being within 8.0% of one another to being within 2.4% and 1.3% of one another respectively. The repeatability of the peak leg force and duration decreases from being within 2.8% and 3.2% of one another respectively to being within 2.3% and 2.1% of one another respectively.

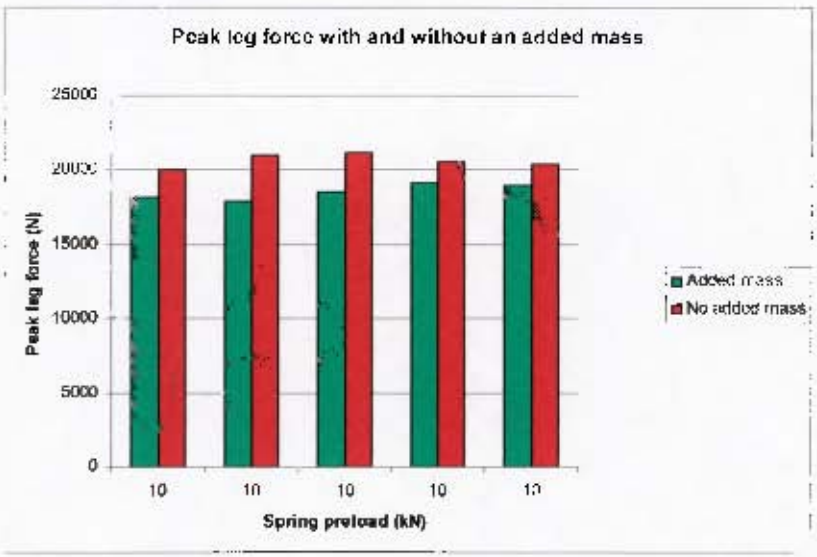

Figure 128: Graph showing 5 samples of peak leg force with and without an added mass at a spring preload of 10kN.

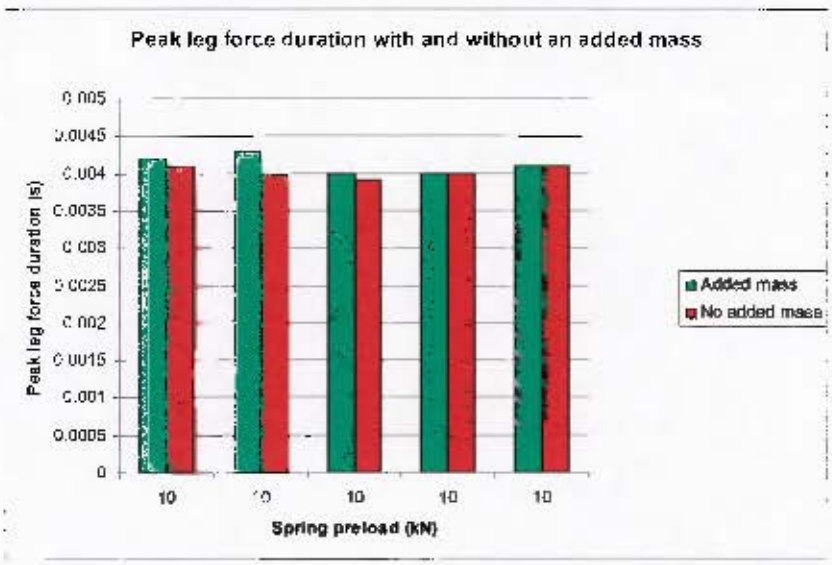

Figure 129: Graph showing 5 samples of the duration of the peak leg force with and without an added mass at a spring preload of 10kN.

3.4.2 Effect of different human surrogates on system performance

In order to investigate the effect that the properties of various human surrogate limbs have on the characteristics and performance of the LLI. a range of limbs and different configurations were used in testing.

Comparison of surrogate leg (serial number 5) setups:

The surrogate leg (serial number 5) was used as the base for four different limb setups. These were described in detail in section 3.3.2. Factors which were explored though these setups include joint stiffness of hip and knee joints, the effect of the ankle joint the effect of the boot and the effect of the prosthetic rubber coating of the Hybrid III ATD foot that is part of the surrogate leg. The tests comparing the various surrogate leg setups were conducted without the additional mass plate attached to the impactor plate of the LLI. The peak leg force recorded for the 25Nm hip and knee joint torque settings are displayed in Figure 130.

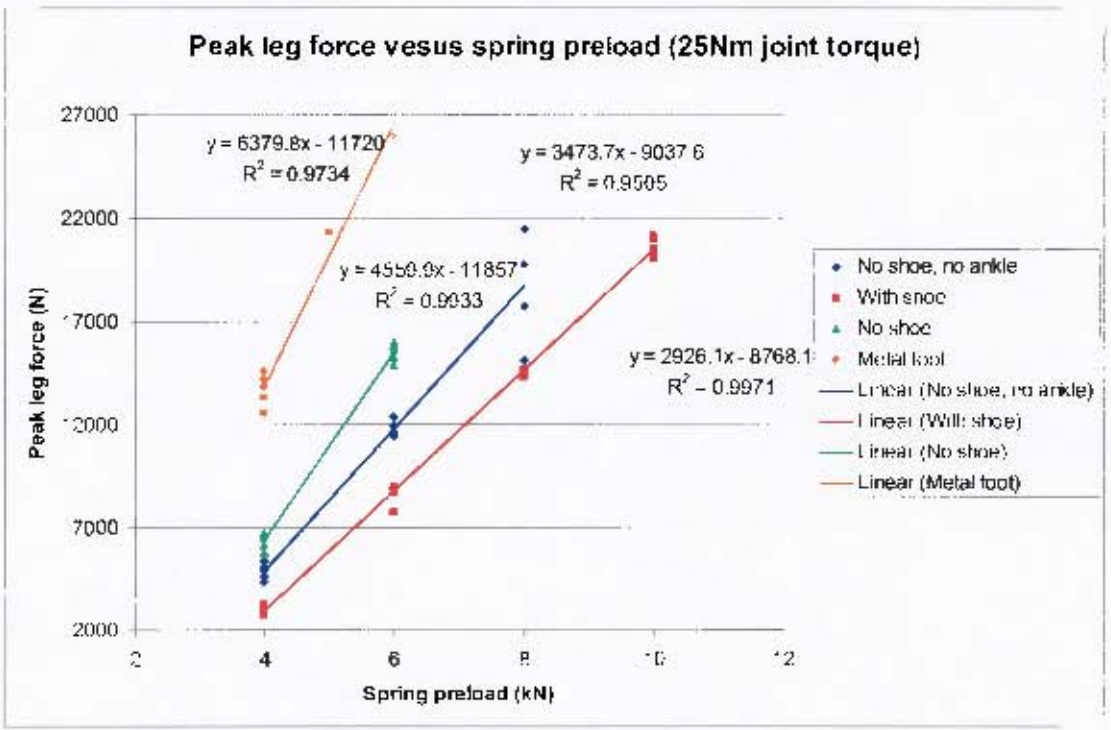

Figure 130: Graph showing peak leg force versus spring preload for various surrogate leg setups at 25Nm joint torque.

Figure 130 shows that the peak leg force was lowest when a boot was worn by the surrogate leg. When the boot was removed, the peak leg force was approximately double that recorded with the boot. The use of the steel foot reduced the damping as the prosthetic rubber coating of the Hybrid III ATD foot was no longer present. This in turn increased the recorded leg force by between 7kN and 10kN depending on the spring preload The effect of no shoe with no ankle joint appeared to read a slightly lower leg force than with an ankle joint. The reason for this was unclear, but could be due to shock absorbing characteristics introduced by the failing weld which would also explain the lack of repeatability in the 8kN spring preload results as after this test the weld broke and testing with this setup was stopped.

Figure 131 shows very little difference in the peak plate velocities for the various setups. This was expected as the peak plate velocity was attained before impact with the limb and thus it should not change based on changing characteristics of the limb (See section 3.3.4 for further explanation).

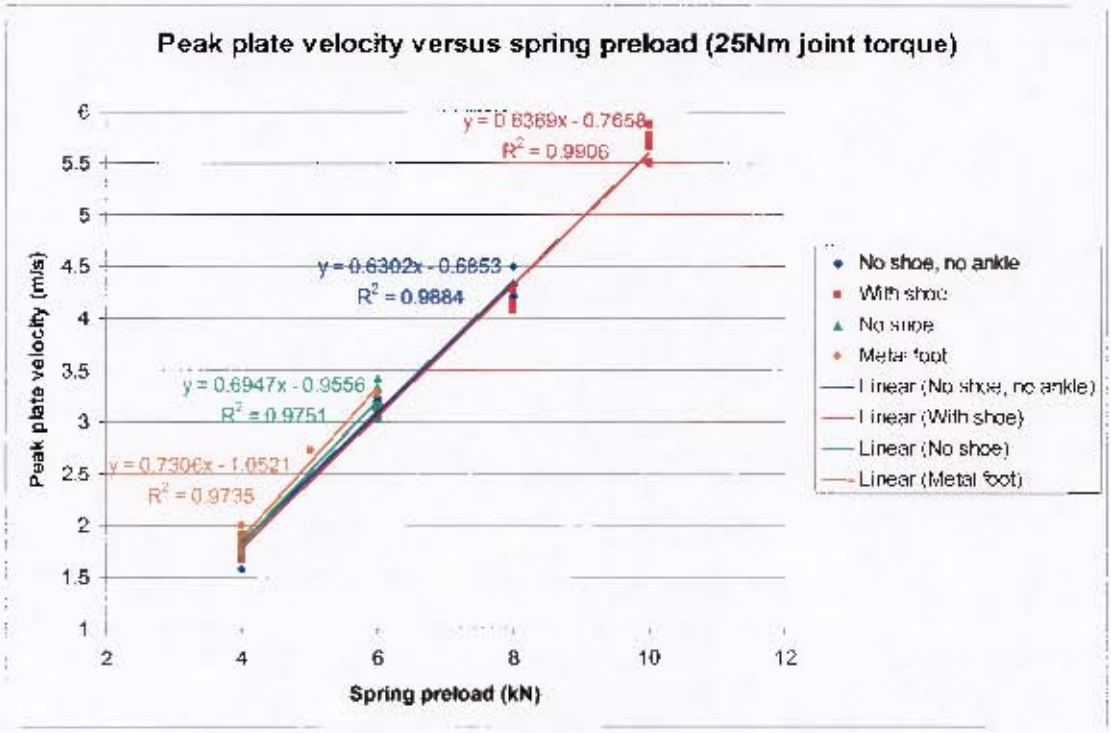

Figure 131: Graph showing peak plate velocity versus spring preload for various surrogate leg setups at 25Nm joint torque.

Comparison of surrogate leg and Hybrid III ATD results:

Tests were conducted with the Hybrid III ATD to enable the performance of the LLI to be compared with the TROSS™. These tests were conducted with the added mass plate. In order to compare results obtained with the Hybrid III ATD and the surrogate leg, additional tests were conducted with the mass plate and the surrogate leg.

The spring was preloaded to 10kN and 5 samples were obtained for both the surrogate leg and the Hybrid III ATD. Figure 132 shows that the surrogate leg recorded forces approximately twice that of the ATD at the 10kN spring preload.
Figure 133 shows that the durations of the peak surrogate leg forces are about half that of the durations of ATD leg forces. This is as expected as an increase in force is directly related to a decrease in duration (See section 3.5.2 for more details)

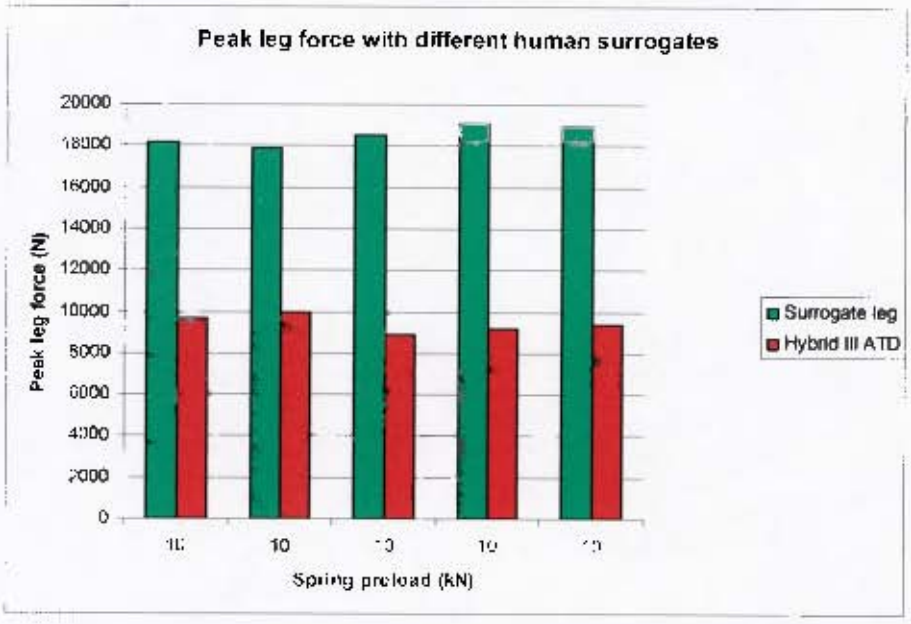

Figure 132: Graph comparing the peak leg force recorded by the Hybrid III ATD and surrogate leg at 10kN spring preload.

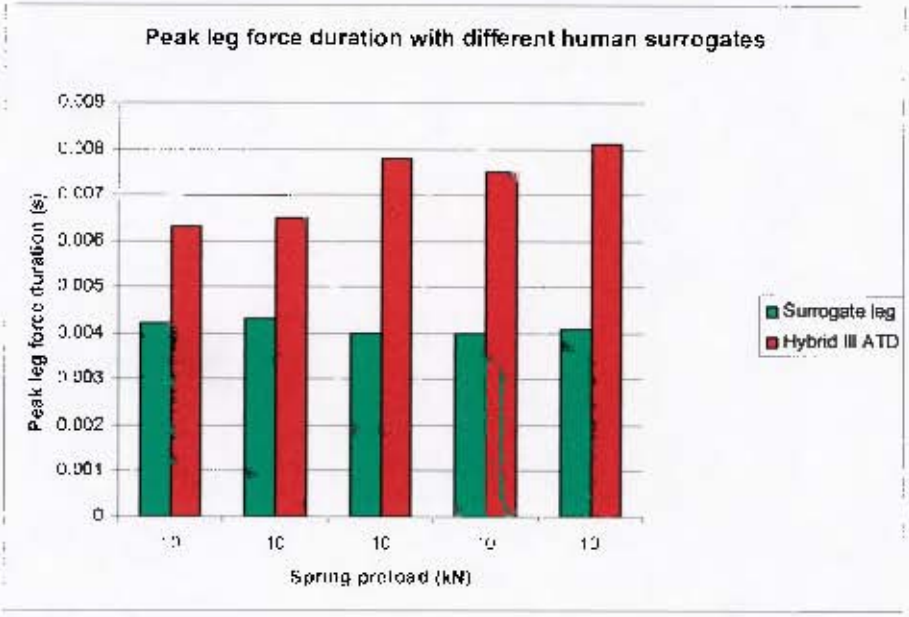

Figure 133: Graph comparing the duration of the peak leg force recorded by the Hybrid III ATD and surrogate leg at 10kN spring preload.

3.5 Discussion of findings related to the LLI

The results of the characterisation of the original LLTS and LLI were presented in the previous section. This section aims to highlight certain results that were discovered during the characterisation process and to bring them together to evaluate the LLI in terms of the aim that was specified based on the literature review that was conducted.

3.5.1 Comparison of simulated and actual LLI results

Figure 134 shows the simulated (by R Ahmed) and actual peak plate velocity at various spring preloads. The simulated peak plate velocity shows a very similar trend to the actual peak plate velocity, but is about 0.5m/s higher than the actual peak plate velocity. This is as expected as the simulation does not take into account the effects of friction and damping which would be present in the actual system.

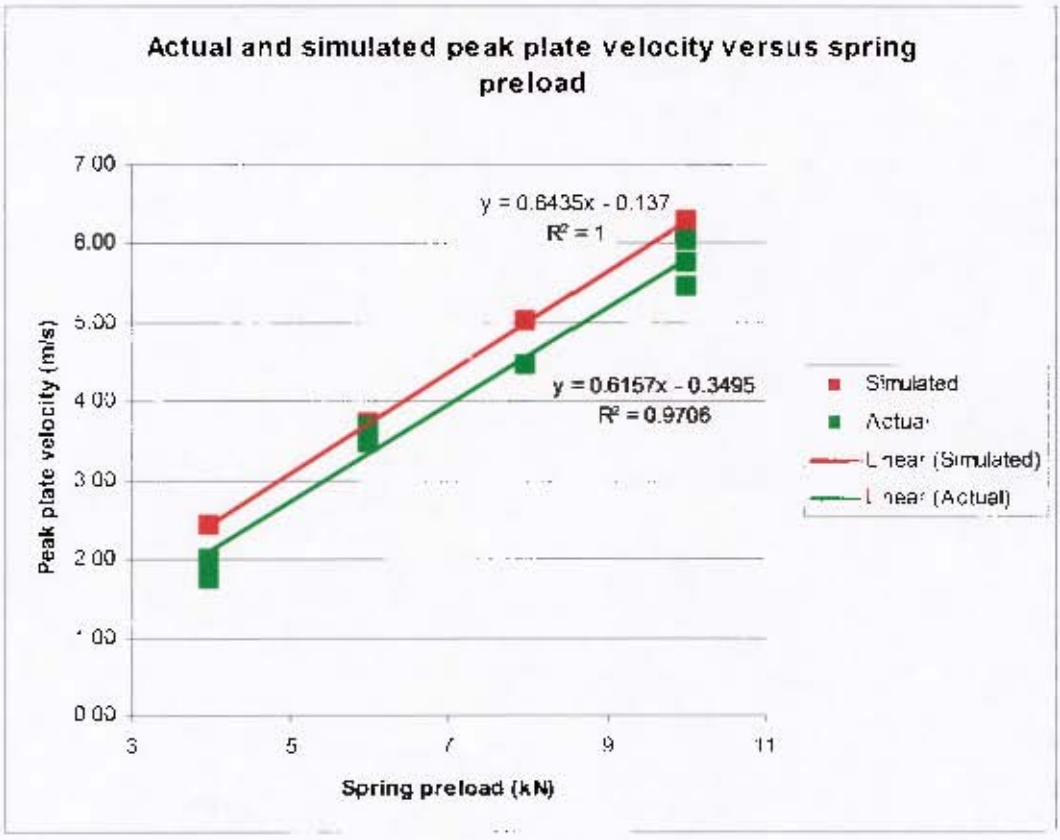

Figure 134: Graph comparing the simulated and actual peak plate velocity results at various spring preloads.

3.5.2 Relationships involving plate velocity and leg force results

The relationship between the output from the LLI (in the form of the impactor plate velocity) and the input to the surrogate leg (in the form of the lower tibia axial force) was explored in Figure 135 and Figure 136. A very strong linear relationship was observed between the peak plate velocity and the peak leg force in Figure 135.

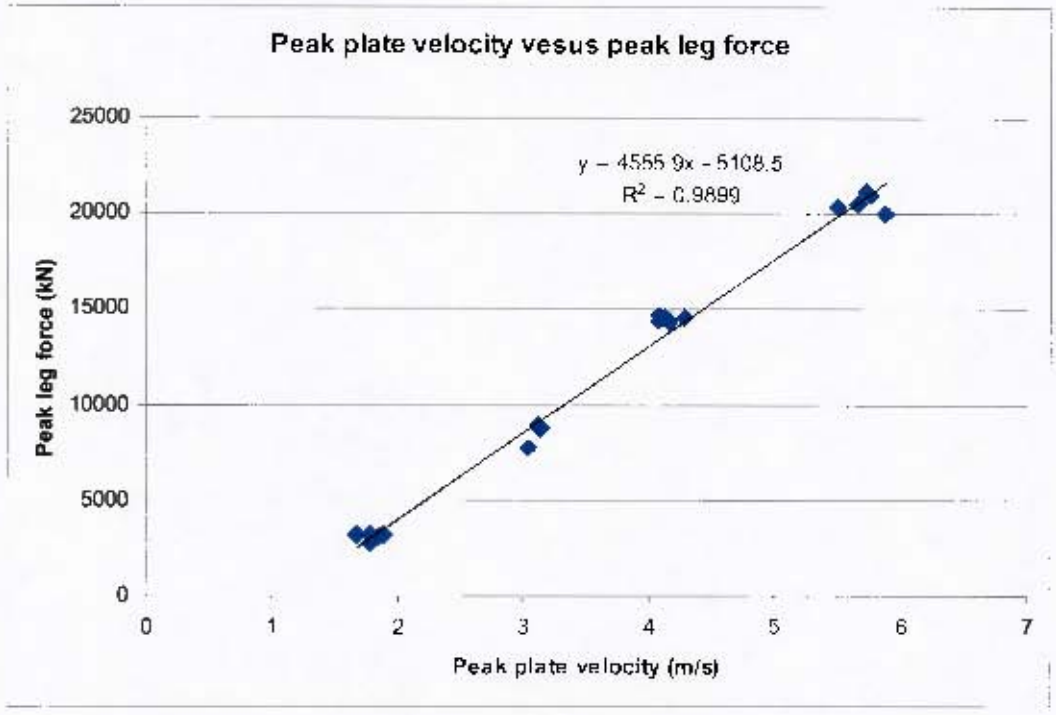

Figure 135: Graph showing the relationship between peak plate velocity and peak leg force.

Figure 136 shows the relationship between the duration of the peak plate velocity and the duration of the leg force. Although this is not a very strong relationship, some correlation is expected as the duration of the peak plate velocity and the duration of the peak leg force are related to the peak plate velocity and the peak leg force respectively (The durations decrease as the peaks increase). Figure 137 shows a much stronger relationship between the peak leg force duration and the peak leg force than the relationship between the peak leg force duration and the peak plate velocity duration. This can be explained by the transfer of momentum – if the leg is impacted more severely (with a higher velocity), it is in contact with the plate for less time which translates to greater force over less time.

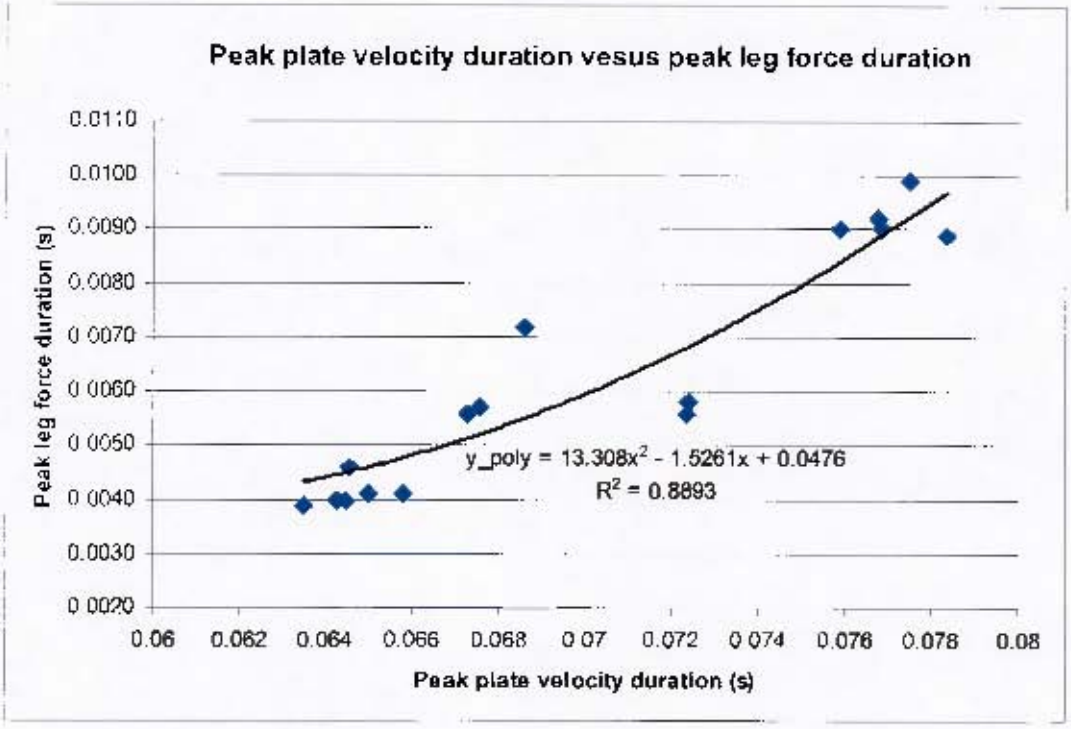

Figure 136: Graph showing the relationship between the duration of the peak plate velocity and the duration of the peak leg force.

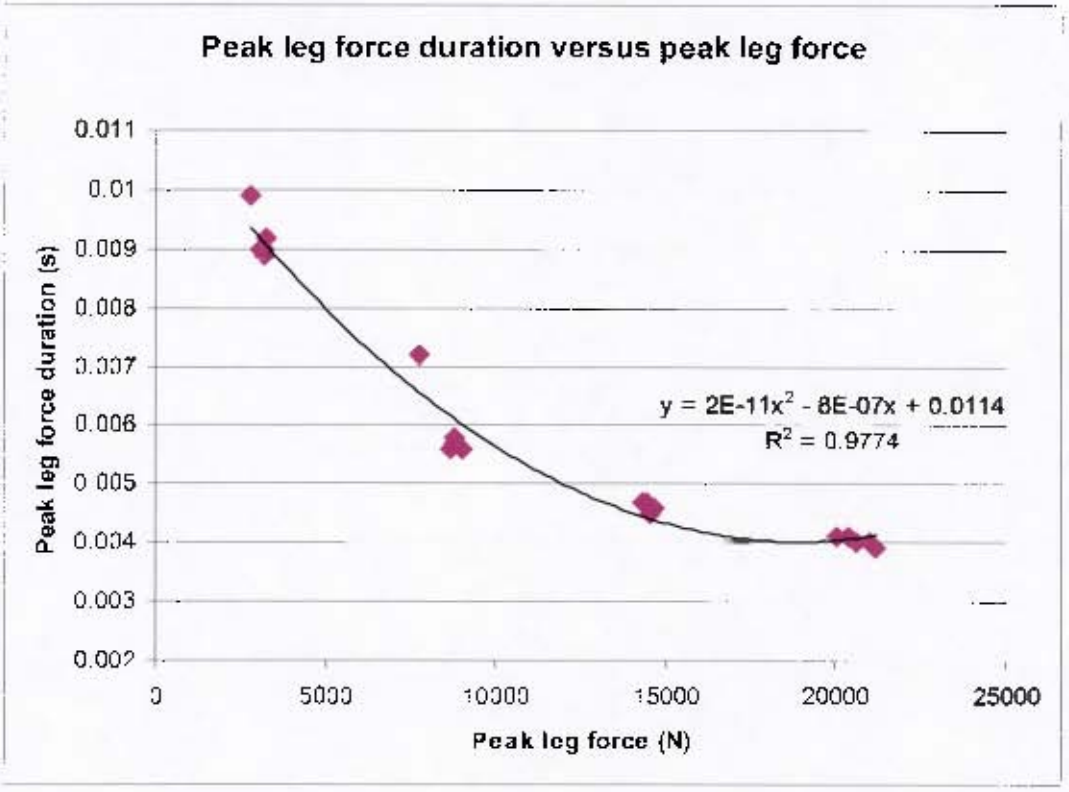

Figure 137: Graph showing the relationship between the peak leg force and the peak leg force duration.

3.5.3 Comparison of original LLTS and LLI results

In order to compare the performance of the original LLTS and the LLI, the same surrogate leg was used and the LLI results were processed and analysed in the same manner as the original LLTS results (in terms of the way in which the peaks and durations were determined). Figure 138 compares the peak plate velocity of the original LLTS and LLI for the various spring preloads. At 4kN spring preload the systems appear to produce similar plate velocities, but as the preload is increased the LLI achieves velocities that are more than double those that could be achieved with the original system. Tests were not conducted below 4kN spring preload with the LLI (due to the chosen offset) and thus the velocities at lower preloads could not be compared.

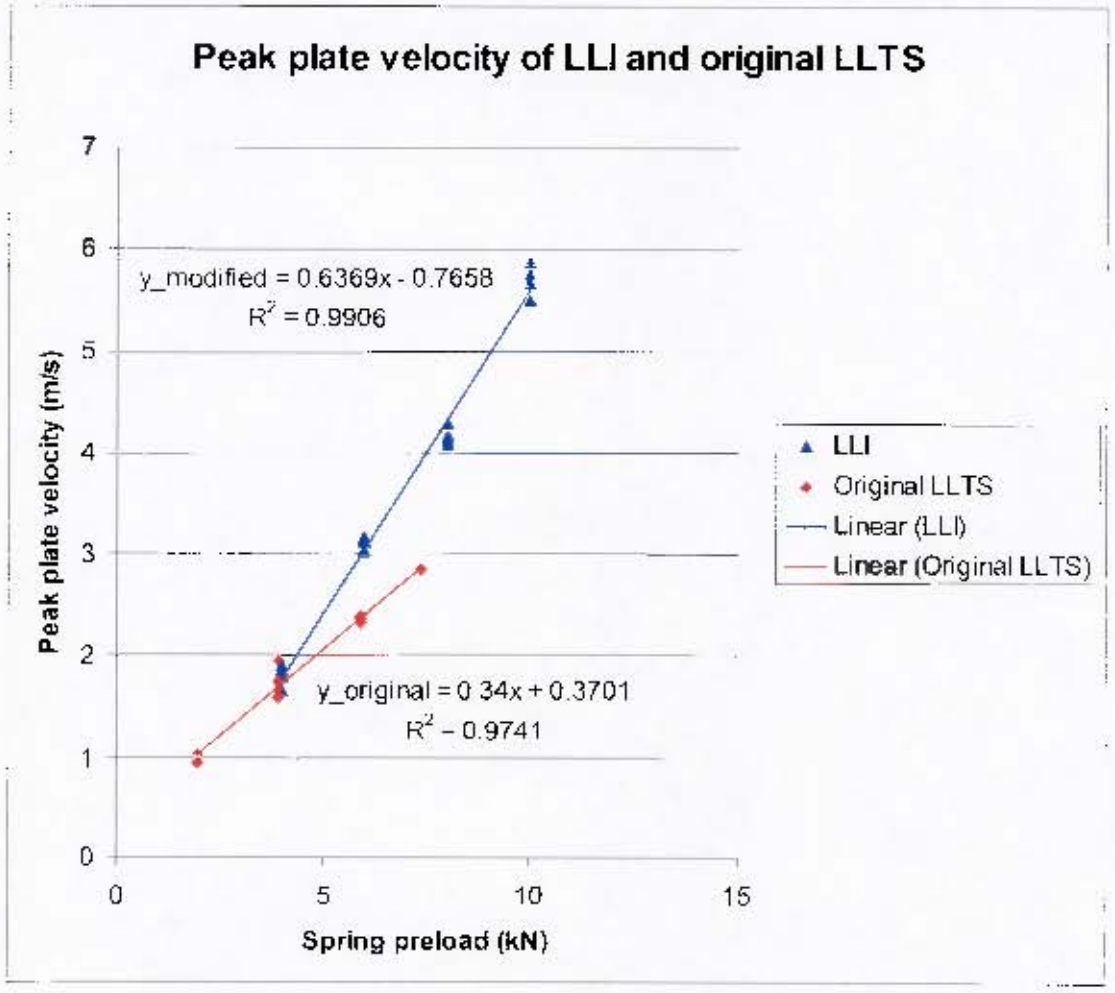

Figure 138: Peak plate velocity versus spring preload for the original LLTS and the LLI.

Similarly in Figure 139 the peak leg forces that can be achieved using the same spring are much greater than those that could be achieved with the original system.

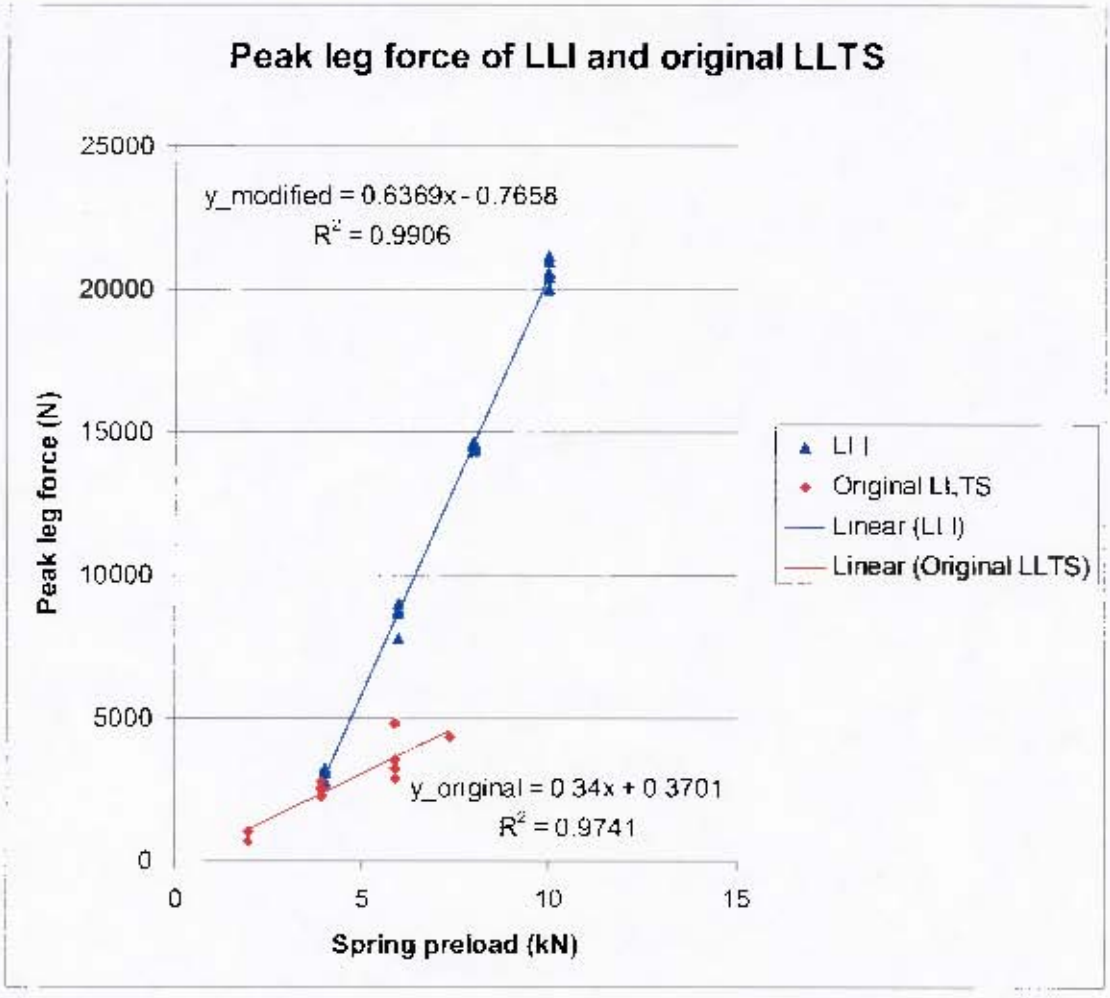

Figure 139: Peak leg force versus spring preload for the original LLTS and the LLI.

The coefficients of determination in both Figure 138 and Figure 139 are noteworthy as they indicate that the variation in peak velocity and peak leg force are more dependant on the variation in the spring preload than they were in the original system. This may reflect on the more efficient and repeatable use of the spring when it is compressed vertically rather than at an angle, as was the case in the original system.

Comparing the repeatability of the original LLTS and the LLI is not strictly meaningful as the number of samples at each of the spring preloads is not consistent. However, the range of repeatability was assessed in order to compare the systems. The repeatability of the original LLTS determined from the peak leg force results recorded by the same surrogate leg ranged from peak leg forces being within 8.3 to 31.3% (an average of 20.9%) of one another. The LLI reflected leg force values within 0.9 to 6.1% (an average of 3.7%) of one another.

3.5.4 Comparison of LLI and LS drop test rig results

As the repeatability of any device used in the testing of surrogate limbs is of paramount importance, the repeatability of results obtained using the LLI was compared to the repeatability of the results obtained using the LS drop test rig[23].

The drop test results recorded in Table 40 reflect the results of a series of drops from a height of 0.5m and the surrogate leg joint stiffness set to 25Nm.

Table 40: Drop test results obtained using the Hybrid III ATD and the surrogate leg.

	Hybrid III ATD	Surrogate leg
Drop number	Peak lower tibia force (kN)	Peak lower tibia force (kN)
1	6.0	8.9
2	6.5	10.3
3	6.5	9.9
4	6.6	10.2
5	7.2	9.2
Average	6.6	9.7
Standard deviation	0.4	0.6
% within	6.5	6.4

The LLI test results recorded in Table 41 reflect the results of a series of tests with a spring preload of 10kN and the surrogate leg joint stiffness set to 25Nm.

Table 41: LLI test results obtained using the Hybrid III ATD and the surrogate leg.

	Hybrid III ATD	Surrogate leg
LLI sample number	Peak lower tibia force (kN)	Peak lower tibia force (kN)
1	9.69	18.28
2	9.97	17.94
3	8.89	18.55
4	9.22	19.02
5	9.42	18.93
Average	9.44	18.54
Standard deviation	0.42	0.45
% within	4.4	2.4

A graphical representation of the above results is shown in Figure 140.

[23] The drop test rig is commonly used to verify human surrogate measurement equipment and to experiment with various parameters which might affect the values obtained when testing with the surrogates.

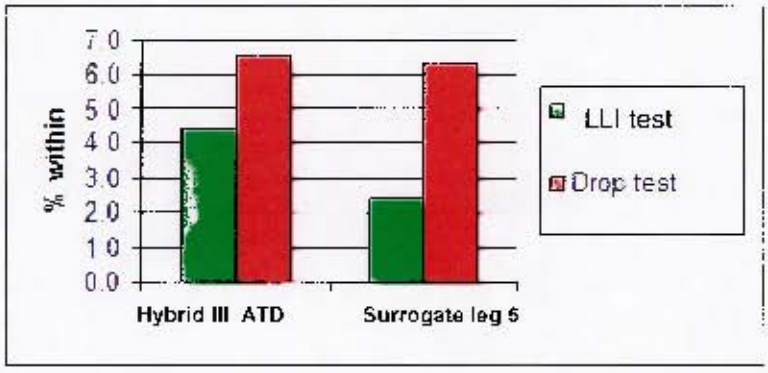

Figure 140: A graphical representation comparing the repeatability of the LLI results and the drop test rig results.

As mentioned before, this comparison of the repeatability is not strictly meaningful as only 5 samples were taken and the loading used in the LLI tests is greater than that used in the drop tests. However, it does give an indication that the repeatability of the results obtained using LLI is at least as good as those obtained using the drop test rig.

3.5.5 Comparison of LLI and TROSS™ results

In order to compare the LLI results with the TROSS™ results outlined in the paper by van der Horst et al. [6], tests needed to be conducted with the Hybrid III ATD. The spring preload was adjusted until a lower tibia axial force of approximately 10kN was recorded by the ATD. This was done in order to match the loading required from the LLI with the *db3* loading that was described in [6] that reflects a tibia force of about 10kN. These results are shown in Figure 141 where the *test db3a* and *test db3b* represent tests conducted with the TROSS™ and *model* represents simulated results.

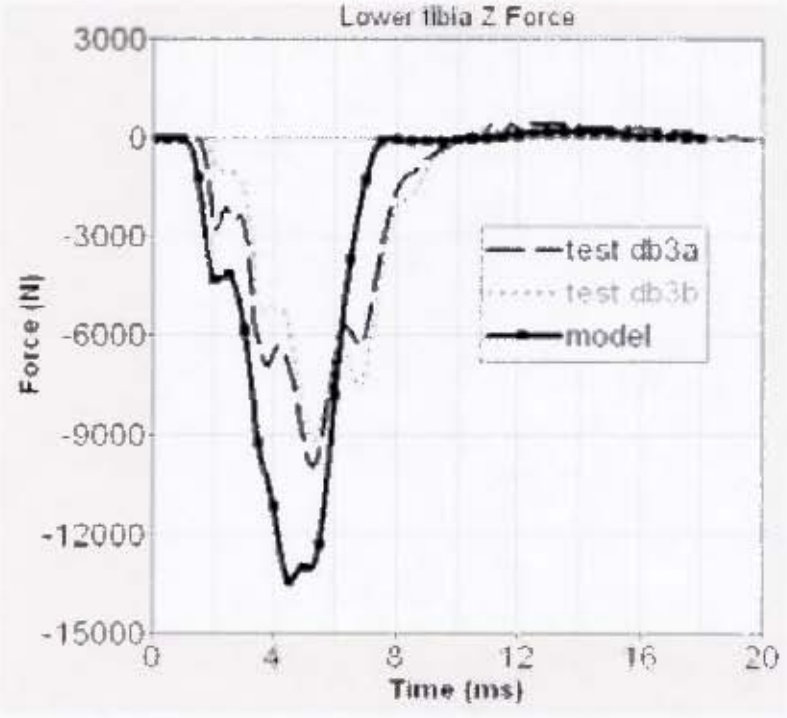

Figure 141: Loading condition db3 lower tibia force results recorded using the TROSS™ and simulated results (from [6]).

The LLI spring preload that produced results that best matched the *db3* results presented in [6] was found to be 10kN. 5 tests were conducted with the LLI and ATD at a spring preload of 10kN (See Figure 142)

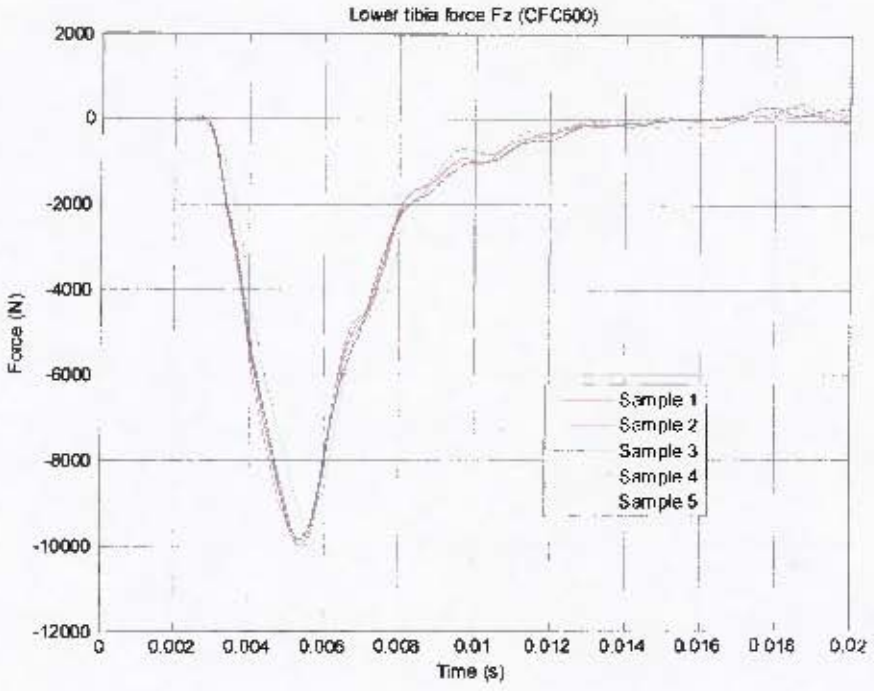

Figure 142: Graph showing 5 samples of the lower tibia axial force recorded by the ATD using the LLI.

The average lower tibia axial force recorded by the ATD using the LLI is 9.4kN. The lower tibia axial forces recorded in Figure 141 labelled *test db3a* and *test db3b* appear to be 10kN and 9kN respectively. Thus, in terms of matching the peak lower tibia axial forces the LLI appears to produce similar results to the TROSS™. The duration of the *test db3a* and *test db3b* peak tibia forces (as determined using a threshold that was set to 10% of the peak) was found to be on average approximately 6.5ms. The duration of the peak tibia forces obtained using the LLI was on average approximately 7ms (with a range between 6 and 8ms which encompasses the 6.5ms duration obtained with the TROSS™). Thus, the lower tibia axial forces recorded by the ATD using the TROSS™ and the LLI appear to be very similar.

In addition to the axial tibia forces, the foot accelerations produced by the TROSS™ and the LLI were compared in Figure 143 and Figure 144. Whilst the peak acceleration produced by the LLI was approximately 500 to 1000m/s^2 greater than that produced by the TROSS™, the time duration and shape of the signals was similar. It was interesting to note that the LLI signal dipped from about 8 to 16ms which could also be seen in the simulated signal (*model*) in Figure 143. However, this was not observed in the TROSS™ *test db3a* and *test db3b* results.

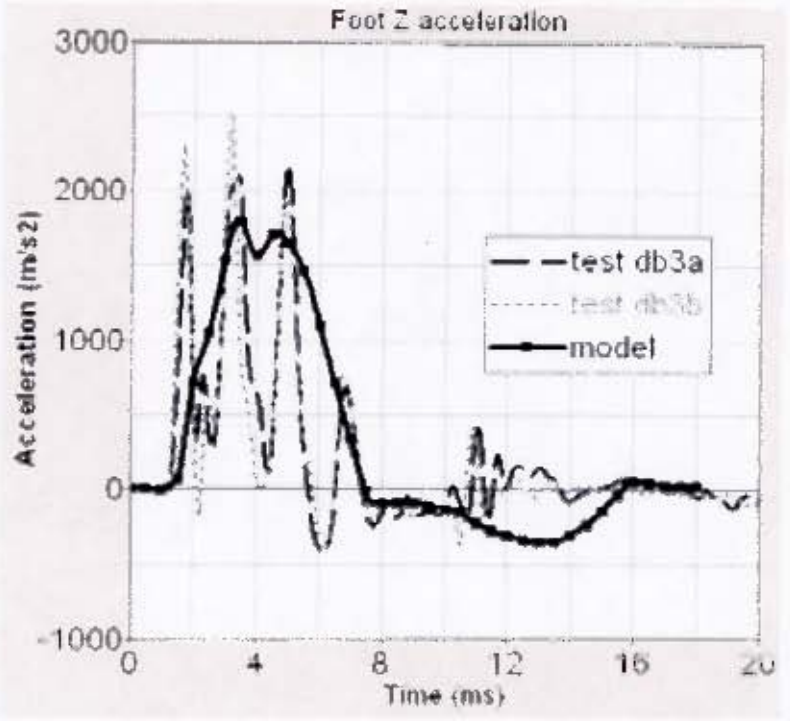

Figure 143: Loading condition db3 foot acceleration results recorded using the TROSS™ and simulated results (from [6]).

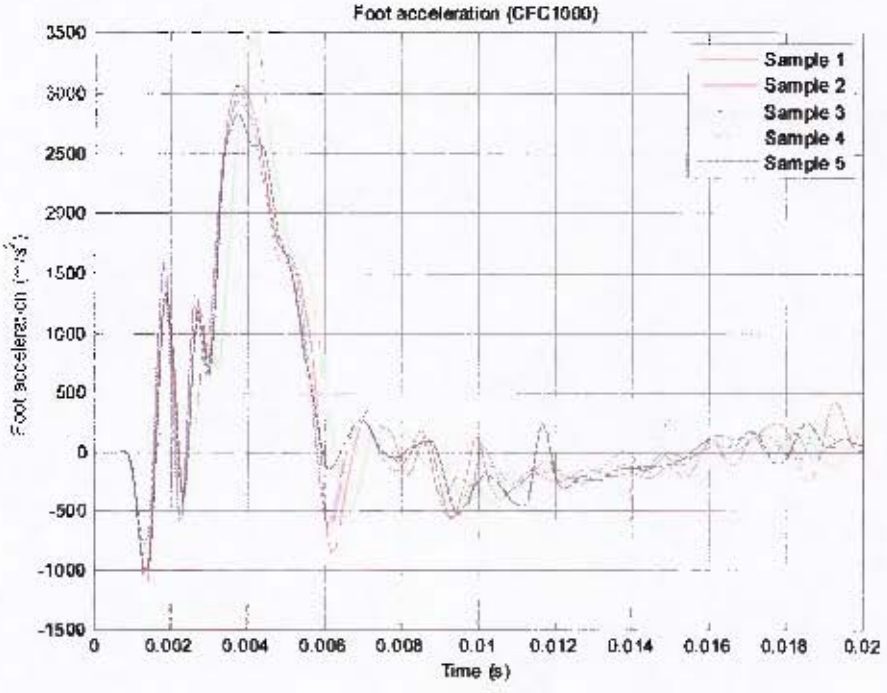

Figure 144: Graph showing 5 samples of the foot acceleration recorded by the ATD using the LLI.

3.5.6 Comparison of LLI results with vehicle test results

The aim of the LLI is to load a human surrogate limb with a force that is similar to that which the limb may experience within a landmine protected vehicle during an explosive event. Thus the range of the peak forces and the range of durations of the peak forces obtained using the LLI were plotted together with data that was recorded during the testing of various landmine protected vehicles. Figure 145 shows that the LLI encompasses most of the results measured by surrogate limbs during explosive events. A shortcoming may be that the LLI does not encompass the peak forces below 3000N, but this is most likely due to the test setup. It is felt that if tests are conducted that do not require a 30mm initial offset, the spring preload will be reduced and thus the peak force recorded by the limb will decrease.

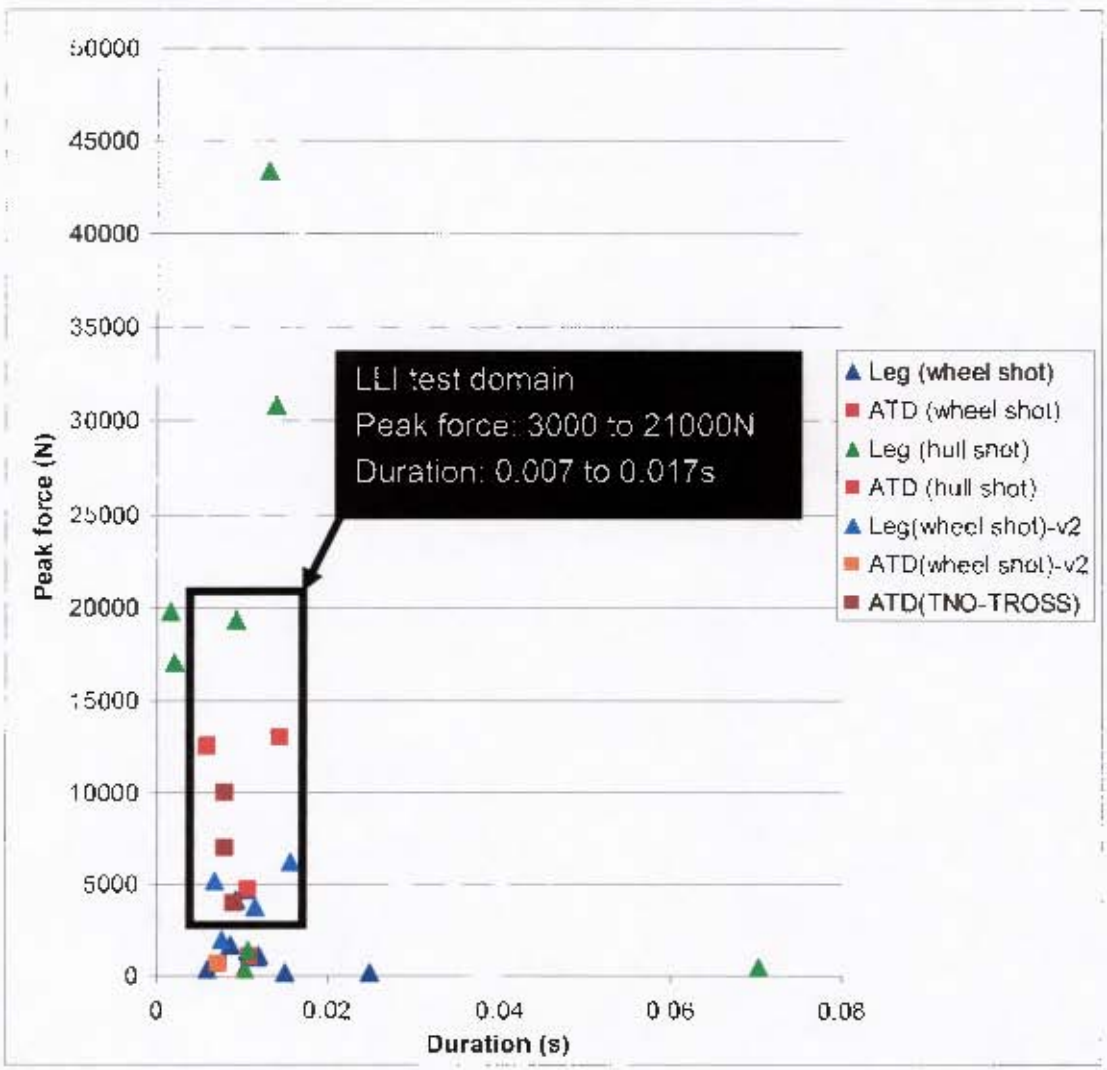

Figure 145: Diagram showing the peak forces and peak force durations recorded with the LLI compare to those recorded during vehicle tests.

4 INVESTIGATION OF FACTORS AFFECTING SURROGATE LIMB MEASUREMENTS

The lower limb HSMD parameters that were considered in this study were lower limb position, boot or no boot and knee and hip joint stiffness. The effect of these parameters on lower limb measurements was examined and their influence on lower limb injury levels considered.

4.1 Effect of lower limb position on injury levels

The experimental design is based on the lower limb position described in [6], the results of which are to be verified experimentally as part of this study

4.1.1 Experimental design setup

The experimental design was setup as follows:

Aim:

To validate the simulation results presented in [6]. These results include the lower tibia axial force (Fz) and moment (My). The acceleration of the foot was also provided (Az)

Apparatus:

A Hybrid III ATD was used with lower tibia tri-axial load cell and a tri-axial ankle load cell. The Hybrid III is also fitted with a 500g[24] foot accelerometer. The LLI was used to apply a force to the Hybrid III limb (See Figure 146).

Figure 146: Photograph of the LLI with the Hybrid III ATD.

[24] A 500g accelerometer should be sufficient as maximum TROSS accelerations (at dB3) are about 2500m/s2 which corresponds to 255g [6]

The foot of the Hybrid III ATD was required to be positioned at a right angle (as will be described in the method below) thus an angular plate was designed that could be attached to the LLI impactor plate. However, this additional angular plate added mass to the impactor plate and would therefore affect the peak velocity that could be delivered by the system. Thus an additional flat plate, with approximately the same mass as the angular plate, was manufactured. The manufactured flat plate attachment is shown in Figure 147 and weighs 7.77kg. The angular plate attachment is shown in Figure 148 and weighs 7.85kg

Figure 147: Photograph of flat plate attached to the LLI impactor plate.

Figure 148: Photograph of angular plate attachment to the LLI impactor plate.

Method:

In [6] a 10kN peak force with a duration of about 8ms was reported in the experimental data with the foot in Position A. The LLI was thus be set up to produce this load on the limb which corresponded to a spring preload setting of 10kN.

The lower tibia z forces and foot acceleration were recorded and compared to the simulation results in [6].

The test domain was set up as shown in Table 42.

Table 42: Test domain for lower leg position investigation.

	Position A	Position B	Position C	Position D
with boot	5 samples	5 samples	5 samples	5 samples
without boot	5 samples	0 samples	0 samples	0 samples

The lower leg positions (See Figure 149) were defined as follows:

- Position A - knee at right angle to horizontal.
- Position B - knee at 45 degrees to horizontal.
- Position C - foot plate and knee at 45 degrees to the horizontal.
- Position D - foot and knee at 45 degrees to the horizontal.

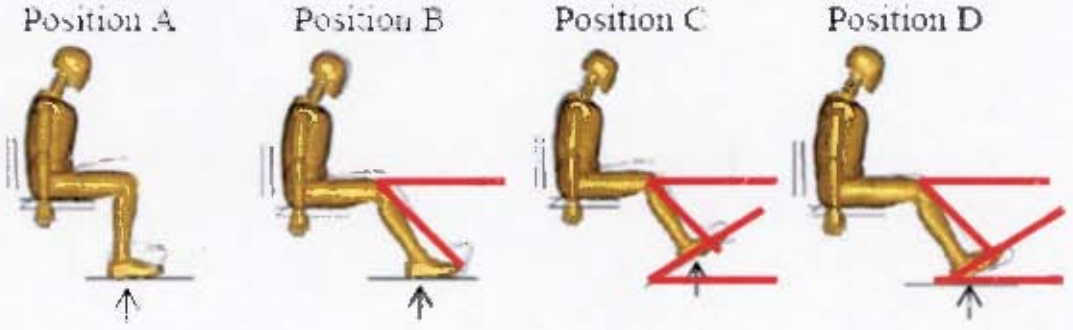

Figure 149: Diagram showing the required angles of the various lower leg positions (adapted from [6]).

However, in practice the required angles that were specified above could not all be achieved A digital spirit level was used to measure the actual angles. The actual angles are specified below:

- Position A - knee at right angle to horizontal.

  This position could be achieved and the angle from the front of the knee to the front of the heel of the boot was measured as 180 degrees.

- Position B - knee at 45 degrees to horizontal

  The 45 degree angle between the line drawn from the front of the knee to front of the toe of the boot and the horizontal could not be achieved as at this angle the boot could not rest flat on the impactor plate. Instead the angle that could be achieved whilst maintaining the flat position of the boot on the impactor plate was 54 degrees as is shown in Figure 150

Figure 150: Diagram illustrating the setup for Position B.

- Position C - foot plate and knee at 45 degrees to the horizontal This position could be achieved with the aid of the angular plate that was manufactured

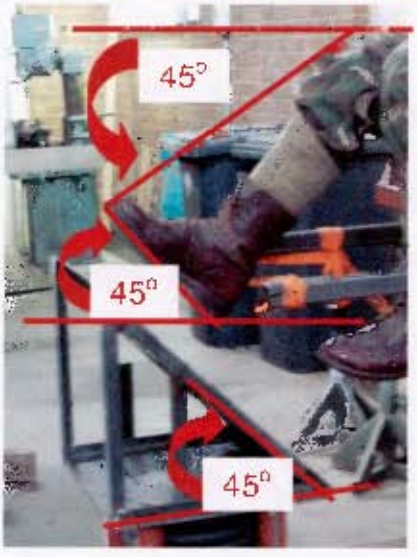

Figure 151: Diagram illustrating the setup for position C.

- Position D - foot and knee at 45 degrees to the horizontal. This position could be achieved and the foot was held in position by a flat tie-down strap.

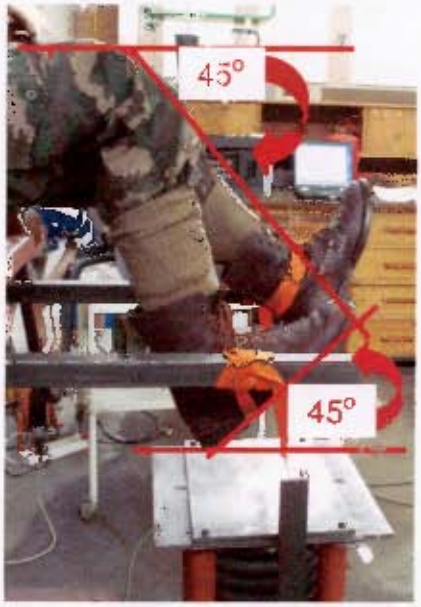

Figure 152: Diagram illustrating the setup for Position D.

In all cases the left limb of the ATD was lifted and secured so that it would not influence the movement of the LLI or the right limb. A flat tie-down was used to secure the left limb of the ATD in the required position whilst the spring was compressed before impact.

Instrumentation:

The following transducers were implemented:

- One 500g accelerometer was fitted to the impactor plate.
- The Hybrid III ATD was instrumented with an ankle load cell, lower tibia load cell and foot accelerometer.
- The hydraulic master cylinder was fitted with a calibrated force gauge and both the hydraulic master and slave cylinders were inspected, repaired and given a safety rating.

Table 43 shows the serial numbers of the instrumentation and the sensitivities of the transducers.

Table 43: Description of the instrumentation used in the characterisation of the LLI and the sensitivities of the transducers.

Instrumentation description:	Serial number:	Sensitivity:
Impactor plate 500g accelerometer (left hand side)	0639-013	0.085mV/g
Hybrid III ATD 2	294	N/A
Hybrid III ATD foot accelerometer	6491-003	0.107mV/g
Hybrid III ATD lower tibia load cell	3287-792	Fz=0.00048mV/N Mx=0.03685mV/Nm My=0.03715mV/Nm
Hybrid III ATD ankle load cell	4218J-80	Fx=0.00126mV/N Fy=0.00127mV/N Fz=0.00048mV/N Mx=0.01931mV/Nm My=0.01914mV/Nm
ATD DAQ data acquisition system	01062006	N/A
Hydraulic pump and cylinder	(ENERPAC P84 hand pump, medium pressure double acting cylinder)	N/A (calibrated with hydraulic cylinder force gauge)
Hydraulic cylinder force gauge	147851	N/A

4.1.2 Data acquisition, processing and analysis

Data acquisition:

Data was acquired using the Compact RIO DAQ system. The signals were sampled for 2 seconds at 10kHz. 0.25 seconds of which was pre-trigger data.

Data processing:

The signals were processed in Matlab™ where the offset was subtracted from each of the channels and the calibration factors (calculated from the sensitivities of the transducers and the channel gains and excitation voltages) were applied. Filtering was also conducted in accordance with AEP-55 Volume 2 [3]. Details of the processing can be found in the Matlab™ code that was used to process the results in accompanying document titled *Matlab™ Script Files*. The codes were named as follows:

- *data_reader_llts_ATD_version1.m* – Used to process the results of each test individually.

- *data_reader_Its_ATDcompareposition_version1.m* – Used to plot the various foot position results on the same axes.

- *data_reader_Its_ATDcomparerepeatability_version1.m* – Used to compare the repeatability of various tests

- *data_reader_Its_ATDcomparesamefile_version1.m* – Used to compare the results from the various sensors for individual tests.

Data analysis:

The manner in which the data was analysed played a large role in the results that were obtained. There is often no hard and fast rule as to how to analyse the data and thus certain decisions were made regarding the analysis of the results. However, as the results could be analysed differently depending on the focus of the research, each of the test graphs were presented in the accompanying document titled *Detailed Results*. This will allow the results to be analysed in an alternative manner should the need arise in the future. A typical example of the graphs that were provided in this document is outlined in Figure 153.

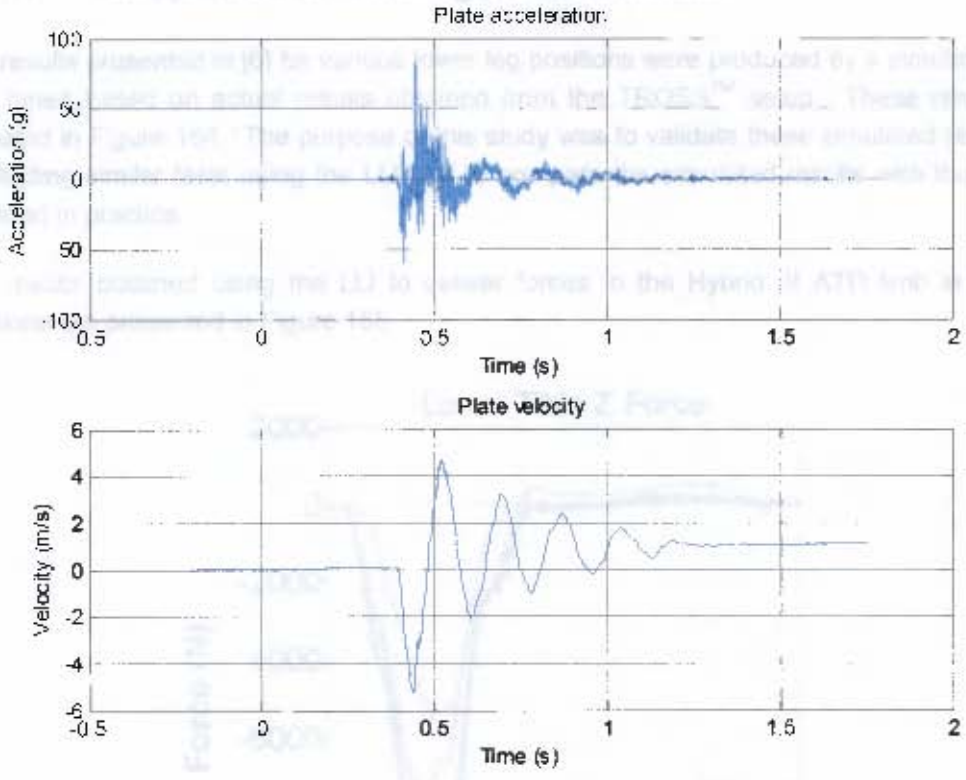

Figure 153: A typical example of the impactor plate acceleration and velocity.

The duration of the peak plate velocity and peak leg force were again determined using threshold value of 10% of the peak.

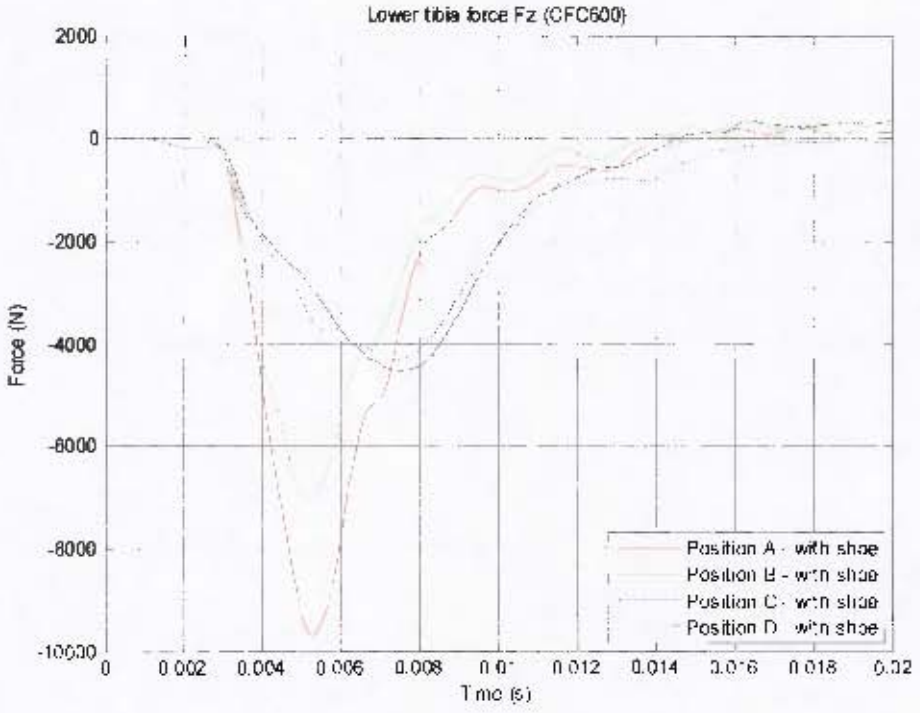

Figure 155: Graph showing the lower tibia axial force recorded with different lower limb positions using the LLI.

The results that were obtained for the different lower limb positions using the LLI are shown in Figure 155. Comparing these results to the simulated results (See Figure 154) the trends appear similar apart from Position C which produced a much higher leg force in the simulated results than in the results obtained using the LLI. This was thought to be due to the practical setup of the lower leg position. The simulation was based on the setup of the TROSS™ where the load on the plate was a blast load which would extend out in a radial and uniform manner from the centre of the explosive charge. The simulation would, most likely, be set up in such a way that all the force would act at a right angle to the plate on which the leg rests. In addition, the simulation was based on keeping the vertical displacement constant and not the input force (or spring preload in the case of the LLT). Using the LLI the force generated by the preloaded spring would act vertically and only a component of the total force would act in the lower tibia axial direction (See Figure 156), in which case it is clear that the pure axial force would be lower than the Position A results

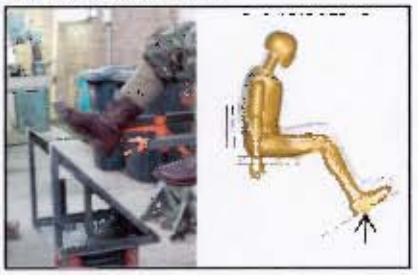

Figure 156: Comparison of LLI and simulation [6] setup for Position C.

Graphs comparing the simulated (from [6]) and LLI results are presented in Figure 157 and Figure 158. With the exception of Position C, the trends in the peak leg force were very similar. The LLI peak forces were consistently higher than the simulated results, but this was also found in [6] when the model was tuned using Position A results obtained from TROSS™ experimental data. The TROSS™ leg force was 9% lower than the simulated leg force. The LLI leg force was 8% lower than the simulated leg force for Position A and, with the exception of Position C, the LLI leg force results are 8-13% lower than the simulated results. The paper [6] suggests that this may be due to the increased effects of damping at higher loading (referring to the db 3 loading condition).

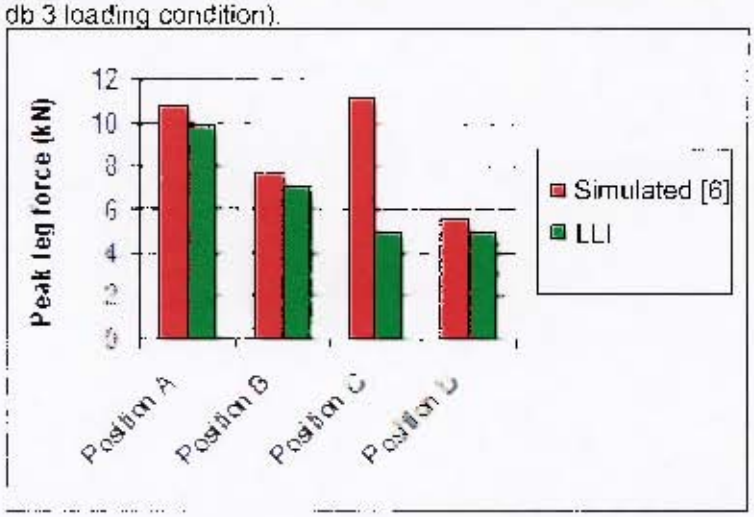

Figure 157: Graph comparing simulated [6] and LLI peak leg force results for various lower leg positions.

The durations of the peak forces obtained for Position A and Position B were similar to those reported in [6] (See Figure 158) where the forces were fairly high. However, the trend whereby the duration of the peak force increases as the magnitude of the peak force decreases does not seem to be supported by the model reported in the paper [6].

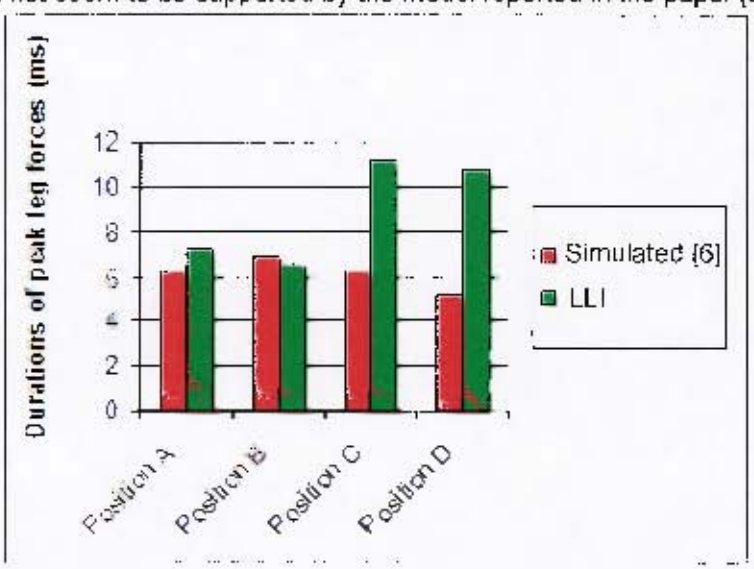

Figure 158: Graph comparing simulated [6] and LLI peak leg force duration results for various lower leg positions.

4.1.4.2 Repeatability assessment at various lower leg positions

The repeatability of results is significant as it provides confidence in the results and is essential for the validation of human surrogate measurement devices. Thus an assessment of the repeatability of the recorded peak tibia force and its duration were assessed for the various lower leg positions. The samples of the peak lower tibia force at each of the lower leg positions and their durations are plotted in Figure 159 and Figure 160 respectively. The results are summarised in Table 44. It was found that the peak forces recorded in Position C were the least repeatable whilst the peak forces recorded in Position A were the most repeatable.

Table 44: Details of the repeatability of the peak lower tibia force at various lower leg positions.

	Average peak lower tibia axial force (kN)	Standard deviation (kN)	% within
Position A - with boot	9.86	0.21	2.1
Position B - with boot	7.14	0.40	5.7
Position C - with boot	4.91	0.64	13.1
Position D - with boot	4.92	0.30	6.1

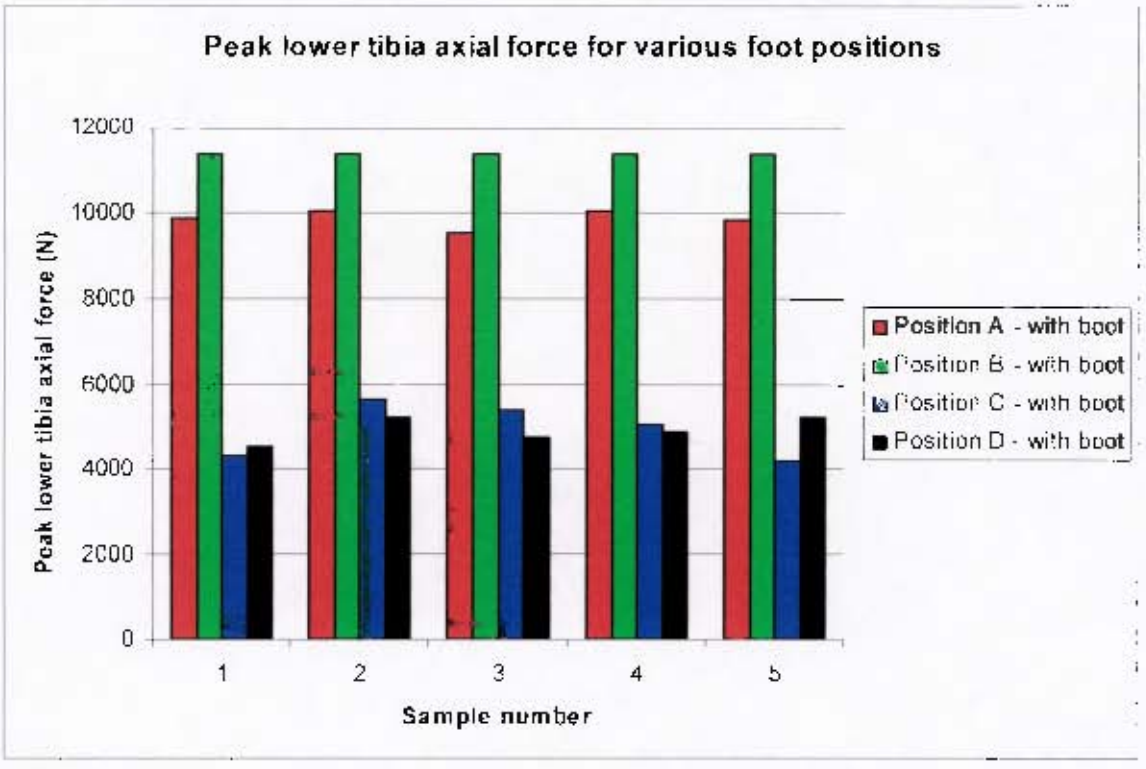

Figure 159: Peak lower tibia force at various lower leg positions.

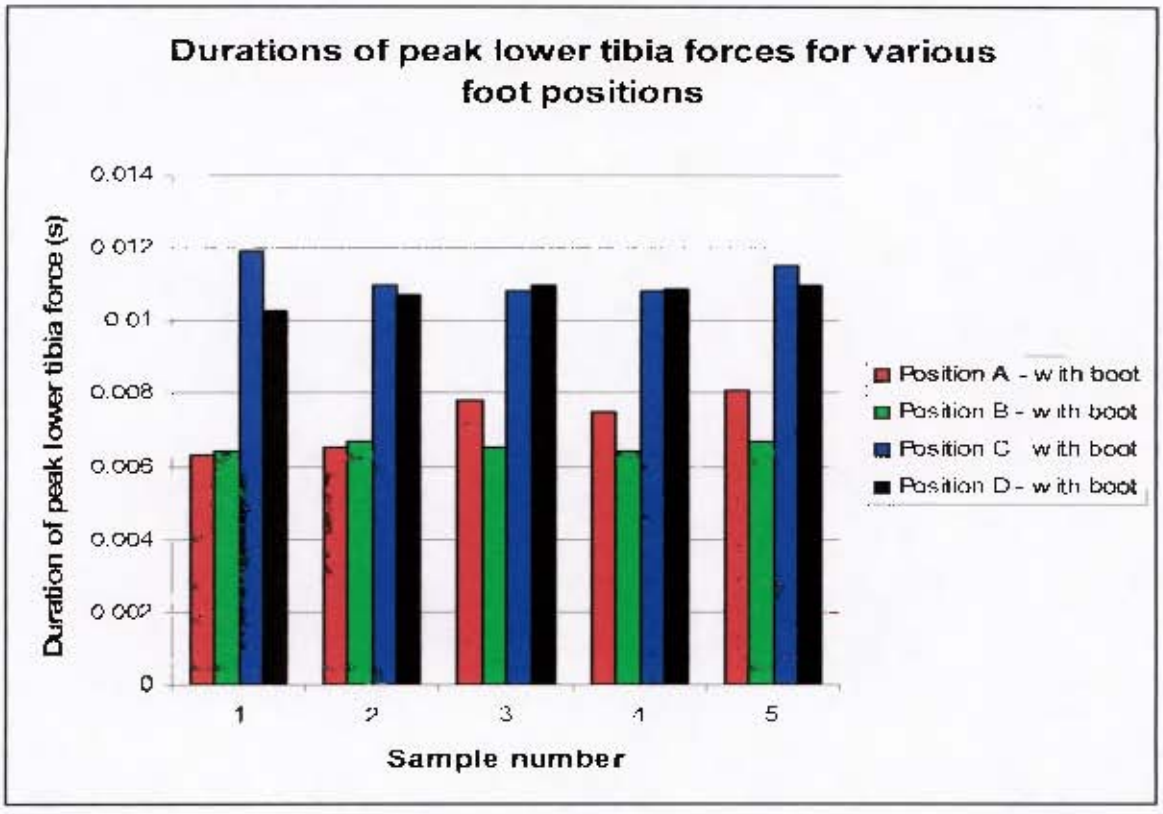

Figure 160: Duration of the peak lower tibia force at various lower leg positions.

The impactor plate velocity gives an indication of the signal input to the limb. Figure 161 and Figure 162 show that the peak plate velocity and its duration were not significantly influenced by the lower leg position which is as expected as the peak occurs prior to impact with the foot. This also confirms that the input velocity of the impactor plate was consistent for all lower leg positions which meant that the deviations in recorded tibia force were as a result of the lower leg position, rather than a change in the input velocity of the impactor plate The peak impactor plate velocities were within 3.4% of each other and the durations of the peaks were within 0.2% of each other.

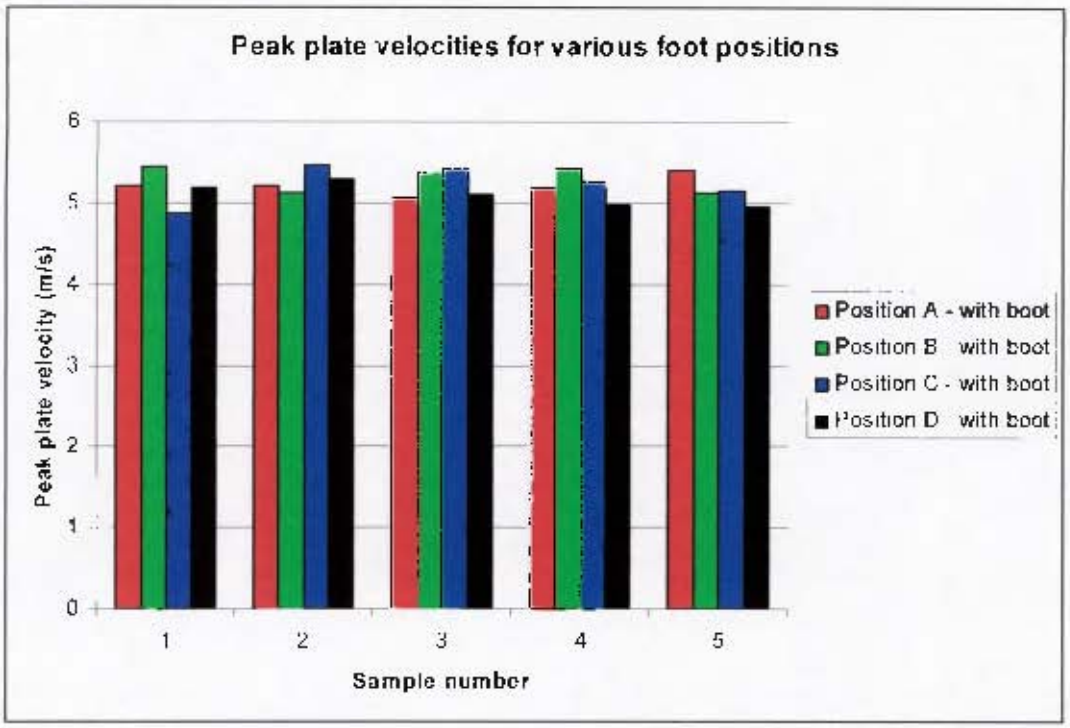

Figure 161: Peak plate velocity for each of the lower leg positions.

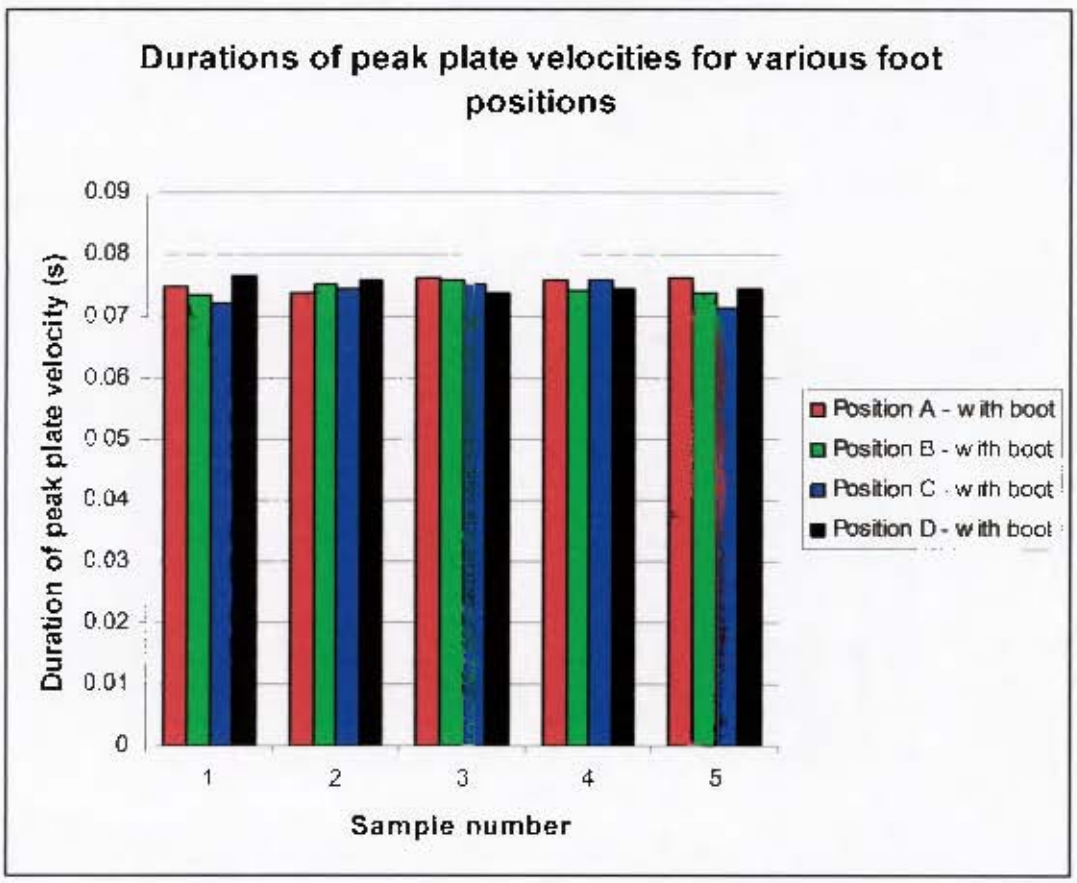

Figure 162: Duration of the peak plate velocity for each of the lower leg positions.

4.2 Effect of wearing a boot on injury levels

The effect of wearing a boot has been reported in the literature to decrease the peak lower tibia axial force significantly [30] [31] [32]. This phenomenon will be explored using a standard issue (South African) army boot in this section.

4.2.1 Experimental design setup

Experiments to investigate the effect of wearing a boot on injury levels were initially conducted using the LS drop test rig. As a significant effect was observed, the LLI was later used to explore this effect further.

The instrumentation and data acquisition, processing and analysis was similar to the setup outlined in sections 4.1.1 and 4.1.2.

4.2.2 Test results and discussion

4.2.2.1 Drop test rig results and discussion

A simple preliminary test was conducted to ascertain the effect of wearing a boot on the force measured by the surrogate leg. Surrogate leg number 5 was dropped from a height of 500mm using the drop test rig. The joint torque of the surrogate leg knee and hip joint was set to 6Nm in each case. The results were processed in Matlab™ and the force/time graphs are shown in Figure 163. The code can be found in the accompanying document titled *MatlabTM Script Files*[35]. Five repeats were conducted with the boot and one drop was done without the boot.

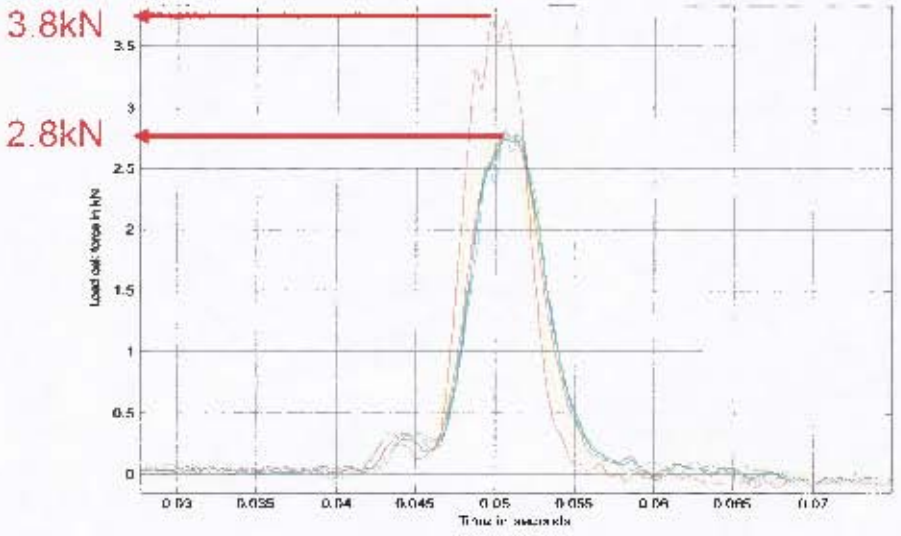

Figure 163: Surrogate leg 5 lower tibia peak force versus time – with and without boots.

[35] The Matlab file saved as *data_reader_drops.m* was used to read in the data and include calibration factors and the file saved as *loadcelliprocdrops.m* was used to line the data up and zoom into the relevant sections of the graphs.

The average of the drops with a boot was found and plotted with the result without a boot in Figure 164.

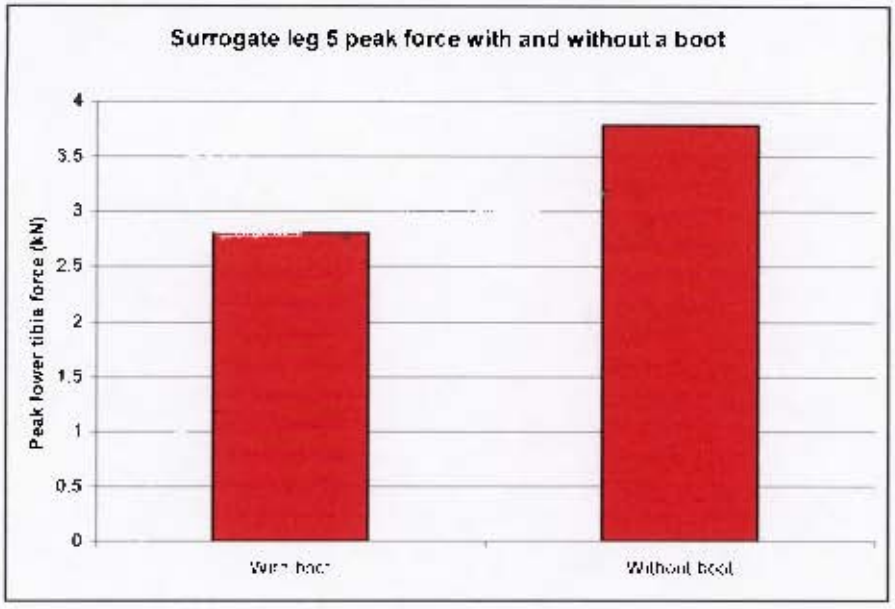

Figure 164: Bar chart of surrogate leg 5 drop test results with and without a boot.

The values of the peak forces were 2.8kN with a boot and 3.8kN without a boot. This translated to the leg reading a 26% lower force with a boot

4.2.2.2 LLI results and discussion

As the effect of the boot was found to be significant in the preliminary testing conducted using the drop test rig, further testing was carried out using the LLI. During the lower leg position investigation 5 additional tests were conducted with the Hybrid III ATD limb in Position A. The results of 1 of the tests are shown in Figure 165.

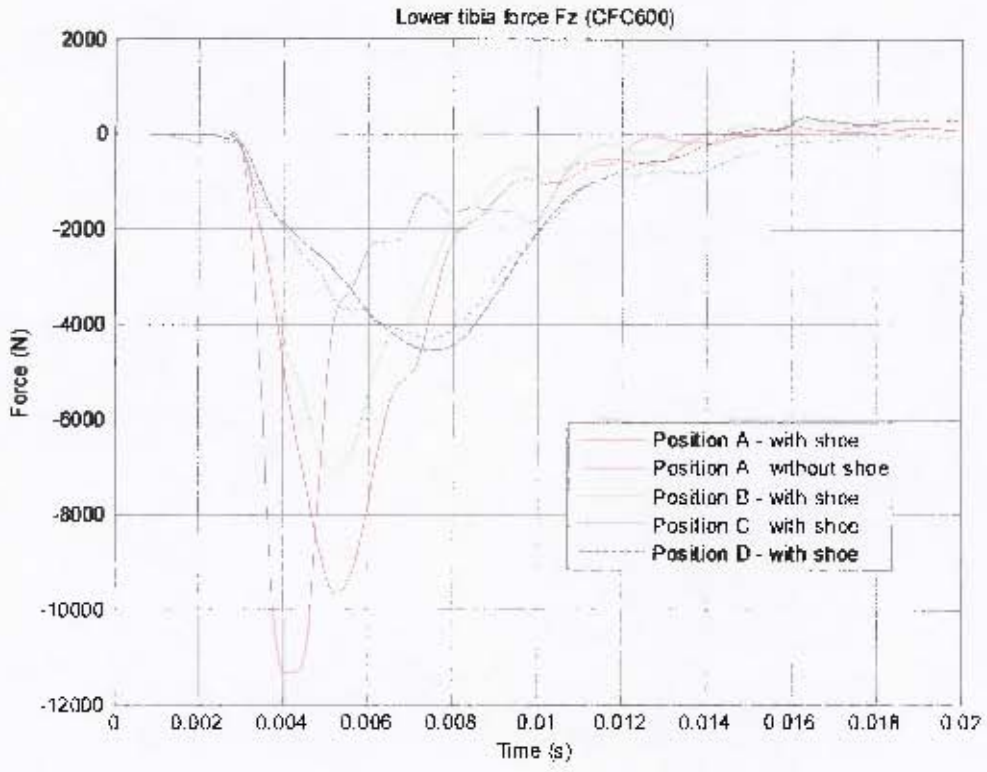

Figure 165: Lower tibia force with and without a boot.

The average peak lower tibia forces are shown in Table 45. The peak lower tibia axial force decreases by 13% by wearing a boot.

Table 45: Average peak lower tibia axial force and duration with and without a boot.

	Average peak lower tibia axial force (kN)	Average peak lower tibia axial force duration (s)
Position A - with boot	9.86	0.007
Position A - without boot	11.35	0.005

As was mentioned in section 2.5.1, it was reported in [32] that the presence of the boots decreased the tibia force by 30-40%. Although the boot did not reduce the force by as much as 30-40% in the LLI or drop testing results, a significant reduction of more than 10% was observed. This deviation may be explained by the use of different boots in the study conducted outlined in [32] as the boots used may have been softer and thus offered more damping and thus greater protection.

4.2.2.3 Repeatability assessment with and without boot using the LLI

During the testing with and without a boot an interesting phenomenon in the repeatability of the results was observed. Repeatability is of significance as human surrogate measurement equipment must be repeatable if it is to be used in the validation of vehicles. The samples taken with and without a boot are shown in Figure 166 and the repeatability is quantised in Table 46.

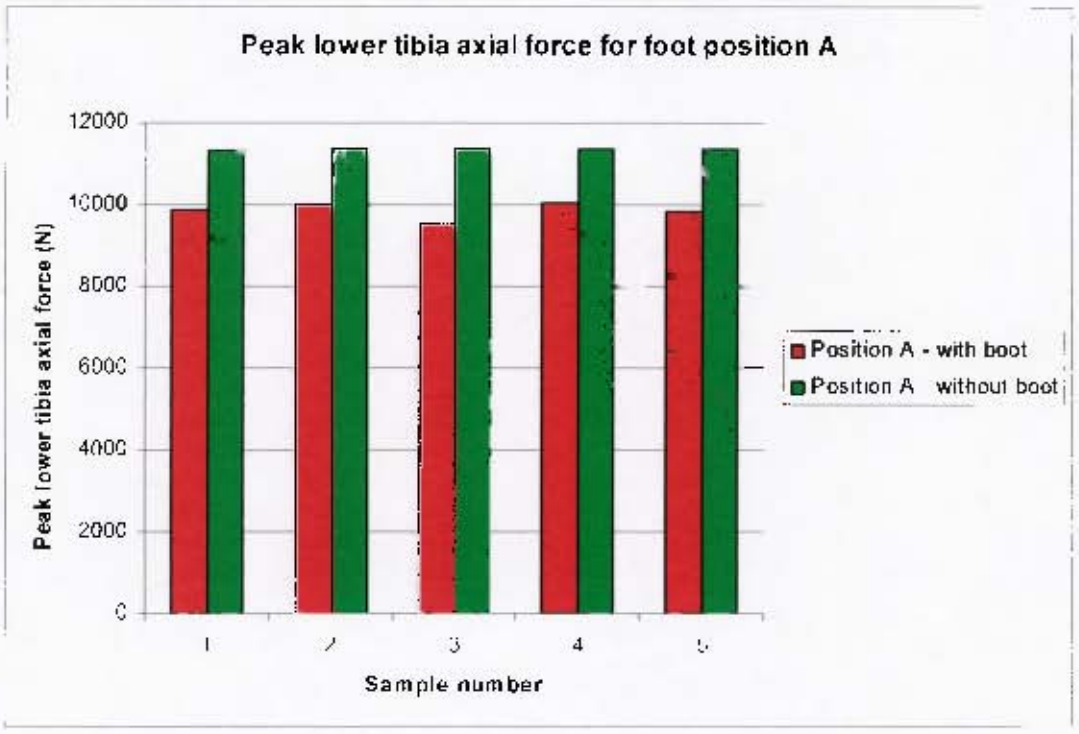

Figure 166: Peak lower tibia axial forces with and without a boot.

Table 46: Peak lower tibia axial force with standard deviation with and without a boot.

	Average peak lower tibia axial force (kN)	Standard deviation (kN)	% within
Position A - with boot	9.86	0.21	2.1
Position A - without boot	11.35	0.01	0.1

The above result was alarming as it reflects that the repeatability of the Hybrid III ATD lower tibia force measurement decreases significantly (the results drop from being within 0.1% of one another to being within 2.1% of one another) with the use of a boot. This means that the accuracy of the measurements obtained using the Hybrid III ATD decreases with the use of a boot which is detrimental to the consistency required during validation testing.

4.3 Effect of hip and knee joint stiffness on injury levels

4.3.1 Experimental design setup

Drop tests were conducted using the surrogate legs set to two different hip and knee joint settings to provide preliminary results regarding the effect of joint stiffness on lower tibia force measurements. In addition to this, two different joint torques were also used during the initial characterisation of the LLTS and later, the effect was further explored using the LLI.

The instrumentation and data acquisition, processing and analysis was similar to the setup outlined in sections 4.1.1 and 4.1.2. However, the surrogate leg was used instead of the Hybrid III ATD as the hip and knee joint stiffness could be easily manipulated. The following transducers were used instead of those specified in 4.1.1 for the Hybrid III ATD (See Figure 167 for the location of the transducers):

- One 500g accelerometer was fitted to the surrogate leg foot.
- Surrogate leg 5 was fitted with a load cell in the lower tibia.

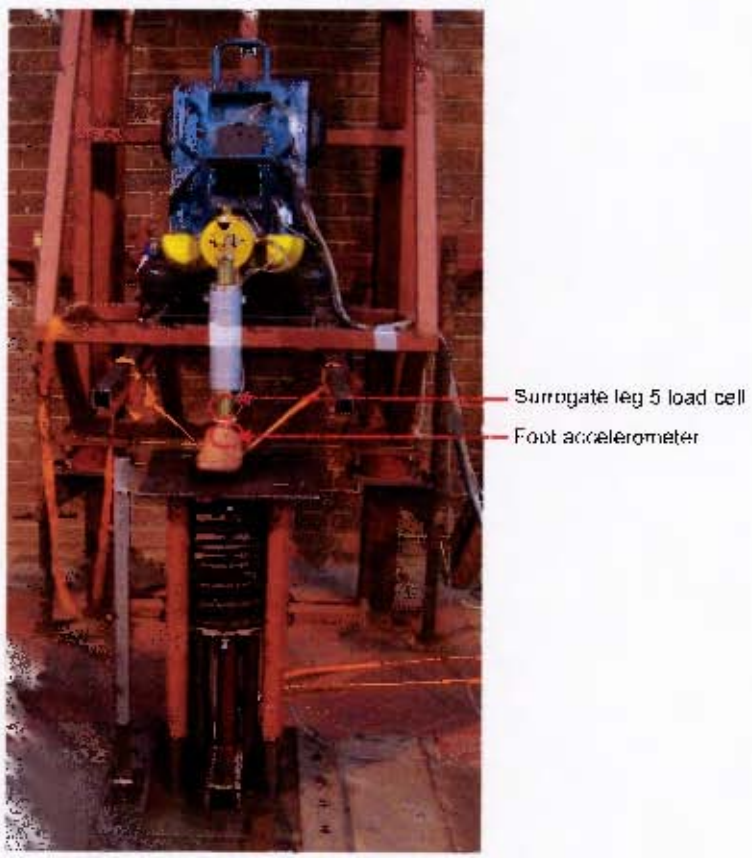

Figure 167: Diagram showing the location of transducers on the LLI and surrogate leg 5.

Table 47 shows the serial numbers of the instrumentation and the sensitivities of the transducers.

Table 47: Description of the instrumentation used in the joint stiffness investigation and the sensitivities of the transducers.

Instrumentation description:	Serial number:	Sensitivity:
Surrogate leg 5	5	N/A
Surrogate leg 5 load cell	5	0.00010mV/N
Surrogate leg 5 500g foot accelerometer	0639-005	0.086mV/g

4.3.2 Test results and discussion

4.3.2.1 Drop test rig results and discussion

The preliminary investigation was conducted with surrogate legs with serial numbers 3, 5, 7 and 8 which were each dropped from a height of 500mm using the drop test rig. The legs were dropped 5 times each at each of the joint torque settings of 6Nm and 25Nm. The results showed good repeatability with an average standard deviation of 0.1kN or within 3-4% of one another. The results are shown in Figure 168.

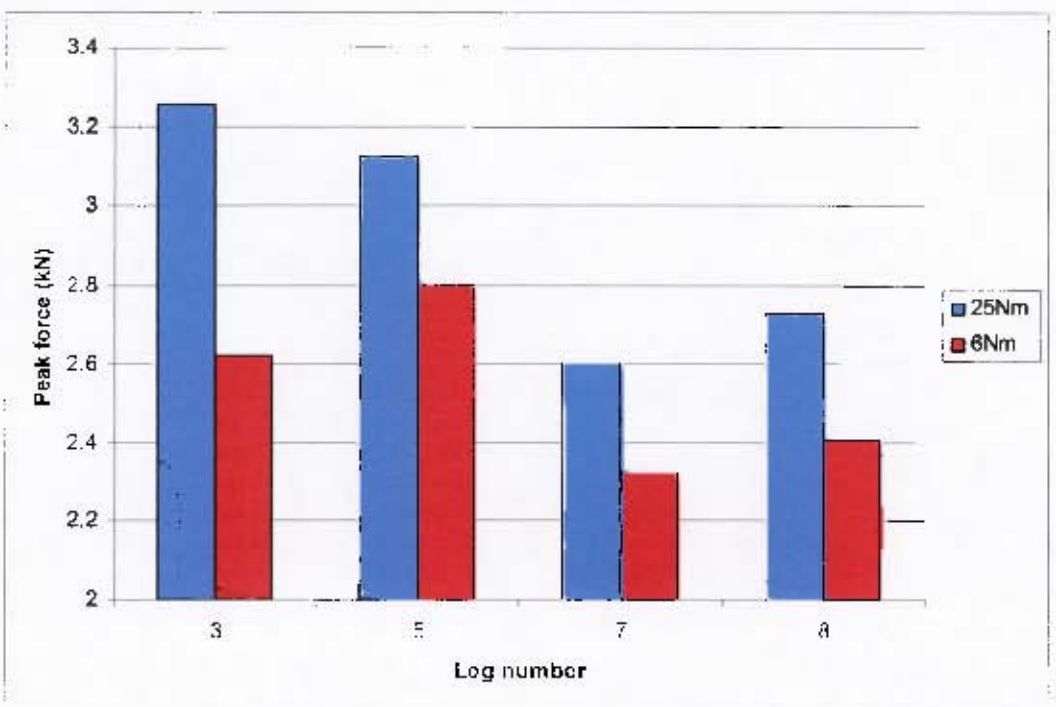

Figure 168: Drop test peak force results for two different joint torque settings.

The results of the drop tests show that as the joint torque decreases, so does the peak force recorded by the surrogate legs

4.3.2.2 LLTS and LLI test results and discussion

Based on the preliminary results, the effect of joint stiffness was further explored using the original LLTS. The results gathered using the original LLTS at two different offset distances (See section 2.5.2.3 of this dissertation for an explanation of offset distance) settings were examined to assess if the trend discovered in the drop test results was confirmed by the LLTS results. The results and trends are highlighted in Figure 169 and Figure 170.

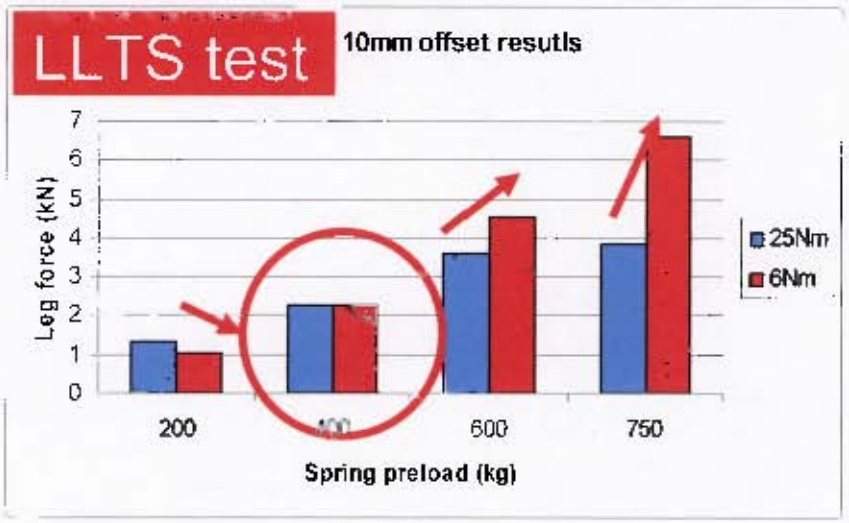

Figure 169: LLTS results using two different joint torque settings using a 10mm offset distance.

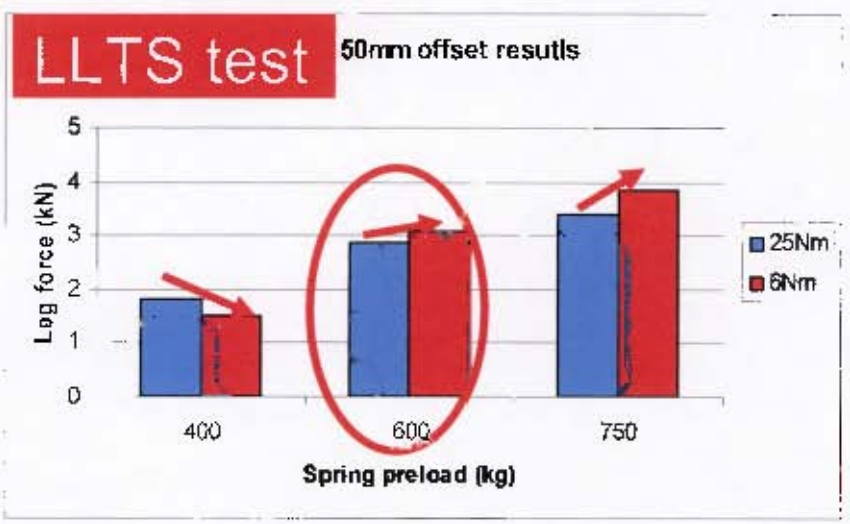

Figure 170: LLTS results using two different joint torque settings using a 50mm offset distance.

It would appear that when the surrogate legs are subjected to forces generated at a low spring preload setting of the original LLTS, the trend observed in drop testing is confirmed as the lower joint torque setting results in a lower force being read by the surrogate leg. However, at higher spring preloads the lower leg joint torque setting reads higher forces than at the larger leg joint torque setting. The circled data points in the figures show the surrogate leg force readings that are comparable to those readings obtained when the leg[26] was drop tested. These LLTS results do not reflect the same trend as was observed during the drop testing of the leg.

Further tests were then conducted using the LLI using surrogate leg 5 with different foot modules (See section 3.4.2 for details on the various foot adaptor modules). The results are illustrated in Figure 171.

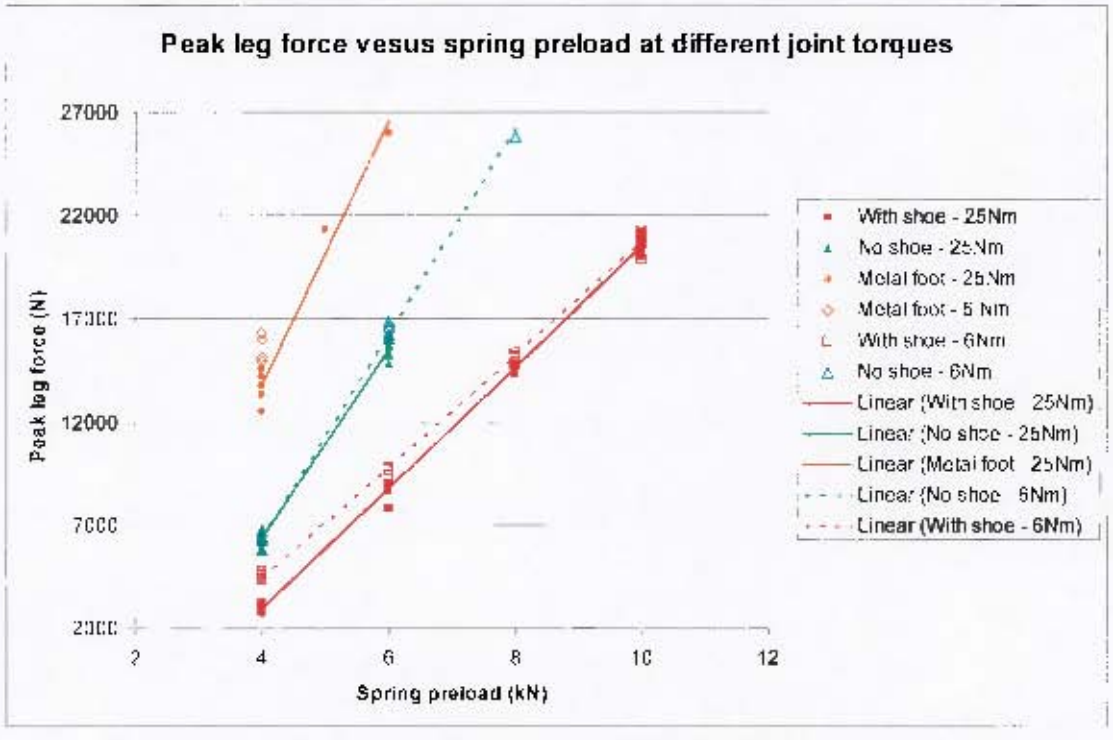

Figure 171: Peak leg force versus spring preload at different joint torques using the LLI.

No obvious trends were found concerning the effect of joint stiffness in the results obtained using the LLI. However, it was clear that joint stiffness may play a role in the peak tibia force that was recorded. To illustrate this fact, the case of the surrogate leg with a shoe was extracted to be more closely examined in Figure 172.

[26] It must be noted that surrogate leg 5 was also used in the LLTS initial characterisation tests

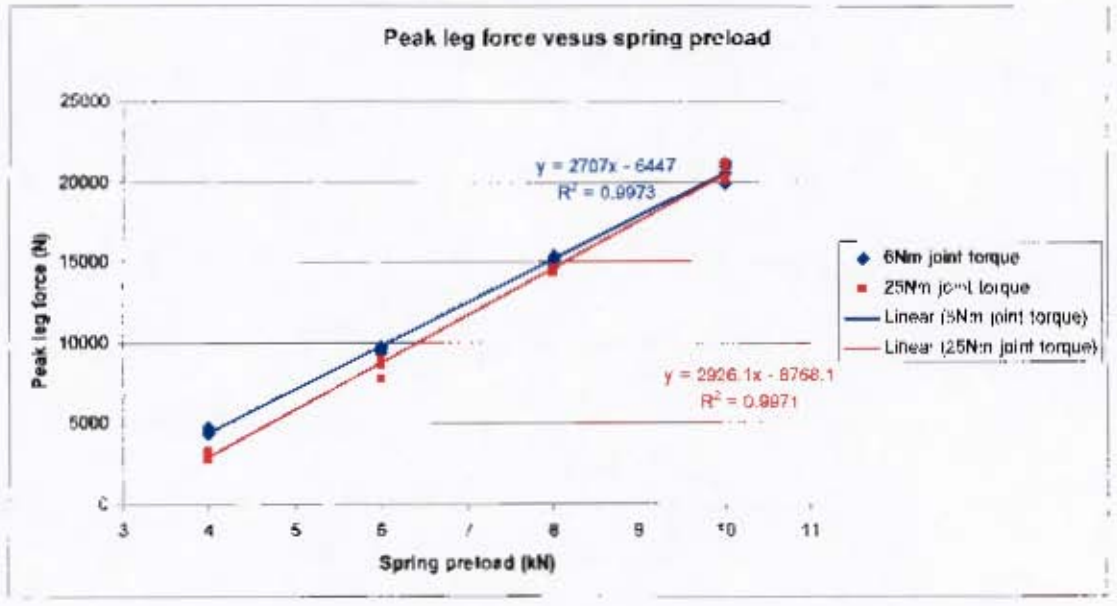

Figure 172: Peak leg force of surrogate leg 5 with a shoe at 6Nm and 25Nm joint torque.

The average peak leg forces at the 4kN spring preload are highlighted in Table 48. These results show a 32% difference in the average peak leg force and the standard deviation of each is only between 3.5% and 6.1% which does not account for the variation.

Table 48: Average peak leg force at 4kN spring preload at 6Nm and 25Nm joint torque.

4kN spring preload	Average peak leg force (kN)	Standard deviation (kN)	% within
6Nm	4.54	0.16	3.5
25Nm	3.10	0.19	6.1

5 CONCLUSIONS AND RECOMMENDATIONS

5.1 Modification and characterisation of the LLI

The conclusions and recommendations regarding the modification and characterisation of the LLI are split up into two sections. The first section examines whether the LLI has met its aim and the second section examines various factors which influence the characterisation and performance of the LLI.

5.1.1 Aim of the LLI

The conclusions on the LLI are presented in terms of the two major aims that were defined for the system:

- **Aim 1: Apply a force of varying peak amplitude and peak amplitude duration to a surrogate limb as the limb might see in the field.**

  In terms of varying the peak amplitude of the force, it has been identified that increasing the preload on the spring increases the peak force. Increasing the peak force appears to decrease the peak force duration. The LLI can produce peak forces that vary between 3000N and 21000N, however, it is expected that if a 30mm offset is not required that peak forces can be lowered. This range exceeds that of the original LLTS and encompasses most forces that a limb can experience within a landmine protected vehicle during an explosive event (See Figure 173). Thus, the LLI meets this aim.

  In addition, the lower tibia axial forces applied by the LLI are very similar to those obtained by the TROSS™ as reported in [6]. This provides added confidence in the ability of the LLI to provide forces which are similar to those that may be experienced by a surrogate limb in a vehicle during an explosive event.

- **Aim 2: The force must be repeatable to allow various parameters to be explored.**

  The repeatability is influenced by the setup of the surrogate leg measurement device and requires many samples to provide conclusive results. However, a preliminary analysis of the repeatability using surrogate leg 5 indicates peak leg forces that are within 0.9% to 6.1% (an average of 3.7%) of each other. This is an improvement on the repeatability of the original LLTS which reveals peak leg forces that are within 8.3% to 31.3% (an average of 20.9%) of each other.

  The repeatability of the LLI results and drop test rig results using a Hybrid III ATD and surrogate leg 5 is comparable (The preliminary study shows that the LLI results are in fact more repeatable than the drop test rig results).

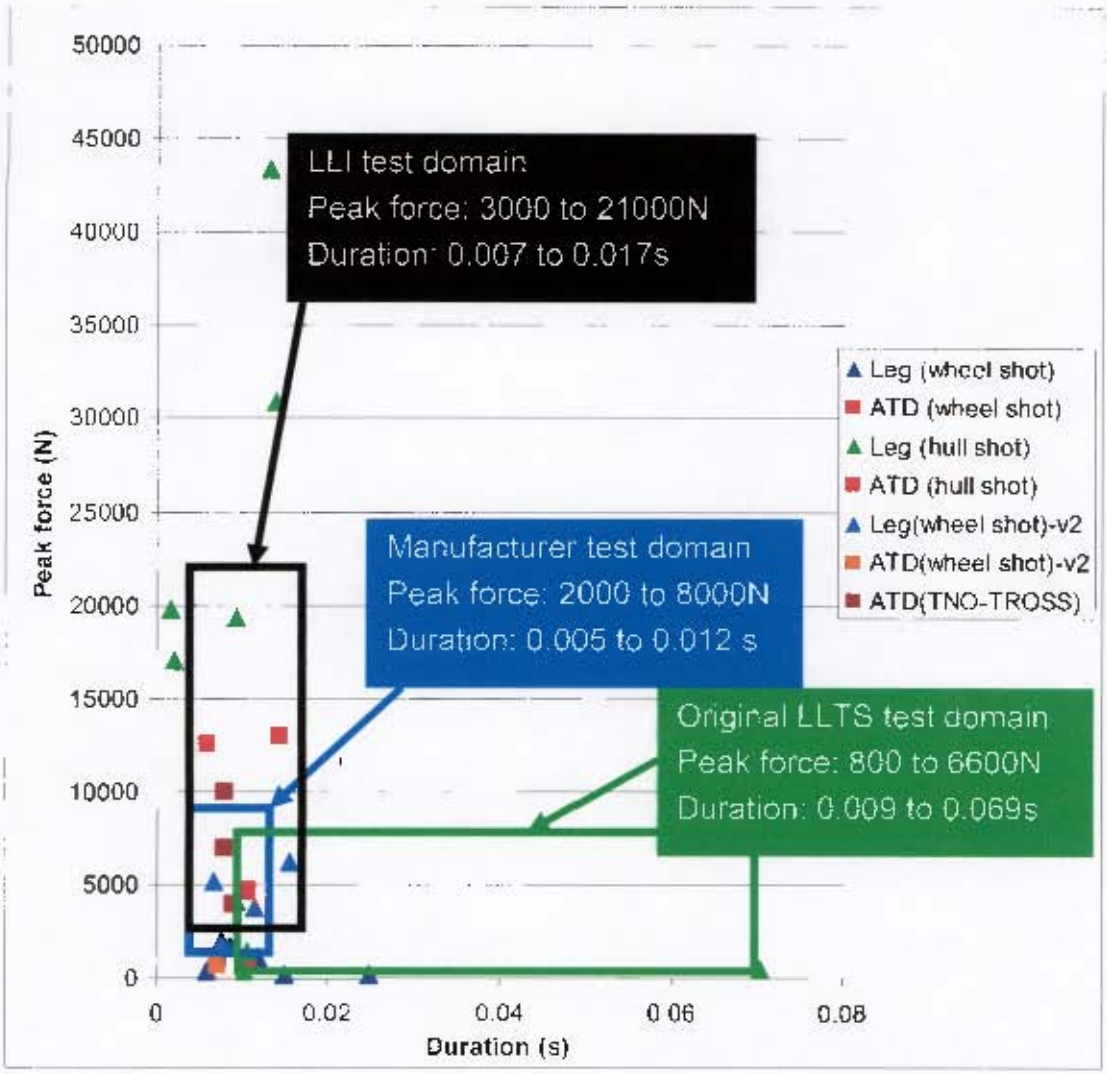

Figure 173: Diagram showing typical peak forces and peak force durations that are recorded by a surrogate limb in the field and the original LLTS and LLI test domains.

5.1.2 Factors affecting the characterisation and performance of the LLI

- The effect of adding a mass plate to the impactor plate decrease the peak velocity of the impactor plate and thus decreases the magnitude of the force that is recorded by the surrogate limb. The addition of the mass plate does not appear to affect the duration of the peak surrogate leg force.

- The use of different surrogate limbs will affect the performance of the system in terms of the peak forces measured. Decreasing the damping offered by the surrogate foot increases the magnitude of the measured force substantially. The use of different surrogate limbs does not affect the peak impactor plate velocity which indicates that the input velocity generated by the LLI is independent of the human surrogate measurement device which allows different human surrogate measurement devices to be legitimately compared.

- When the LLI is setup to provide severe loading, the surrogate leg records axial tibia forces that are approximately double those recorded by the Hybrid III ATD. Whilst previous experiments show that the surrogate leg records forces that are slightly higher than those recorded by the ATD, this difference is extreme. It is recommended that the results obtained by the surrogate leg under severe loading conditions be validated.

- The input to the surrogate leg is currently obtained from the impactor plate peak velocity which is calculated from an accelerometer measurement. The integration process that is required to obtain a velocity reading from the accelerometer reading is not generally regarded as good practice. A displacement meter should be used in future to verify the velocity reading.

5.2 Investigation of factors affecting surrogate leg measurements

- The lower leg position tests carried out with the use of the LLI were used to experimentally verify the simulation results in [6]. The trends observed in the peak leg force results in [6] were the same as those obtained using the LLI for lower limb position A, B and D

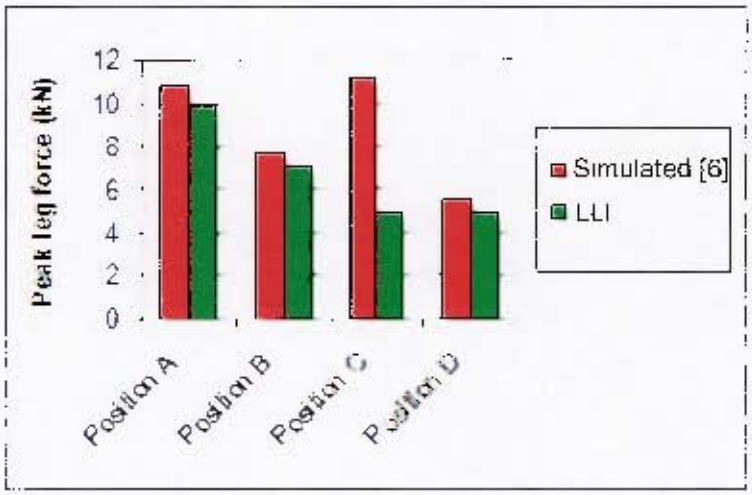

Figure 174: Graph comparing simulated [6] and LLI peak leg force results for various lower leg positions.

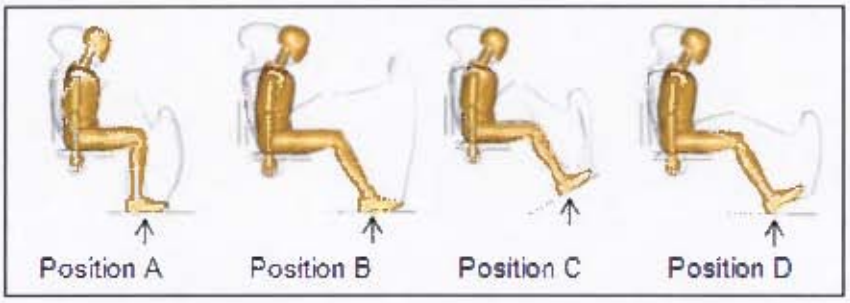

Figure 175: Diagram illustrating the various lower leg positions (from [6]).

These results can be interpreted as follows:

- The highest axial loading on the lower tibia is experienced in Position A which means that in this position the occupant would have the highest risk of injury due to the axial loading.
- Position B follows position A in terms of risk of injury due to the axial loading.
- Position D is the position in which there is the least risk of injury due to axial loading
- The effect of Position C will not be discussed at this stage as the results obtained with the LLI and the simulated results do not reflect a similar trend. It is recommended that the details of the setup of the simulation be obtained in order to investigate the deviation of the LLI results with those stated in [6].

One must keep in mind that these results are related only to injury due to pure axial loading of the lower tibia. Other injury mechanisms do exist and should be evaluated

at the various lower leg positions. Although a certain lower leg position may reduce the risk of injury due to pure axial loading, it may increase the risk of injury due to other loading regimes and injury mechanisms. It is recommended that PMHS tests be conducted at the various lower leg positions in order to determine the effects of injury mechanisms other than pure axial loading of the lower limb.

The durations of the peak forces for Positions A and B are similar to those obtained in [6] where the peak forces are relatively high. However, for position D the duration of the peak force in [6] is much lower than the duration obtained using the LLI. The trend of the duration of the peak force decreasing as the peak force increases does not appear to be supported by the results reflected in [6], but it is clear in the results obtained using the LLI. This trend or lack thereof should thus be further investigated.

The repeatability of the peak leg force results was best in Position A which indicates that tests conducted in this position to investigate variables other than lower leg position (e.g. The effect of different boots on injury levels) will provide the most repeatable results.

- The use of the boot was reported in [32] to decrease the peak lower tibia axial force by 30-40%. Although the boot did not reduce the force by as much as 30-40% in the LLI or drop test rig results, a significant reduction of more than 10% was observed. The deviation in the amount by which the boot decreases the force may be explained by the use of different boots in the study reported in [32] (The boots used may have been softer and thus offered more damping and thus greater protection). It is recommended that the use of different boots be investigated as the effect that wearing the boots has on the risk of injury due to axial loading of the lower tibia is significant.

  The boot was found to negatively affect the repeatability of the lower tibia axial force results. This should be carefully considered as repeatability is important during vehicle validation testing and research into various lower limb parameters where the accuracy of the results is necessary.

- The lower limb response to various loading regimes needs to be carefully examined. The effect of joint stiffness provided conflicting results in the drop tests, original LLTS tests and LLI tests. The most variation in peak forces recorded using different joint stiffnesses was observed in the drop test results where the initial condition of the limb (position of the limb just prior to impact) is less defined than when using the LLI. However, in some cases the LLI did reflect differences using the two different joint stiffnesses of up to 32% at low spring preloads (4kN) and decreasing to no difference at high spring preloads (10kN). Thus, the effect of joint stiffness on the forces recorded by a surrogate limb is not clearly understood and should be further investigated with emphasis put on the repeatable setting of the initial condition of the limb.

- These investigations should lead one closer to **relating** measurements from **human surrogate limbs** to **actual injuries** (via defining more accurate and detailed injury criteria – For example: Not only the lower tibia axial force should be considered, but the forces along other axes and the moments should also be taken into account in the determination of the injury risk). This in turn will enable one to **better protect** people against injury and advise them on how to protect themselves (e.g. Which vehicles offer the best protection? What clothing or boots could be used to prevent or minimize injuries? Which sitting posture is best (e.g. Foot position, kit bag not on lap)?).

Figure 176: Diagram showing an overview of how research into lower limb surrogate measurement parameters can lead to improved protection mechanisms.

6 REFERENCES

[1] Geneva International Centre for Humanitarian Demining (GICHD) October 2004. *Humanitarian impact from mines other than anti-personnel mines*, Geneva.

[2] S. Nell. 2000. *Landmine protected wheeled vehicles. design, development and evaluation of*, RSA-MIL-STD-37, Issue 3.

[3] Procedures for Evaluating the Protection Level of Logistic and Light Armoured Vehicles, AEP-55 Volume 2 Edition 1, September 2006.

[4] S. Backaitis and H. Mertz. 1994. *Hybrid III: the first human-like crash test dummy*, SAE International. PT-44, USA.

[5] R. Dieterich August 2003. *Foot ankle/complex detail design report*. K1578081, Issue B.

[6] M van der Horst, C. Simms, R. van Maasdam and P. Leerdam. 2005 *Occupant lower leg injury assessment in landmine detonations under a vehicle*. IUTAM Symposium on Biomechanics of Impact. From Fundamental Insights to Applications. Dublin, Ireland.

[7] K Schmitt, P Niederer and F. Walz. 2004. *Trauma biomechanics: Introduction to accidental injury*. Berlin, Heidelberg, New York: Springer-Verlag.

[8] W. Whiting and R Zernicke. 1998. *Biomechanics of musculoskeletal injury*, Human Kinetics, USA.

[9] F Martini 2004 *Fundamentals of anatomy and physiology: Sixth Edition*, Benjamin Cummings, USA.

[10] J. Pike 1990. *Automotive safety: Anatomy, injury, testing and regulation*, Society of Automotive Engineers, Inc USA

[11] Association for the Advancement of Automotive Medicine (AAAM). 2005 *AIS 2005: Abbreviated Injury Scale 2005*, AAAM, Editors T. Gennarelli and E. Wodzin. Barrington, IL 60011, USA.

[12] C. Gadd. 1961. *Criteria for injury potential*, Impact Acceleration Stress Symposium, National Academy of Sciences. Washington, National Research Council Publication Number 977. pp. 141-144.

[13] Hertz. 1993. *A note on the head injury criterion (HIC) as a predictor of the risk of skull fracture*, 37th Annual Proceedings of the AAAM.

[14] N. Jones. 1989. *Structural impact*, Cambridge University Press, UK, Cambridge, ISBN: 0521301807

[15] G. Klopp, J. Crandall, G. Hall, W. Pilkey, S. Hurwitz and S. Kuppa. 1997. *Mechanisms of injury and injury criteria for the human foot and ankle in dynamic axial impacts to the foot,* IRCOBI Conference, Hannover.

[16] P. Begeman and P. Prasad. 1990. *Human ankle impact response in dorsiflexion.* In S. Backaitis and H. Mertz. 1994. *Hybrid III: the first human-like crash test dummy,* SAE International, PT-44, USA.

[17] F. Schueler, R. Mattern, F. Zeidler and D. Scheunert. 1995. *Injuries of the lower legs – foot, ankle joint, tibia; mechanisms, tolerance limits, injury criteria evaluation of a recent biomechanic experiment series,* The Biomechanics of Impact International Conference, Brunnen, Switzerland.

[18] N. Yoganandan, F. Pintar, M. Boynton, P. Begeman, P. Prasad, S. Kuppa, R. Morgan and R. Eppinger. 1996. *Dynamic axial tolerance of the human foot-ankle complex,* SAE 962426, USA: Society of Automotive Engineers.

[19] J. Funk, J. Crandall, L. Tourret, C. MacMahon, C. Bass, J. Patrie, N. Khaewpong and R. Eppinger. 2002. *The axial injury tolerance of the human foot/ankle complex and the effet of Achilles tension,* Journal of Biomechanical Engineering, Vol 124, Issue 6, pp.750-757.

[20] A. Hirsh. 1964. *Man's response to shock motions.* Reprint of a paper presented at the Winter Annual Meeting, Philadelphia, Pa., November 17-22, 1963 of the American Society of Mechanical Engineers. Report 1797 S-F0151404.

[21] H. Mertz. 1984. *Injury assessment values used to evaluate Hybrid II response measurements.* In: S. Backaitis and H. Mertz. 1994. *Hybrid III: the first human-like crash test dummy,* SAE International, PT-44, USA.

[22] S. Kuppa, J. Wang, M. Haffner and R. Eppinger. 2001. *Lower extremity injuries and associated injury criteria,* National Highway Traffic Safety Administration, USA, Paper no. 457.

[23] S.Nell, 2000.*Landmine protected wheeled vehicles: design, development and evaluation of, Handbook for,* RSA-MIL-HDBK-38, Issue 1.

[24] H. Yamanda. 1970. *Strength of biological materials.* R. E. Krieger Publ., New York.

[25] E. Welbourne and N. Shewchenko. 1998. *Improved measures of foot and ankle injury risk from the Hybrid III tibia.* 16th International Technical Conference on the Enhanced Safety of Vehicles (ESV), Windsor, Ontario, Canada, May 31- June 4.

[26] A. Barbir. 2005. *Validation of lower limb surrogates as injury assessment tools in floor impacts due to anti-vehicular landmine explosions.* Thesis submitted in partial fulfilment of the requirements for the degree of Master of Science, Major: Biomedical Engineering (Impact Biomechanics), Graduate School of Wayne State University, Detroit, Michigan.

[27] G. Turner and J. Reinecke. 2005. *Project Hoefyster test report.* DEF 2005/159 issue 2.

[28] R. Levine. 2002. *Injuries to the extremities, in accidental injury – Biomechanics and prevention,* Springer Verlag, New York.

[29] P. Manning, A. Wallace, C. Owen, A. Roberts, C. Oakley and R. Lowne. 1998. *Dynamic response and injury mechanism in the human foot and ankle and an analysis of dummy biofidelity.* The University of Nottingham and The Transport Research Laboratory, United Kingdom, 98-S9-O-11.

[30] J. Manseau and M. Keown. 2005. *Development of an assessment methodology for lower leg injuries resulting from anti-vehicular landmines,* IUTAM Symposium on Biomechanics of Impact: From Fundamental Insights to Applications, Dublin, Ireland.

[31] J. Geurts, M. van der Horst, P. Leerdam, C. Bir, H. van Dommelen and J. Wismans. 2006. *Occupant safety: mine detonation under vehicles – a numerical lower leg injury assessment,* IRCOBI Conference, Madrid, Spain.

[32] C. Bir, A. Barbir, M. Wilhelm, M. van der Horst, F. Dosquet and G. Wolf. 2006. *Validation of lower limb surrogates as injury assessment tools in floor impacts due to antivehicular land mines,* IRCOBI Conference, Spain, Madrid.

[33] M. Latash and V. Zatsiorsky. 1993. *Joint stiffness: myth or reality?* Human Movement Science, Vol 12, Issue 6, pp. 653-692.

[34] M. Gunther and R. Blickhan. 2002. *Joint stiffness of the ankle and the knee in running,* Journal of Biomechnaics, Vol. 35, pp. 1459-1474.

[35] S. Zinder, K. Granata, D. Padua, B. Gansneder. Accepted December 2006. *Validity and reliability of a new in vivo ankle stiffness measurement device,* Journal of Biomechanics.

[36] M. Latash. 1992. *Virtual trajectories, joint stiffness, and changes in the limb natural frequency during single-joint oscillatory movements,* Neuroscience, Vol. 49, No. 1, pp. 209-220.

[37] L. Zhang and G. Wang. 2001. *Dynamic and static control of the human knee joint in abduction-adduction,* Journal of Biomechanics, Vol. 34, pp. 1107-1115.

[38] M. Pithioux, P. Chavet, N. St-Onge and C. Nicol. *Influence of muscle preactivation of the lower limb on impact dynamics in case of frontal collision,* Online: http://acxiv.org/abs/physics/0510185.

[39] A. Esteki and J. Mansour. 1996. *An experimentally based nonlinear viscoelastic model of jonit passive moment,* Journal of Biomechanics, Vol 29, No 4, pp. 443-450.

[40] R. Davis and P. DeLuca. 1996. *Gait characterization via dynamic joint stiffness,* Gait and Posture, Vol 4, pp224-231.

[41] R. Selles, X. Li, F. Lin, S. Chung, E. Roth and L. Zhang. 2005. *Feedback-controlled and programmed stretching of the ankle plantarflexors and dorsiflexors in stroke: effects of a 4-week intervention program,* Arch Phys Med Rehabil, Vol. 86.

[42] R. Riener and T. Edrich. 1999. *Identification of passive elastic joint moments in the lower extremities,* Journal of Biomechanics, vol 32, pp.539-544.

[43] E. Hardin, A. Su and A. van den Bogert. 2003. *Foot and ankle forces during an automobile collision: the influence of muscles,* Journal of Biomechanics, Vol. 37, pp. 637-644.

[44] M. McHugh and D. Hogan. 2004. *Effect of knee flexion angle on active joint stiffness,* Acta Physiologica Scandinavica, Vol 180, Issue 3.

[45] C. English and D. Russell. 1999. *Mechanics and stiffness limitations of a variable stiffness actuator for use in prosthetic limbs,* Mechanism and Machine Theory, Vol. 34, pp. 7-25.

[46] C. English and D. Russell. 1999. *Implementation of variable joint stiffness through antagonistic actuation using rolamite springs,* Mechanism and Machine Theory, Vol. 34, pp. 27-40.

[47] K. Holt, R. Wagenaar, M. LaFiandra, M. Kubo and J. Obusek. 2003. *Increased musculoskeletal stiffness during load carriage at increasing walking speeds maintains constant vertical excursion of the body center of mass,* Journal of Biomechanics, Vol. 36, pp. 465-471.

[48] J. Ochala, D. Lambertz, M. Pousson, F. Goubel and J. van Hoecke. 2004. *Changes in mechanical properties of human plantar flexor muscles in ageing,* Experimental Gerontology, Vol. 39, pp. 349-358.

[49] S. Lark, J. Buckley, S. Bennett, D. Jones and A. Sargeant. 2003. *Joint torques and dynamic joint stiffness in elderly and young men during stepping down,* Clinical Biomechanics, Vol. 18, pp. 848-855.

[50] P. Stiff. 1986. *Taming the landmine.* Alberton: Galago Publishing.

[51] A. Medin, H. Axelsson and A. Suneson, 1998. *The reactions of the crew in an armoured personnel carrier to an anti-tank mine blast. A Swedish incident in Bosnia 1996.* FOA defence research establishment, ISSN 1104-9154.

[52] V. Radonic, L. Giunio, M. Biocic, A. Tripkovic, B. Luksic and D. Primorac. 2004. *Injuries form antitank mines in Southern Croatia.* Military Medicine, Vol. 169, April.

[53] M. Huang. 2002. *Vehicle Crash Mechanics,* CRC Press LLC, USA.

[54] J. Meriam and L. Kraige. 1998. *Engineering Mechanics Dynamics Fourth Edition,* John Wiley and Sons, Inc, Canada.

[55] K. Griesel. February 2006. *TROSS detail design report*, R/1/00507/4 Issue 4, KT527081.

[56] K. Griesel. February 2006. *LLTS test instruction*, R/4/000507/1 Issue 1, KT527081.

[57] K. Griesel. February 2006. *LLTS test report*, R/5/000507/1 Issue 1, KT527081.

[58] S. Boyd. 2000. *Acceleration of a plate subject to explosive blast loading – trial results.* Maritime Platforms Division Aeronautical and Maritime Research Laboratory, DSTO-TN-0270, Australia.

[59] J. Wang, R. Bird, B. Swinton and A. Krstic. 2004. *Protection of lower limbs against floor impact in army vehicles experiencing landmine explosion.* Journal of Battlefield Technology, Volume 4, Number 3.

[60] G. Keller and B. Warrack. 2003. *Statistics for management and economics,* Thomson Learning, Inc, USA.

[61] H. Kaufmann, T. Rothacher, G. Rubin and R. Meier. 2001. *Shock reduction power of different materials in plate targets.* 19th International Symposium of Ballistics, 7-11 May, Interlaken, Switzerland.

Appendix A Calibration Documentation

Appendix Removed due to visible signatures

A.2 Instrumentation certificates

Calibration document for surrogate leg 5:

CSIR

NATIONAL METROLOGY LABORATORY
TOTAL QUALITY MANAGEMENT SYSTEM

APPENDIX B
CALIBRATION DATA SHEET

Certificate No

CUSTOMER
EQUIPMENT
SERIAL NUMBER
MODEL No

INDICATOR (Model)
Serial Number
Resolution
Reading (units)

(X) Applied	(Y) Indicated				
	Run 1	Run 2	Run 3	Run 4	AVERAGE
	4. [V]	5. [V]	8. [V]	7. [V]	
0kN	0	0	0	0	
2	0,139	0,139	0,1432	0,142	
4	0,283	0,282	0,282	0,283	
6	0,424	0,422	0,425	0,425	
8	0,566	0,563	0,566	0,566	
10	0,708	0,706	0,709	0,709	
12	0,849	0,845	0,851	0,852	
14	0,991	0,987	0,992	0,992	
16	1,132	1,128	1,134	1,134	
18	1,275	1,269	1,275	1,276	
20	1,418	1,412	1,417	1,418	

Temperature Maximum 20,3
Minimum 20

(X) (Y)

Conversion
Calibrated in Tension Compression
Equipment Used 7696? Indicator 2mV/4025
Serial No 7696? Port
Present E. Jacobs Date 10/02/06
OC Witness

Calibration certificates for top plate accelerometer, surrogate leg 5 accelerometer and bottom plate accelerometer respectively:

measurement Accelerometer Calibration Certificate

Measurement Specialties Inc.
PH: 1-949-716-5377
FX: 1-949-916-5677
www.meas-spec.com
vibration@meas-spec.com
Calibration Date: **12/21/05** By: ZP

Model: **3022-500** S/N: **0639-008**
With 5VDC supply and 25°C:
Output Resistance: **4.28** kΩ
Zero Offset: **1.54** mV
Sensitivity: **0.085** mV/g at 100Hz

LOWER LEG 005 SHEET

measurement Accelerometer Calibration Certificate

Measurement Specialties Inc.
PH: 1-949-716-5377
FX: 1-949-916-5677
www.meas-spec.com
vibration@meas-spec.com
Calibration Date: **12/21/05** By: ZP

Model: **3022-500** S/N: **0639-005**
With 5VDC supply and 25°C:
Output Resistance: **4.22** kΩ
Zero Offset: **-0.24** mV
Sensitivity: **0.086** mV/g at 100Hz

LOWER bottom plate

10,5 Ω

measurement Accelerometer Calibration Certificate

Measurement Specialties Inc.
PH: 1-949-716-5377
FX: 1-949-916-5677
www.meas-spec.com
vibration@meas-spec.com
Calibration Date: **12/21/05** By: ZP

Model: **3022-500** S/N: **0639-013**
With 5VDC supply and 25°C:
Output Resistance: **4.18** kΩ
Zero Offset: **3.14** mV
Sensitivity: **0.085** mV/g at 100Hz

Appendix Removed due to visible signatures

A.3 Documentation for hydraulic system

50 Lorentz Street (Between Mitchell & Soutter – between Nedbank & Engen Garage)
P.O. Box 19301, Pretoria West 0117
Republic of South Africa
Tel: +27(0)12 327 3075,2831,2849,2849
Fax: +27(0)12 327 7530
Web: www.hytec.co.za

HYTEC
Inland - Pretoria
A Division of Afripower (Pty) Ltd
Reg No. 1973/013536/07

Rexroth
Bosch Group
Authorised Distributor

HYDRAULICS & PNEUMATICS

WORK REPORT

To:	C S I R	Prepared by:	DEVA GOVINDER
Fax No:	(012)	Cell No:	082 887 9838
Att:	Miss Tammy Whyte	E-mail Address:	devago@hytec.co.za
		Our Order No:	DG2156
		Our Job No:	
		Date:	05/03/07
Your Ref:		Page:	1 of 3
Re:	LAND MINE SHOCK SIMULATION TEST COMPONENTS		

Dear Madam

We thank you for utilising Hytec for consultation, servicing and repairing of your hydraulic equipment. We take pleasure in providing the following feedback report regarding the equipment repaired and prepared for use in your land mine shock simulation testing.

Hydraulic cylinder
Hydraulic cylinder - condition

- Shaft in good condition no scratch marks
- Barrel bore in good condition, no scratch marks
- Cylinder piston in good condition, no signs of pitting or wear
- Cylinder seals in good condition, no signs of excessive wear and tear
- Cylinder port rewelded with brass welding, unsuitable for high pressure operation

Hydraulic cylinder suitability for test application

- Cylinder size: 40mm bore x 20mm shaft
- Hydraulic forces available from above sizes at 210 Bar pressure: 25.8 kN push, 19.4 kN pull
- Test force of 20 kN requires 217 Bar pressure.
- Hydraulic cylinders are designed to operate at a safety factor of 3.0 versus the operating pressure. The supplied cylinder's seals can cope with 210 Bar but the internal design reflects an intended working pressure of 140 Bar, i.e the cylinder can operate at 217 Bar but the safety factor drops to 1.9 from 3.0.
- In light of the above Hytec advises that CSIR carefully considers the use of this cylinder in the proposed test application. The cylinder can possibly work for very short periods of time at 217 Bar pressure but all testing must cease immediately upon any seal failure, signs of leaking or pressure loss. This is not a written consent to use the cylinder but a recommendation for consideration in light of current cylinder delivery times and testing dead lines.

Hand pump - condition

Hand pump suitability

- Hand pump is an Enerpac P84 double acting unit.
- Enerpac (and its main competitor Power Team – both US companies) produce the most robust and well designed high pressure hydraulic equipment in the world.
- The P84 unit can generate a maximum pressure of 700 Bar, regulated by an untamperable internal pressure relief valve.
- For this application the hand pump's internal pressure relief valve can be set to 220 Bar in order to protect the cylinder and reset to factory specification of 700 Bar once testing is completed

Equipment repair breakdown

Hydraulic cylinder

- Stripped, cleaned and inspected
- Replaced sealkit
- Refurbished port
- Replaced port protection plugs
- Assembled, tested, painted and packaged
- Test certificate to be provided (included in this feedback report)

Hand pump

- Striped, cleaned and inspected
- Replaced sealkit
- Replaced high pressure relief valve
- Re-seated low pressure relief valve
- Replaced hand pump grip
- Repair/replaced control valve
- Assembled, tested, painted and packaged
- Test certificate to be provided (included in this feedback report)

Final comments on component capabilities

- After initial discussions on my visit, the components available were required to deliver a pulling force of 20 kN.
- The repaired cylinder offered a 40mm bore x 20mm shaft.
- At maximum design pressure of 140 Bar this equated to a 13.2 kN of pulling force.
- After assessment of the unit in stripped condition we advised that the cylinder could be pressurised to 210 Bar resulting in 19.8 kN
- We however advised that this pressurisation be carried out over short intervals and be stopped immediately if the cylinder showed signs of stress.

Please use the following table as a reference of pulling force (retraction of the shaft) against supplied pressure

Please refer to the last remaining pages for test and calibration certificates

Hoping that we have interpreted your requirements correctly and looking forward to being of service to you in the future

Kindest regards

Deva Govinder
External Sales

Appendix Removed Due To Visible Signatures

Appendix B FEM Simulations

B.1 Simulation of LLTS

UNIVERSITY OF CAPE TOWN

Department of Mechanical Engineering

BLAST IMPACT AND SURVIVABILITY RESEARCH UNIT

BISRU

Finite Element Analysis of Structural Performance of the LLTS

Prepared for	:	CSIR/Defencetek
Prepared by	:	Victor Balden
Date	:	October 2006

Engineering Research That Saves Lives

1 Document Information

Document Title	*Finite Element Analysis of Structural Performance of the LLTS*
Contract No. **Project Designation**	-
Prepared by:	Victor Balden BISRU, UCT
Date	27 October 2006
Approved by:	Prof Gerald Nurick Director, BISRU, UCT
Date	27 October 2006
Distribution List:	Mr. David Reinecke & Mrs T Whyte CSIR Landwards Sciences PO Box 395 Pretoria 0001, South Africa Tel +27 21 8832141 +27 12 8414049 e-mail :
Revision History RevA, 27 October 2006	Release of Approval within BISRU

2 Table of Contents

3 List of Figures

4 Scope of Work

The scope of work to be undertaken by BISRU is divided into the following tasks:

- Generate a finite element model of the LLTS using geometry supplied by CSIR
- Simulate the LLTS dynamic response
- Deliver a rudimentary report outlining the simulation methods and results

5 Finite Element Model

5.1 CAD Geometry

The completed CAD model of the LLTS is shown in Figure 1. The CSIR supplied drawings from the manufacturer of the LLTS, which were used to generate the CAD geometry. The geometry was realized using shell surfaces, rather than solids, as the geometry is to be used in finite element simulations in which shell realization is more appropriate than continuum elements.

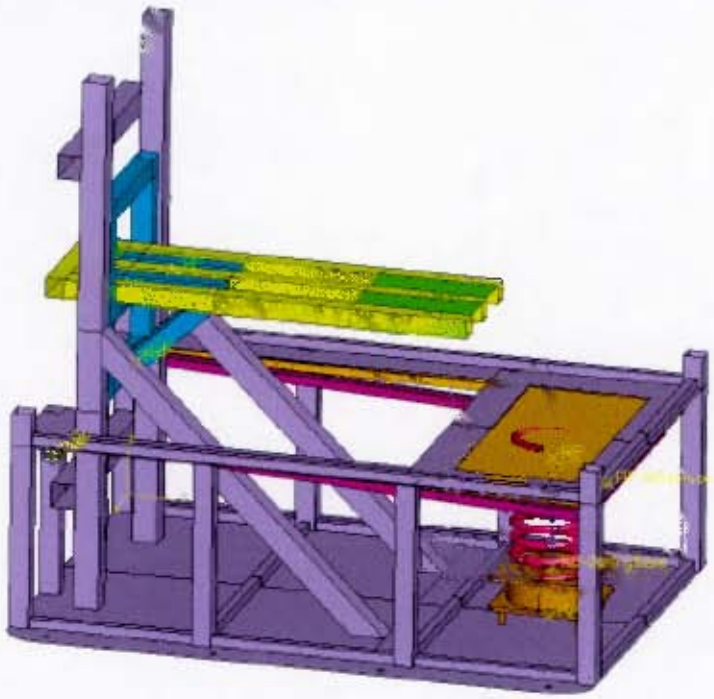

Figure 1: Completed CAD geometry of the LLTS

5.2 Mesh

All components of the assembled shelter are discretised using shell elements, ABAQUS element type S4R. These elements account for finite membrane strains and arbitrarily large rotations and hence are suitable for large-strain analysis. The default element size used throughout the model is 16mm. The completed mesh is shown in Figure 2 and Figure 3.

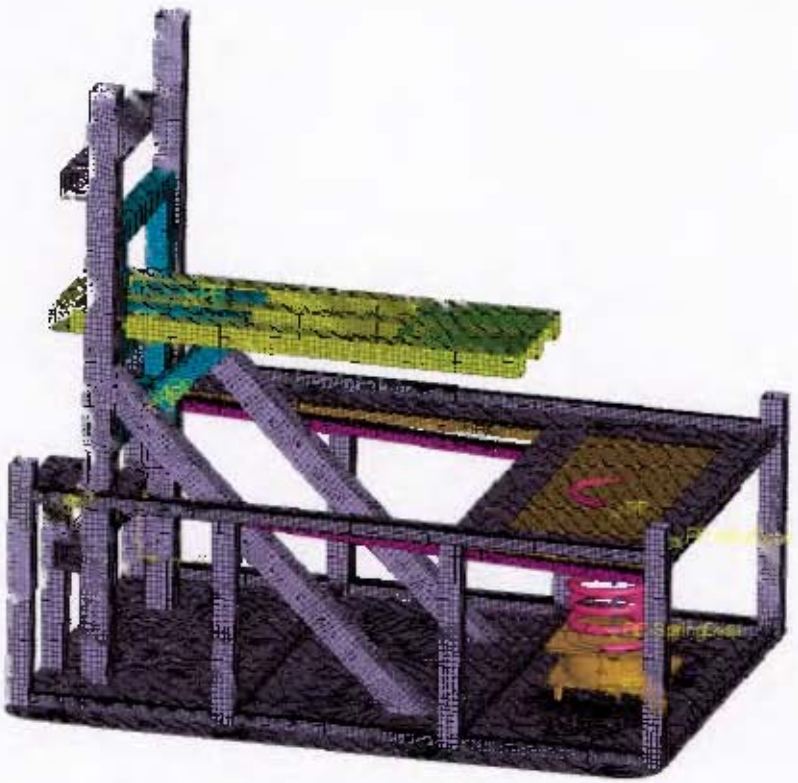

Figure 2: Finite element mesh of LLTS

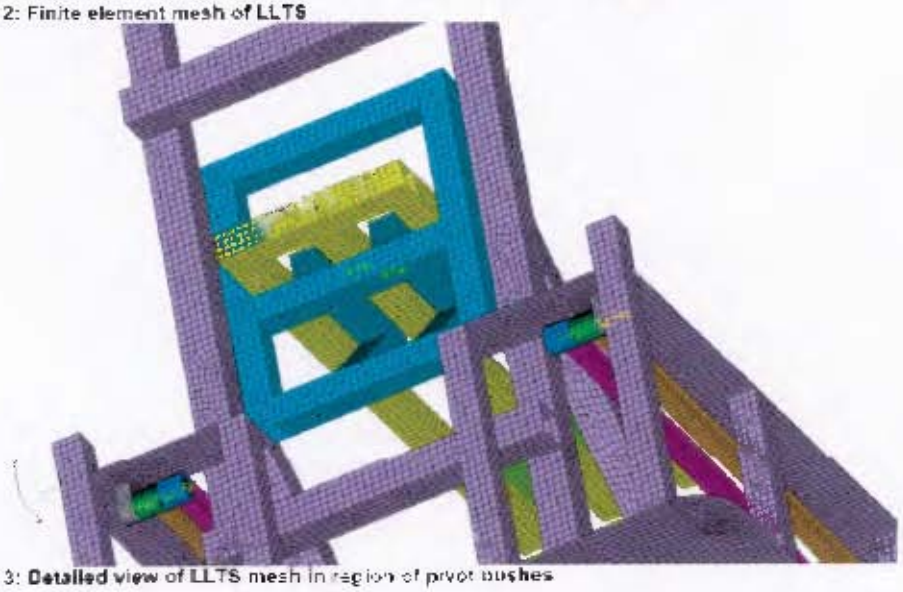

Figure 3: Detailed view of LLTS mesh in region of pivot bushes

1.1 Contact & Interactions

The following contact and interactions were defined in the model:

- Contact between the Striker Plate & Top Plate. Hard kinematic contact was implemented, using a coefficient of friction μ=0.0
- Contact between the Top Plate & Frame. For this contact definition hard kinematic contact was also implemented, using a coefficient of friction μ=0.0
- The respective pivot bearing surfaces of both the Top Plate and Striker Plate were independently coupled to centrally positioned reference points, as was the two mounting frame bearing surfaces. Hinge type connector elements were then connected between the respective pivot plate's reference points and the frame mounting bearing's reference points. In this way both Top Plate and Striker Plate are able to rotate about the axis of the Frame mounting bearing block. In the simulations friction was ignored in these bearing connections.
- The spring was not explicitly modelled, rather a computationally less expensive axial spring element was used instead, as shown in Figure 4.
- The interaction between the top of the spring and the Striker Plate occurs over an annulus on the lower face of the Striker Plate. The annulus is defined by the inner and outer diameters of the spring, as shown in Figure 4. The base of the spring is mounted to a spacer, which in turn is bolted to the base plate of the Frame. Figure 4 shows that these spring mounting bolts were coupled together and then tied to the lower end of the spring, thus simulating realistic load transfer from the spring into the Frame.
- The lugs on the Striker Plate which are used to preload the spring were coupled together to a single reference point, as shown in Figure 4, to allow a concentrated load to be easily applied during numerical simulations.

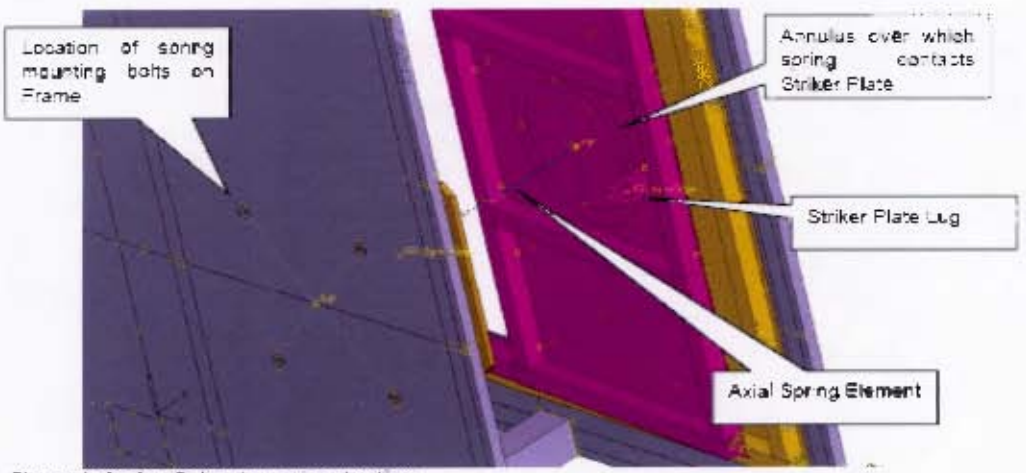

Figure 4: Spring finite element realization

5.3 Boundary Conditions

The eight mounting bolts on the lower skirt of the frame were encastre, as shown in Figure 5

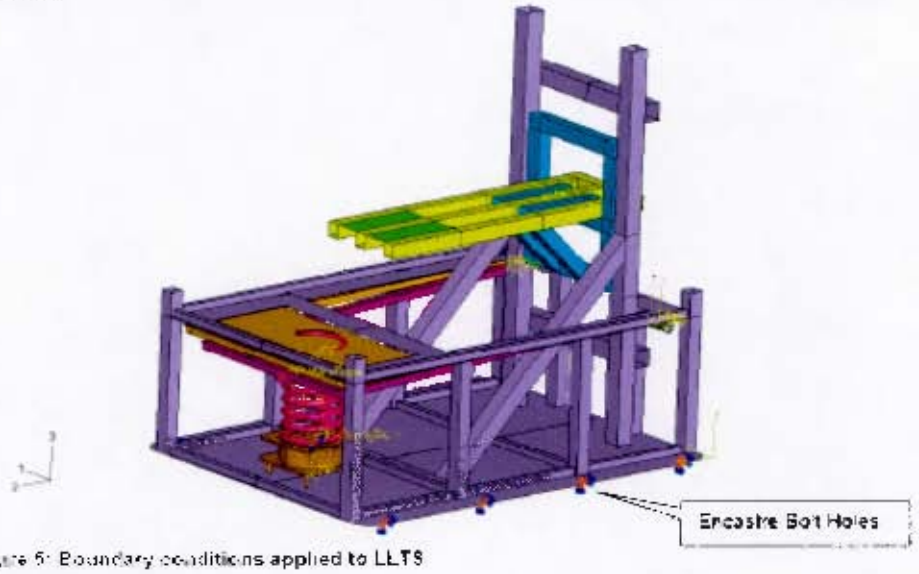

Figure 5: Boundary conditions applied to LLTS

5.4 Materials

Only linear material behaviour was considered. The material is a typical SABS 300W mild low carbon steel, thus a Young's Modulus of 208GPa and Poisson Ratio of 0.3 are appropriate.

5.5 Loading

The results of three simulations are presented here:

Load Case 1. Eigenmode analysis

Load Case 2. Dynamic Simulation of LLTS
- i. Gravity loading of the entire assembly in the global negative '3' direction.
- ii. Spring Preload, as applied to the Striker Plate lugs of 12kN

Load Case 3 Dynamic Simulation of LLTS, using truncated geometry
- i. Gravity loading of the entire assembly in the global negative '3' direction.
- ii. Spring Preload, as applied to the Striker Plate lugs of 750kg
- iii. Top Plate to Frame Offset 10mm

6 Simulation Results

6.1 EigenMode Analysis

The initial eight eigenmodes are shown in Figure 6. Notice that both the Striker and Top Plate exhibit closely spaced low frequency modes, indicating almost that these two sub-assemblies are very flexible. It is also interesting to note that the upper plate of the Top Plate, which strikes the boot, processes a large low frequency fundamental resonance which may disturb the boot / Top Plate interaction.

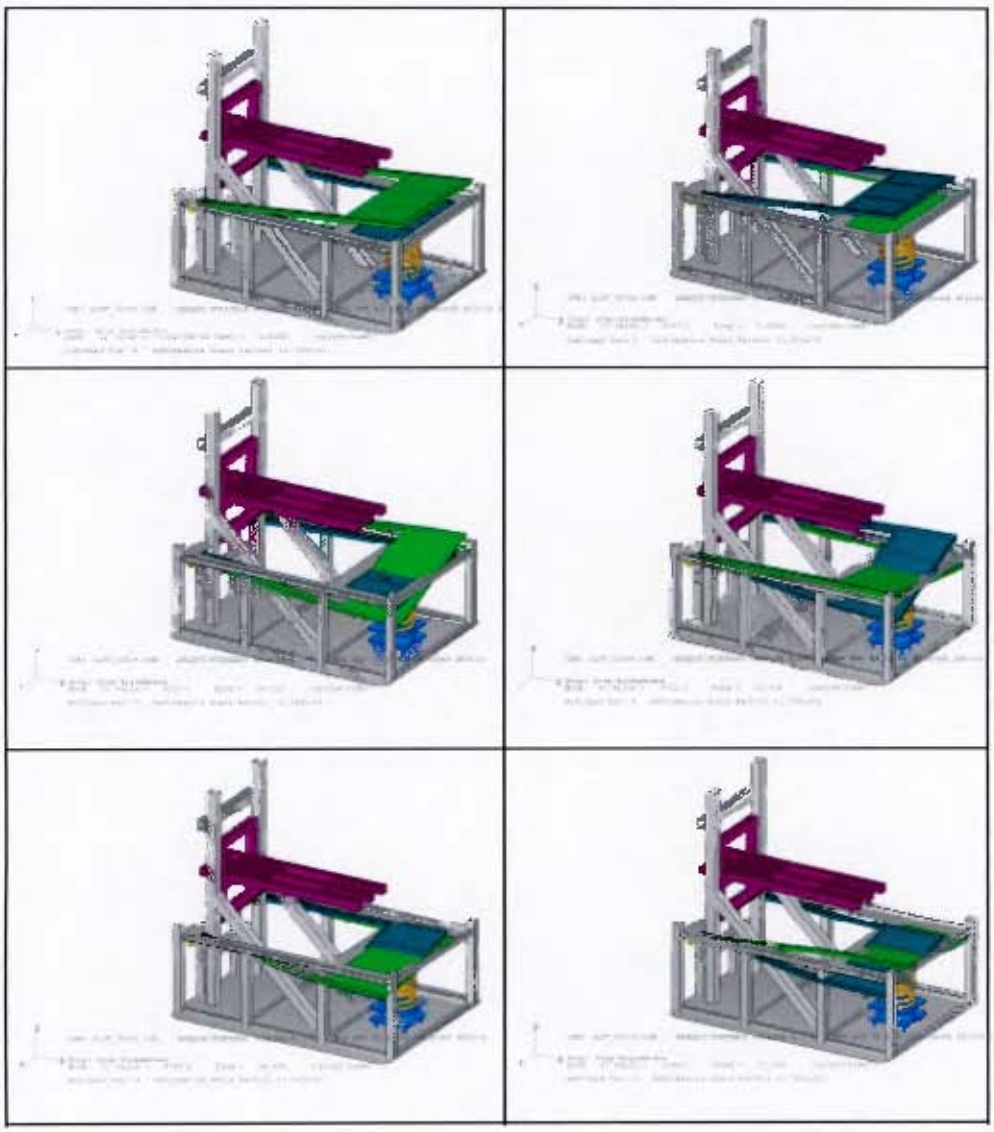

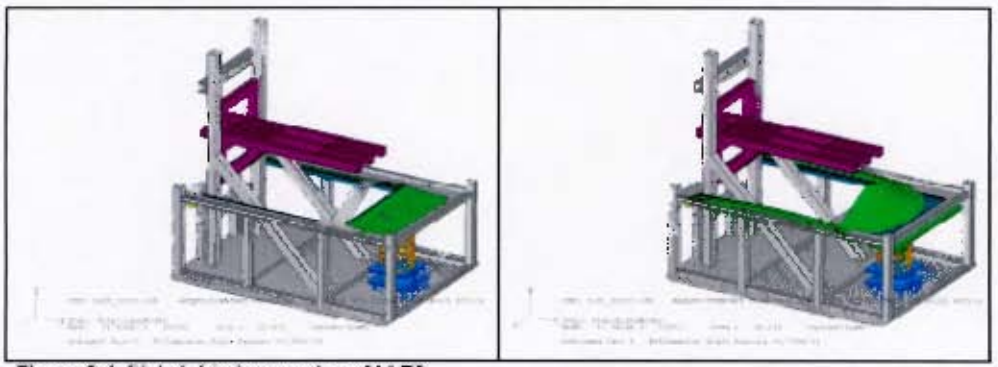

Figure 6: Initial eight eigenmodes of LLTS

6.2 *Dynamic Simulation of LLTS*

Initially the LLTS was preloaded by 12kN, the static finite element results are shown in Figure 7 and 8. The static structural results indicate that the maximum mises stress in the Striker Plate is 159MPa, as highlighted in the figures. Figure 9 presents the deformation of the Striker Plate, it is noticeable that the sub-assembly is deforming about the spring mounting. This behaviour could be expected given the position of the spring with respect to the applied Striker Plate preload.

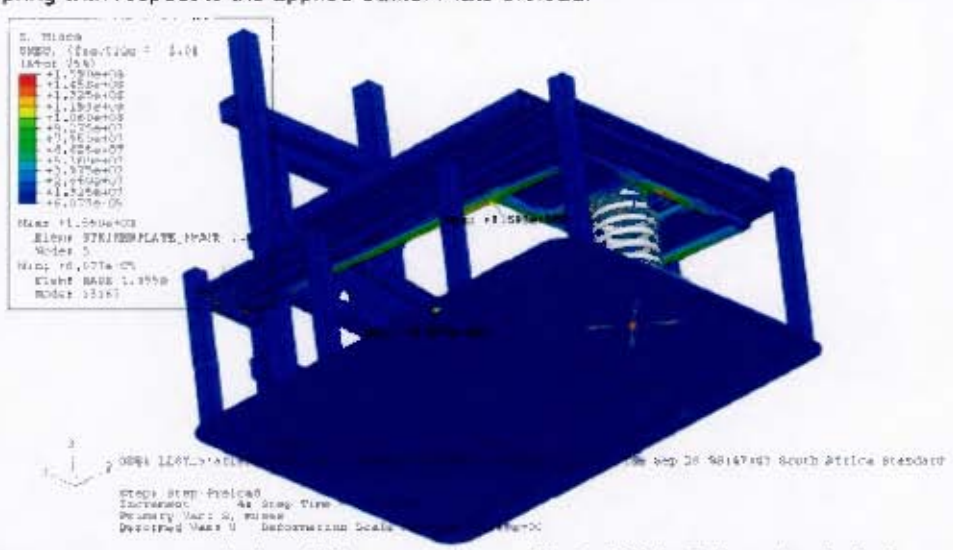

Figure 7: Contour distribution of Mises stress (Legend limit: 159MPa, Deformation Scale Factor: x1, Units: Pa)

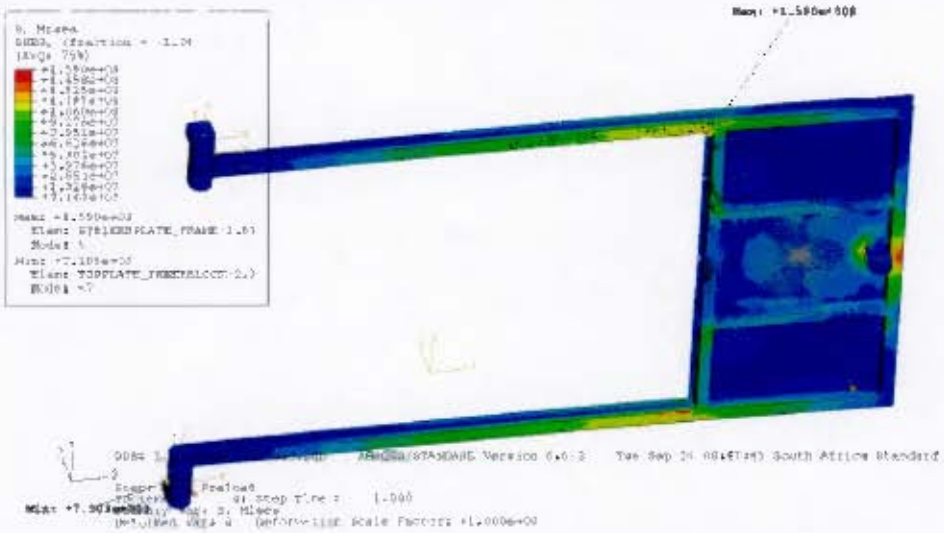

Figure 8: Contour distribution of Mises stress on Striker Plate (Legend limit: 159MPa, Deformation Scale Factor: x1, Units Pa)

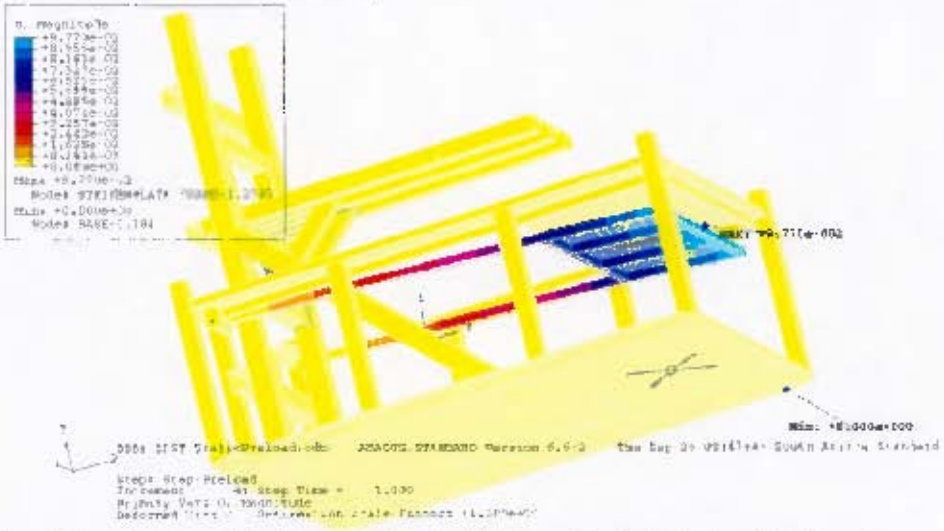

Figure 9: Contour plot of Displacement Magnitude (Deformation Scale Factor x1, Units: m)

A selection of the dynamic simulation results are shown in Figure 10.

Figure 10: Sectioned view of the Mises stress distribution @ 62ms (Legend limit: 300MPa, Deformation Scale Factor. x1, Units. Pa)

Figure 11: Sectioned view of the Mises stress distribution @ 86ms (Legend limit: 300MPa, Deformation Scale Factor. x1, Units. Pa)

6.3 *Dynamic Simulation of LLTS, Truncated Model*

To facilitate comparison of the simulation results to CSIR models, it was decided to truncate the model, by omitting all components except the Striker, Top Plate, and essential portions of the Frame. The complete truncated model is shown in Figure 12.

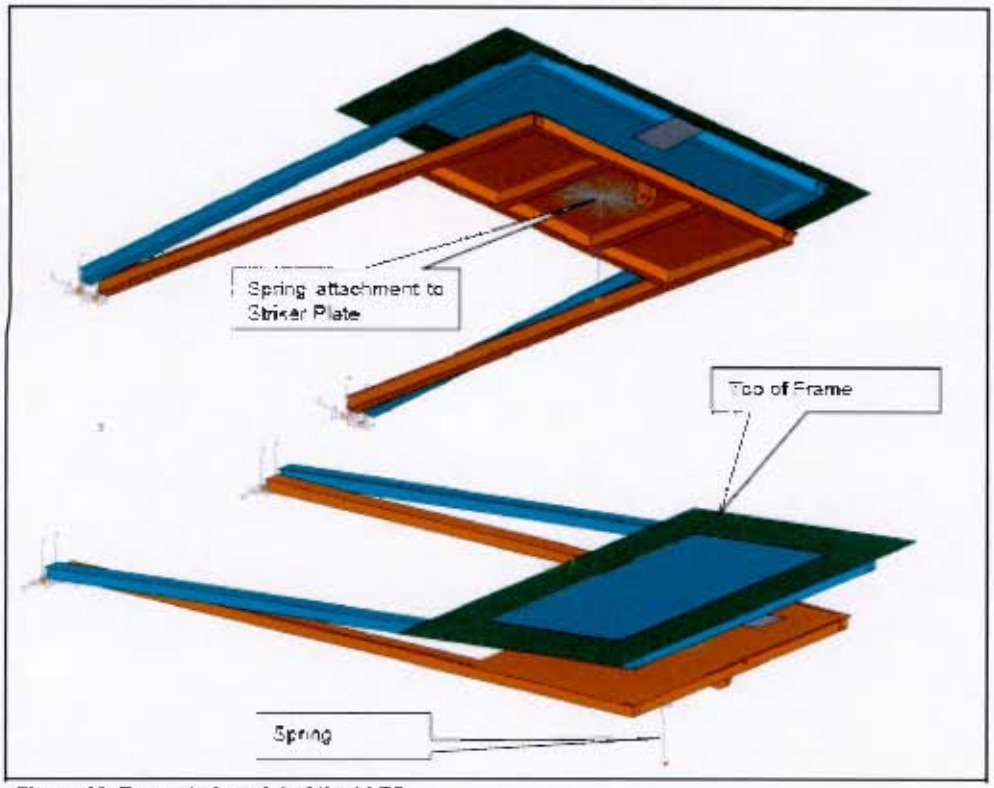

Figure 12: Truncated model of the LLTS.

The simulation results for this model are presented in the next series of figures. Figure 13 show the relative velocities of the Top Plate and Striker Plate, in locations were the CSIR have placed accelerometers.

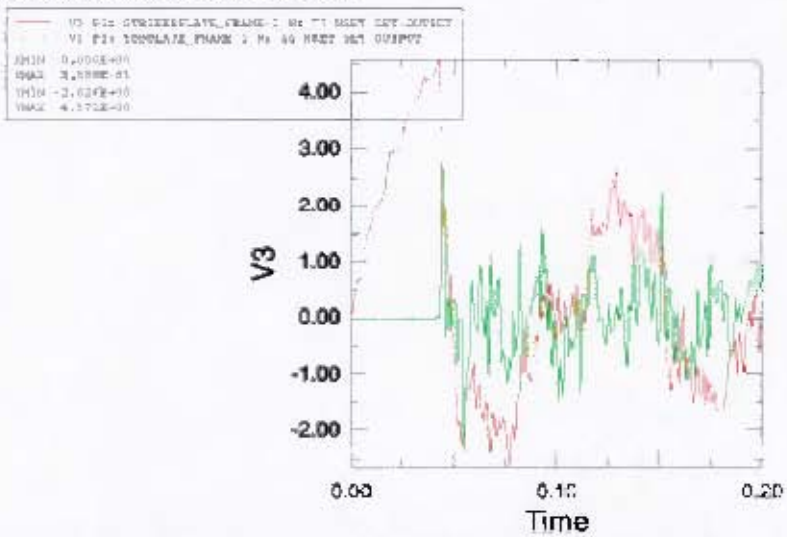

Figure 13: Graph of the relative velocities of the Striker Plate and Top Plate

The graph indicates that the Striker Plate acquires a velocity of 4m/s before interacting with the Top Plate, following this contact both sub-assemblies move at approximately 2.5m/s. These simulation results are in agreement with CSIR experimental results of the LLTS for similar preload and offset parameters

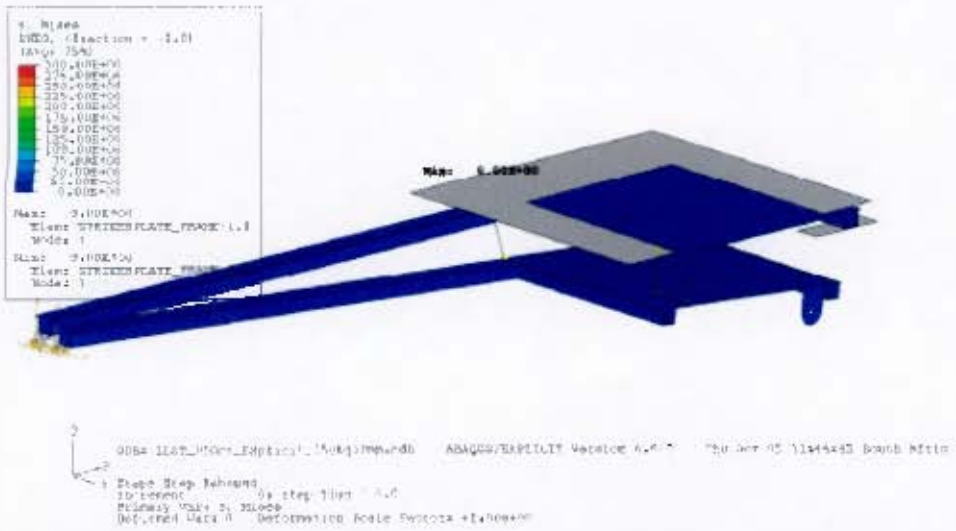

Figure 14: Sectioned view of the Mises stress distribution @ 0ms (Legend limit: 300MPa, Deformation Scale Factor: x1, Units: Pa)

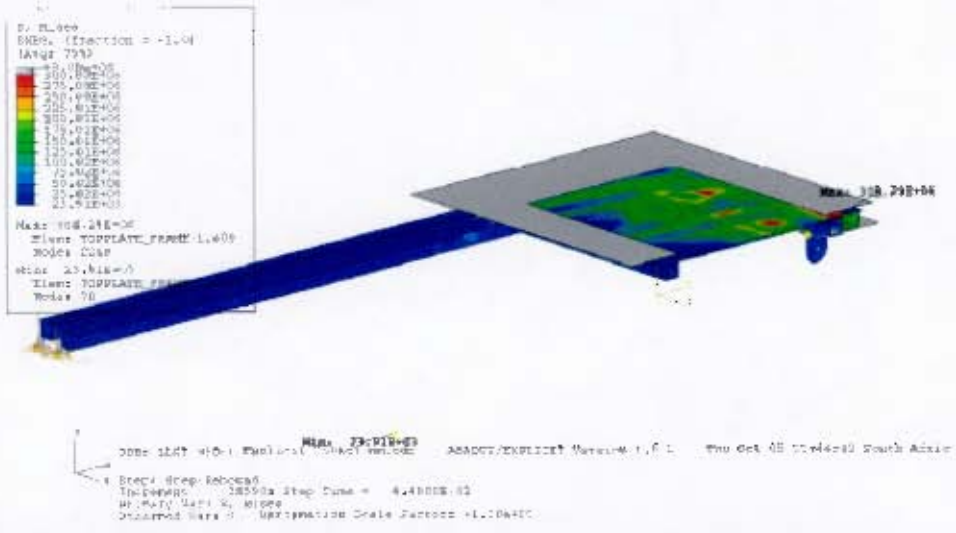

Figure 15: Sectioned view of the Mises stress distribution @ 44ms (Legend limit: 300MPa, Deformation Scale Factor: x1, Units: Pa)

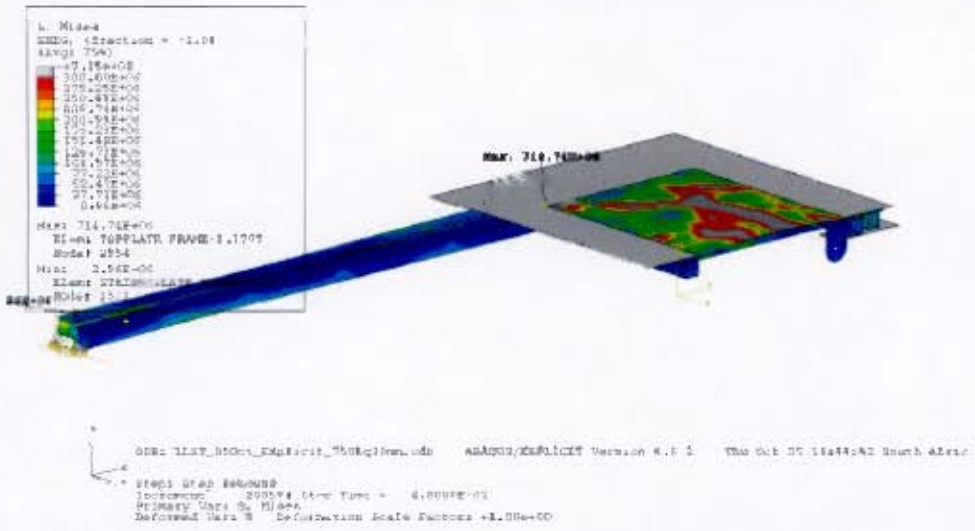

Figure 16: Sectioned view of the Mises stress distribution @ 48ms (Legend limit: 300MPa, Deformation Scale Factor: x1, Units: Pa)

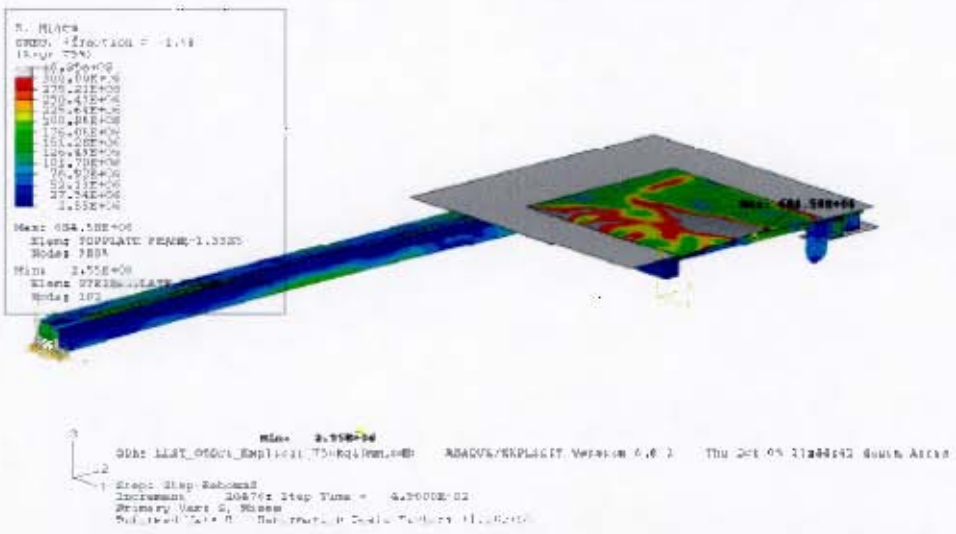

Figure 17: Sectioned view of the Mises stress distribution @ 48ms (Legend limit: 500MPa, Deformation Scale Factor: x1, Units: Pa)

B.2 Simulation of lower limb position

UNIVERSITY OF CAPE TOWN

Department of Mechanical Engineering

BLAST IMPACT AND SURVIVABILITY RESEARCH UNIT

BISRU

Numerical of Structural LMT Surrogate Leg

Prepared for	:	CSIR/Defencetek
Prepared by	:	Victor Balden
Date	:	October 2006

Engineering Research That Saves Lives

1 Document Information

Document Title	*Numerical Simulation of LMT Surrogate Leg*
Contract No. **Project Designation**	-
***Prepared* by:**	Victor Balden BISRU, UCT
Date	27 October 2006
Approved by:	Prof. Gerald Nurick Director, BISRU, UCT
Date	27 October 2006
Distribution List:	Mr. David Reinecke & Mrs. T Whyte CSIR Landwards Sciences PO Box 395 Pretoria 0001, South Africa Tel : +27 21 8832141 +27 12 8414049 e-mail :
Revision History RevA, 27 October 2006	Release for Approval within BISRU

2 Table of Contents

3 List of Figures

4 Scope of Work

The scope of work to be undertaken by BISRU is divided into the following tasks:

- Generate a finite element model of the LMT Surrogate Leg, using geometry supplied by CSIR
- Simulate the dynamic response of the leg
- Deliver a rudimentary report outlining the simulation methods and results

5 Finite Element Model

5.1 CAD Geometry

The completed CAD model of the surrogate leg is shown in Figure 1. The CSIR supplied drawings from the manufacturer which were used to generate the CAD geometry. At this time the ankle and ankle locating plate are omitted from the model, as the foot geometry is currently not available.

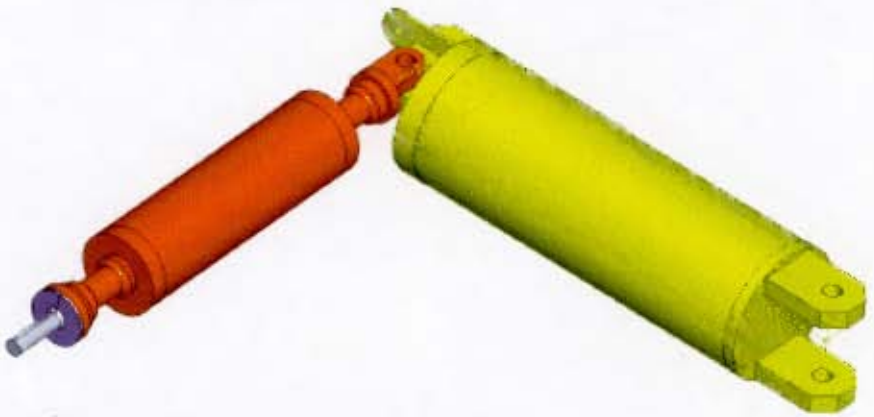

Figure 1: Completed CAD geometry of the surrogate leg

Figure 2 shows a sectioned view of the leg assembly, indicating those components which have internal cavities.

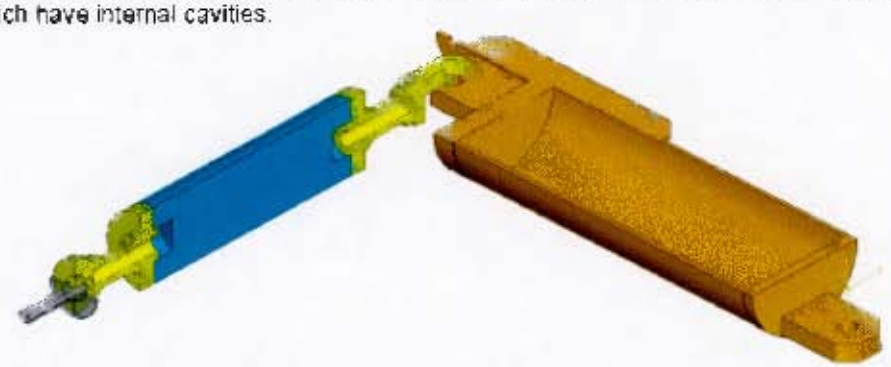

Figure 2: Sectioned view of the completed surrogate leg

5.2 Model Development

The simulation of the surrogate leg, as depicted in Figure 1 and 2 will involve considerable computational expense. Instead a beam element model was developed using the exact geometry of the leg sub-assemblies. In this way the mass and inertia properties of the beam element model are identical to the 3D model, while processing a low computational overhead. Figure 3 shows the beam model superimposed onto the sectioned view of the complete 3D geometry.

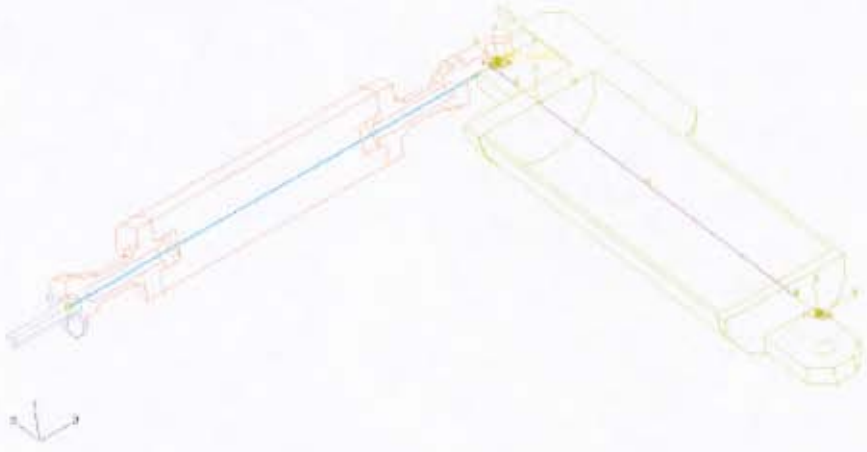

Figure 3: Wireframe sectioned view, showing beam element model representation.

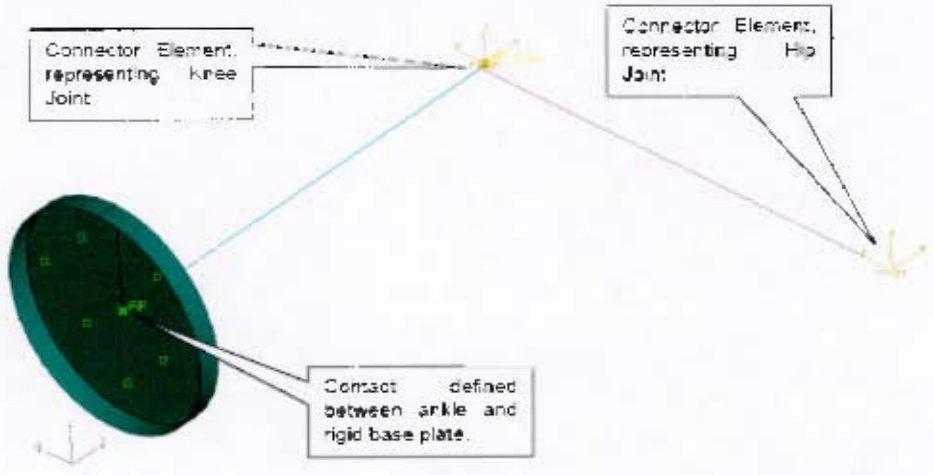

Figure 4: Beam element model of LMT surrogate leg. Notice rigid circular base added.

In Figure 4 a circular rigid base was added to the model, where by the ground reaction loading could be applied to the lower leg (ankle joint), while accounting for the size of the foot and also allowing translation of the ankle joint along the plane representing the ground loading.

5.3 Mesh

Beam elements. ABAQUS explicit element type B31, where used to discretise the surrogate leg model. The default element size used throughout the model is 10mm.

1.1 Contact & Interactions

The following contact and interactions were defined in the model:

- Contact between the ankle joint and circular rigid base was modelled as hard kinematic, using a coefficient of friction μ=0.0
- A hinge type connector element was defined for the hip joint, as shown in Figure 4. The rotational friction coefficient was defined as μ=0.3 and the rotational damping was arbitrarily defined as 10Nm/rad/s.
- A hinge type connector element was defined for the knee joint, as shown in Figure 4. The rotational friction coefficient was defined as μ=0.3 and the rotational damping was arbitrarily defined as 10Nm/rad/s.

5.4 Boundary Conditions

The pelvis side of the connector element, representing the hip joint, was encastre.

5.5 Materials

Only linear material behaviour was consicered. Both lower and upper tibia load cell components are machined from EN36A. The tibia central region is manufactured from Acetal, while all other components are constructed from mild steel material, typically SABS 300W mild low carbon steel. For the steel materials a density of 7850kg/m^3, Young's Modulus of 208GPa and Poisson Ratio of 0.3 are appropriate, while for the Acetal the density is 1410kg/m^3, Young's Modulus of 31GPa and Poisson Ratio of 0.3.

5.6 Loading

Initially the published results in the paper "Occupant lower leg injury assessment in landmine detonations under a vehicle" by van der Horst et. al of the TNO, Nederland were used to access the capability of the developed numeric model. Figure 5 shows the configuration of the tests undertaken by van der Horst et. al.

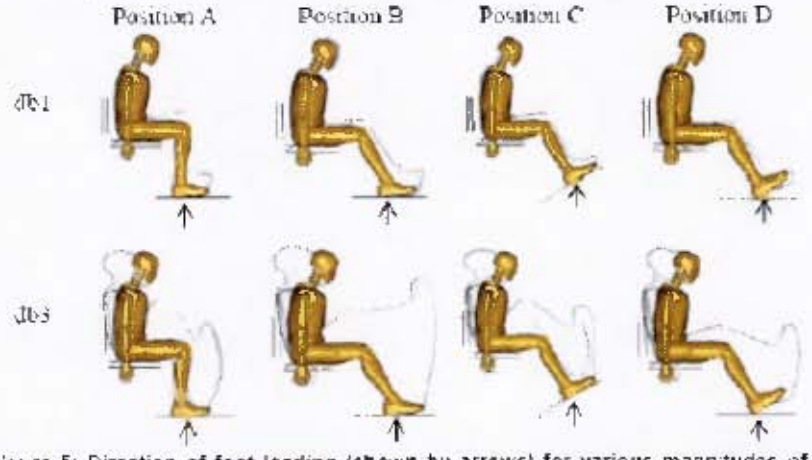

Figure 5: Direction of foot loading (shown by arrows) for various magnitudes of loading (db1, db3). The wireframe outline is understood to depict the final displacement of the respective leg sub-assemblies.

The foot was not included in the numeric model of the surrogate leg and hence only the loading case A was considered. The published acceleration data for load case 'db3' was estimated and applied to the rigid foot, as shown in Figure 6.

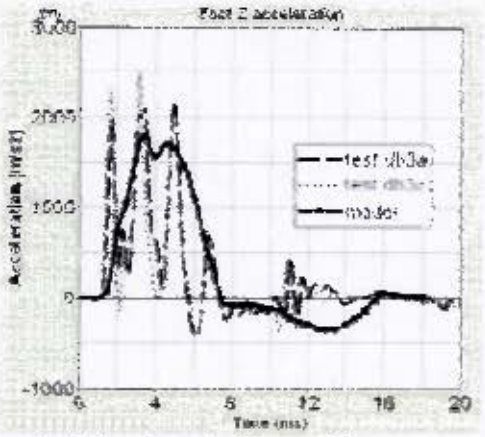

Figure 6: Foot Acceleration for db3 test [van der Horst et. al.]

This acceleration was estimated as a half sinusoidal waveform of duration 8ms, reaching a maximum of 2000m/s^2

6 Comparative Simulation Results

The displaced shape of the surrogate leg at 8ms is shown in Figure 7, there seems to a comparison with this predicted final position and the van der Horst results of Figure 7.

Figure 7 : The position of the surrogate leg components after 8ms

Figure 8 shows the comparison the simulated tibia lower force for the LMT surrogate leg and van der Horst et.al. data. The magnitude of the LMT surrogate leg model marginally over-predict the lower tibia force, however it is pleasing that the global trends between the data sets correlate well.

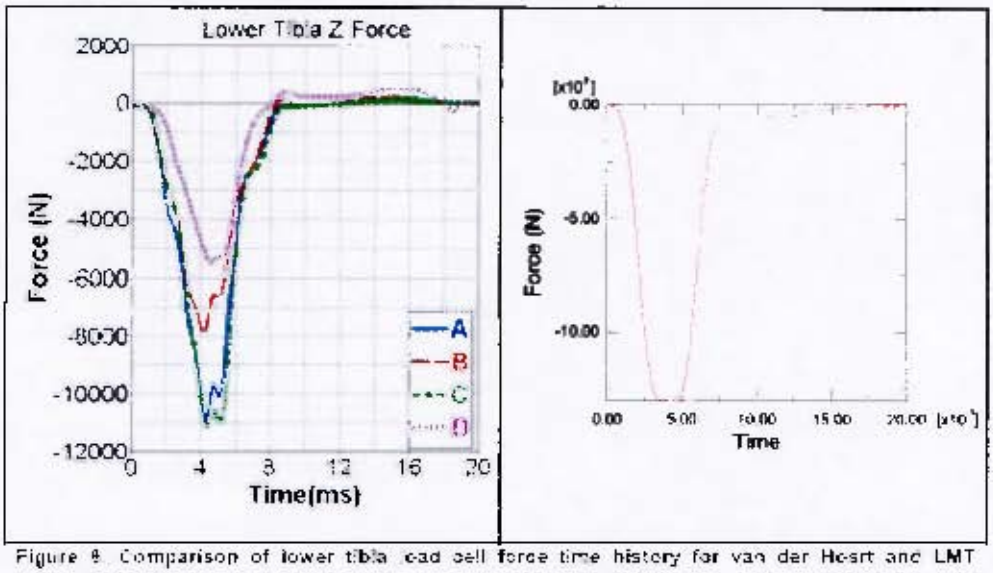

Figure 8 Comparison of lower tibia load cell force time history for van der Horst and LMT surrogate leg.

7 Discussion

This report describes the initial work that was undertaken by Victor Balden, of BIRU. It is suggested to refine the LMT surrogate leg model by the inclusion of the foot. It is then suggested to perform a numerical optimization study to determine the optimum joint friction and damping values to more accurately correlate with experimental data.